

Predicting Scour of Bedrock in Wisconsin

Hani H. Titi, Ph.D., P.E.

Qian Liao, Ph.D.

Alexander Laflin

Department of Civil and Environmental Engineering
University of Wisconsin-Milwaukee

Jeffrey R. Keaton, Ph.D., P.E., PG, D.GE, ENV-SP

Amec Foster Wheeler

William Kean, Ph.D.

Department of Geosciences
University of Wisconsin-Milwaukee

WisDOT ID no. 0092-12-07

April 2017



RESEARCH & LIBRARY UNIT



WISCONSIN HIGHWAY RESEARCH PROGRAM

WISCONSIN DOT
PUTTING RESEARCH TO WORK

DISCLAIMER

This research was funded through the Wisconsin Highway Research Program by the Wisconsin Department of Transportation and the Federal Highway Administration under Project 0092-12-07. The contents of this report reflect the views of the authors who are responsible for the facts and accuracy of the data presented herein. The contents do not necessarily reflect the official views of the Wisconsin Department of Transportation or the Federal Highway Administration at the time of publication.

This document is disseminated under the sponsorship of the Department of Transportation in the interest of information exchange. The United States Government assumes no liability for its contents or use thereof. This report does not constitute a standard, specification or regulation.

The United States Government does not endorse products or manufacturers. Trade and manufacturers' names appear in this report only because they are considered essential to the object of the document.

Technical Report Documentation Page

1. Report No. WHRP-0092-12-07	2. Government Accession No	3. Recipient's Catalog No	
4. Title and Subtitle Predicting Scour of Bedrock in Wisconsin		5. Report Date April 2017	
		6. Performing Organization Code Wisconsin Highway Research Program	
7. Authors Hani H. Titi, Qian Liao, Alexander Laflin, Jeffrey R. Keaton, and William Kean		8. Performing Organization Report: No.	
		9. Performing Organization Name and Address Department of Civil and Environmental Engineering University of Wisconsin-Milwaukee 3200 N. Cramer St. Milwaukee, WI 53211	
10. Work Unit No. (TRAIS)		11. Contract or Grant No. WHRP 0092-12-07	
		12. Sponsoring Agency Name and Address Wisconsin Highway Research Program Wisconsin Department of Transportation WisDOT Research & Library Unit 4805 Sheboygan Avenue, Room 104 P.O. Box 7915 Madison, WI 53707	
13. Type of Report and Period Covered Final Report, 11/2011– 10/2016		14. Sponsoring Agency Code	
		15. Supplementary Notes	
16. Abstract <p>This research evaluates the scour potential of rocks supporting Wisconsin DOT bridge foundations. Ten highway bridges were selected for this study, of which seven are supported by shallow foundations, and five were built on sandstone in rivers/streams. The remaining bridges are supported by foundations on degradable granite, gneiss, and dolostone. The research study included modified slake durability tests on core and hand-picked rock specimens obtained from streams/river of seven bridge sites (10 bridge structures), field work that included site visits and geologic characterization of bedrocks, hydrographic bottom channel surveys, and hydraulic modeling and analysis to estimate scour depth of bedrocks on both the river bed and around bridge piers.</p> <p>Based on the analysis of the modified slake durability test results, the sandstone exhibited significant mass loss during the continuous abrasion test. The geotechnical scour numbers and the abrasion numbers were calculated for the investigated rock specimens, which provided higher values for the sandstone compared with the other investigated rock types. This indicates that under high stream powers such degradable rock (i.e., sandstone) is more susceptible to higher scour rates compared with the other investigated rock types. It should be noted that the scour is water-rock interaction phenomenon; while the effective stream powers applied to these specimens in the modified slake durability test are high, the bedrocks that support bridge foundations in a river may not be subjected to these extreme stream power values and therefore they may degrade/abrade at a slower rate. The hydraulic modeling and analysis presents the details of the rock scour prediction at each bridge site based on stream flow data collected/analyzed from gauge stations near the investigated project sites and the results of the modified slake durability tests.</p> <p>The hydraulic modeling and analysis on six bridge sites demonstrated that the estimated annual scour depths of the investigated rocks on both the river bed foundations and around bridge piers are typically small to negligible except for two bridge sites on the Wisconsin River and the Black River. When using continuous stream power without the threshold of a "channel-forming" condition, the 75-year scour depths at STH13-WR are estimated as 7.7 and 10.2 ft. on the river bed and around the bridge pier, respectively. These numbers likely overpredict scour considering the sediment deposition that covers the channel bed. Scour depths with flood frequency analysis are generally close to that of the cumulative stream power from daily flow series with "channel-forming" threshold conditions.</p>			
17. Key Words		18. Distribution Statement No restriction. This document is available to the public through the National Technical Information Service 5285 Port Royal Road Springfield, VA 22161	
19. Security Classif.(of this report) Unclassified	20. Security Classif. (of this page) Unclassified	21. No. of Pages 204	22. Price

Acknowledgements

This research project is financially supported by Wisconsin Highway Research Program (WHRP) and Wisconsin Department of Transportation (WisDOT).

The research team would like to acknowledge and thank Mr. Daniel Reid of WisDOT for his help, support, and input during the various phases of the research project. His expertise and knowledge in Wisconsin rock geology contributed to this research project significantly.

The input and guidance of WHRP Geotechnical Oversight Committee members and WisDOT engineers Mr. Robert Arndorfer, Mr. Jeffrey Horsfall, Mr. Andrew Zimmer, Mr. Michael Perkins, and Ms. Najoua Ksontini is greatly appreciated.

The research team would like to thank Mr. Joel Ruda and his WisDOT drilling crew for their extensive effort to get the core samples from the river beds.

Collins Engineers conducted the hydrographic surveys. The help of Mr. Steven Miller and Christopher Hartzell is acknowledged.

The research team also acknowledges the help and support of UW-Milwaukee Professors, staff, and students for their help and support in various capacities for this project: Prof. Benjamin Church, Dr. Dong Zheng, Mr. Joshua Harris, Mr. Nicholas Coley, Dr. Roonak Ghaderi, Mr. Brett Ketter, Ms. Priscila Rodrigues Silva, Mr. Cristhian Cuellar Martinez, Mr. Cristian Tejedor Bonilla, and Mr. Mahmoud Dakwar.

Table of Contents

Chapter 1: Introduction -----	1
1.1 Problem Statement -----	1
1.2 Research Objectives -----	2
1.3 Background-----	2
1.4 Organization of the Research Report -----	4
Chapter 2: Background -----	5
2.1 Classification of Scour -----	5
2.2 Threshold of Scour -----	6
2.3 Stream Power-----	7
2.4 Scour on Rock-----	10
2.4.1 Dissolution of Soluble Rock -----	11
2.4.2 Cavitation -----	12
2.4.3 Physical/Chemical Weathering -----	14
2.4.4 Quarrying/Plucking-----	15
2.4.5 Abrasion -----	21
2.5 Modified Slake Durability Test -----	22
Chapter 3: Estimating Stream Power of Wisconsin Rivers -----	35
3.1 Introduction -----	35
3.2 Stream Data Extraction-----	35
3.3 Stream Power Calculation -----	36
3.4 Probability-Weighted Flood Frequency Approach -----	38
Chapter 4: Research Methodology -----	45
4.1 Selection of Project Site Locations -----	45
4.2 Field Investigation – Rock Sampling -----	47
4.3 Waterway Geometry and Hydraulics -----	59
Chapter 5: Evaluation of Bedrock Geology of Investigated Sites -----	61
5.1 Geology of Locations 4 and 5, STH 13/16/23 over Wisconsin River and Location 7 and 8, I90/94 over Spring Brook -----	61
5.2 Geology of Locations 9 and 10, IH 94 over Red Cedar River-----	63
5.3 Geology of Location 6 USH-10 over Black river near Neillsville, WI Clark Co. (B-10- 131) -----	65
5.4 Geology of Location 11, Business USH51 over Eau Claire River, Wausau, WI- 5.5 Geology Location 3, Memorial Drive over the Fox River, Appleton, Outagamie Co. WI -----	68
5.6 Geology of Locations 1 and 2, IH 43 and USH 10 over Manitowoc River, Manitowoc Co. WI -----	70
5.7 X-Ray Diffraction -----	72

Chapter 6: Results and Analyses of Laboratory Testing -----	76
6.1 Modified Slake Durability Test Results – Sandstone-----	76
6.2 Modified Slake Durability Test Results of Dolostone and Gneiss-----	94
6.3 Eau Claire River Granite-----	100
6.4 Evaluation of Modified Slake Durability Test Results for Investigated Bedrock -	106
Chapter 7: Hydraulic Modeling Analysis -----	113
7.1 Selected Bridge Sites for Scour Analysis-----	113
7.2 Hydrological Data Analysis-----	112
7.3 Hydraulic Modeling-----	121
7.4 Bridge Scour Estimation-----	125
7.4.1 Standard Method-----	125
7.4.2 Long-term rock scour based on flood frequency analysis-----	128
7.4.3 Effects of the critical stream power for rock scour-----	131
7.4.4 Annual scour depth at all test sites-----	132
7.5 Summary and Discussion-----	132
7.6 Proposed New Guidelines for WisDOT Bridge Bedrock Scour Analysis-----	134
Chapter 8: Conclusions -----	138
References	140
Appendix A	
Appendix B	

List of Figures

Figure 2.1: Horseshoe and wake vortices (HEC-18 – Richardson and Davis, 1991)-----	5
Figure 2.2: Force balance for particles subject to turbulent flow (taken from Annandale, 2007)	6
Figure 2.3: Shields diagram (after Annandale, 2007) -----	8
Figure 2.4: Available and applied stream power vs. depth (Annandale, 2006) -----	9
Figure 2.5: Energy balance of mean motion in near bed region (Schlichting and Gersten, 2000) -----	10
Figure 2.6: Flow velocity vs. flow depth, showing cavitation regions, taken from Keaton (2013)	13
Figure 2.7: Forces acting on an intact jointed rock block (after Hancock et al.1998)-----	15
Figure 2.8: Forces acting on an intact jointed rock block (after Hancock et al.1998)-----	16
Figure 2.9: Threshold power necessary for erosion (after Annandale, 1995; Note that the units of stream power should be expressed as kW/m ²)-----	19
Figure 2.10: Forces acting on an intact jointed rock block, after Annandale (1998)-----	20
Figure 2.11: Standard drum showing critical dimensions (ASTM)-----	23
Figure 2.12: Comparison of Standard Slake Durability test and continuous abrasion test (Dickenson and Baillie, 1999)-----	25
Figure 2.13: Stream power as a function of time (taken from Costa and O’Conner, 1995)	26
Figure 2.14: Available stream power at peak of date of Schoharie Creek bridge failure, with scour resistance (based on UCS) of bed material (taken from Annandale, 2000) -----	26
Figure 2.15: Contour map of P-β-Av. erosion surface, taken from Dickenson and Baillie (1999)-----	30
Figure 3.1: Rating curves developed for the USGS stream station 04066003 (Menominee River below Pemene Creek near Pembine, WI)-----	36
Figure 3.2: Daily mean discharge and annual peak flow recorded at USGS stream station 04066003 (Menominee River below Pemene Creek near Pembine, WI) -----	37
Figure 3.3: Estimating the mean daily stream power with and without threshold conditions for the USGS stream station 04066003-----	38
Figure 3.4. Data and regression lines for modified slake durability tests for rock samples (Keaton et al., 2012) -----	39
Figure 3.5: Relation between the average event duration to the flood recurrence interval (return period) for the USGS stream station 04066003-----	40
Figure 3.6: Probability distribution of stream power as a function of annual flood frequency for the USGS stream station 04066003 -----	41
Figure 3.7: (a) Relation between the frequency weighted annual stream power to the mean annual stream power with a 2-year flow threshold. (b) Relation between the frequency weighted annual stream power to the mean daily stream power without threshold flow condition	41
Figure 3.8: Map of the daily mean stream power $\bar{\Omega}$ without threshold flow condition ----	42
Figure 3.9: Map of the daily mean stream power $\bar{\Omega}_2$ with a 2-year flow threshold -----	43
Figure 3.10: Map of the frequency weighted annual stream power $\bar{\Omega}_F$ -----	44
Figure 4.1: Map of the bedrock geology of Wisconsin, developed by the Wisconsin Geological and Natural History Survey, University of Wisconsin-Extension -----	46

Figure 4.2: STH 13 bridges (B-11-01 and B-11-104) on the Wisconsin River, Wisconsin Dells – Cambrian Sandstone-----	49
Figure 4.3: STH 47 bridge (B-44-98) on the Fox River, Appleton – Dolomite -----	50
Figure 4.4: USH 10 bridge (B-10-131) on the Black River, Neillsville – Gneiss -----	51
Figure 4.5: IH-94 bridges (B-17-208, B-17-209, B-17-211) on the Red Cedar River, Menomonie – Cambrian Sandstone -----	52
Figure 4.6: IH 43 bridges (B-36-72, B-36-73) on the Manitowoc River, Manitowoc – Dolomite -----	53
Figure 4.7: USH 51 bridge (B-37-280) on the Eau Claire River, Schofield – Granite-----	54
Figure 4.8: IH 90/94 bridges (B-56-42, B-56-43) on Spring Brook, Lake Delton – Cambrian Sandstone -----	55
Figure 4.9: Bedrock coring conducted by a WisDOT drill crew with the drilling rig mounted on a barge -----	57
Figure 4.10: Bedrock hand sampling conducted by the research team -----	58
Figure 4.11: The research team conducting hydrographic field surveys using the single beam echo sounder system on Spring Brook, Lake Delton -----	60
Figure 4.12: Hydrographic field survey section locations upstream and downstream of the USH 51 bridge on the Eau Claire River in Schofield-----	60
Figure 4.13: Typical hydrographic field survey results for section 1 downstream of the USH 51 bridge on the Eau Claire River in Schofield-----	60
Figure 5.1: Geologic Map of in the Wisconsin Dells area. This includes locations 4 and 5 which are in the Dells and locations 7 and 8 which are over Interstate 90/94 crossing Spring Brook. Map modified from Clayton and Attig 1990-----	61
Figure 5.2: East side borings showing about 10 feet of sand in some locations over sandstone -----	62
Figure 5.3: West side of the Wisconsin River boring log showing almost completely sandstone in the subsurface -----	62
Figure 5.4: Boring Log data for sites 7 and 8-----	63
Figure 5.5: Modified from Brown (1988). Eau Clair Formation is in Gray color -----	64
Figure 5.6: Photo from the “Devil’s Punchbowl” showing outcrop of the Eau Claire Formation. Univ of Wisconsin –Staut, 2004-----	64
Figure: 5.7: Boring Logs for Locations 9 and 10 -----	65
Figure 5.8: modified from Brown, 1988, Agn is gneiss and migmatite: Pgr is biotite granite. The ages of these rocks vary between 2500-1800 Ma -----	66
Figure 5.9: Boring Logs for Location 6 -----	66
Figure 5.10: Geologic map of the bridge site, modified from the Geologic Map of Marathon Co. (La Berge and Meyer, 1983.) -----	67
Figure 5.11: Core sample from the area over the Eau Claire River at Wausau -----	68
Figure 5.12: Boring Logs from USH 51 – Eau Claire River location-----	68
Figure 5.13: Geologic Map of the Appleton area modified from Brown (2005) -----	69
Figure 5.14: Boring logs for location 3-----	69
Figure 5.15: Modified from the Bedrock Geologic Map of Wisconsin (Mudrey et.al., 1982) -----	70
Figure 5.16: Boring logs for location 1. (B-36-72)-----	71
Figure 5.17: Boring log for second bridge at location 1 -----	71
Figure 5.18: X-ray diffractogram for bedrock sample from Fox River -STH 47 (Dolomite) -----	72

Figure 5.19: X-ray diffractogram for bedrock sample from Balck River - USH 10 (Gneiss)	73
Figure 5.20: X-ray diffractogram for bedrock sample from Wisconsin River -STH 13 (Sandstone)	73
Figure 5.21: X-ray diffractogram for bedrock sample from Manitowoc River -IH 43 (Dolomite)	74
Figure 5.22: X-ray diffractogram for bedrock sample from Red Cedar River -IH 94 (Sandstone)	74
Figure 5.23: X-ray diffractogram for bedrock sample from Spring Brook -IH 90/94 (Sandstone)	75
Figure 5.24: X-ray diffractogram for bedrock sample from Eau Claire River -USH 51 (Granite)	75
Figure 6.1: Sandstone samples from Wisconsin River, Spring Brook, and Red Cedar River bridge sites	77
Figure 6.2: Sandstone specimens from Wisconsin River at various stages of the continuous abrasion test (modified slake durability test): (a) Initial sample, (b) after 4 runs, (c) after 8 runs, (d) after 12 runs, (e) after 16 runs, and (f) after 20 runs. -----	78
Figure 6.3: Various presentations of the equivalent scour depth versus equivalent stream power -----	81
Figure 6.4: The equivalent hourly scour depth versus equivalent hourly stream power for Wisconsin River sandstone based on the mean weight. -----	82
Figure 6.5: Cumulative sample loss versus cumulative test time for core sandstone samples from Wisconsin River. -----	82
Figure 6.6: Cumulative sample loss versus cumulative test time in natural logarithmic scale for core sandstone samples from Wisconsin River -----	84
Figure 6.7: Equivalent hourly scour depth versus equivalent hourly stream power for sandstone samples from Wisconsin River with the first point of data included -----	85
Figure 6.8: Equivalent hourly scour depth versus equivalent hourly stream power for sandstone samples from Wisconsin River with the first point of data neglected -----	87
Figure 6.9: Degradable and durable rock characterization based on modified slake durability test (Keaton 2013)-----	92
Figure 6.10: Dolostone specimens (core samples) from Fox River at various stages of the continuous abrasion test (modified slake durability test)-----	95
Figure 6.11: Gneiss specimens (hand-picked samples) from Black River at various stages of the continuous abrasion test (modified slake durability test)-----	95
Figure 6.12: Results of modified slake durability test plotted as equivalent hourly scour depth versus equivalent hourly stream power for Fox River dolostone core specimens (neglecting initial data point) -----	96
Figure 6.13: Results of modified slake durability test plotted as equivalent hourly scour depth versus equivalent hourly stream power for Black River Gneiss hand-picked specimens (neglecting initial data point) -----	97
Figure 6.14: Cumulative sample loss for Dolomite and Gneiss -----	98
Figure 6.15: Intact rock from core samples (note heavy, erratic jointing) -----	101
Figure 6.16: Samples of rock for use in modified slake durability test procedure-----	102
Figure 6.17: Samples before first test cycle [(a) and (b)], and after first cycle [(c) and (d)]	102

Figure 6.18: Core samples used in test; prior to immersion in water [(a) and (b)], and after 10 minutes of soaking in water [(c) and (d)]-----	104
Figure 6.19: Comparison of maximum loss as a percent of the initial weight of the specimen for all bedrock samples at the investigated bridge sites -----	107
Figure 6.20: Results of modified slake durability test for representative rock specimens obtained from the investigated bridge sites (the initial data point was neglected in the analysis)-----	108
Figure 6.21: Geotechnical Scour Number for all investigated rocks – (95 percentile) ---	109
Figure 6.22: Threshold values of equivalent hourly stream power required to initiate scour of the investigated rock types obtained from the modified slake durability test (minimum, median and maximum values)-----	111
Figure 6.23: Maximum and minimum abrasion number values for investigated rocks --	112
Figure 7.1: Daily stream flow rates (vertical lines) and annual peak flow rates (circles) recorded by USGS stream flow stations near the six bridge sites. Flood flow of 10, 100 and 500 year events are estimated from frequency analysis based on the annual peak flow series of each site	114
Figure 7.2: Tests of the goodness of fit of a log-Pearson Type III distribution with the annual peak flow series recorded at the selected USGS stream stations -----	118
Figure 7.3: Relation between the average event duration to the flood recurrence interval (return period) at the selected USGS stream stations -----	120
Figure 7.4: River cross-sections survey for river bed topography at site US10-BR.	122
Figure 7.5: Sample hydraulic simulation result for site US10-BR with HEC-RAS -----	122
Figure 7.6: Rating curves between the stream power and the river discharge reconstructed from HEC-RAS simulation results -----	124
Figure 7.7: Time series of daily stream power over the river bed at all six project sites, calculated from USGS daily stream flow and power-discharge rating relations-----	125
Figure 7.8: Cumulative stream power over the river bed under the bridge and around bridge piers at the six project sites. Dashed lines are linear regression of the cumulative stream power, and the numbers represents the slope of the linear regression, i.e., the annual average stream power, $\bar{\Omega}$, over the period of stream flow observation -----	127
Figure 7.9: Cumulative stream power with a 2-year flow threshold (“channel-forming”) at the six project sites. Dashed lines are linear regressions of the cumulative stream power, and the numbers represents the slope of the linear regressions, i.e., the annual average stream power, $\bar{\Omega}_2$, over the period of stream flow observation -----	128
Figure 7.10: Probability distribution of the cumulative stream power over a flood event for all six project sites-----	129
Figure 7.11: Estimated annual average scour depths on the rock foundation and around bridge piers with different methods-----	132
Figure 7.12: Conceptual relationship of this rock scour research with HEC-18, HEC-20, and HEC-23, adapted from Keaton et al. (2012)-----	135

List of Tables

Table 4.1: Summary of bridge structure information for bridges selected for the rock scour study -----	47
Table 4.2: Summary of coring and hand sampling conducted at the investigated project sites -----	59
Table 6.1: Sample calculations of equivalent stream power and equivalent scour depth from the modified slake durability test on sandstone core sample at pier 1 on the STH13 bridge on Wisconsin River. -----	80
Table 6.2: Calculated equivalent hourly scour depth (EHSD) and equivalent hourly stream power (EHSP) based on the 15-minute time increment for sandstone core sample at pier 1 on the STH13 bridge on Wisconsin River -----	81
Table 6.3: Geotechnical Scour Number as well as threshold of equivalent hourly stream power for sandstone samples from Wisconsin River (with the first point of test data considered in the calculations) -----	88
Table 6.4: Geotechnical Scour Number as well as threshold of equivalent hourly stream power for sandstone samples from Wisconsin River (with the first point of test data omitted in the calculations) -----	90
Table 6.5: The Abrasion Number values for sandstone core and hand-picked samples from Wisconsin River from the modified slake durability test -----	93
Table 6.6: Geotechnical Scour Number for dolostone samples from Fox River -----	99
Table 6.7: Abrasion Number for dolostone samples from Fox River -----	99
Table 6.8: Geotechnical scour numbers and abrasion numbers for tested samples -----	100
Table 6.9: Geotechnical Scour Numbers and Abrasion Numbers for Bulk Core Samples -----	100
Table 6.10: Geotechnical scour number of granite samples from Eau Claire River -----	103
Table 6.11: Abrasion number for granite samples from Eau Claire River -----	103
Table 6.12: Geotechnical scour numbers and abrasion numbers for Bulk Core Samples -----	104
Table 7.1: List of selected project sites for bridge scour analysis -----	114
Table 7.2: Flood flow rates (in cubic feet per second, cfs) with occurrence interval of $T= 2, 5, 10, 25, 50, 100,$ and 500 years -----	119
Table 7.3: Annual average stream power with and without “channel-forming” threshold ($\bar{\Omega}$ and $\bar{\Omega}_2$), and the long term average stream power from flood frequency analysis ($\bar{\Omega}_F/365/24$). (Note stream power units are: [ft-lb s-1 ft-2]) -----	131
Table 7.4: Estimated average rock scour depths over a 75-year period. (Scour depth unit: [ft]) -----	133

Chapter 1

Introduction

1.1 Problem Statement

The Wisconsin Department of Transportation (WisDOT) employs shallow foundations on bedrock in waterways for the construction of some bridge structures. As part of the design process of these foundations, the project's structural engineer, hydraulic engineer and geotechnical engineer must estimate the anticipated depth of scour that will occur at the foundation over the life of the project. The following text quotes the current WisDOT methodologies:

Bridge Manual Section 8.3.2.7

Conduct Scour Evaluation

Evaluating scour potential at bridges is based on recommendations and background from FHWA Technical Advisory "Evaluating Scour at Bridges" dated October 28, 1991 and procedures from the FHWA Hydraulic Engineering Circular No. 18, Evaluating Scour at Bridges, Fourth Edition, May 2001, and Hydraulic Engineering Circular No. 20, Stream Stability at Highway Structures, Third Edition, March 2001.

All bridges shall be evaluated to determine the vulnerability to scour. In the FHWA publication Recording and Coding Guide for Structure Inventory and Appraisal of the Nation's Bridges, a code system has been established for evaluation. A section in this guide "Item 113 - Scour Critical Bridges" uses a single-digit code to identify the status of the bridge regarding its vulnerability to scour. A reproduction of this item is given in 8.8 Appendix 8-C.

There are three main components of total scour at a bridge site. They are Long-term Aggradations and Degradation, Contraction Scour, and Local Scour. In addition, lateral migration of the stream must be assessed when evaluating total scour at substructure units. Contraction and local scour will be evaluated in the context of clear-water and live bed scour conditions.

Alternatively, NCHRP Project 24-29 "Scour at Bridge Foundations on Rock" recommends a procedure, which involves testing the bedrock and examining hydraulic factors over the life of the structure. WisDOT is funding this research project to allow for the use of this method on existing structures/structures currently under design/construction structures in Wisconsin.

The purpose of this research is to apply an alternative method for evaluating scour for Wisconsin bedrock as described in NCHRP Project 24-29 "Scour at Bridge Foundations on

Rock” and perform testing and hydraulic evaluation to document the procedures on several existing structures.

1.2 Research Objectives

The objective of this research is to assess the ability of the newly developed methods described in NCHRP Project 24-29 “Scour at Bridge Foundations on Rock” to characterize the scour potential for various types of Wisconsin bedrock and structures throughout the state. The study will evaluate the need to refine the test procedures and establish a range of typical test parameter values for use with Wisconsin bedrocks. The research will also compare the new methods with current practices and communicate any potential benefits that can be realized through WisDOT implementation of the newly developed methods.

1.3 Background

Bridge scour is the erosion or removal due to flowing water of sediment (sand or rock) around the pier or abutment of a bridge, thereby compromising the integrity of the structure. Bridge scour is a major cause of highway bridge failure in the United States. After the collapse of the Schoharie Creek Bridge on I-90 in 1987 during a flood, the Federal Highway Administration (FHWA) issued Technical Advisory in 1988 that require evaluation of all bridges to determine the vulnerability to scour. In order to provide guidance to determine the probable depth of scour under various hydraulic, geological and structural conditions, the FHWA Hydraulic Engineering Circular No. 18 (HEC-18): Evaluating Scour at Bridges (Richardson and Davis, 2001) has been developed as the technical standard for bridge scour analysis. Additional documents are also available, including HEC-20: Stream Stability at Highway Structures (Lagasse et al., 2001a) and HEC-23: Bridge Scour and Stream Instability Countermeasures (Lagasse et al., 2001b). These documents are also utilized by WisDOT as the standard procedures for bridge scour analysis, which are detailed in the *Wisconsin Bridge Manual* (http://on.dot.wi.gov/dtid_bos/extranet/structures/bridge-manual/index.htm). Based on these procedures, a single-digit code can be assigned to a bridge to identify the status of the bridge regarding its vulnerability to scour.

The standard procedures documented in HEC-18 can be summarized as the following:

- (1) Hydrological analysis: select the design flood event (e.g., a 100-year flood and a super flood: 500-year flood or overtopping flood).
- (2) Hydraulic analysis: determine the water surface profile and local flow velocities using WSPRO or HEC-RAS software based on the design flood event.
- (3) Compute the total scour depth in combination with structural and geotechnical inputs from the bridge site, which is assumed as the sum of three major components:
 - a. Long-term aggradation and degradation of the river bed.
 - b. General scour at the bridge due to contraction and other factors.

- c. Local scour at the pier and the abutment due to vortex structures around the obstruction.
- (4) Plot the total scoured depth on the cross-section (scour prism) for evaluation.

Most – if not all – scour equations documented in HEC-18 address the erosion of non-cohesive, granular bed materials. These equations are based on previous research on sediment erosion, transport and deposition. At the level of basic physical principles, the scour of granular sediment depends on the local peak hydrodynamic conditions such as the velocity or bed shear stress, as well as the physical properties of the sediment particles including size, specific weight, and the critical shear stress, etc. Also, the effects of sediment loading in the stream are considered, i.e. clear-water scour vs. live-bed scour. For bridges constructed with shallow foundations on bedrock in which the bed materials are cohesive, cemented or indurated (i.e. rock or rock-like formations), models in HEC-18 would usually result in overestimated erosion depth. In order to address this issue, the National Cooperative Highway Research Program (NCHRP) has funded research project “Scour at Bridge Foundations on Rock” (NCHRP Project No. 24-29) to develop a new methodology for estimating the rate and design depth of scour in rock over the service life of a bridge, and to create guidelines for application of the improved methodology.

The mechanisms of rock erosion are more complicated than granular sediment erosion alone. In general, they can be classified into (1) hydraulic erosion of un-jointed intact rock, (2) hydraulic erosion of jointed rock masses (plucking), (3) abrasive erosion due to either bed load or suspended load, (4) cavitation, and (5) dissolution and weathering of rock material. While cavitation and dissolution are not common in natural streams and channels, other mechanisms can be modeled with well-defined hydraulic conditions. There has been recent progress towards modeling rock erosion rate, such as through mechanical-process based methods (Sklar and Dietrich, 2004) or even through microscopic-scale modeling (Pan et al., 2010). Practically, empirical models (Annandale, 2006) are still the most accepted methods in the analysis of bed-rock erosion of bridge scour even though they were developed for unlined spillway channels rather than for natural channels. The hydraulic erosion rate is often described as a power function of the bed shear stress or the stream power. Many empirical models of erosion rates can be generalized into a “stream-power family of models” (Whipple and Tucker, 1999). A model may also include a threshold shear stress for erosion and may consider the influence of sediment loads (either saltating bed loads or suspended loads) on the incision rate.

Keaton et al. (2010), Keaton and Mishra (2010), and Mishra et al. (2010) published methodologies and sample results developed for NCHRP Project 24-29 in papers presented at the 5th International Conference on Scour and Erosion (ICSE-5). The new method focuses on degradable rock scour, which is believed to be gradual and cumulative over a long period (life span of a bridge). Hence a cumulative hydraulic load is defined as the time integral of stream power, which is the product of bed shear stress and the stream velocity. With available onsite historical stream flow data as well as the amount of scour observed at a bridge location, an

empirical Scour Number can be determined and can be applied for predicting the future scour depth over the remaining life of a structure. The obtained Scour Number can also be applied to other existing structures with foundations in the same or similar rock formation and with similar stream flow. The scour depth due to future hydraulic loads is modeled through a probability weighted approach, which captures the range of flow conditions and is converted to an average annual scour (Mishra et al., 2010). For cases where the empirical Scour Number cannot be obtained due to the lack of onsite scour depth observations, a geotechnical Scour Number can be estimated as a surrogate. A modified slake durability test has been developed for this purpose, where sample rock fragments collected at the bridge site are submerged in a rotating drum. The measured cumulative sample mass loss can be converted to an equivalent scour depth vs. a normalized cumulative power taken to represent equivalent stream power. A calibration test was conducted for two samples of thinly bedded siltstone from the Sacramento River at Redding (California). The obtained geotechnical Scour Number was found to be similar to an empirical Scour Number for the same site (Keaton et al., 2010).

Because some bridges in Wisconsin are constructed using shallow foundations on bedrock in waterways, the Wisconsin Highway Research Program (WHRP) is requesting proposals to predict the scour of these bedrocks using methods similar to those described in NCHRP Project 24-29.

1.4 Organization of the Research Report

This research report is organized in eight chapters. Chapter One presents the problem statement and the objectives of the research project. Background information on rock scour with focus on NCHRP project 24-29 are compiled in Chapter Two. In Chapter Three, details of the analysis conducted on gage data to estimate stream power of Wisconsin rivers are presented. Chapter Four presents the research methodology executed at the selected sites as well as in the laboratory to accomplish the objectives of the research project. Evaluation of the bedrock geology of the investigated sites is summarized in Chapter Five. Chapter Six presents the results, evaluation and discussion of the laboratory testing program conducted on the collected rock samples. The hydraulic modeling analysis of the investigated sites is presented in Chapter Seven. Conclusions of the research project are presented in Chapter Eight.

Chapter 2 Background

This chapter presents the results of the literature review of rock scour characterization with emphasis on degradable rocks. The modified slake durability test is discussed in detail because it was selected by NCHRP project 24-29 for laboratory evaluation of rock scour.

2.1 Classification of Scour

Three distinct types of scour are noted to occur at channels spanned by bridges:

- 1) Contraction scour: This is the removal of bed material by a flow caused by the increase of flow velocity corresponding to a decrease in cross-sectional flow area. This can be caused by an accumulation of debris on the upstream side of a bridge foundation, or by bridge approaches extending into a floodplain to allow the bridge structure to be shorter.
- 2) Local scour: This refers to scour that takes place in direct proximity of a bridge pier, and it is caused by acceleration of flow around the pier. This is primarily due to the formation of horseshoe vortices from a turbulent flow regime. Figure 2.1 shows a schematic of the mechanisms that cause local scour.

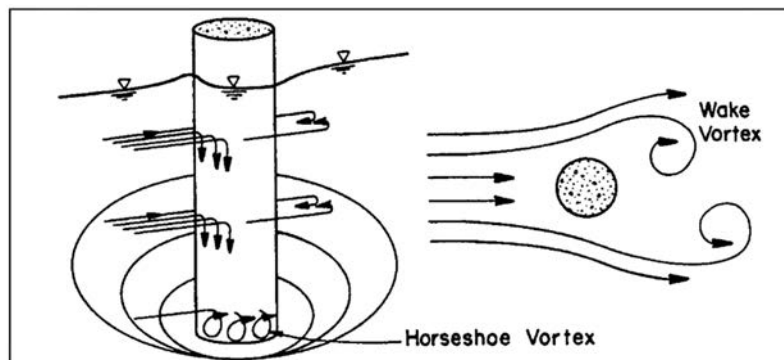


Figure 2.1: Horseshoe and wake vortices (HEC-18 – Richardson and Davis, 1991)

Local scour depends on several factors, including flow velocity and flow depth, pier width and shape, bed material characteristics and configuration, and angle of attack of flow (Richardson and Davis, 1993).

- 3) General scour or degradation: This is the long-term removal (degradation) of material from a streambed.

The summed effects of these three types of scour constitute the total scour, which must be considered in a complete bridge scour analysis.

Scour can be classified into two types: Clear water scour and live bed scour. Clear water scour describes conditions where bedload and suspended sediment are largely absent from the flow, while live bed scour considers bedload and suspended sediment as dominant factors.

2.2 Threshold of Scour

The theory and methods applied in HEC-18 (Richardson and Davis, 1991), as well as the majority of the existing literature surrounding sediment transport, assume that shear stress acting on streambed material is the driving force behind scour and erosion. Annandale (2007) points out that this assumption is only valid for cases of laminar flow. Annandale (2007) cites the work of Hinze (1975), which shows that under turbulent flow conditions, the root mean square of the fluctuating pressures on a streambed, denoted by p' , is empirically related to the turbulent boundary shear stress τ_t (not to be confused with shear stress at the stream bed) by:

$$p' = 3\tau_t \quad (2.1)$$

This is not to imply that erosion is caused by a shear stress mechanism; rather, it is simply an empirical observation relating the two quantities (Annandale, 2006).

Annandale (2006) cites Emmerling (1973), which found that pressure peaks present in turbulent flow regimes can be as high as $6p'$; when combined with Equation (2.1), this yields maximum pressures that are eighteen times the magnitude of the turbulent boundary layer shear stress. Figure 2.2 is a diagram that illustrates the forces acting on a particle under turbulent flow conditions.

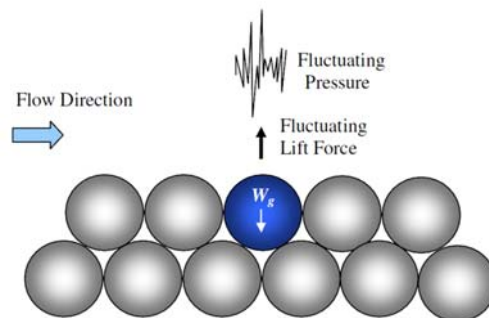


Figure 2.2: Force balance for particles subject to turbulent flow (taken from Annandale, 2007)

From Figure 2.2, it can be seen that the uplift force required for incipient motion is equal to the submerged weight of the particle (neglecting frictional force between the particles). That is:

$$\frac{\pi}{4} \cdot d^2 \cdot \Delta p = \frac{\pi}{6} \cdot d^3 \cdot (\rho_s - \rho_w) \cdot g \quad (2.2)$$

where:

$$\begin{aligned} d &= \text{Particle diameter \{L\}} \\ \Delta p &= \text{Change in pressure \{ML}^{-1}\text{T}^{-1}\} \\ \rho_s &= \text{Density of particle \{ML}^{-3}\} \\ \rho_w &= \text{density of water \{ML}^{-3}\} \\ g &= \text{gravitational acceleration \{LT}^{-2}\} \end{aligned}$$

Substitution of Equation (2.1) into Equation (2.2) and rearranging yields the following result:

$$\frac{\tau_t}{(\rho_s - \rho_w)gd} = \frac{4}{18 \cdot 6} \approx 0.037 \quad (2.3)$$

The left-hand side of Equation (2.3) is the dimensionless shear stress, i.e. the Shields (1936) parameter. The right-hand side is the minimum value of critical shear stress for incipient motion in turbulent flow; this minimum can be observed on the Shields diagram. This condition is only satisfied over a certain range of particle Reynolds numbers, for transitional (smooth) turbulent flow. Annandale (2006) notes the relation in Equation (2.3) is only valid when the negative pressure fully encapsulates the particle.

The relation in Equation (2.3) shows that the critical dimensionless shear stress required for frictionless particle motion in turbulent flow is approximately equal to 0.037. The conclusion reached by Annandale (2007) is substantiated by the Shields (1936) diagram, shown in Figure 2.3. This diagram, derived empirically, plots the relationship between the dimensionless shear stress and the Reynolds number for a characteristic particle. The Shields parameter is denoted θ , equivalent spherical particle diameter d , unit weight of sediment γ_s , unit weight of water γ , relative flow velocity u_0 , and kinematic viscosity of water ν . The diagram shows a dimensionless shear stress threshold approximately equal to 0.037 for turbulent flow, as derived in the above analysis by Annandale (2006). The empirical nature of the Shields diagram indicates that friction between grains is in fact incorporated in the relation in Equation (2.3).

2.3 Stream Power

The term “stream power” describes the rate of energy transferred to (or by) water as it flows. For uniform flow in natural channels, where specific energy ($y + v^2/2g$) remains constant, the energy gained by the water is balanced by the energy dissipated by the water through means of friction. Energy is not dissipated uniformly over the cross section of flow; rather, the dissipation of energy is concentrated in the near-bed region. Annandale (2006) analyzes the

distribution of stream power over a depth of flow by differentiating the stream power, as defined by Equation 2.4, with respect to flow depth y , which yields:

$$\frac{d}{dy}(\tau u) = u \frac{d\tau}{dy} + \tau \frac{du}{dy} \quad (2.4)$$

where the first term on the right-hand side of Equation 2.4 is the power available to drive flow per unit volume of water, and the second term on the right-hand side is the power per unit volume of water that is applied to the streambed. By assuming a power law velocity distribution given as a function of depth, Annandale (2006) plotted curves of the stream power distributions with depth, shown in Figure 2.4.

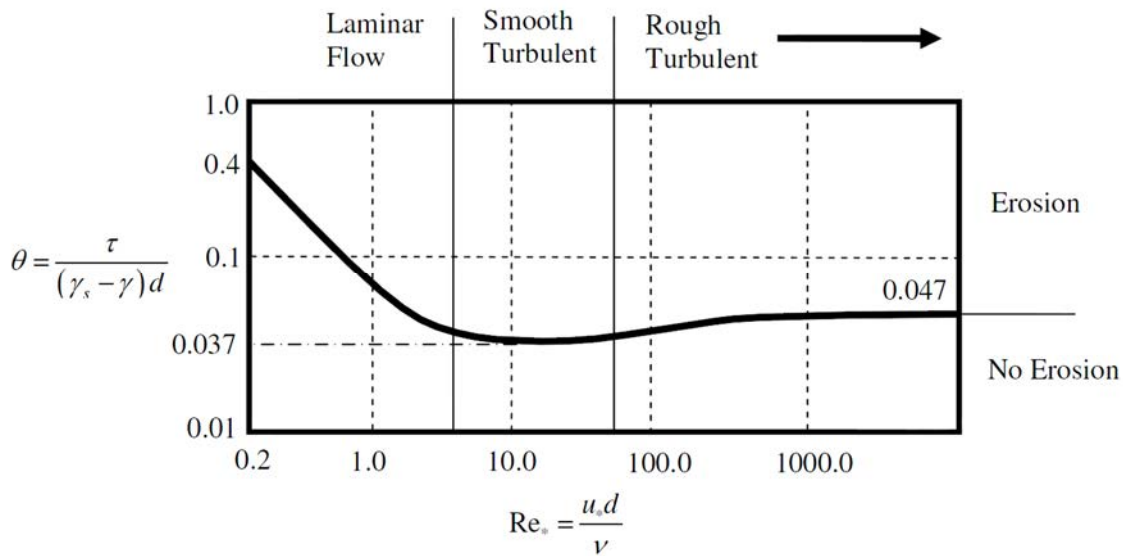


Figure 2.3: Shields diagram (after Annandale, 2007)

Figure 2.4 shows that the available stream power is mainly concentrated in the center of the stream, while the applied stream power is at a maximum at the stream bed. Stream power is transferred to the stream bed from the center of the stream, where it will dissipate into heat energy. As mentioned above, a certain portion of the stream energy is dissipated outside the near-bed region, with the remaining portion dissipated inside the near-bed region. The energy dissipated in the near-bed region is of primary importance with respect to scour (Annandale, 2006).

Schlichting and Gersten (2000) plot the energy balance in the near-bed region; this plot is shown in Figure 2.5.

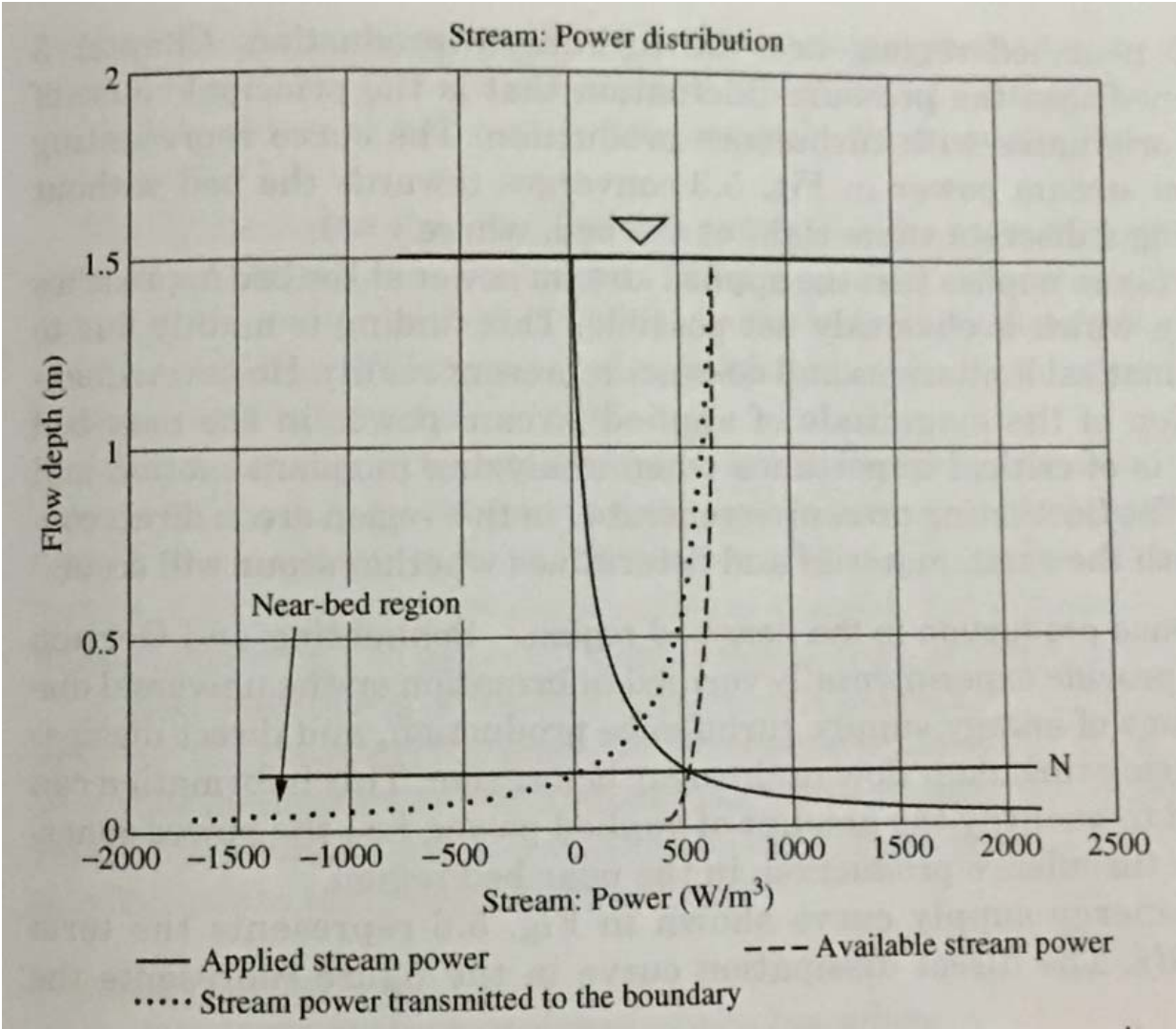


Figure 2.4: Available and applied stream power vs. depth (Annandale, 2006)

Annandale (2006) points out that the unique curve for the dimensionless turbulence production is described by the following equation:

$$\tau_t^+ \frac{du^+}{dy^+} = \frac{1}{-0.1117 \times 10^2 + 0.6254 y^+ + 0.9429 \times 10^{-3} / y^+} + 0.5976 \times 10^{-3} y^+ \quad (2.5)$$

Integration (numerical) of this function with respect to flow depth over the near bed region yields the following:

$$\tau^+ u^+ = 7.853 \quad (2.6)$$

This expression allows for the estimation of the magnitude of pressure fluctuations in the near bed region, which is the driving force behind the quarrying mode of scour (Annandale, 2006). This mechanism also contributes to grain-scale plucking.

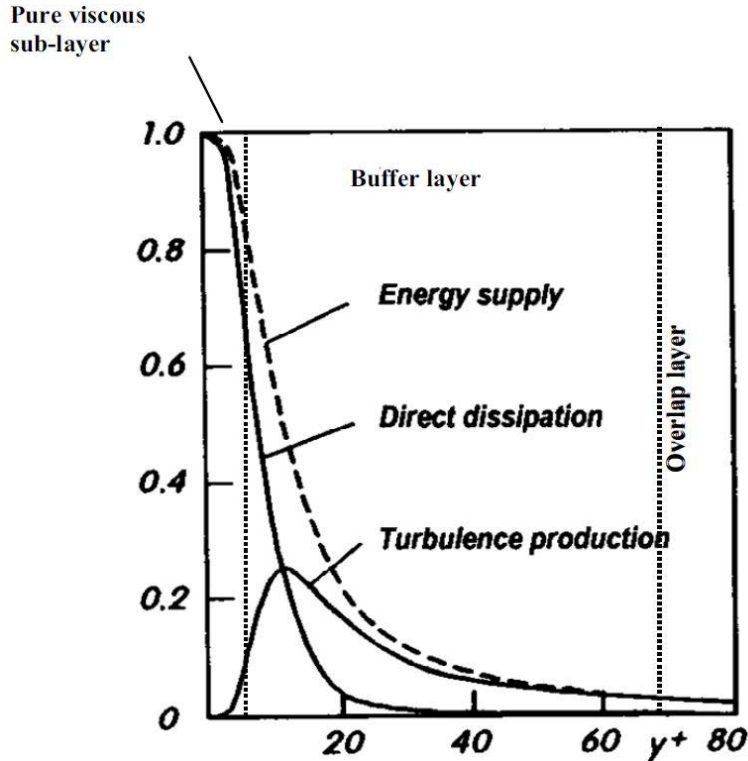


Figure 2.5: Energy balance of mean motion in near bed region (Schlichting and Gersten, 2000)

2.4 Scour on Rock

At the present, a standardized testing program for weak rock is lacking; neither rock mechanics nor soil mechanics methods can be fully applied to determine the engineering properties of weak rock (Nickmann et al., 2006). Weak rock is, of course, commonly encountered in engineering projects. For structures where underwater foundations are necessary, such as bridges, the presence of weak rock poses a particular challenge from an engineering standpoint. The geomaterials that encase and support the foundations of bridges over water are constantly subject to the erosive forces of flowing water and the sediment suspended therein at the rock-water interface. Excessive scour of foundation materials occurring within the design life of a structure places it at risk for failure, and scour is in fact the leading cause of highway bridge failure in the United States (USDA, 1998). A notable example of scour-related failure is that of the Schoharie Creek Bridge, which, in April 1987, failed during an estimated 50-year flood. Subsequent investigations revealed that the failure was due to the cumulative effects of scour, with inadequate countermeasures taken to prevent these effects. The Schoharie Creek Bridge failure prompted the FHWA to issue a mandate requiring the evaluation of all highway bridges over water for vulnerability to scour; i.e. “scour critical” bridges. While methods exist for estimating the design scour depth for alluvial channels (as outlined in Hydraulic Engineering Circular [HEC] 18), the scour depths predicted by these methods are overly conservative when applied to most rock bed channels. The rate and severity of scour in rock-lined channels is

dependent on the durability and condition of the rock material, which cannot be quantified by a single material property or index (FHWA 1991). Moreover, hydraulic conditions play an integral role in the erosion/scour process, and these conditions must be considered in a complete assessment of scour susceptibility.

HEC-18 (4th Ed., Appendix M) (Richardson and Davis, 2001) notes that additional research is needed in the area of weak rock scour durability, recommending a focus on general geological, geomorphologic, and geotechnical analyses; flume tests; further investigation of the erodibility index (Annandale, 1995) method; as well as adherence to FHWA Memo HNG-31, titled “Scourability of Rock Formations” (FHWA, 1991). This memo lists the Standard Slake Durability test as a plausible method for determining the scourability of rock, in addition to other procedures such as the sodium/magnesium sulfate soundness (ASTM C88) and LA abrasion (ASTM C131/C131M) tests. HNG-31 lists the rock quality designation (RQD) and the unconfined compressive strength (determined per ASTM D2938) as two key parameters to be used in estimating the scour durability of rock.

The existing methods for estimating rock scourability have limitations. Keaton (2013) notes that the LA abrasion test, with its relatively high power as well as steel ball bearings, would rapidly degrade soft rock samples and would therefore have little use in assessing the durability of such samples with respect to the forces of flowing water. Index-based methods for determining scour threshold (i.e. erodibility index [Annandale, 1995] and headcut erodibility index [(NRCS, 2001)]) do not consider the rate of erosion, but rather predict a threshold stream power at which erosion will occur.

Scour of rock bed channels can be attributed to five separate mechanisms (Keaton et al., 2010):

- 1) Dissolution of soluble rock
- 2) Cavitation
- 3) Physical/chemical weathering of exposed rock surfaces
- 4) Quarrying and plucking
- 5) Abrasion due to bedload and suspended particles or grain scale abrasion

The scour modes listed above are dependent on a variety of factors, such as geologic condition of the channel, channel geometry, sediment concentration, stream velocity, and so forth. These factors dictate which scour modes are active in a channel and which mode dominates for a given channel. Each of these modes is described below in greater detail:

2.4.1 Dissolution of Soluble Rock

Some minerals are soluble in water to some degree. Minerals exhibit varying rates of dissolution depending on the mineral type and the conditions of the surrounding environment

(e.g. temperature, pH, concentration of ions). Dissolution of soluble rock is not considered to be a contributor to scour for the following reasons (Keaton et al., 2012):

- Mineral types that undergo dissolution in engineering timescales (e.g. halite, sylvite, anhydrite) are usually identified in subsurface investigations in the primary stages of the construction process, and structures would not be founded on these rock types due to their general poor load bearing ability.
- Stronger soluble mineral types that are suitable for support of foundations (e.g. limestone, dolostone) dissolve in geologic timescales, on the order of centuries. As such, it can be expected that the total loss of material over the design life of a bridge is likely to be negligible. Formations of these rock types that have undergone significant dissolution will contain voids that would most likely be detected by subsurface investigation.

While rock dissolution is not, for the reasons given above, considered to be a significant source of scour in and of itself, dissolution of rock may play an indirect role in the scour phenomenon. Pre-existing dissolution features, such as voids contained within a rock mass, can contain rock rubble that acts to enhance turbulence which can promote the exceedance of threshold conditions for scour and hasten scour of susceptible materials (Keaton, 2013).

2.4.2 Cavitation

Cavitation occurs when the pressure levels present in a liquid flow field fall below that of the vapor pressure of the liquid, causing the formation of water vapor-filled cavities (i.e. bubbles). When flow pressure returns to a level above that of the partial pressure of water vapor in the surrounding atmosphere, the bubbles implode, releasing significant amounts of energy into the flow or onto adjacent surfaces. Cavitation is capable of pitting and damaging very hard materials such as steel, and is therefore undesirable behavior in most civil engineering applications. Cavitation damage has been documented along concrete lined dam spillways, where the advance of damage of this type is often quite drastic and rapid.

While cavitation effects certainly have sufficient power to be a source of bridge scour, the conditions necessary for cavitation to occur seldom exist in natural channels (Tinkler and Parrish, 1998; Hancock, 1998). Barnes (1956) expressed the Bernoulli equation in cavitation-relevant terms as:

$$\frac{p_a}{\gamma_w} + \frac{v_m^2}{2g} + z_s = \frac{p_v}{\gamma_w} + \frac{v_c^2}{2g} + z_b \quad (2.7)$$

where:

$$\begin{aligned} p_a &= \text{Atmospheric pressure } \{ML^{-1}T^{-2}\} \\ \gamma_w &= \text{Unit weight of water, equal to } \rho_w g \{ML^{-2}T^{-2}\} \\ v_m &= \text{Mean channel velocity } \{LT^{-1}\} \\ g &= \text{gravitational acceleration } \{LT^{-2}\} \end{aligned}$$

- z_s = Elevation at stream surface {L}
- p_v = Vapor pressure of water {ML⁻¹T⁻²}
- v_c = Local velocity at point of cavitation, equal to kv_m
{LT⁻¹}
- z_b = Elevation at bottom of channel {L}

Solving Equation 2.7 for v_m (the mean channel velocity necessary for cavitation to occur) with $z_b = 0$ (datum) and $z_s = H$ (the depth of flow) and including the parameter k , yields:

$$v_m = \left[\frac{2(p_a - p_v)}{(k - 1)\rho_w} + \frac{2gH}{(k - 1)} \right]^{1/2} \quad (2.8)$$

As Equation 2.8 demonstrates, the mean flow velocity required for cavitation decreases with increasing vapor pressure and flow depth, and increases with decreasing atmospheric pressure. Figure 2.6 shows a plot of mean flow velocity versus flow depth, showing combinations of depths and velocities where cavitation is likely to occur, unlikely to occur or impossible.

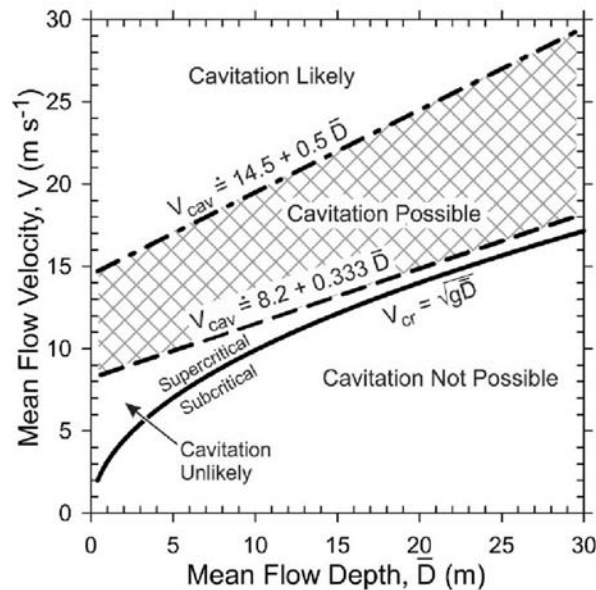


Figure 2.6: Flow velocity vs. flow depth, showing cavitation regions, taken from Keaton (2013)

Velocities of the required magnitude can be caused by a drastic change in slope or a sharp contraction of the flow area, or at an abrupt change in elevation such as a knickpoint. Thus, cavitation in natural channels is likely to occur at very steep or narrow portions of a channel. However, even at such channel sections, vigorous flow patterns serve to entrain air into the

water, which can inhibit cavitation by increasing the compressibility of the water (Hancock et al., 1998). This provides “cushioning” against implosion, thereby reducing the impact of the collapsing bubble. Moreover, the narrowness of such channels would likely obviate the need for placement of submerged foundations in the channel bed as the bridge would likely span the entire channel width in such cases (Keaton et al., 2012).

Research into cavitation by Arndt (1981) establishes the cavitation index, σ , as the fundamental parameter in the description of the phenomenon. The cavitation index is given by:

$$\sigma = \frac{p_0 - p_v}{\frac{1}{2} \rho U_0^2} \quad (2.9)$$

where:

$$\begin{aligned} \sigma &= \text{Cavitation index } \{1\} \\ p_0 &= \text{Hydrostatic pressure } \{\text{ML}^{-1}\text{T}^{-2}\} \\ p_v &= \text{Vapor pressure of liquid } \{\text{ML}^{-1}\text{T}^{-2}\} \\ \rho &= \text{Density of liquid } \{\text{ML}^{-3}\} \\ U_0 &= \text{Freestream velocity } \{\text{LT}^{-1}\} \end{aligned}$$

The cavitation index is then the ratio of the difference between the hydrostatic and vapor pressures to the freestream dynamic pressure (the velocity head from the Bernoulli equation multiplied by the density of the fluid). Theoretically, cavitation will occur when the cavitation index takes a value below unity (Whipple et al., 1999). However, the cavitation index was found to be dependent on fine sediment concentration, the degree of aeration, and the Reynolds number of the flow. Cavitation requires nucleation sites to occur, which could be an existing small air bubble or a grain of fine sediment suspended in the flow. Turbulent flows (i.e. flows with high Reynolds numbers) generate vortices whose cores are likely to be at pressures below that of the mean freestream dynamic pressure, facilitating the formation of cavitation bubbles.

2.4.3 *Physical/Chemical Weathering*

Physical and chemical weathering processes are not erosive processes per se, as they occur in-situ without motion of fluid or particles. However, these processes can reduce the durability of rock formations, “conditioning” the rock surfaces for other modes of scour. Mechanical weathering processes include wetting and drying cycles, freezing and thawing cycles, and growth of vegetation into joints, while chemical weathering involves the disintegration of a rock’s mineral structure by means of chemical reactions.

2.4.4 Quarrying/Plucking

Quarrying and plucking describe a mode of scour where intact blocks of varying size are lifted from a rock mass by hydraulic forces. Quarrying/plucking can occur in rock when exposed rock masses are jointed at a sufficiently small scale (Keaton et al. 2012). Pressure fluctuations induce uplift forces that lift rock pieces out of the rock mass and into the flow field, allowing them to be carried downstream as bedload. These pressure fluctuations are induced by turbulent flow.

Hancock et al. (1998) hypothesize that quarrying and plucking are the most rapid form of streambed degradation when rock mass jointing conditions permit. The researchers developed two simplified physical quarrying models to identify the flow conditions necessary for quarrying and plucking to occur. The first model considered the uplift force generated by pressure differences in the flow, while the second model was based on the block sliding and rotation due to shear stress acting on the exposed surfaces of the block. The uplift model is based on the Bernoulli equation, and it establishes the minimum velocity necessary to induce pressure differences that result in an uplift force. Figure 2.7 shows the forces acting on a jointed block of intact rock.

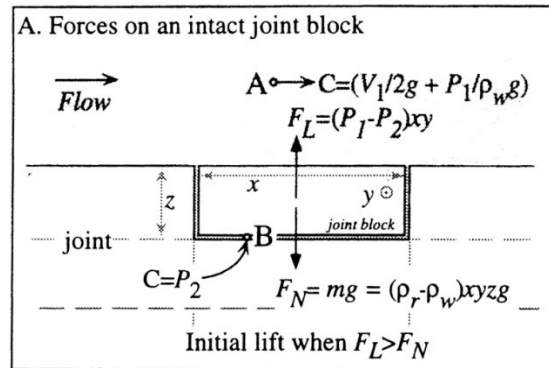


Figure 2.7: Forces acting on an intact jointed rock block (after Hancock et al.1998)

Equating forces from Figure 2.7 with the assumption that $P_1 = P_2 - v_1^2/2g$, it can be shown that the minimum flow velocity necessary to initiate upward motion of the block is:

$$v_t = \left[\frac{2gz}{\rho_w} (\rho_r - \rho_w) \right]^{1/2} \quad (2.10)$$

The authors note that this simple analysis neglects the frictional resistance force from the neighboring blocks. It should be noted, also, that the analysis neglects the increase in hydrostatic pressure corresponding to the height of the block with respect to the water level. Bollaert (2002) provides a similar, but much more detailed analysis, taking into account the resistive force due to

friction between the block and the surrounding rock mass. The model of this is shown in Figure 2.7.

Annandale (2007) divides the quarrying and plucking mode of scour into three classifications, based on the mode of failure:

- Block removal: Completely jointed rock is lifted out of the rock mass which is accomplished by transient pressure fluctuations. This occurs when the uplift force overcomes the submerged weight of the block and the frictional forces occurring between jointed rock blocks, and results in immediate scour and block entrainment
- Brittle fracture: This occurs when the stress intensity at a pre-existing fissure exceeds the fracture toughness of the rock. This will result in abrupt, explosive failure and scour.
- Sub-critical failure: This occurs as pressure fluctuations act in a cyclic manner which causes the eventual fatigue failure of the rock. Eventually, material that is subject to this type of failure will be vulnerable to block removal, as the blocks are reduced to a size that allows block removal.

Annandale (2007) notes that the comprehensive scour model developed by Bollaert (2002) has little practical use for bridge scour at the present time, as there is a lack of pragmatic procedures for calculating pressure fluctuation characteristics around bridge piers and abutments. With such methods, scour can be treated analytically, and the time rate of scour due to fatigue and other time-dependent modes can be determined based on a physical basis.

The second quarrying model from the Hancock et al. (1998) study, based on a sliding mechanism of failure, assumes the rock block slides due to shear stress. Figure 2.8 shows the forces acting on a block under such conditions:

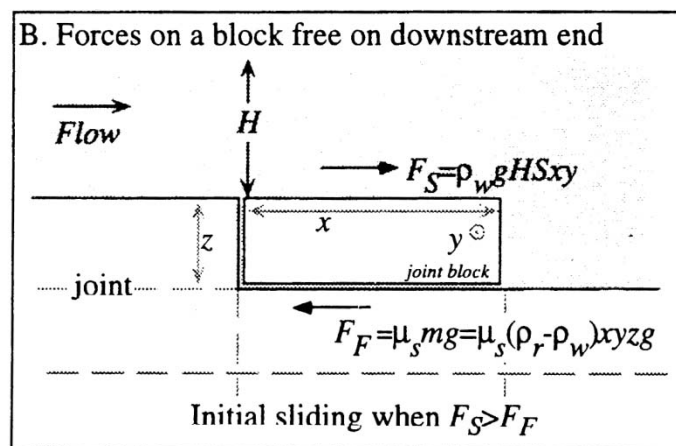


Figure 2.8: Forces acting on an intact jointed rock block (after Hancock et al.1998)

In a similar manner to the previous analysis, summing forces acting on the block yields an expression for the depth-slope product (shear stress divided by unit weight of fluid) necessary to initiate translational motion of the block, given by:

$$HS_f = \frac{z\mu_s}{\rho_w}(\rho_r - \rho_w) \quad (2.11)$$

where:

H	=	Depth of flow {L}
S_f	=	Energy grade line slope {1}
z	=	Height of block {L}
ρ_r	=	Density of rock block {ML ⁻³ }
ρ_w	=	Density of water {ML ⁻³ }
μ_s	=	Coefficient of static friction for rock-rock interface {1}

Hancock et al. (1998) noted the previously undocumented phenomenon of hydraulic wedging, where clasts become lodged in rock joints and fractures after they are temporarily widened by pressure fluctuations in the flow. This effect is theorized to accelerate the weathering process, and is also suspected to play a role in the preparation of rock masses for quarrying/plucking mode scour.

Annandale (1995) developed an index-based model to describe the plucking mode of scour, the erodibility index method, which is identical to Kirsten's (1982) excavatability index method; this is in turn based on the Barton et al. (1974) Q-system method for rock classification. The erodibility index method is suited for both granular soil types as well as rock. The erodibility index parameter quantifies a material's resistance to erosion, and establishes a threshold relation to the rate of energy dissipation (i.e. stream power) necessary to induce erosion in a given material. This threshold stream power is expressed as a function of the erodibility index (Annandale, 1995), that is:

$$P = f(K_h) \quad (2.12)$$

The erodibility index, K_h , is the product of four sub-indices, each of which can be estimated using standard field or laboratory tests. These are listed and explained below:

- Mass strength number, M_s : The mass strength number represents the strength of the material without respect to the geologic heterogeneity of the mass (Annandale, 1995). This parameter is defined as the product of a material's uniaxial unconfined compressive strength (UCS) and its coefficient of relative density (the bulk density normalized to 27.0 kN/m³). An alternative definition of the parameter, for rock, is given by the unconfined

compressive strength of the sample, in megapascals (MPa), if over 10 MPa. If under 10 MPa, M_s is given by $0.78 \times UCS^{1.05}$. The degree of weathering of exposed rock will result in a decrease in the value of M_s , as the rock's strength diminishes with the degree of weathering. Assigning a proper value of M_s to exposed, weathered rock formations is left to engineering judgment and experience. Alternate procedures are used to determine M_s for cohesive and non-cohesive soils; results from the shear vane test are used for cohesive soils and results from the standard penetration test (ASTM D1586) are used for non-cohesive soils to determine M_s .

- Particle/block size number, K_b : For rock materials, the primary means of calculating K_b is given by the formula:

$$K_b = \frac{RQD}{J_n} \quad (2.13)$$

where:

$$\begin{aligned} K_b &= \text{Block size number} \\ RQD &= \text{Rock Quality Designation} \\ J_n &= \text{Joint set number} \end{aligned}$$

The rock quality designation is a standard core recovery parameter, defined by Deere (1963) as the percentage of the sum of lengths of core pieces greater than 100 mm to the total length of the core run (normally 1.5 m). The joint set number is related to the number of joints present in the rock mass as well as the spacing of the joints. J_n takes a value of unity for an intact rock with few or no joints, while the upper limit of J_n is 5.00, specified for rock masses with more than four joint sets.

- Discontinuity/inter-particle shear strength number, K_d : For rock, this value represents the relative strength of discontinuities, and is defined by:

$$K_d = \frac{J_r}{J_a} \quad (2.14)$$

where:

$$\begin{aligned} K_d &= \text{Discontinuity/inter-particle shear strength} \\ &\quad \text{number} \\ J_r &= \text{Joint roughness number} \\ J_a &= \text{Joint wall alteration number} \end{aligned}$$

The joint roughness number and joint alteration number represent the degree of roughness of opposing faces of a rock discontinuity and the degree of alteration of the materials that form the face of the discontinuity, respectively (Annandale, 2001).

- Relative ground structure number, J_s : This parameter represents the relative resistance to erosion with respect to the structure of the ground. It takes into account the least favorable dip angle of the rock discontinuity with respect to the direction of flow, as well as the shape of the rock blocks. The dip of the least favorable discontinuity, known as the effective dip, is determined by the orientation of the block with respect to the flow, and is corrected for bed slope. The shape of the rock blocks is determined by the joint spacing ratio, defined as the average spacing of the joint sets in the vertical plane.

Annandale (1995) plotted results from this analysis on a log-log scale, shown in Figure 2.9.

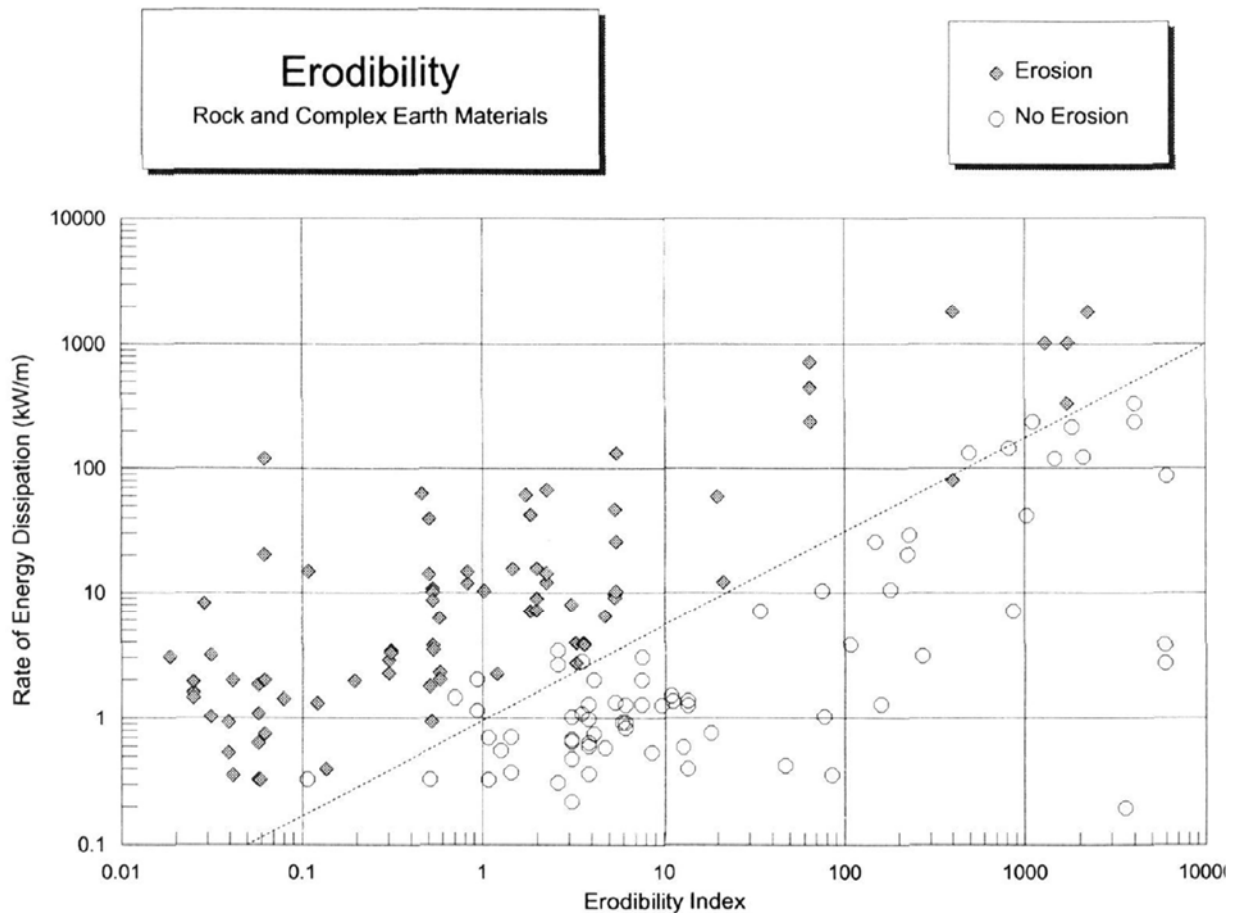


Figure 2.9: Threshold power necessary for erosion (after Annandale, 1995; Note that the units of stream power should be expressed as kW/m^2)

The above plot demonstrates that the threshold power required to initiate erosion is a power function of the erodibility index, with the exponent given by the slope of the line of the log-log plot, which is seen to be approximately $3/4$. Thus, by inspection of the regression line, it can be seen that the approximate relationship between the threshold rate of energy dissipation

(stream power in kW/m²) necessary for erosion and the erodibility index can be written explicitly as:

$$P \approx K_h^{3/4} = (M_s K_b K_d J_s)^{3/4} \quad (2.15)$$

The erodibility index method only addresses the quarrying/plucking mode of scour; neither the time rate nor the severity of scour is considered. This method simply assigns a threshold stream power to a rock mass; predicting scour to occur when this threshold is exceeded.

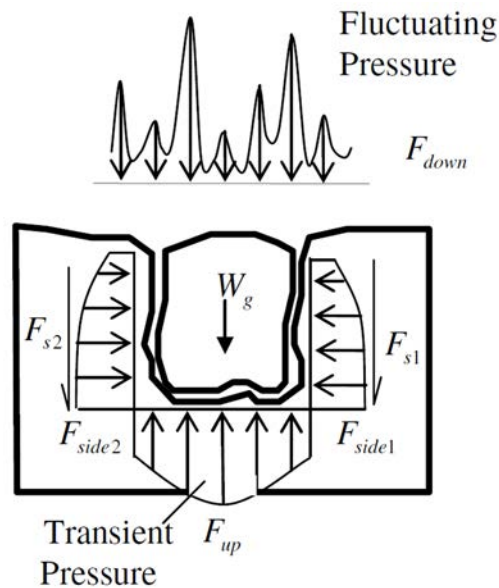


Figure 2.10: Forces acting on an intact jointed rock block, after Annandale (1998)

Bollaert (2002) provides a detailed physical analysis of the plucking mode of rock scour as it pertains to the spillways of dams, termed the comprehensive scour model.

Bollaert (2010) modeled quarrying/plucking scour in a bridge pier setting (i.e. local scour) using a two-phase numerical simulation. The model considered three components of the total uplift force acting on a block:

- 1) Static uplift: The buoyant force equal to the weight of the displaced volume of water. This is a function of the block density (as well as fluid density).
- 2) Quasi-steady uplift: Depends on local flow velocity over scour hole, as well as the protrusion of the block. This is a function of the approach velocity of the flow.
- 3) Turbulent uplift: Caused by pressure fluctuations present in turbulent flow. This is a function of time, approach velocity, pressure fluctuations, and shear stresses.

Stated symbolically:

$$F_{tot} = F_{static} + F_{LS} + F_{LT} = f(\rho_w) + f(V_a) + f(t, V_a, P_a, \tau_a) \quad (2.16)$$

The main hydraulic parameter in Bollaert's (2010) model is stream power, which, for a channel bed, can be expressed as the product of average flow velocity and average bed shear stress. Bollaert (2010) used an adjusted stream power was calculated, per HEC-18 (Richardson and Davis, 1993), which accounts for both pier shape and angle of attack of the flow with the inclusion of two factors. In the model, a sinusoidal boundary pressure signal was applied in order to represent the pressure fluctuations present in a turbulent flow pattern; this was modeled to act simultaneously at the joints of both sides of the block. A net uplift impulsion, produced when the resultant uplift force acting on the block is positive, was converted to a net uplift velocity, which was in turn converted to a net uplift height. Block removal was considered to be achieved when the net uplift height was greater than or equal to 20% of the block height. Scour was considered to occur on a layer-by layer basis, where the removal of a single block constituted the scour of an entire layer.

Keaton et al. (2012) note that the headcut erodibility index (Kirsten, 1988) and erodibility index (Annandale, 1995) methods are not directly applicable for scour analysis at bridges. These methods were developed for dam spillway channels which experience much higher rates of hydraulic energy dissipation (i.e. stream power) than those present at a typical bridge site. Moreover, these methods only address the quarrying/plucking mode of scour, which may or may not be the dominant form of scour depending on the conditions of the waterway.

2.4.5 Abrasion

The abrasion mode of rock occurs both due to bedload motion (translation and saltation), as well as by suspended particles. Sediment flow decoupling after expansion, recirculation. Bedrock channels carry more sediment than alluvial channels (Howard and Kerby, 1982).

Bedload, present in many rivers, contributes to scour of riverbeds in some capacity through its motion depending on the flow conditions. Dickenson and Baillie (1999) documented scour in channels of the Oregon Coast Range, and conducted laboratory tests to attempt to correlate observed scour depths with a model that employs both geotechnical and hydraulic parameters. The researchers modified the standard test method for slake durability of shales and similar weak rocks (ASTM D4644), a procedure to determine the vulnerability of weak rock types to slaking, developed by Franklin and Chandra (1972). This procedure was developed for assessing the durability of rock materials being considered for use as riprap for erosion protection.

Abrasion scour caused by suspended sediment is a complex topic, and the understanding of the physical process is still in its formative stages (Annandale, 2006). Hancock et al. (1998) posit that abrasion by entrained sediment, along with quarrying and plucking, are the dominant forms of erosion for most channel beds. Where rock masses are not jointed at a sufficiently small

scale as necessary for quarrying, rock erosion must be carried out by abrasion. Hancock et al (1998) give a treatment of bedrock channel erosion that is analogous to aeolian abrasion, and developed an expression for the time rate of erosion based on the work of Anderson (1986). The abrasion erosion rate is expressed as:

$$\frac{dz}{dt} = \frac{S_a C_{sed} v_g^2 v_w}{2\rho_r} \quad (2.17)$$

where:

$$\begin{aligned} \frac{dz}{dt} &= \text{Time rate of erosion by abrasion } \{LT^{-1}\} \\ S_a &= \text{The “susceptibility” of a material to erosion} \\ &\quad \{1\} \\ C_{sed} &= \text{Mass concentration of a particular grain size} \\ &\quad \{1\} \\ v_g &= \text{Grain velocity relative to channel bed } \{LT^{-1}\} \\ v_w &= \text{Water flow velocity } \{LT^{-1}\} \\ \rho_r &= \text{Density of target rock } \{ML^{-3}\} \end{aligned}$$

The susceptibility parameter, S_a , depends primarily on material properties such as density, hardness, and fracture mechanical properties, and relates kinetic energy flux to mass of target material removed (Anderson, 1986). With the assumptions that the sediment concentration, C_{sed} , is proportional to the bed shear stress and that the particle velocity is equal to the flow velocity, the researchers make the observation that the time rate of abrasion appears to be proportional to the fifth power of velocity. However, they also note that particle concentration is not sufficient to indicate the rate of erosion. They note that the particles must separate from the flow, as the flow velocity goes to zero at the surface of the channel bed. The rate of erosion is also highly dependent on the concentration of sediment in the flow; a lack of entrained particles precludes erosion by suspended sediment abrasion, while too much sediment acts to shield the riverbed from abrasion (Sklar and Dietrich, 1997). Erosion by suspended particles takes the form of sculpted erosional forms (e.g. flutes and potholes); the presence of these forms in the bedrock of a channel bed indicates that erosion of this type is taking place. These forms were noted to appear on the downstream side of bedrock crest features, where flow separation causes decoupling of particles from the flow field.

2.5 Modified Slake Durability Test

The Standard Test Method for Slake Durability of Shales and Similar Weak Rocks (ASTM D4644), after the work of Franklin and Chandra (1972), is a standard test procedure used to provide qualitative estimates of weak rock durability, as well as to provide a means to assign index-type durability values to weak rocks (e.g., Franklin shale rating system). In the test

procedure, a sample of weak rock is subject to tumbling and soaking action over a 10-minute test period in a standard drum (see Figure 2.11) which is partially immersed (with the rock sample fully immersed) in slaking fluid (distilled water) and rotated at $20 \pm 5\%$ revolutions per minute. The standard calls for a total sample mass of 450-550 grams, with the sample comprised of 10 roughly equidimensional pieces with a mass of 40-60 grams each. Each test run is followed by drying of the sample in a thermostatically controlled oven capable of maintaining a temperature of $110 \pm 5^\circ\text{C}$ ($230 \pm 9^\circ\text{F}$). The natural water content of the rock is measured per ASTM D2216, and the temperature of the slaking fluid is measured before and after each test run.

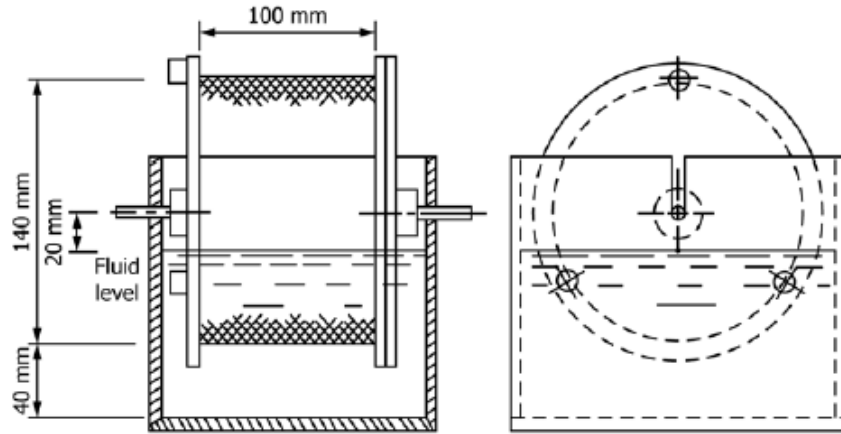


Figure 2.11: Standard drum showing critical dimensions (ASTM)

A total of two test runs are conducted in the ASTM D4644 method; however, the results (mass losses accrued over 10 minutes of tumbling and abrasion) of the first test run are not used in the final calculations. From the results of the second run, the slake durability index is calculated as follows:

$$I_d(2) = \left[\frac{(W_F - C)}{(B - C)} \right] \times 100\% \quad (2.18)$$

where:

- $I_d(2)$ = Slake durability index (second cycle)
- B = Mass of drum plus oven-dried specimen before first cycle
- W_F = Mass of drum plus oven-dried specimen after second cycle
- C = Mass of empty drum

The slake durability index is then simply the percent of mass lost from the sample during the two 10-minute test runs and subsequent oven-dryings.

As the name of the standard suggests, a primary objective of the standard slake durability test is to determine the susceptibility of rock specimens to slaking; that is repeated cycles of wetting and drying. Other tests exist which classify weak rock based on its slaking behavior, such as the jar slake test (Wood and Deo, 1975) and the slake index test (Wood, 1972). The factor that differentiates the slake durability test from the above listed procedures is the inclusion of a mechanical abrasion action, i.e. the tumbling of the drum. Abrasion of the specimen is caused both by the impact of other specimen pieces and the mesh cage; this abrasion action is somewhat analogous to that experienced by bedload motion across a riverbed (Dickenson and Baillie, 1999; Keaton et al., 2012). The standard slake durability test then appears to be a sort of composite test, where sample degradation occurs due to the slaking effect as well as abrasion.

The oven-drying after each test run is likely to cause additional mass losses in rock specimens, especially weak sedimentary rock. Slaking is a common behavior of weak rocks; however, some rock types that slake heavily with wetting and drying cycles will tend to remain intact if their moisture content is not subject to fluctuation (Morgenstern and Eigenbrod, 1974). Dickenson and Baillie (1999) noted the accelerated degradation of sedimentary rock specimens induced by the oven drying portion of the slake durability test. The streambeds in Dickenson and Baillie's region of study, the Oregon coastal range, are likely to be submerged year-round or dried to the point of partial saturation as a worst case scenario. Complete desiccation such as that imparted by oven drying is very unlikely to occur in natural conditions (Dickenson and Baillie, 1999). This being the case, the researchers assert that the standard slake durability test, with the oven drying component, is not well suited for determining the susceptibility of continuously submerged streambed rock to abrasion-mode scour.

Dickenson and Baillie (1999) modified the standard slake durability test by eliminating the oven drying portion of the procedure to eliminate the mass losses solely due to slaking. In addition to the omission of the oven drying process, test segment time intervals were lengthened to 30 minutes for the first two hours of the test and to 1 hour segments thereafter. As the sample is continuously immersed in water without drying, the masses/weights of the specimens are measured in a saturated surface dry (SSD) state. As the slaking portion was effectively removed from the procedure, the researchers used the term "Continuous Abrasion Test" in place of "Standard Slake Durability Test" to better reflect the nature of their modified procedure. Mass losses were calculated repeatedly (after each test run) rather than calculating a single mass loss after the second test run as prescribed by the standard slake durability test (ASTM D4644). The mass losses from each test run were plotted against the natural logarithm of the elapsed test time to calculate an *abrasion number* (β), defined as the slope of the regression line of the cumulative loss vs. natural logarithm of time plot. Dickenson and Baillie (1999) assert that the abrasion number is a better diagnostic measure for evaluating the degradation behavior of weak rock specimens than the slake durability index as calculated from the results of the standard slake durability test. A comparison plot showing the percent weight loss vs. time for both methods (with matching sample type) is shown in Figure 2.12:

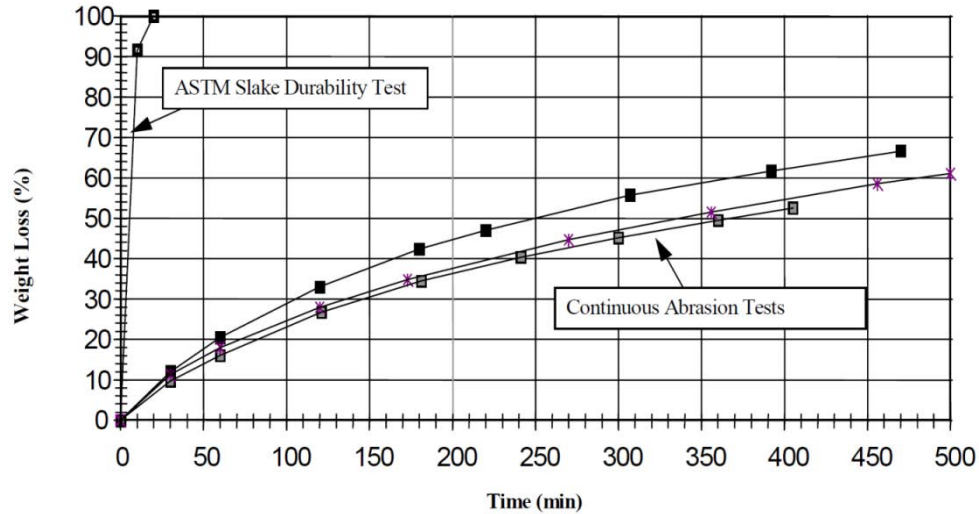


Figure 2.12: Comparison of Standard Slake Durability test and continuous abrasion test (Dickenson and Baillie, 1999)

Figure 2.12 shows that the sample degraded completely by the second run of the standard slake durability test, whereas the sample exhibited a much more gradual rate of weight loss when subjected to the continuous abrasion test. This disparity in the rate of weight loss is due to the degradation caused by the wetting/drying cycles of the standard test; this process is absent from the continuous abrasion test. This clearly demonstrates the deleterious effect of wetting and drying cycles on the engineering properties of sedimentary rock.

As scour is a soil-water interaction phenomenon, a hydraulic parameter is needed in addition to a geotechnical parameter to assess the vulnerability of material to scour (Keaton et al., 2012). Some of the existing research into scour has made use of stream power, which is a measure of the time rate of energy dissipation of a flow. Stream power is a useful parameter for scour analysis, as it encompasses several other parameters pertinent to streambed scour such as velocity and shear stress (Keaton, 2013). For appreciable erosion to occur in a geomaterial, a certain threshold level of stream power must be exceeded (Annandale, 1995); this threshold level relates to the durability and condition of the material itself. Figure 2.13, taken from Costa and O’Conner (1995), demonstrates that a flood event must have both sufficient stream power and occur over a sufficient duration to cause significant erosion, according to the threshold concept of erosion. The energy available to erode bedrock is the area under the stream power-time curve (i.e. the time integral of stream power as a function of time), with the threshold stream power for a given material as a lower bound.

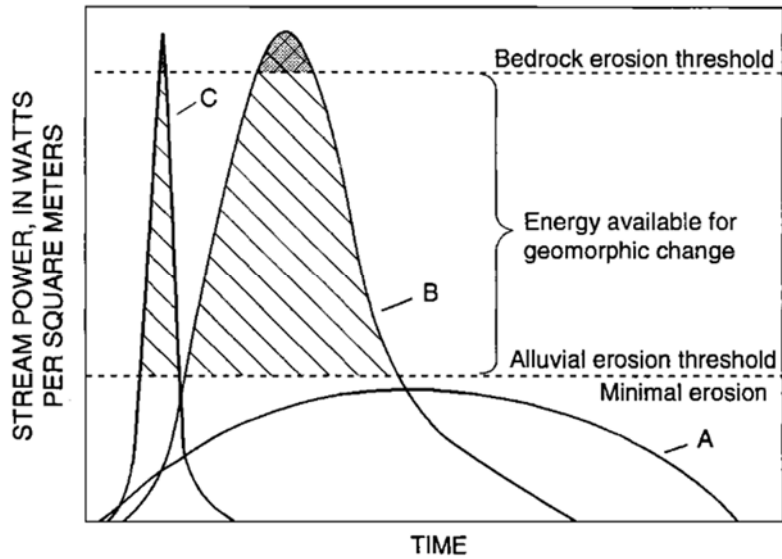


Figure 2.13: Stream power as a function of time (taken from Costa and O’Conner, 1995)

Figure 2.14, taken from Annandale (2000), shows the available stream power at the Schoharie Creek Bridge during the peak of the April 5, 1987 flood, along with the threshold levels of stream power required to initiate scour in the streambed material (riprap and glacial till):

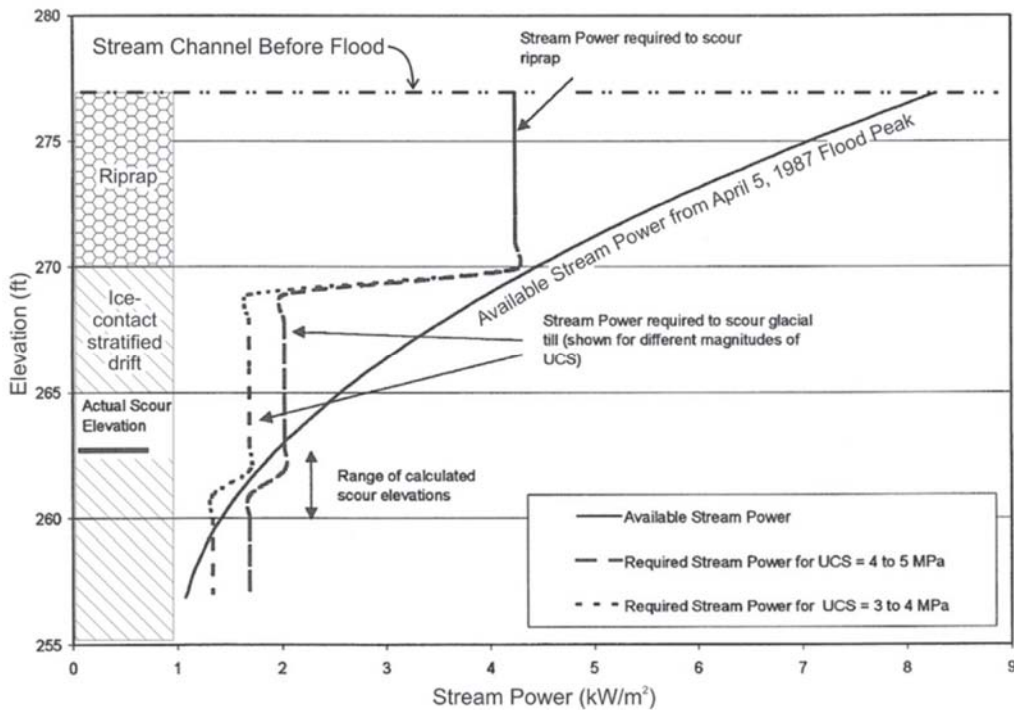


Figure 2.14: Available stream power at peak of date of Schoharie Creek bridge failure, with scour resistance (based on UCS) of bed material (taken from Annandale, 2000)

Figure 2.14 shows that the available stream power of the 1987 flood exceeded the threshold stream power necessary to induce erosion in both the riprap and the glacial till, which led to scour of the erodible bed material and subsequent failure of the structure.

Annandale (2006) explains that stream power is a suitable surrogate variable, unlike bed shear stress or average flow velocity, for describing the erosive capacity of water. Use of this parameter yields results that are internally consistent, that is it produces results that are consistent with the laws of physics.

The main hydraulic parameter in Dickenson and Baillie's (1999) scour model is integrated stream power, i.e. the total energy expended during a period of flow (e.g., a flood event) as shown above in Figure 2.14. This parameter, denoted Ω by the researchers, is defined mathematically (Costa and O'Conner, 1995) as:

$$\Omega = \int_{t_0}^{t_f} \omega(t) dt \quad (2.19)$$

with $\omega(t)$ being instantaneous stream power per unit area of the channel as a function of time. For a particular instant, the stream power is given by:

$$\omega = \gamma_w q \Delta E = \frac{\rho_w g Q S_f L}{wL} = \frac{\rho_w g Q S_f}{w} = \gamma_w q S_f \quad (2.20)$$

where:

- ω = Stream power per unit area of channel
- γ_w = Unit weight of water (~ 9.81 kN/m³)
- q = Flow rate per unit width of channel (unit discharge)
- ΔE = Energy head losses over length of flow
- ρ_w = Density of water (~ 1000 kg/m³)
- g = Gravitational acceleration
- Q = Volumetric flow rate
- S_f = Energy grade line slope (head loss per unit length)
- L = Length of flow
- w = Width of channel

Dickenson and Baillie (1999) assumed that flow was uniform in their studied channels, i.e. S_f is equal to the slope of the channel bed, S_0 . The SI units of stream power per unit area are watts per square meter (W/m²); integrating this quantity over the area of the channel bed would yield the total rate of energy dissipation for a given channel cross-section. Thus, the total energy

expended by water during a flow event at a given channel cross-section is the area under the stream power vs. time curve (see Figure 2.13), bounded by the points t_0 (the beginning of the flow event) and t_f (the conclusion of the flow event).

An alternative formulation of stream power is given by the product of bed shear stress and flow velocity. The mean shear stress acting on a section of the channel bed can be written as a generalized form of the depth-slope product (that is the “hydraulic radius-slope product”), which can be derived by summing the forces acting on a control volume of flow (with some simplifying assumptions; namely the validity of the small angle approximation and a uniform flow condition). As shear stress is defined as the stress component acting parallel to a surface or cross-section (from which a resultant force can be resolved), and power can be defined as the dot product of force and velocity (which are coincident vectors in this case), the power expended per unit area of the channel bed can be written as:

$$\omega = \tau \bar{V} = \gamma_w S_f R_h \cdot \frac{Q}{A} = \gamma_w S_f \frac{A}{P} \cdot \frac{Q}{A} = \frac{\gamma_w S_f Q}{P} \quad (2.21)$$

where:

- ω = Stream power per unit area of channel bed
- τ = Mean shear stress at bed-water interface
- \bar{V} = Mean velocity of flow
- γ_w = Unit weight of water ($\sim 9.81 \text{ kN/m}^3$)
- Q = Volumetric flow rate
- A = Cross-sectional area of channel
- S_f = Energy grade line slope (head loss per unit length)
- P = Wetted perimeter of channel section
- R_h = Hydraulic radius of channel section; defined as A/P

This quantity is in fact equal to the previous formulation of shear stress (Equation 2.21) divided by the area of the channel bed under consideration; i.e. the total area under consideration is the length of the channel multiplied by its wetted perimeter, or:

$$\frac{\gamma_w Q S_f L}{A_{bed}} = \frac{\gamma_w Q S_f L}{PL} = \frac{\gamma_w Q S_f}{P} \quad (2.22)$$

With the assumption that stream power is constant over the cross-section of the channel as well as the length of flow, this quantity can simply be taken as the stream power for the entire given stream cross-section divided by the area of the channel bed, i.e. the wetted perimeter multiplied by a unit length. Furthermore, the wetted perimeter of many natural (wide) channels can simply be approximated as the width of the channel. Following from this assumption,

Substitution of w in place of P in Equation 2.21 yields Equation 2.22 exactly. This quantity, as described above, indicates the average rate of energy dissipation per unit area of channel bed.

Keaton et al. (2012) note that the average bed shear stress, as given by the depth-slope product, is valid only when analyzing global scour of an entire channel cross section; its assumptions are invalid when considering local scour around bridge piers or contraction scour. Following from the continuity equation, turbulent flow induced by the presence of the bridge piers acts to increase flow velocity and, in turn, the shear stress acting on surfaces adjacent to the pier. This effect becomes evident upon inspection of the boundary shear stress expression as derived from Manning's equation, via solving for the energy gradient and substituting the result into the depth-slope product. An addition of a velocity enhancement factor K_p is made to account for pier shape. Shear stress can then be given by:

$$\tau = \left(\frac{nK_p V}{c} \right)^2 \left(\frac{\gamma_w}{y_0^{1/3}} \right) \quad (2.23)$$

where:

- τ = Shear stress at boundary layer
- V = Velocity of flow
- K_p = Velocity enhancement factor
- γ_w = Unit weight of water (~ 9.81 kN/m³)
- n = Manning's roughness coefficient
- c = Unit conversion factor; 1.0 for SI and 1.486 for U.S. customary
- y_0 = Depth of approach flow

Thus the stream power at the pier boundary varies proportionally with the cube of velocity when the shear stress-velocity product is computed with the above expression. Scour in the direct proximity of a bridge pier (local scour) will thus be more drastic than that of the surrounding bed, assuming uniform scour resistance over the entire channel bed.

Dickenson and Baillie (1999) monitored the depth of erosion in their channels of interest by surveying stream cross sections over a period of several years. More recent cross sections were compared with the initial cross-sections, and the change in cross-sectional area was divided by the channel width to yield an average scour depth. A second method to determine scour depth was employed in which average change in depth was measured, over the width of the channel, in 30-60 cm increments.

Dickenson and Baillie (1999) measured or calculated several hydraulic variables for the stream sections under study, including stream power. Stream power was calculated per Equation

2.21, with the channel discharge readily available from daily flow series. Channel slope was found to vary over a wide range depending in the source of the data and the method employed. This presented a problem from an analysis standpoint, as stream power depends heavily on the bed slope. The researchers ultimately chose the channel slopes as given by the USGS 7.5-minute quadrangle topographic maps, which tended to give to give the most highest estimate for bed slope. Channel cross-sections, bed slope, and an estimated Manning's roughness coefficient were used as inputs to the USACE HEC-RAS program, which provides stream power as an output.

Dickenson and Baillie (1999) examined the trends between erosion depth and abrasion number, and between erosion depth and stream power; a weak trend was noted between these single parameters and erosion depth. The researchers also plotted the observed average scour depth against both integrated stream power and abrasion number, forming a surface plot. A contour map of the surface plot is shown in Figure 2.15, with the abrasion numbers as contours.

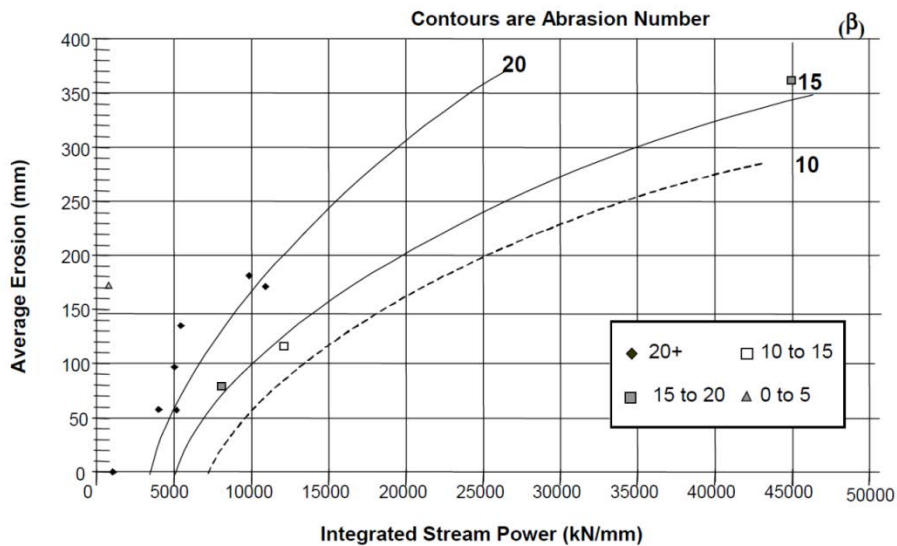


Figure 2.15: Contour map of P - β - A_v .erosion surface, taken from Dickenson and Baillie (1999)

Dickenson and Baillie (1999) note that abrasion numbers (β) for the tested samples took values between 3 and 30: abrasion numbers for very hard rock and basalt were determined to lie in the $1 \leq \beta \leq 10$ range, in the $10 \leq \beta \leq 20$ range for hard to weak sandstones, and in the $20 \leq \beta \leq 30$ range for soft siltstones and shales. The sparse data used in the study (11 samples) as well as a large gap in the 15,000-45,000 kN/mm range precluded a rigorous statistical analysis of the data (Dickenson and Baillie, 1999). Moreover, the analysis considered only scour by bedload abrasion; the researchers acknowledge that other modes of scour were evident at their chosen sites (e.g., hydraulic jacking and quarrying, abrasion by suspended sediment). Nonetheless, the researchers recommend that the continuous abrasion test be used as a preliminary screening tool

for determining the scour durability of rock, as well as a point of departure for future studies of rock scour.

Keaton (2010) proposed further modifications to the modified slake durability (continuous abrasion) test. The sample mass is normalized to 500 grams, and mass losses used in the calculations of equivalent scour depth are taken to be proportional to the normalized sample. Normalization of the sample mass allows for direct comparison of all rock types (Keaton, 2013). The normalized sample mass is defined as follows:

$$m_{i,N} = m_{0,N} \left[\frac{m_i}{m_0} \right] \quad (2.24)$$

with the normalized incremental losses given by:

$$\Delta m_{i,N} = m_{i-1,N} - m_{i,N} \quad (2.25)$$

where:

- $m_{0,N}$ = Initial normalized mass of specimen (500 g)
- m_0 = Initial mass of specimen
- m_i = Mass of specimen after i^{th} run
- $m_{i,N}$ = Normalized mass after i^{th} run
- $\Delta m_{i,N}$ = Normalized incremental losses

A notable addition to the modified slake durability (continuous abrasion) procedure by Keaton et al. (2012) is the calculation of the stream power parameter directly from the test data. Keaton (2013) notes the change in mass of the specimen is due to the dissipation of mechanical energy into the samples. Though the slake durability test is not meant to model the movement of water over a rock bed channel per se, the sample losses can nonetheless be expressed in units of power (Keaton, 2013). Equivalent stream power, as described by Keaton (2010), can be expressed in the following way:

$$\text{Equivalent stream power} = \frac{\text{distance traveled} * \text{average normalized weight}}{\text{time interval} * \text{normalizing area}} \quad (2.26)$$

This equation expresses a force multiplied by distance, divided by a time interval yielding units of power. This quantity is normalized by a unit area (1 m²) to yield units of power per unit area (W·m⁻²), which are the SI units of the shear stress-velocity product for stream power.

The distance “traveled” by the sample can be expressed by the following equation:

$$\text{distance traveled} = \Delta x_{eq} = \dot{\theta} C_{dr} \Delta t \quad (2.27)$$

where:

$$\begin{aligned} \dot{\theta} &= \text{Angular velocity of motor (20} \pm 5\% \\ &\quad \text{rev/min)} \\ C_{dr} &= \text{Circumference of drum} \\ \Delta t &= \text{Time interval of test run} \end{aligned}$$

For trials after the first trial, the average normalized mass of the specimen can be written as:

$$\frac{W_{i,N} + W_{i-1,N}}{2} = \frac{g}{2} (m_{i-1,N} + m_{i,N}) \quad (2.28)$$

where:

$$\begin{aligned} W_{i,N} &= \text{Normalized weight of specimen after } i^{\text{th}} \\ &\quad \text{run} \\ g &= \text{Gravitational acceleration, 9.807 m/s}^2 \\ m_{i,N} &= \text{Normalized mass of specimen after } i^{\text{th}} \text{ run} \end{aligned}$$

For the first trial, the average normalized mass of the specimen can be written as:

$$\frac{W_{i,N} + W_{0,N}}{2} = \frac{g}{2} (m_{i,N} + m_{0,N}) \quad (2.29)$$

where $W_{0,N}$ and $m_{0,N}$ are the normalized initial weight and mass, respectively, of the specimen. However, the results from the first trial are not used in analysis due to edge rounding of the samples, which produces a spurious high rate of degradation that is not likely to be representative of the in-situ characteristics of the rock.

Keaton et al. (2012) take the normalizing area to be the bottom eighth of the drum, that is:

$$\text{normalizing area} = A_N = \frac{C_{dr} L_{dr}}{8} \quad (2.30)$$

where L_{dr} is the length of the drum (100 mm). Combining Equations 2.27, 2.28, 2.29, and 2.30 yields:

$$\begin{aligned} \frac{\Delta x_{eq} \cdot W_{i,N,av}}{A_N \cdot \Delta t} &= \frac{\dot{\theta} C_{dr} \Delta t \cdot \frac{g}{2} (m_{i,N} + m_{i-1,N})}{\frac{C_{dr} L_{dr}}{8} \cdot \Delta t} = \frac{8\dot{\theta} g}{L_{dr}} \cdot \frac{(m_{i,N} + m_{i-1,N})}{2} \\ &= \frac{8\dot{\theta} g}{L_{dr}} \cdot m_{N,av} \end{aligned} \quad (2.31)$$

This shows the stream power as a function of the angular speed $\dot{\theta}$, gravitational acceleration g , the length of the drum L_{dr} , and the average normalized mass of the specimen for each interval and the previous trial $m_{N,av}$. As the angular velocity of the motor and the length of the drum are standardized, the stream power can be expressed as a constant multiplied by the average mass of the specimen during a given test run, as:

$$\frac{8\dot{\theta} g}{L_{dr}} \cdot m_{N,av} = \frac{8 \times \frac{1}{3} \text{ rev/s} \times 9.807 \text{ m/s}^2}{0.1 \text{ m}} \cdot m_{N,av} = 261.52 \cdot m_{N,av} \quad (2.32)$$

with the sample mass given in kilograms. It should be noted that the use of these standard parameters yields a theoretical maximum equivalent stream power of 130.76 W/m^2 , with the assumption of no material loss during the first test run ($8 \times 1/3 \text{ s}^{-1} \times 9.807 \text{ m/s}^2 \times [0.1 \text{ m}]^{-1} \times 0.5 \text{ kg} = 130.76 \text{ W} \cdot \text{m}^{-2}$) (Keaton, 2013). As most natural channels will have a stream power that exceeds this level, extrapolation is necessary to apply the results for practical uses. Also of note is the strong nonlinear response of the sample during the initial test runs, in which the specimen loses a higher amount of material due to edge rounding (Keaton, 2013). This effect may be blocked simply by excluding initial mass losses from the results. The equivalent stream power is also much higher during the initial stages of the procedure, as the mass of the sample diminishes from the maximum.

Equivalent scour depth is then calculated by determining the loss in volume of the specimen, and normalizing it over a unit area (1 m^2). In order to do this, the specific weight of the sample is determined (per ASTM C127), and the equivalent scour depth is then taken as the difference in normalized sample weights (or masses) before and after the i th test run, divided by the unit weight (or density) of the sample. This is described symbolically by the following:

$$ESD_i = \frac{W_{i-1,N} - W_{i,N}}{\gamma} \cdot \frac{1}{A_{unit}} = \frac{m_{i-1,N} - m_{i,N}}{\rho} \cdot \frac{1}{A_{unit}} \quad (2.33)$$

Equation 2.33 yields units of length (m^3/m^2), which are dimensionally consistent with the units of scour depth. More durable samples, after a sufficient number of test runs, will eventually reach a point of negligible mass loss. This signifies that the equivalent stream power, given the sample mass, can no longer exceed the threshold necessary for significant erosion to occur in the

samples. However, this threshold stream power may not be suitable for predicting scour at bridge sites, due to the differing nature between natural erosion mechanisms and those induced by the continuous abrasion test (Keaton et al. 2012).

These differences notwithstanding, the modified slake durability/continuous abrasion test yields what may be useful parameters for determining rock durability and scour resistance. Keaton (2010) defines the geotechnical scour number as the slope of the equivalent hourly stream power vs equivalent hourly scour depth (ESP_i vs. ESD_i ; regression line, the y-intercept of which is forced to zero, as depicted in Figure 2.16. The geotechnical scour number can be used to predict a design scour depth for a bridge site with a given design stream power. To do this, the geotechnical scour number for a given rock material is multiplied by the cumulative stream power and by the design life of the bridge ($m \cdot [W \cdot m^2]^{-1} \times W \cdot m^2 \cdot s^{-1} \times s = m$) to determine the design scour depth at the site. The cumulative stream power at a site can be determined from daily flow series, as shown by Keaton et al. (2012). This approach is elaborated in Chapter 3 of this report.

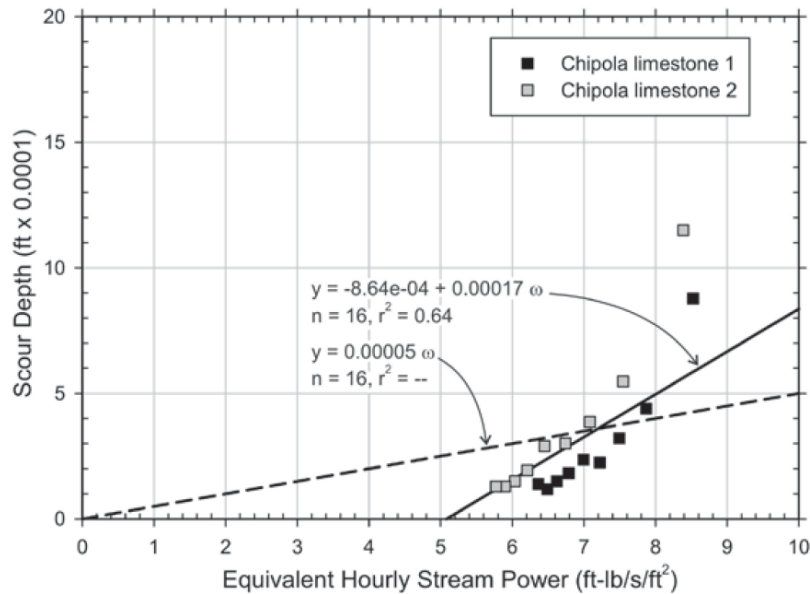


Figure 2.16: Modified slake durability test results and geotechnical scour numbers for limestone from the I-10 bridges site Chipola River, Florida (Keaton et al. 2012)

Chapter 3

Estimating Stream Power of Wisconsin Rivers

This chapter presents the results of the hydraulic analysis of flow data obtained from USGS stream gage stations located in Wisconsin rivers. The objective is to determine the stream power at stream gage stations located in close proximity of bridges supported by shallow foundations on rock.

3.1 Introduction

In this project, we focus on the rock scour at bridges due to abrasion, which is a progressive, grain-scale erosion of degradable rock material in response to water flows. The stream power of a river flow has been considered as the most appropriate loading parameter. The stream power can be estimated from available hydraulic data, i.e., from USGS stream gage stations.

In order to facilitate the process of identifying candidate field study sites, we have conducted a thorough review and analysis of the hydraulic parameters of major Wisconsin rivers and streams. Specifically, we have estimated the annual average stream power based on all available USGS stream gage data, in light of the assumption that higher annual average stream power may produce a deeper scour depth on rocks with the same geological properties. Following the scour number approach (Keaton et al., 2010), the annual scour depth can be estimated as

$$y_s = K_s \Omega \quad (3.1)$$

where y_s is the predicted annual scour depth, Ω is the annual average cumulative stream power and K_s is the Scour Number, either the empirical value from in situ site inspection or the geotechnical estimate from laboratory tests, e.g., the modified slake durability test.

3.2 Stream Data Extraction

The list of all USGS streamflow stations was obtained from the site <http://waterdata.usgs.gov/wi/nwis/current?type=flow>. An automatic web data program was developed in Matlab to extract streamflow data automatically from the USGS site, starting from this list page. Data extracted include historical daily flow time series, annual peak flows, and the field measurements data.

There are 232 stations in total in Wisconsin; however not all of them are suitable for stream power analysis. Stream power calculation requires the simultaneous measurement of water depth (as an estimate of hydraulic radius) and the mean velocity, while most stations only report the estimated discharge. Therefore, we have selected stations that also include field

measurement data. Two rating curves are developed to empirically relate the velocity (V) and water depth (H) to the discharge (Q) based on periodic field calibration data. Power law relations are assumed for both the two rating curves, i.e.:

$$H = H_0 + a_1 Q^{n_1} \quad (3.2)$$

$$V = a_2 Q^{n_2} \quad (3.3)$$

where H_0 is the gauge height (water depth) when there is no flow.

Figure 3.1 shows an example of rating curves fitting for station ID 04066003. Field measurements data for several stations do not fit well with the rating relations, and they are excluded from this study.

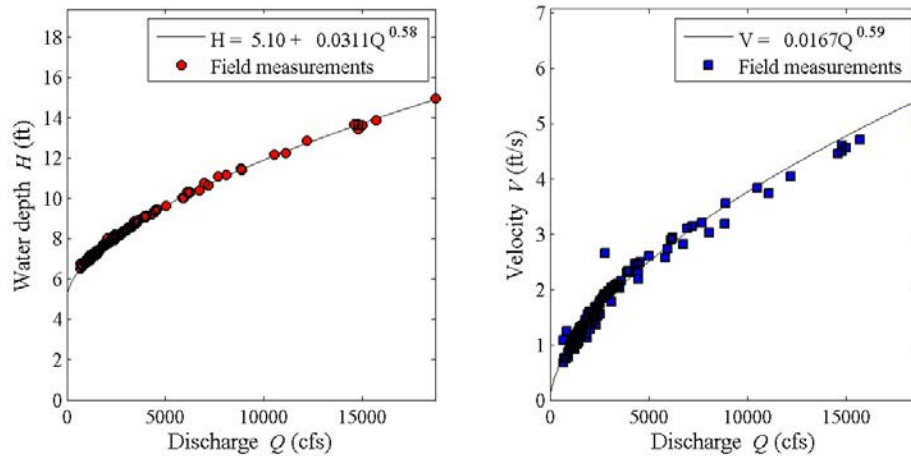


Figure 3.1: Rating curves developed for the USGS stream station 04066003 (Menominee River below Pemene Creek near Pembine, WI).

3.3 Stream Power Calculation

Stream power can be estimated with the following equation:

$$\Omega = \tau V = \left(\frac{nV}{1.486} \right)^2 \left(\frac{\gamma}{H^{1/3}} \right) V \quad (3.4)$$

where γ is the specific weight of water (62.4 lb/ft³) and the Manning's roughness n is chosen to be 0.032 as a representative to natural streams, although this value could be changed in the future when field surveys are conducted. Since Equation (3.4) is developed from the Manning's equation, the unit for velocity must be [ft s⁻¹] and the unit for the depth is [ft]; as a result, stream power has units of [lb-ft s⁻¹ ft⁻²], i.e. the power of friction per unit area of river bottom.

An example of daily discharge data obtained from USGS station 04066003 is shown in Figure 3.2, along with the recorded annual peak flow. A time series of stream power can be constructed based on the daily discharge following Equation (3.4) and the two rating functions (3.2) and (3.3). In order to account for the enhanced local flow and turbulence near a bridge pier, a factor of 1.7 has been applied to the estimated stream velocity. In order to estimate the mean daily stream power, cumulative stream power is plotted against time (in days). A linear regression is applied to the data, and the slope of the linear fit is considered as the average daily stream power. This value times 365 (days/year) and 86,400 (seconds/day) will be the total work done by the stream flow in one year over one squared foot of river bottom. However, in the following analysis, we will keep the unit of stream power as $[\text{lb}\cdot\text{ft}\ \text{s}^{-1}\ \text{ft}^{-2}]$ for convenience. We denote the annual mean stream power from this cumulative power analysis as $\bar{\Omega}$

Some scour process occurs only when a threshold hydraulic condition is exceeded (Mishra et al., 2010). Such a threshold condition could be a critical velocity, a critical shear stress or a critical stream power, or in some cases, a “channel-forming” flow condition. In order to account for this condition, we can estimate the effective mean daily stream power base on a threshold condition, i.e., plot the cumulative power of the flow with a threshold of the 2-year flow magnitude, and the slope of a linear regression is denoted as $\bar{\Omega}_2$. Figure 3.3 shows an example of this analysis.

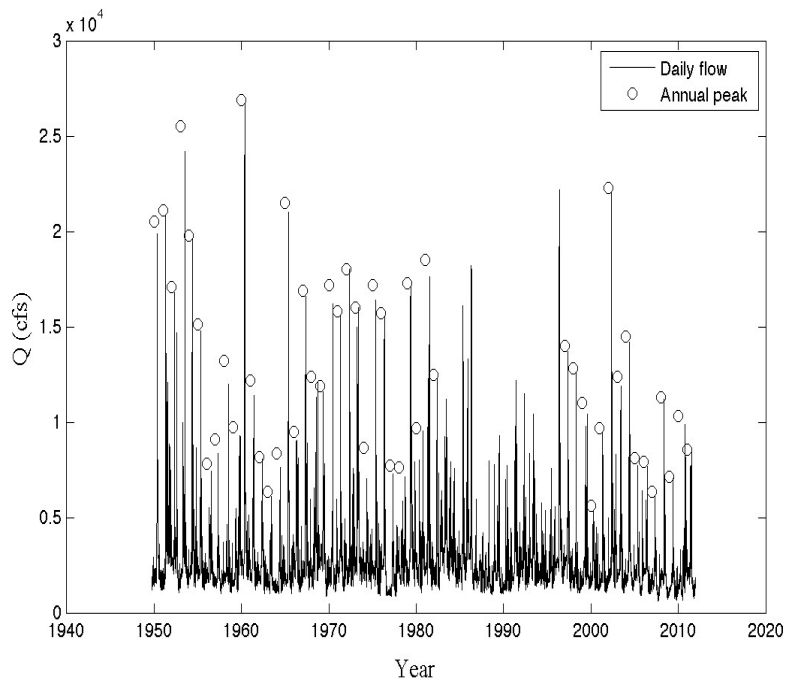


Figure 3.2: Daily mean discharge and annual peak flow recorded at USGS stream station 04066003 (Menominee River below Pemene Creek near Pembine, WI).

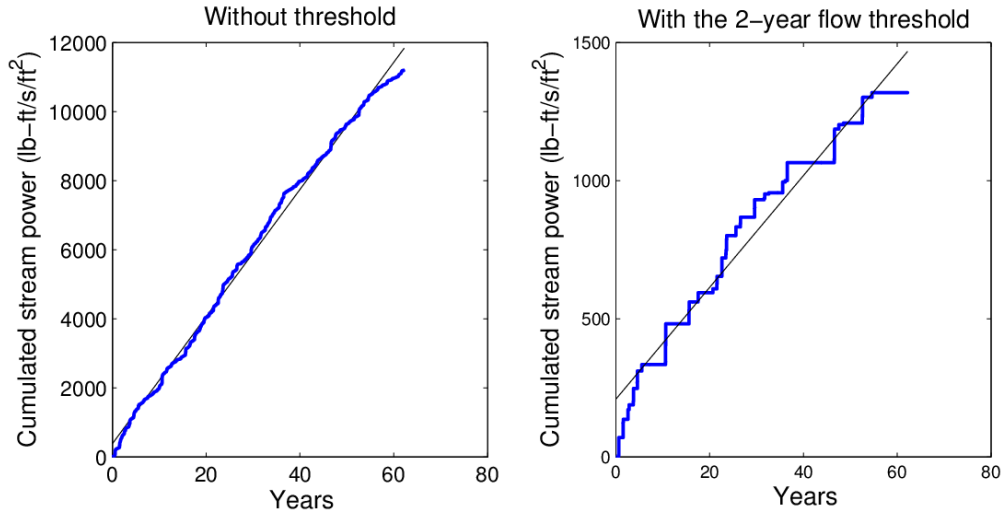


Figure 3.3: Estimating the mean daily stream power with and without threshold conditions for the USGS stream station 04066003.

We have also computed the mean daily stream power with a specified threshold of stream power. The threshold values are 1, 2, ... 9 ($\text{lb-ft s}^{-1} \text{ft}^{-2}$), respectively, with the expectation that future geotechnical test (such as the modified slake durability test) may indicate that the scour depth \sim stream power relation is better modeled with a threshold stream power value for some type of rocks, i.e.:

$$y_s = K_s(\Omega - \Omega_{crit}) \quad (3.5)$$

For example, previous studies with the modified slake durability tests which relate the equivalent scour depth to the equivalent stream power for some limestones, siltstones and sandstones clearly demonstrated the existence of a threshold condition may be modeled by a threshold stream power (see Figure 3.4).

3.4 Probability-Weighted Flood Frequency Approach

The probability-weighted approach has been used to predict the long-term rock erosion depth based on the return period (recurrence interval) of flood events. Similarly, we can estimate the annual effective stream power with the flood frequency analysis, which can be easily converted to an annual erosion depth in light of the scour number approach, i.e., Equation (3.1).

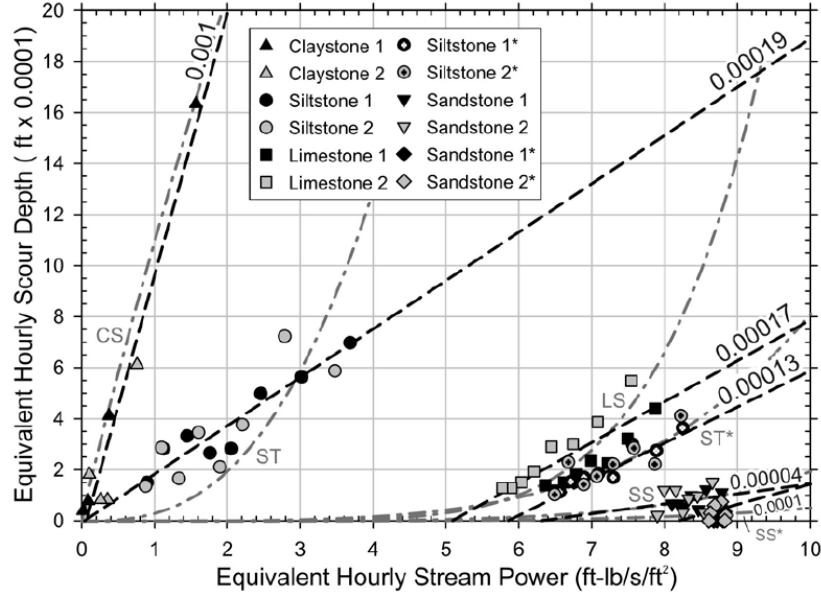


Figure 3.4: Data and regression lines for modified slake durability tests for rock samples (Keaton et al., 2012).

This analysis is only applied to stations where the annual peak flow data is available. The magnitude of flood (Q_T) of a given return period (T) can be estimated from the annual peak series and assuming a log-Pearson type III probability distribution. Given a series of annual peak flow, Q_1, Q_2, \dots, Q_n , we can construct a series $y_i = \log_{10} Q_i$, ($i = 1, 2, \dots, n$). Denoting μ_Y , σ_Y , and G_S as the sample mean, sample standard deviation and sample skewness of the series y_i , the magnitude Q_T of a T year event can be estimated using the frequency factor method:

$$\log_{10} Q_T = \mu_Y + K(T, G_S)\sigma_Y \quad (3.6)$$

where K is the frequency factor as a function of the return period T and the skewness G_S , and which can be calculated using Kite's Equation:

$$K = z + (z^2 - 1)k + \frac{1}{3}(z^3 - 6z)k^2 - (z^2 - 1)k^3 + zk^4 + \frac{1}{3}k^5 \quad (3.7)$$

where $k = \frac{G_S}{6}$, $z = \Phi^{-1}\left(1 - \frac{1}{T}\right)$, and Φ^{-1} is the inverse function of the cumulative distribution function (CDF) of a standard normal distribution.

Meanwhile the average duration of a T year event, D_T , can be estimated by analyzing the daily flow time series. A T year event is defined as a consecutive daily flow series that is higher than Q_T . All these events are identified from the historical series, and their durations are averaged as an estimate for D_T . A power-law relation is applied to fit the relation $D_T \sim T$, and the

best-fit function is used to calculate D_T for any given recurrence interval T . Figure 3.5 shows an example of this analysis.

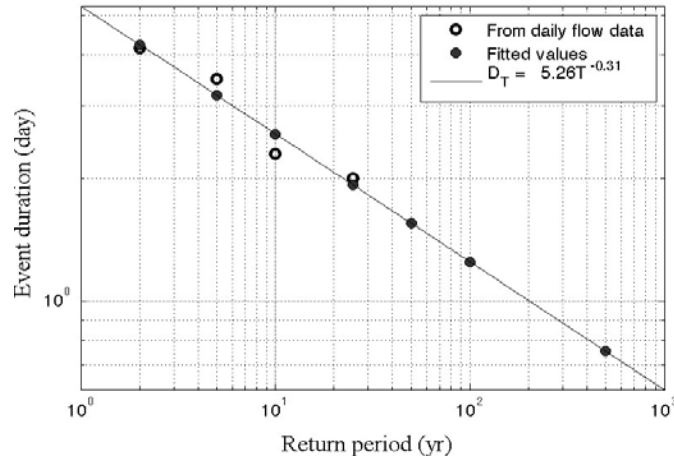


Figure 3.5: Relation between the average event duration to the flood recurrence interval (return period) for the USGS stream station 04066003.

Flood magnitude for $T = 2, 5, 10, 25, 50, 100$ and 500 years are calculated and converted to a stream power following rating relations. These stream power values are then multiplied by the estimated average duration D_T to represent the cumulative power of a T year event. Figure 3.6 shows a typical probability distribution of stream power. Eventually, the annual average stream power ($\bar{\Omega}_F$, where the subscript F denotes “frequency-weighted”) can be calculated with the following probability-weighted equation:

$$\bar{\Omega}_F = \int \Omega_T dP_T \quad (3.8)$$

where Ω_T is the cumulative stream power of a T year event and $P_T = 1/T$ is the corresponding probability of the occurrence of a T year event for any given year.

Conceptually, we postulate that the frequency weighted annual stream power $\bar{\Omega}_F$ is equivalent to the mean daily stream power with a 2-year flow threshold $\bar{\Omega}_2$ multiplied by 365 (days/year). This is verified by plotting $\bar{\Omega}_F$ against $365\bar{\Omega}_2$, as shown in Figure 3.7(a). A good correlation is found between these two measures. However, there are not clear correlations between $\bar{\Omega}_F$ and $\bar{\Omega}$, i.e. the mean daily stream power without threshold condition, as shown in Figure 3.7(b).

Maps of all selected stations and their corresponding stream powers $\bar{\Omega}$, $\bar{\Omega}_2$, and $\bar{\Omega}_F$ are presented in Figures 3.8 to 3.10. These maps along with the geological distribution of bed rocks will be used to facilitate the selection of field investigations.

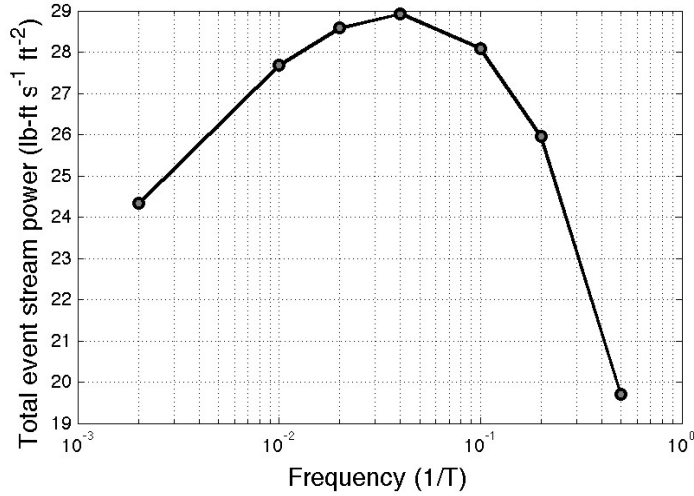


Figure 3.6: Probability distribution of stream power as a function of annual flood frequency for the USGS stream station 04066003.

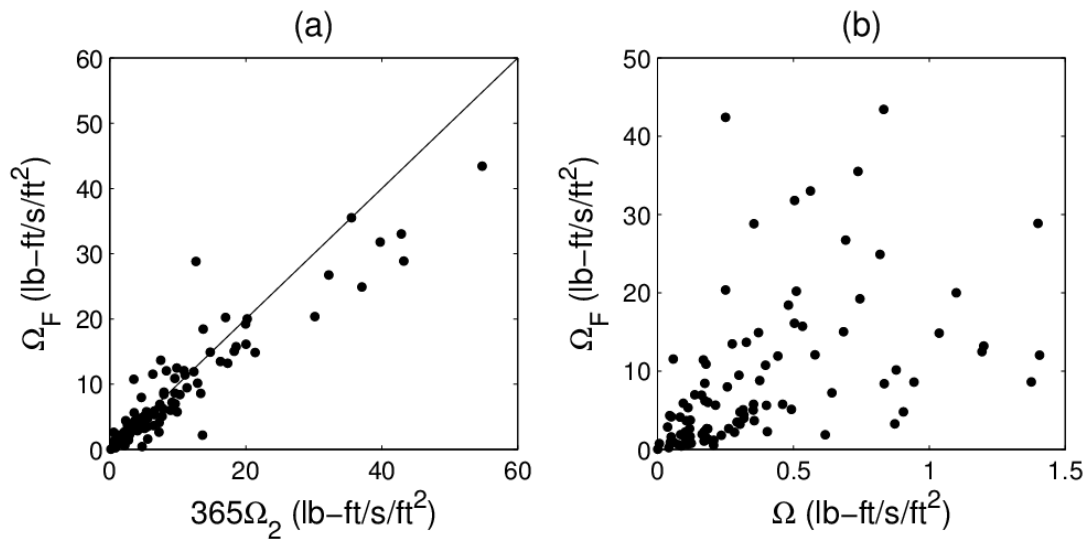


Figure 3.7: (a) Relation between the frequency weighted annual stream power to the mean annual stream power with a 2-year flow threshold. (b) Relation between the frequency weighted annual stream power to the mean daily stream power without threshold flow condition.

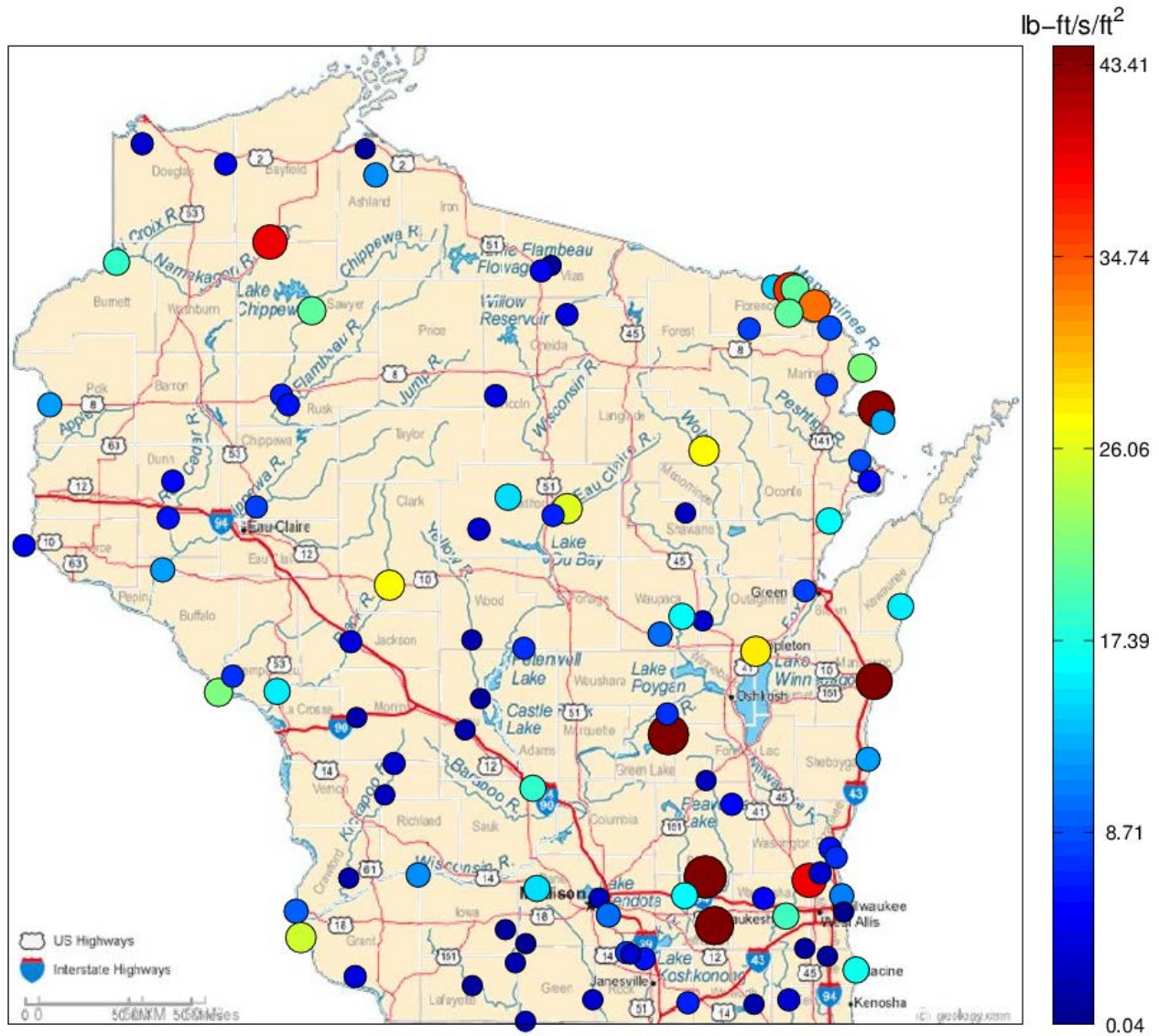


Figure 3.10: Map of the frequency weighted annual stream power $\bar{\Omega}_F$.

Chapter 4

Research Methodology

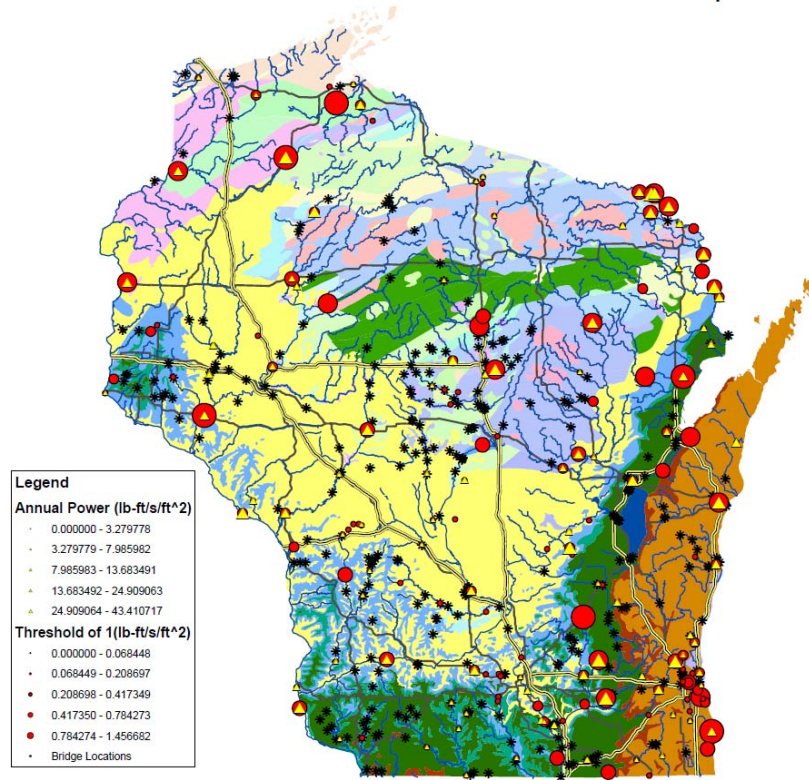
This chapter presents the methodology executed to achieve the goals of the research. It describes the process of identifying candidate project sites as well as the selection of the final list of projects. It details the field reconnaissance of the selected projects, rock sampling using a WisDOT drill rig and hand sampling, and channel bottom hydrographic surveys.

4.1 Selection of Project Site Locations

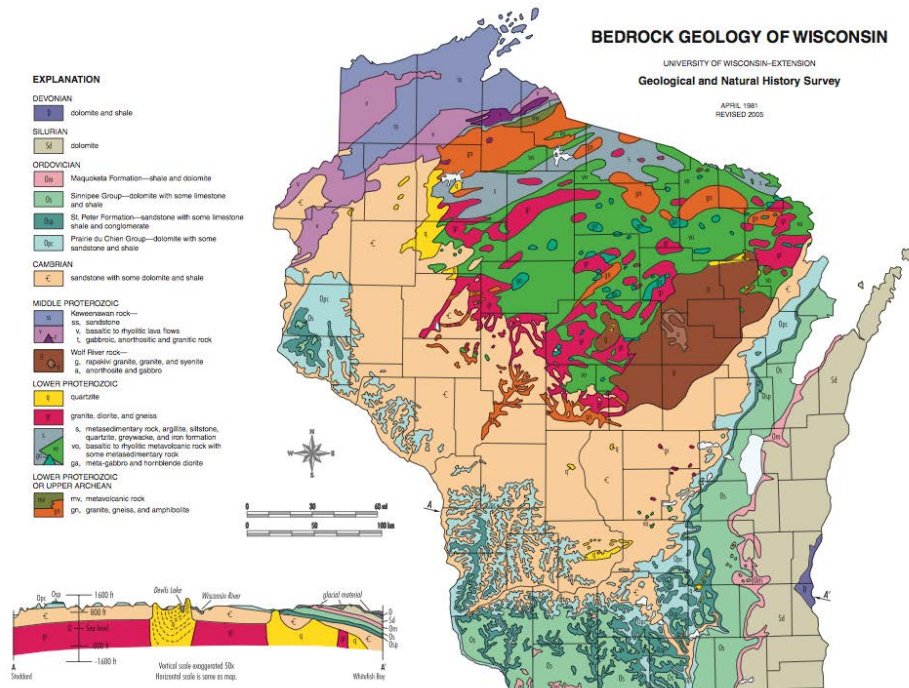
The research team conducted a comprehensive hydraulic analysis (as presented in Chapter 3) and identified the locations of USGS stream gage stations with measured flows that resulted in high stream power in Wisconsin rivers and streams. Figure 4.1a shows the annual as well as threshold stream power for various Wisconsin rivers graphed on Wisconsin bedrock map. Bridge structures that are supported by shallow foundation systems are also shown on the map. The research team identified a list of 22 candidate project sites for field study based on input and guidance from the Project Oversight Committee (POC). These project sites satisfied the selection criteria, which included: bridge structures with piers supported by spread footings/shallow foundation systems, bridge foundations on bedrock representative of the rock formations encountered in Wisconsin, and bridge foundations located in rivers or streams with high stream power. The WisDOT Bridge Inventory database was also used in part to identify the candidate projects and to obtain information which included boring logs, bridge structure plans, and underwater inspection reports.

The focus of the laboratory testing described in the RFP is on the modified slake durability test, which applies to progressive scour of degradable rock. This laboratory focus suggests that the potential field test locations should include degradable rock conditions which are susceptible to progressive scour. The initial identification of potential field tests locations consists of geologic screening of bedrock formations, as well as reviewing WisDOT Bridge Inventory data. Figure 4.1 depicts a map of geological bedrock formations in Wisconsin which was used as a reference for candidate project site selection.

The research team met with the POC and discussed the various aspects of the 22 candidate project sites based on the selection criteria. The meeting resulted in the identification of the 10 project sites summarized in Table 4.1 for field and laboratory investigations. As presented in Table 4.1, four of the selected bridge structures are supported by shallow foundations on degradable rocks (Cambrian Sandstone). The exceptions to the selection criteria are: the I-94 Red Cedar River bridge which is supported by drilled shafts in sandstone, and the US-51 Eau Claire River bridge which is supported by steel H-piles in degradable/weathered granite. These were selected due to the rock type supporting the bridge foundations.



(a) Stream Power and WisDOT structure map



(b) Bedrock geology

Figure 4.1: Map of the bedrock geology of Wisconsin, developed by the Wisconsin Geological and Natural History Survey, University of Wisconsin-Extension.

4.2 Field Investigation – Rock Sampling

The research team conducted comprehensive evaluations of the bedrock geology at the selected project locations. Geologic maps and historical geotechnical boring and coring data were used to characterize the bedrock at the selected locations. In addition, the research team and the POC chair conducted field reconnaissance visits to the selected project sites and discussed plans for rock sampling that included coring and hand sampling. Figures 4.2 to 4.8 show pictures of the field visits and features of the bridge structures, bedrock, and rivers/streams.

Table 4.1: Summary of bridge structure information for bridges selected for the rock scour study.

Bridge Structure ID	Bridge Structure Description	Year Built	GPS Location (Latitude, Longitude)		Bedrock Geology
B-36-72	IH 43 over Manitowoc River	1979	44.129394	-87.732972	Silurian carbonates (dolomite)
B-36-73			44.127892	-87.732242	
B-44-98	STH 47 Memorial Drive over Fox River	1982	44.253333	-88.415000	Sinnipee Group (Galena or Platteville Fms., dolomite)
B-11-01	STH 13 over Wisconsin River 16 (N. of WI. Dells)	1955	43.627803	-89.778792	Cambrian sandstone
B-11-104		1991	43.627636	-89.781611	
B-10-131	USH 10 over Black River (S, of Neillsville)	1993	44.552219	-90.608931	Pre-Cambrian granite, (sub unit: Wgh)
B-56-42	IH 90/94 over Spring Brook	1961	43.596644	-89.813950	Cambrian sandstone
B-56-43			43.596389	-89.813206	
B-17-208	IH 94 over Red Cedar River	2013	44.908242	-91.897630	Cambrian sandstone (Tunnel City Group)
B-17-209			44.908012	-91.897630	
B-17-211			44.907935	-91.897490	
B-37-280	Bus. USH 51 over Eau Claire River	1997	44.916290	-89.611586	Pre-Cambrian granite/felsic volcanics

Table 4.1 (cont.): Summary of bridge structure information for bridges selected for the rock scour study.

Bridge Structure ID	Bridge Structure Description	Year Built	Number of Piers	Pier Type	Foundation Type
B-36-72	IH 43 over Manitowoc River	1979	3	Hammer Head	Shallow Foundation
B-36-73			3		
B-44-98	STH 47 Memorial Drive over Fox River	1982	3	Hammer Head	Shallow Foundation
B-11-01	STH 13 over Wisconsin River 16 (N. of WI. Dells)	1955	2	Round Column Bent	Shallow Foundation
B-11-104		1991	2	Hammer Head	
B-10-131	USH 10 over Black River (S, of Neillsville)	1993	2	Individual Column in Line	Shallow Foundation
B-56-42	IH 90/94 over Spring Brook	1961	2	Individual Column in Line	Shallow Foundation
B-56-43			2	Individual Column in Line	
B-17-208	IH 94 over Red Cedar River	2013	2	Round Column Bent	Drilled Shaft
B-17-209			2		
B-17-211			2		
B-37-280	Bus. USH 51 over Eau Claire River	1997	3	Round Column Bent	Steel H-Piles



Figure 4.2: STH 13 bridges (B-11-01 and B-11-104) on the Wisconsin River, Wisconsin Dells – Cambrian Sandstone.



Figure 4.3: STH 47 bridge (B-44-98) on the Fox River, Appleton – Dolomite.



Figure 4.4: USH 10 bridge (B-10-131) on the Black River, Neillsville – Gneiss.

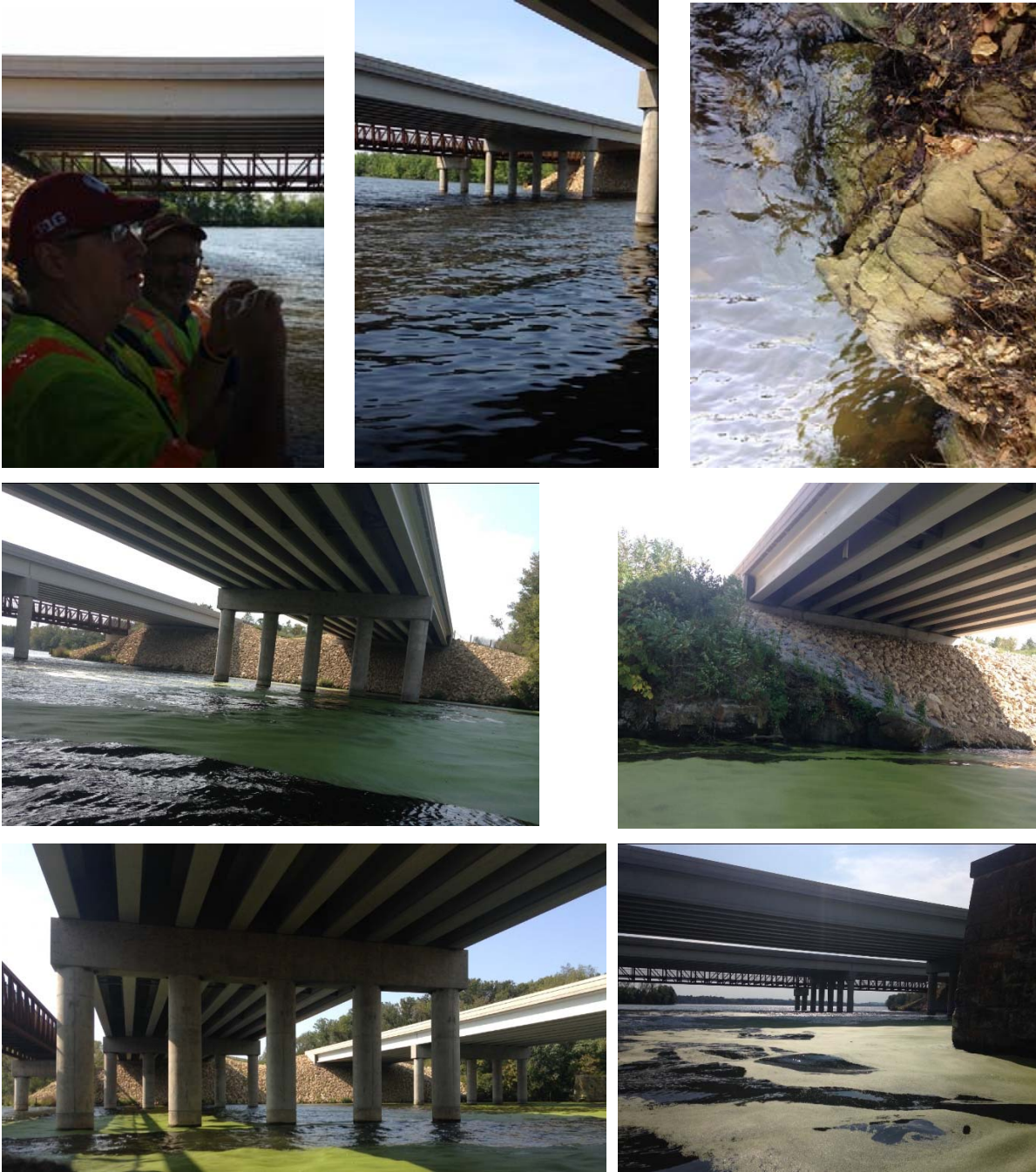


Figure 4.5: IH-94 bridges (B-17-208, B-17-209, B-17-211) on the Red Cedar River, Menomonie – Cambrian Sandstone.



Figure 4.6: IH 43 bridges (B-36-72, B-36-73) on the Manitowoc River, Manitowoc – Dolomite.



Figure 4.7: USH 51 bridge (B-37-280) on the Eau Claire River, Schofield – degradable (rotten) Granite.



Figure 4.8: IH 90/94 bridges (B-56-42, B-56-43) on Spring Brook, Lake Delton – Cambrian Sandstone.

The coring of bedrock was initially planned for all selected bridge site locations. However, the coring process required the use of a barge to carry the drill rig and also required waterway access to tug the barge to the bridge locations from a boat landing or similar facility. The WisDOT drilling team faced significant waterways access challenges, for example, at the STH 13 bridge on the Wisconsin River due to the difficult terrain and absence of an accessible launch point. For other locations such as the Black River, Manitowoc River, and Spring Brook, it was not possible to access their bridge site locations with the available equipment. Therefore, due to the difficulties encountered, it was decided to perform coring at the three accessible bridge site locations (STH 13 on the Wisconsin River, STH 47 on the Fox River, and USH 10 on the Eau Claire River) and to hand pick samples from bedrock formation outcrops within the streams/river from the following project sites: USH 10 on the Black River, IH-90/94 on Spring Brook, and IH 43 on the Manitowoc River. Cores from the Red Cedar River were supplied by

WisDOT NW Region since the bridge was recently constructed and significant coring had been performed for the design of drilled shafts for the new bridge. Figures 4.9 and 4.10 show pictures of the coring and hand sampling of bedrock at the selected project sites. The coring plan resulted in acquiring rock samples according to the summary presented in Table 4.2.

The collected core and hand samples were wrapped in boxes, jars, and plastic bags to preserve moisture and minimize the potential for slaking in air. The retrieved core and hand samples from each project were then transported to the geotechnical research laboratory at UW-Milwaukee for evaluation and laboratory testing. The following evaluation and laboratory testing procedures were conducted on representative samples:

1. Geologic characterization and evaluation of the rock core samples.
2. X-ray diffraction to determine the mineralogical composition of the rock samples.
3. The modified slake durability (continuous abrasion) test as described in NCHRP Report 717 (Keaton et al. 2012) and also in Chapter 2 of this report.
4. Flume test on slab sample of sandstone from Wisconsin River

The research team did not perform the unconfined compression tests on the bedrock samples due to the limited number of collected core samples. These samples were selected for the modified slake durability test.



Figure 4.9: Bedrock coring conducted by a WisDOT drill crew with the drilling rig mounted on a barge.



Figure 4.10: Bedrock hand sampling conducted by the research team.

Table 4.2: Summary of coring and hand sampling conducted at the investigated project sites.

Bridge Structure ID	Bridge Structure Description	Rock Samples Types	Core/Samples Location			
			Pier #	Core Run	Depth (ft)	Recovery
B-36-72	IH 43 over Manitowoc River	Hand	West side of the river – outcrop			
B-36-73			West side of the river – outcrop			
B-44-98	STH 47 Memorial Drive over Fox River	Core	P2	4	9.5-14.5	100%
			P3	3	8.5-13.5	100%
			P4	2	6-11	100%
			P5	1	7-12	100%
B-11-01	STH 13 over Wisconsin River 16 (N. of WI. Dells)	Core	P2	1	31.5-36	90%
			P2	2	36-40.5	90%
			P1	1	40.5-45	85%
			P1	2	45-49.5	100%
		Hand	Various Locations and depths			
B-11-104		Hand	Various Locations and depths			
B-10-131	USH 10 over Black River (S. of Neillsville)	Hand	East side of river – north of structure – outcrop			
B-56-42	IH 90/94 over Spring Brook	Hand	East and west sides of the waterway – outcrop between the two bridges			
B-56-43						
B-17-208	IH 94 over Red Cedar River	Core	P1 P2	Shaft1, 2, 3, 4, and 5	Various depth	Various values
B-17-209			P1 P2	Shaft1, 2, 3, 4, and 5	Various depth	Various values
B-17-211			P1 P2		Various depth	Various values
B-37-280	Bus. USH 51 over Eau Claire River	Core	P2	1, 2	15-19	Various values
			P3	1 2,3,4,5	15.5-18 18-29.5	

4.3 Waterway Geometry and Hydraulics:

The research team and Collins Engineers, Inc. conducted hydrographic field surveys using the single beam echo sounder system as shown in Figure 4.11. The research team conducted six survey sections at each project location. This provided six floodplain valley cross-sections needed for the bridge hydraulics analyses: three upstream and three downstream sections, four of which are roughly one and two bridge lengths away from the structure on both sides, and two cross-sections of both faces of the bridge. Figure 4.12 presents the hydrographic field survey locations for the USH 51 bridge on the Eau Claire River. A sample result of the hydrographic field survey for the USH 51 bridge on the Eau Claire River is presented in Figure 4.13. The hydrographic field survey results for all projects are presented in Appendix A.



Figure 4.11: The research team conducting hydrographic field surveys using the single beam echo sounder system on Spring Brook, Lake Delton.



Figure 4.12: Hydrographic field survey section locations upstream and downstream of the USH 51 bridge on the Eau Claire River in Schofield.

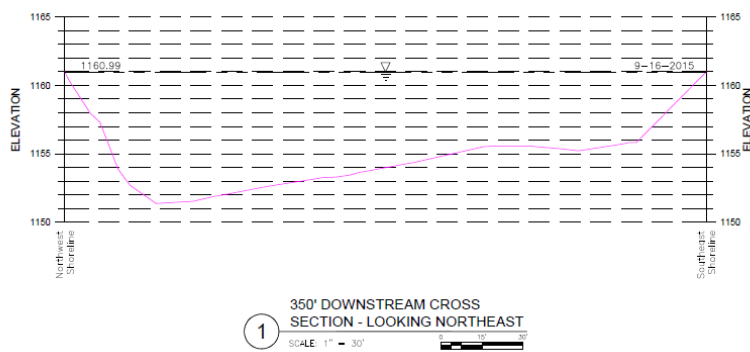


Figure 4.13: Typical hydrographic field survey results for section 1 downstream of the USH 51 bridge on the Eau Claire River in Schofield.

The borings for the bridge over the Wisconsin River at this location are provided below in Figures 5.2 and 5.3. They are dominated by surface sand deposits on the western side underlain by the local sandstone. On the eastern side the subsurface is all sandstone. It appears that all bridge supports – piers – are located completely into areas of only sandstone. This also suggests that the river has sufficient flow under the bridge to deter deposition of sediments.

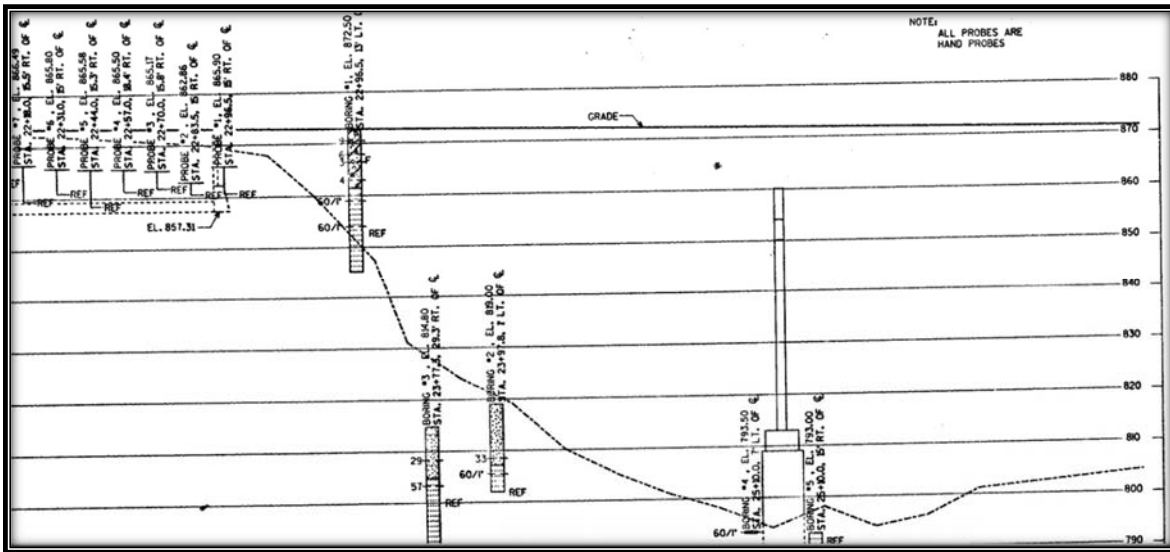


Figure 5.2: East side borings showing about 10 feet of sand in some locations over sandstone.

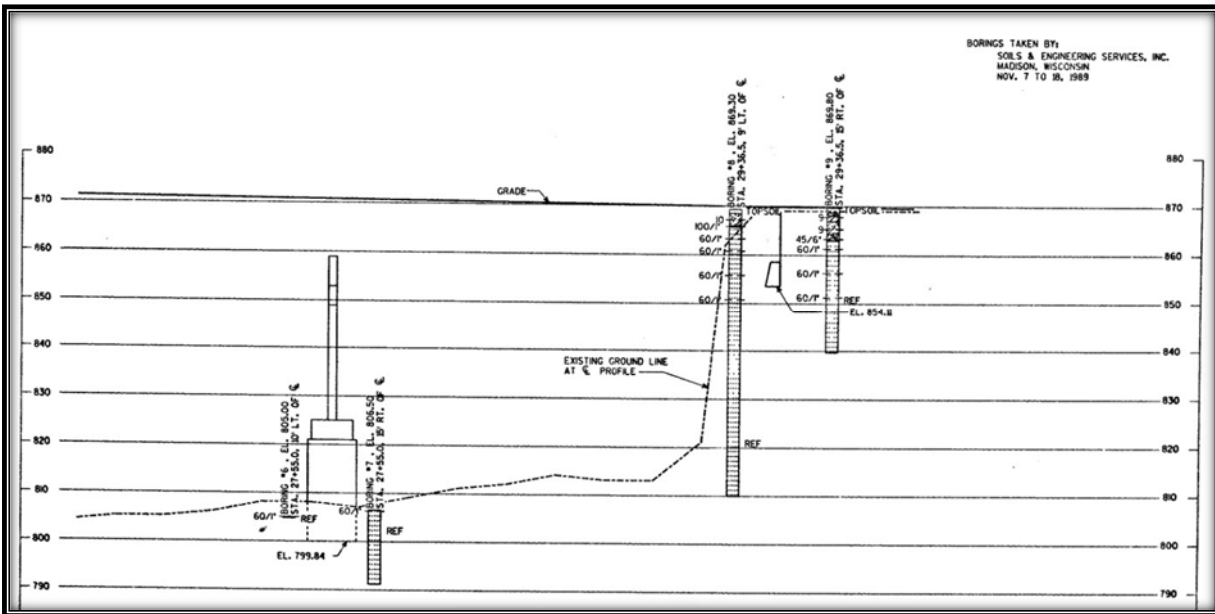


Figure 5.3: West side of the Wisconsin River boring log showing almost completely sandstone in the subsurface.

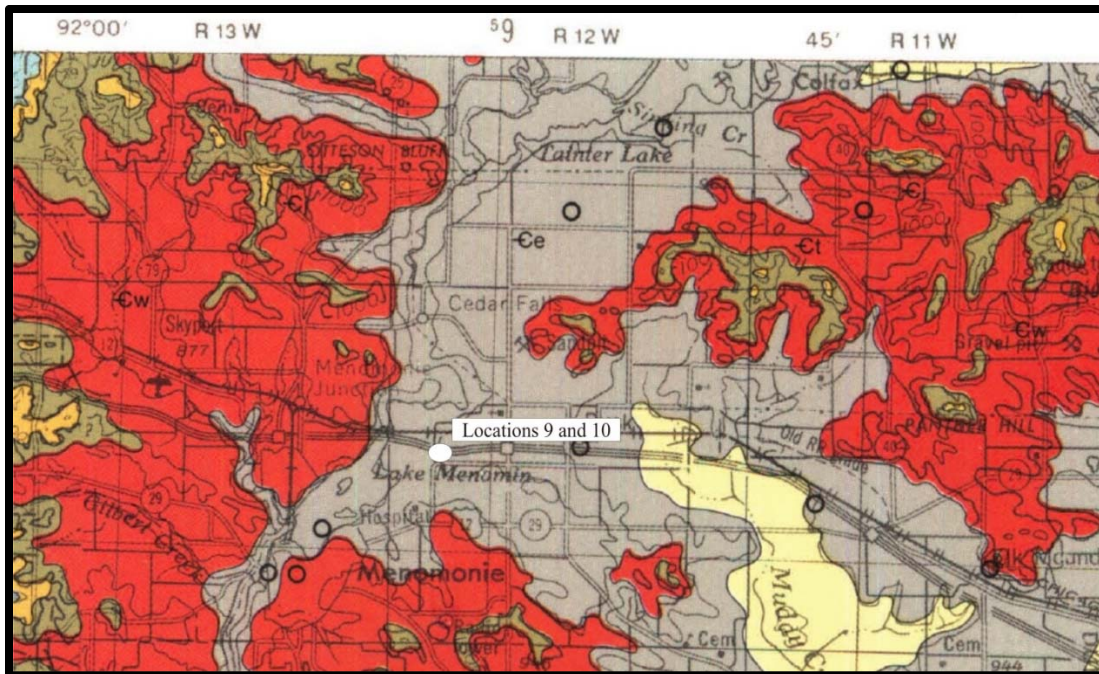


Figure 5.5: Modified from Brown (1988). Eau Clair Formation is in Gray color.



Figure 5.6: Photo from the “Devil’s Punchbowl” showing outcrop of the Eau Claire Formation. University of Wisconsin –Stout, 2004.

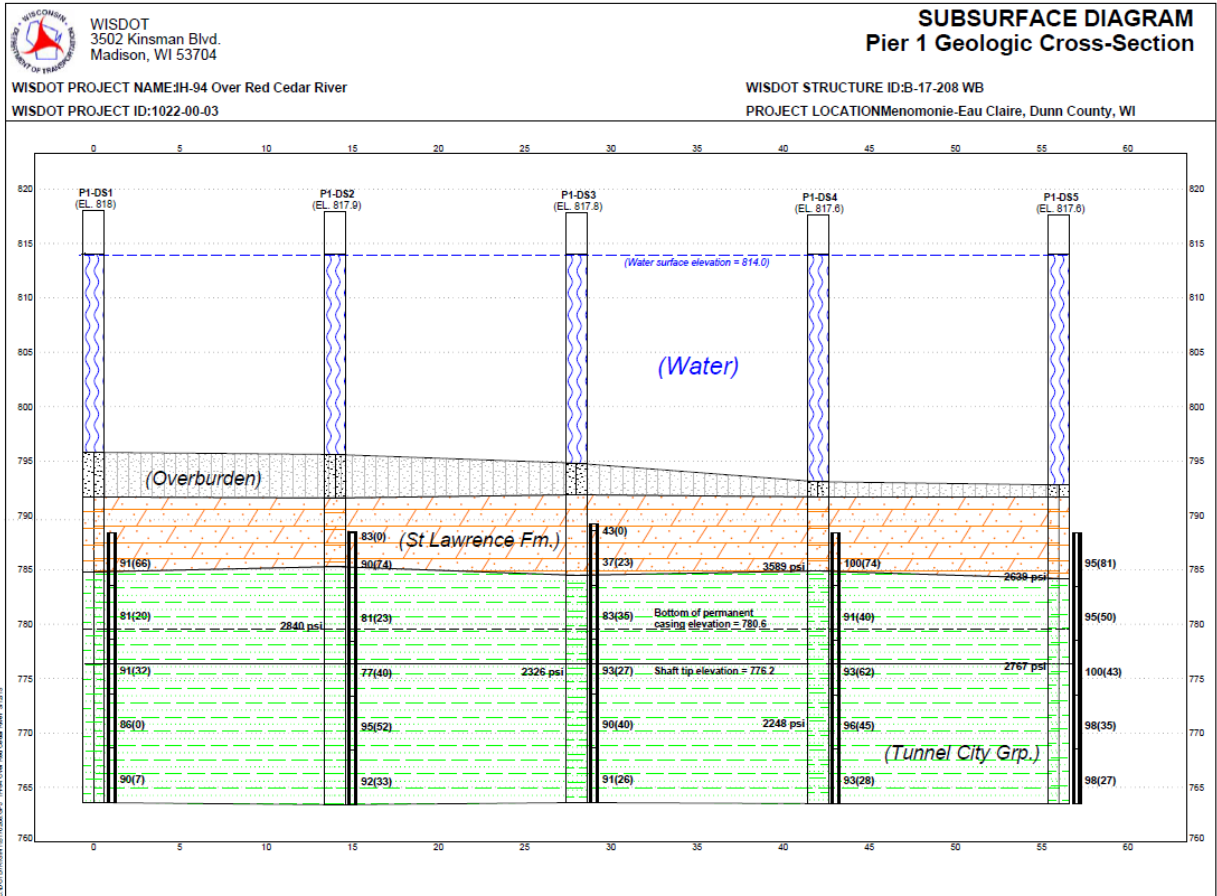


Figure 5.7: Boring Logs for Locations 9 and 10.

5.3 Geology of Location 6 USH-10 over Black river near Neillsville, WI Clark Co. (B-10-131)

The rocks along the Black river near Neillsville, WI are Archean to Early Proterozoic in age. This makes them between 2700 and 1800 million years old. The rocks are a variety of metamorphic gneisses and migmatites. At the bridge location, the rocks to the north are biotite granites (Pgr) and at the bridge and southward are the gneiss and migmatite (Agn), as shown in Figure 5.8. Both of these rock types are of strong and, as typical of these rock types, have interlocking mineral grains. They do not weather easily as do the surrounding Cambrian Sandstone. The boring logs for this site (Figure 5.9) show between 5 and 10 feet of clay or fill over an irregular surface of the igneous/metamorphic rocks as noted above.

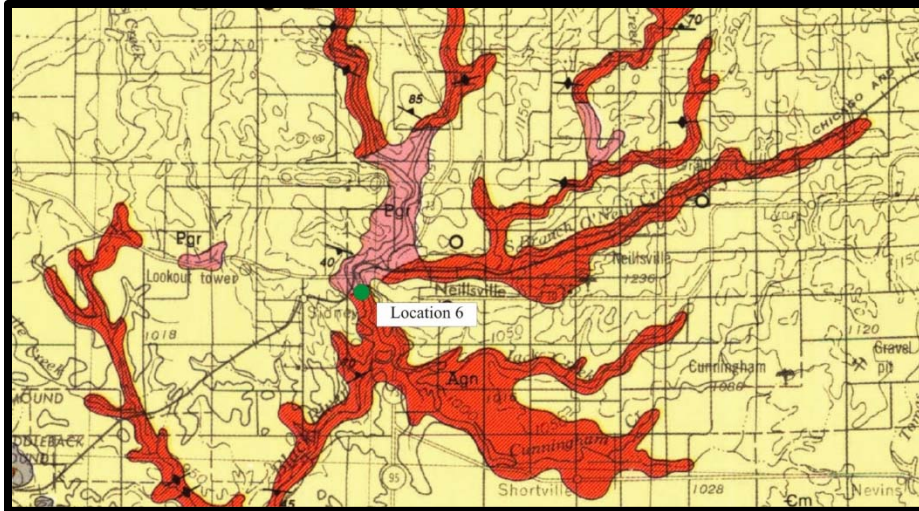


Figure 5.8: modified from Brown, 1988, Agn is gneiss and migmatite: Pgr is biotite granite. The ages of these rocks vary between 2500-1800 Ma.

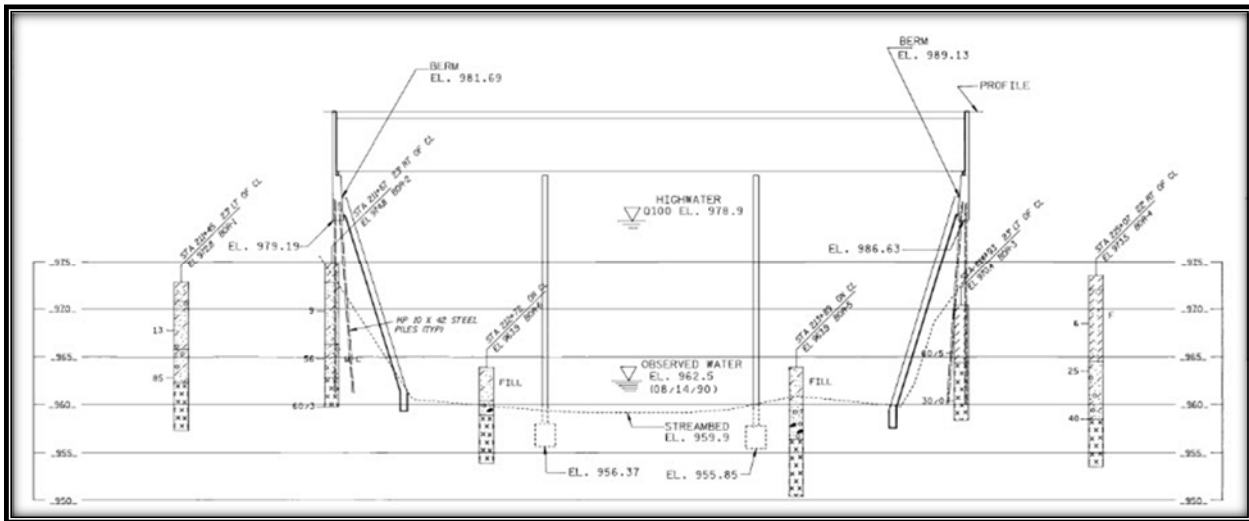


Figure 5.9: Boring Logs for Location 6.

5.4 Geology of Location 11, Business USH51 over Eau Claire River, Wausau, WI.

The Geology of the Wausau is some of the most complex in the state because it records intrusive granitic rocks and significant metamorphism of the surrounding rocks. These rocks are all quite old being lower and middle Proterozoic in age (1950 to 1850 Ma). The region has syenite (Isy) (light blue color), felsic metavolcanics (Fv) (green color), metagabbros (Mg)(dark green), granite (Lg)(pink) and mafic metavolcanics (Mv)(dark dark green). Lastly there is



Figure 5.11: Core sample from the area over the Eau Claire River at Wausau.

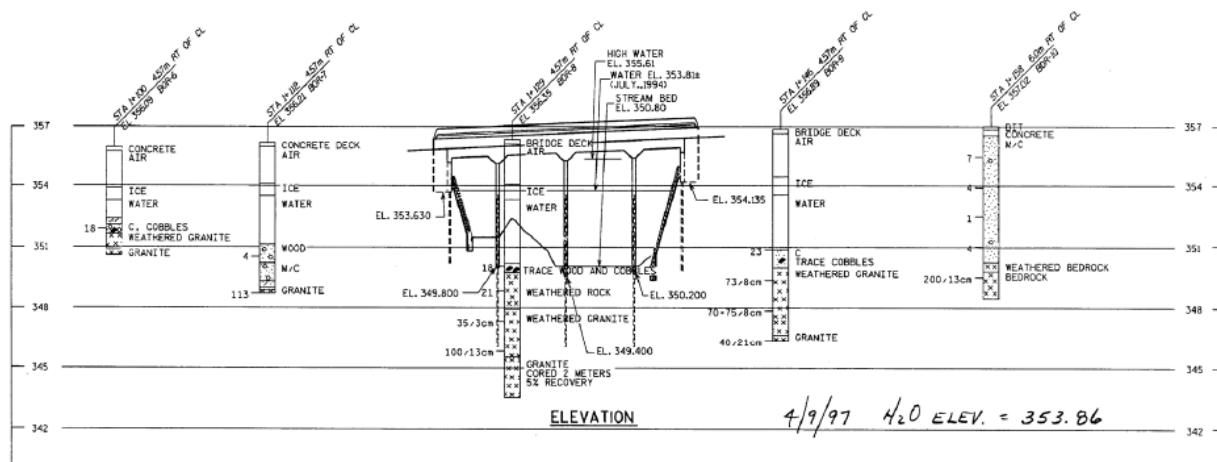


Figure 5.12: Boring Logs from USH 51 – Eau Claire River location.

5.5 Geology Location 3, Memorial Drive over the Fox River, Appleton, Outagamie Co. WI

The rock near Appleton is Ordovician in age, part of the Sinipee group, with an age of about 460 -470Ma. In the bridge location two formations could be present, namely Prairie Du Chien (Op) (pale green-yellow color) or the Sinnipee group (Os) (light blue color) as seen on the geologic map (Figure 5.13) below. It would appear that the bridge is built on Prairie Du Chien Formation.

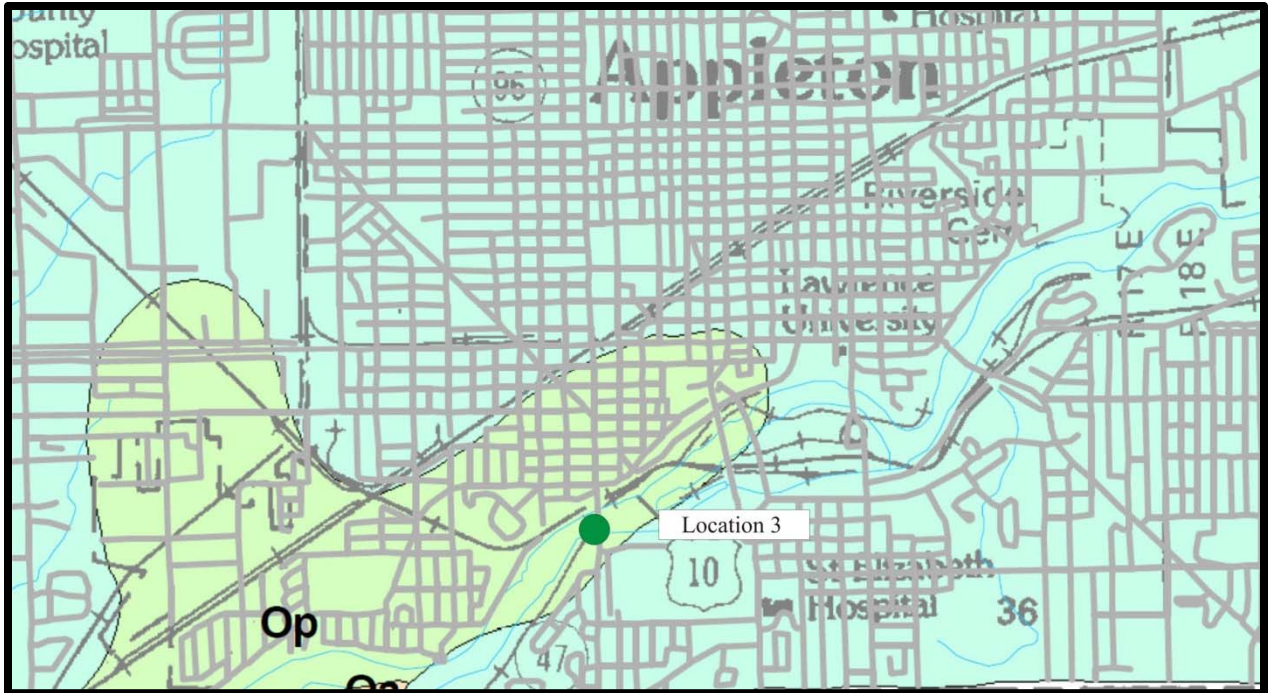


Figure 5.13: Geologic Map of the Appleton area modified from Brown (2005).

The boring logs for this bridge (B-44-98) as seen in Figure 5.14 indicate the bedrock as limestone of the Prairie Du Chien Formation. The unconsolidated sediments noted as brown sand on the edges of the bridge area is river sediments from glacial outwash.

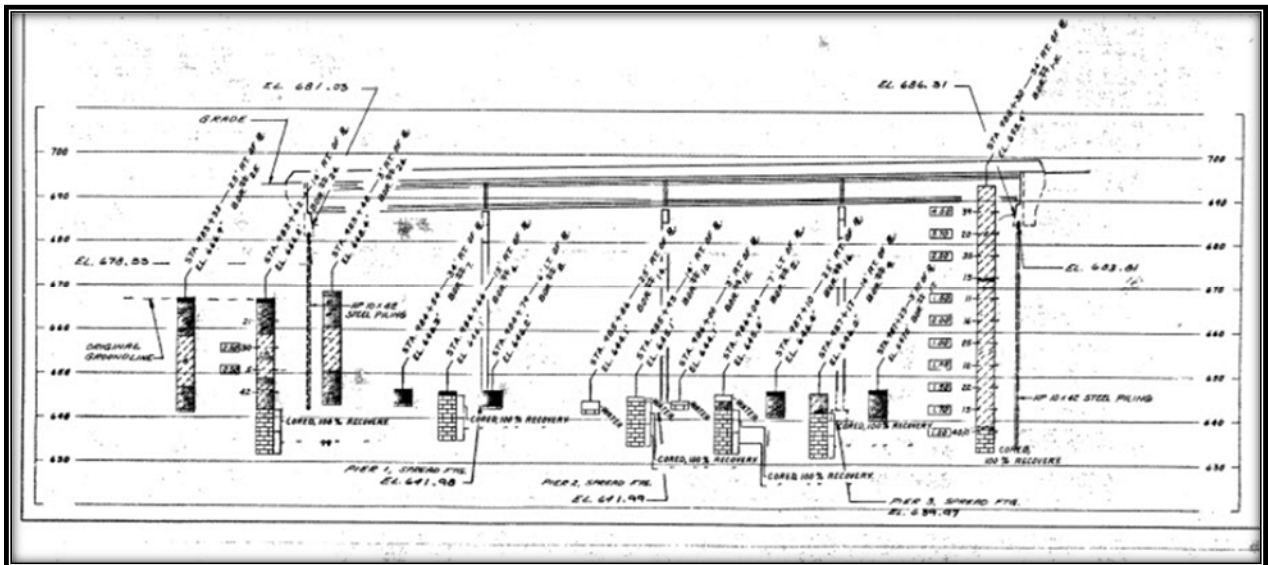


Figure 5.14: Boring logs for location 3.

5.6 Geology of Locations 1 and 2, IH 43 and USH 10 over Manitowoc River, Manitowoc Co. WI.

The Eastern side of Wisconsin is dominated by the Silurian Dolomite which makes it about 350 This ridge of dolomite continues through Door Co, to parts of Canada and eventually forms Niagara Falls in Western New York and Southern Ontario. Dolostones are a calcium, magnesium carbonate, similar to limestone which is calcium carbonate. The Silurian dolostone of eastern Wisconsin is quite compact and hard. It is a common building stone in the Midwest. It does have a dominant fracture pattern which is NE-SW.

The geology of the area is quite uniform as noted in the general geologic map of the area Figure 5.15 below. There appears not to be a detailed geologic map of Manitowoc Co., but the surface rock is known to be one of Silurian formations, most likely the Burnt Bluff Group or the Mayville Formation. In either case the rock is quite hard and fairly thick beds.

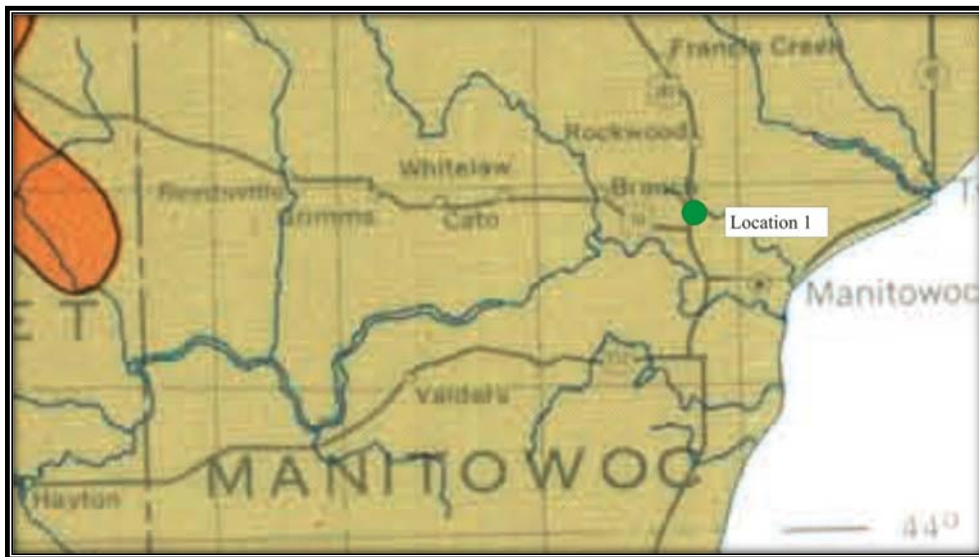


Figure 5.15: Modified from the Bedrock Geologic Map of Wisconsin (Mudrey et.al., 1982).

The boring logs are provided in Figure 5.16 and show gravel in some locations of up to 20 feet on top of the bedrock. Within the channel, the gravel is at most 5 ft. thick on top of the bedrock dolostone.

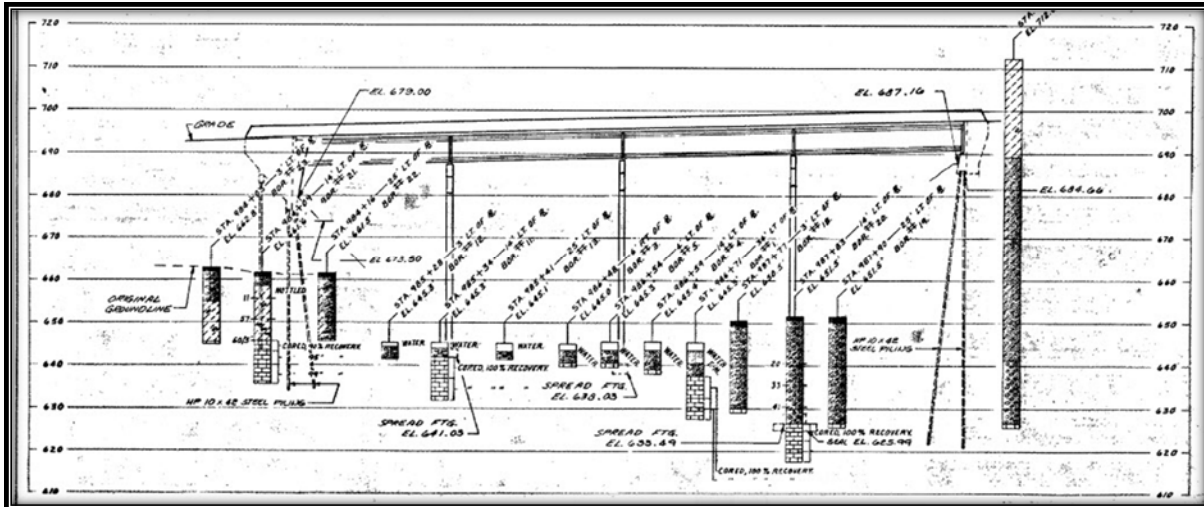


Figure 5.16: Boring logs for location 1. (B-36-72).

The borings under the second bridge at this location (Figure 5.17) shows surface material that is dominantly clay material on top of the bedrock away from the center of the river. Having clays in one location and gravels in the other location very nearby suggests the surface material is glacial deposits probably diamictite (till). (B-36-73)

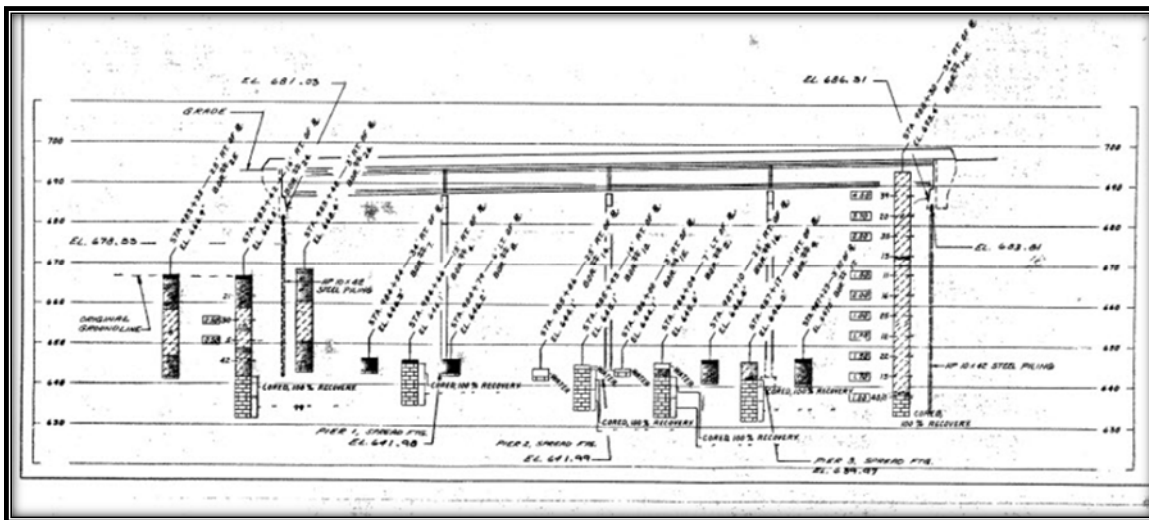


Figure 5.17: Boring log for second bridge at location 1.

5.7 X-Ray Diffraction

Sample Preparation

A ball mill, grinder, consist of hallow cylindrical and two stainless steel balls was used to grind the rock sample and prepare a powder. First the cylindrical chamber has been washed with ethanol and filled with sample of rock. Then, the cylindrical chamber placed in shaker device for 3 minutes in order to achieve consistent and fine powders. Powders have been used for XRD analysis.

X-Ray Diffraction

The samples were subjected to X-ray diffraction using Bruker D8 Discover system. The source of X-ray is Cu Ka with 40 kV primary beam. The angle of analysis (2θ) set to be between 10° to 80° and the tests have been performed at room temperature for 30 minutes on each sample. The X-ray diffractograms of the investigated bedrock samples are depicted in Figures 5.18 to 5.25. The identification of the mineralogical compositions of these rocks is also presented in each figure confirming the type of the bedrock identified in the geological description.

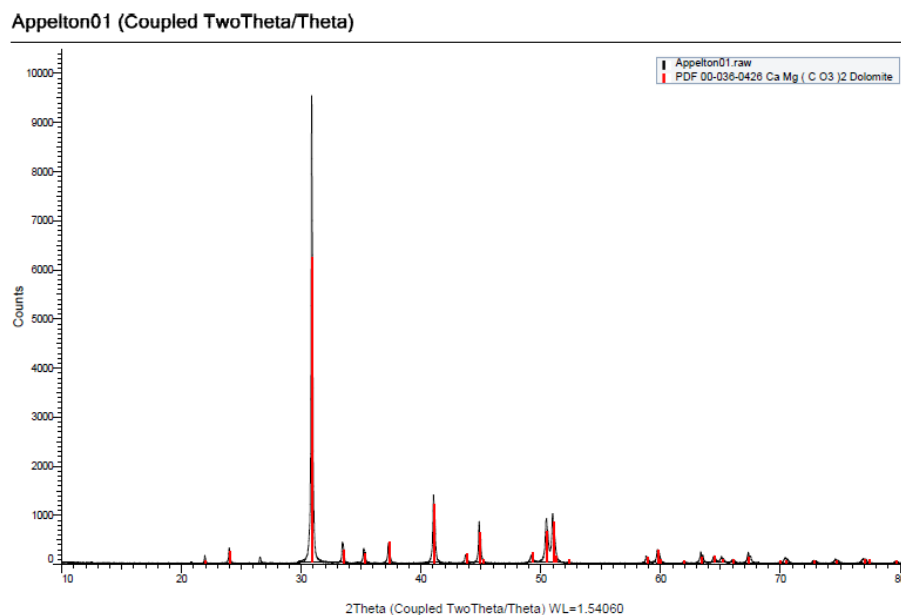


Figure 5.18: X-ray diffractogram for bedrock sample from Fox River -STH 47 (Dolomite).

Black River (Coupled TwoTheta/Theta)

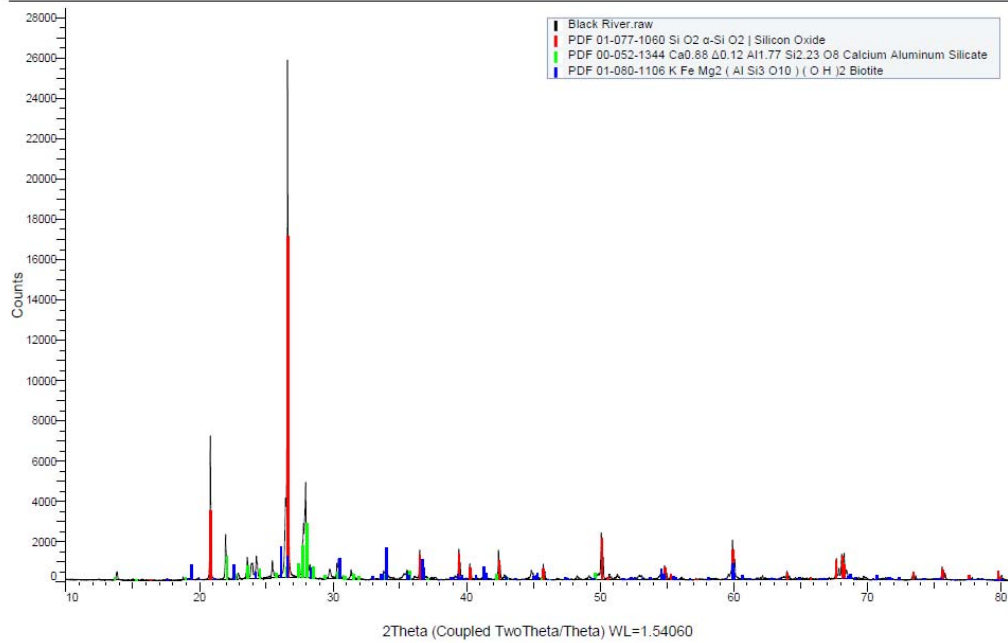


Figure 5.19: X-ray diffractogram for bedrock sample from Balck River - USH 10 (Gneiss).

3 (Coupled TwoTheta/Theta)

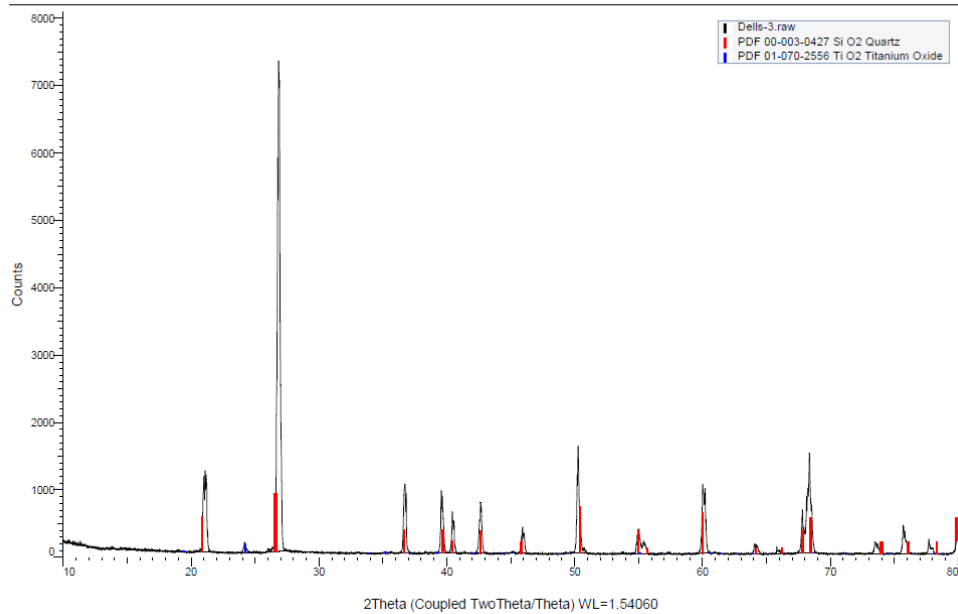


Figure 5.20: X-ray diffractogram for bedrock sample from Wisconsin River -STH 13 (Sandstone).

Manitowac (Coupled TwoTheta/Theta)

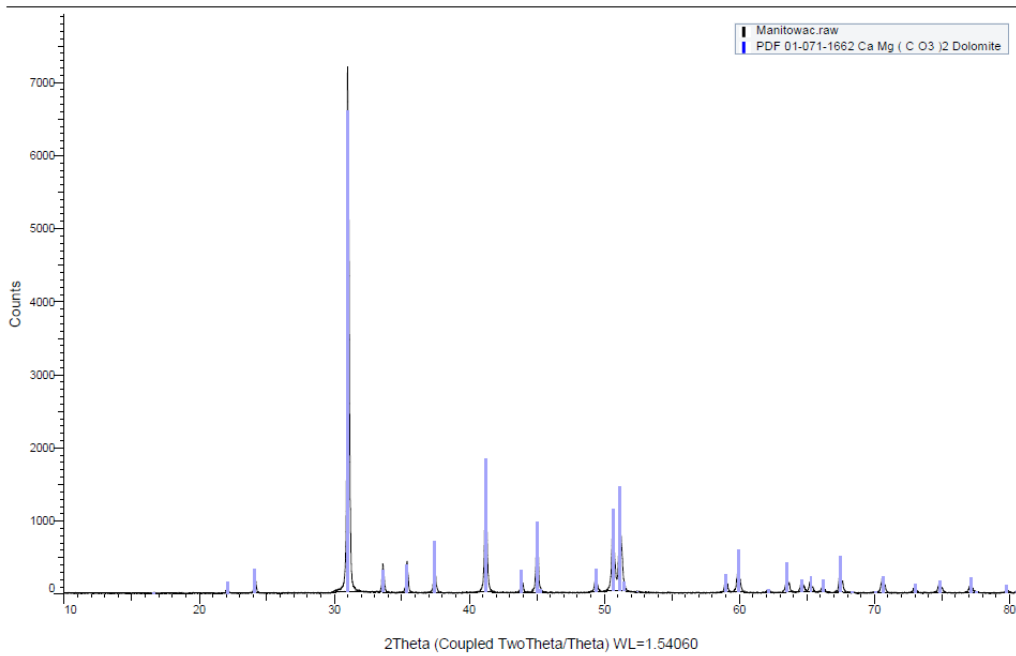


Figure 5.21: X-ray diffractogram for bedrock sample from Manitowac River -IH 43 (Dolomite).

4 (Coupled TwoTheta/Theta)

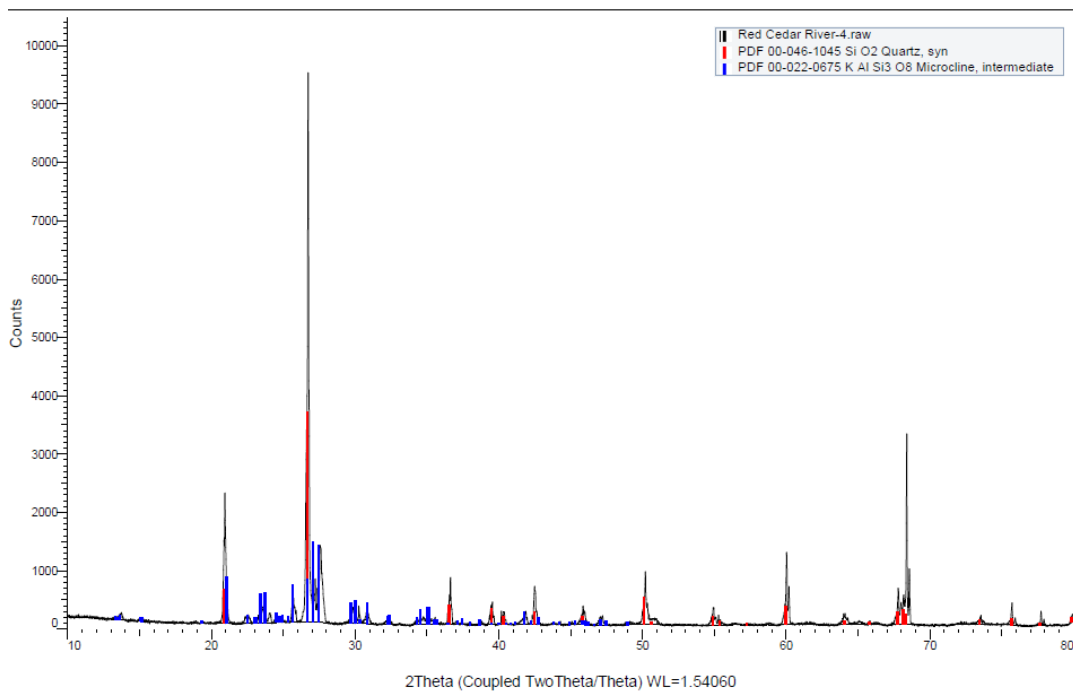


Figure 5.22: X-ray diffractogram for bedrock sample from Red Cedar River -IH 94 (Sandstone).

Spring Brook (Coupled TwoTheta/Theta)

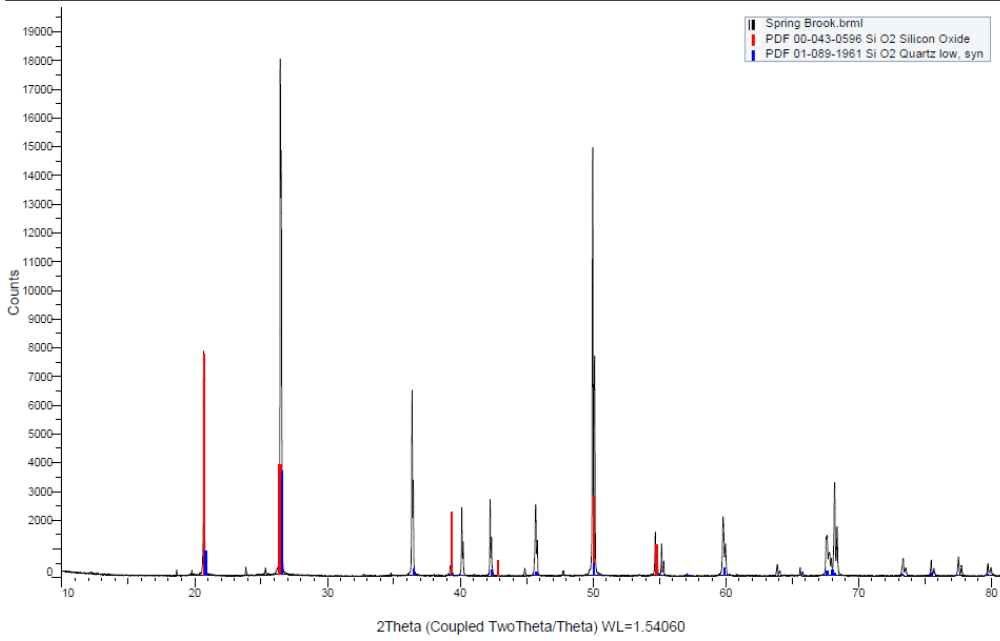


Figure 5.23: X-ray diffractogram for bedrock sample from Spring Brook -IH 90/94 (Sandstone).

2 (Coupled TwoTheta/Theta)

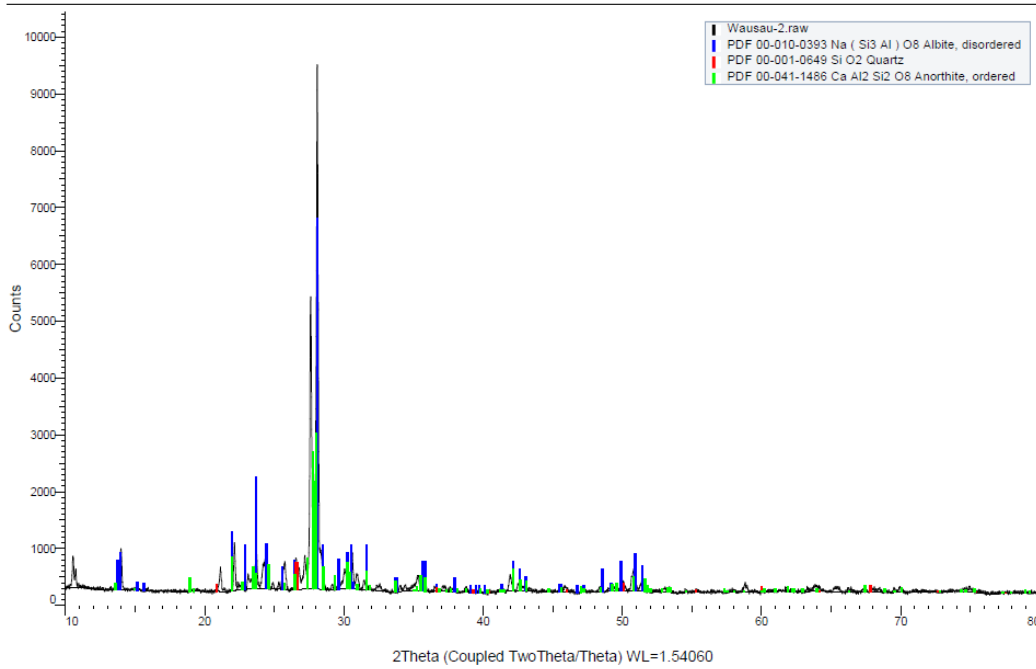


Figure 5.24: X-ray diffractogram for bedrock sample from Eau Claire River -USH 51 (Granite).

Chapter 6

Results and Analyses of Laboratory Testing

This chapter presents the results of the modified slake durability test on the collected rock samples (cores and hand-picked) from all investigated project sites. The equivalent hourly scour depth versus the equivalent hourly stream power relationship was plotted to estimate the geotechnical scour number. The abrasion number was also estimated for all investigated rock samples. Statistical analysis was also conducted to evaluate the variations in test results.

6.1 Modified Slake Durability Test Results – Sandstone

Sandstone samples from the Wisconsin River, the Red Cedar River, and Spring Brook were subjected to the modified slake durability (continuous abrasion) test as described in Chapter 2. The test was conducted on a total of 112 different core sandstone samples from the Red Cedar River, 43 (19 hand-picked and 24 core) samples from the Wisconsin River, and 12 hand-picked samples from Spring Brook. Slab hand-picked samples were also obtained from the Wisconsin River sandstone for flume tests. However, the flume tests did not yield significant results and will not be reported herein. The Red Cedar River samples had been in storage for several months. The remaining samples had been taken more recently and stored in plastic bags/glass jars, and hence had a significant portion of remaining natural moisture content. The samples were generally weak and friable, with the exception of some samples that showed some cementation. Representative images of samples from each test site are shown in Figure 6.1.

The Wisconsin River sandstone is mostly light brown, with some pink regions, as can be seen in Figures 6.1(a), 6.1(b) and 6.1(c). The outcrops at this location are of the Mount Simon Formation, which is the lowest member of the Elk Mound Group. Samples from exposed regions often show induration due to case-hardening. The Spring Brook sandstone (Figure 6.1(d)) is also from the Mount Simon formation. The Red Cedar River sandstone is from the Eau Claire formation, and is interbedded with shale as can be seen in Figure 6.1(e).

Modified slake durability tests were performed on the sandstone specimens, where initially trials were made to decide on the appropriate time increments. Given the apparent weakness of the samples and the amount of specimens' weight loss, 15 minute increments were selected for test cycle length. The tests consisted of 20 runs, for a total test length of 300 minutes. Photographs of the samples were taken after each test run. A selection of photographs showing sample degradation over the tests is shown in Figure 6.2.

As shown in Figure 6.2, the sandstone sample shows significant mass loss in the initial stages of the test. The rate of mass loss gradually decreases as the test progresses.



(a) Wisconsin River – core samples



(b) Wisconsin River – handpicked samples



(c) Wisconsin River – slab sample



(d) Spring Brook – handpicked samples



(e) Red Cedar River core samples



(f) Red Cedar River core samples

Figure 6.1: Sandstone samples from the Wisconsin River, Spring Brook, and Red Cedar River bridge sites.



(a)



(b)



(c)



(d)



(e)



(f)

Figure 6.2: Sandstone specimens from the Wisconsin River at various stages of the continuous abrasion test (modified slake durability test): (a) initial sample, (b) after 4 runs, (c) after 8 runs, (d) after 12 runs, (e) after 16 runs, and (f) after 20 runs.

Use of the modified slake durability procedure precluded the calculation of the slake durability index in accordance with the standard method (i.e. ASTM D4644). Instead, the data were analyzed per Dickenson and Baillie's (1999) method to calculate Abrasion Number (β), and the Keaton et al. (2012) method was applied to find Geotechnical Scour Number (GSN), along with statistical parameters from the equivalent hourly scour depth versus the equivalent hourly stream power (*EHSD* vs. *EHSP*) dataset. It should be noted that the geotechnical scour number was calculated considering the first test cycle, as well as without (neglecting) the first test cycle. The reason for this is to provide information on both cases since the mass loss due to edge rounding in the first test cycle is significant only when the core specimens are of disk like shape created by saw cutting.

In scour depth and stream power calculations, Keaton et al. (2012) normalized the weight of the rock specimen to an initial weight of 500 grams. ASTM C127-15 Standard Test Method for Relative Density (Specific Gravity) and Absorption of Coarse Aggregate was used to determine the saturated, surface dry (SSD) unit weight of the rock materials. Specimen weight measurements at the end of each run during the modified slake durability test were obtained, and the cumulative weight loss was used to calculate the equivalent scour depth. The energy dissipation during one-hour test run normalized to the test drum area occupied by the rock fragments was used to calculate equivalent hourly stream power. Table 6.1 presents sample calculations of equivalent stream power and equivalent scour depth from the modified slake durability test on sandstone core sample at pier 1 on the STH13 bridge on the Wisconsin River. It should be noted that for sandstone specimens the time increment is 15 minutes; therefore, the equivalent scour depth and the corresponding equivalent stream power values are for 15-minute increments. Various methods were attempted to calculate the equivalent hourly scour depth and the corresponding equivalent hourly stream power values from the 15-minute increments, which included the mean weight with time offset of 15, 30, and 45 minutes. Table 6.2 depicts the equivalent hourly scour depth and the corresponding equivalent hourly stream power values calculated based on the mean weight using offset of 15, 30, and 45 minutes and Figure 6.3 depicts the result of other attempts of calculations. The equivalent hourly scour depth and the corresponding equivalent hourly stream power values based on the mean weight were adopted herein to represent the modified slake durability test results, as shown in Figure 6.4.

The cumulative sample loss in percent of the initial mass is plotted against the cumulative test time for four Wisconsin River sandstone core samples as presented in Figure 6.5. Inspection of the figure shows after 300 minutes of modified slake durability test time, the sandstone specimens' percent loss ranged from 33 to 81%, indicating significant loss. Mass loss in the first 15 minutes of test time varied between 5.3 and 41%. Abrasion of the core fragments for each tested specimen generally indicates that sandstone degraded with different rates, but with a faster rate in the initial phases of the test. The slower abrasion rate is due to the decrease in the equivalent stream power since a threshold of stream power must be exceeded to initiate scour in degradable rocks.

Table 6.1: Sample calculations of equivalent stream power and equivalent scour depth from the modified slake durability test on sandstone core sample at pier 1 on the STH13 bridge on the Wisconsin River.

trial	Δt (min)	t_{cum} (min)	$m_{i,tot}$ (SSD) (g)	m_i (SSD) (g)	Δm_i (g)	% loss	% loss (cum.)	$m_{i,n}$ (g)	$\Delta m_{i,n}$ (g)	$m_{n,av}$ (g)	ESD_i ($m^3/m^2 \times 10^{-4}$)	ESP_i (W/m^2)
0	0	0	1800.29	525.99	0.00	0.00	0.00	500.00	0.00	500.00	0	130.76
1	15	15	1752.01	477.71	48.28	9.18	9.18	454.11	45.89	477.05	0.180686648	124.76
2	15	30	1727.68	453.38	24.33	4.63	13.80	430.98	23.13	442.54	0.091054394	115.73
3	15	45	1706.41	432.11	21.27	4.04	17.85	410.76	20.22	420.87	0.079602424	110.07
4	15	60	1686.04	411.74	20.37	3.87	21.72	391.40	19.36	401.08	0.076234197	104.89
5	15	75	1667.01	392.71	19.03	3.62	25.34	373.31	18.09	382.35	0.071219282	99.99
6	15	90	1650.33	376.03	16.68	3.17	28.51	357.45	15.86	365.38	0.062424468	95.55
7	15	105	1634.52	360.22	15.81	3.01	31.52	342.42	15.03	349.94	0.059168515	91.52
8	15	120	1620.41	346.11	14.11	2.68	34.20	329.01	13.41	335.71	0.052806309	87.80
9	15	135	1608.01	333.71	12.40	2.36	36.56	317.22	11.79	323.11	0.046406678	84.50
10	15	150	1593.88	319.58	14.13	2.69	39.24	303.79	13.43	310.50	0.052881159	81.20
11	15	165	1583.36	309.06	10.52	2.00	41.24	293.79	10.00	298.79	0.039370827	78.14
12	15	180	1572.64	298.34	10.72	2.04	43.28	283.60	10.19	288.69	0.040119322	75.50
13	15	195	1563.36	289.06	9.28	1.76	45.04	274.78	8.82	279.19	0.034730159	73.01
14	15	210	1554.49	280.19	8.87	1.69	46.73	266.35	8.43	270.56	0.033195745	70.76
15	15	225	1547.69	273.39	6.80	1.29	48.02	259.88	6.46	263.11	0.025448824	68.81
16	15	240	1540.07	265.77	7.62	1.45	49.47	252.64	7.24	256.26	0.028517652	67.02
17	15	255	1534.62	260.32	5.45	1.04	50.51	247.46	5.18	250.05	0.020396484	65.39
18	15	270	1527.77	253.47	6.85	1.30	51.81	240.95	6.51	244.20	0.025635947	63.86
19	15	285	1522.92	248.62	4.85	0.92	52.73	236.34	4.61	238.64	0.018150999	62.41
20	15	300	1517.12	242.82	5.80	1.10	53.84	230.82	5.51	233.58	0.02170635	61.09

Table 6.2: Calculated equivalent hourly scour depth (EHSD) and equivalent hourly stream power (EHSP) based on the 15-minute time increment for sandstone core sample at pier 1 on the STH13 bridge on the Wisconsin River (see Table 6.1).

Cumulative time (min.)	$EHSD_i$ (m^3/m^2)	$EHSP_i$ (W/m^2)
60	4.2758E-05	112.71
75	3.1811E-05	108.19
90	2.8948E-05	103.09
105	2.6905E-05	98.49
120	2.4562E-05	93.48
135	2.2081E-05	90.29
150	2.1126E-05	86.46
165	1.9146E-05	83.19
180	1.7878E-05	79.45
195	1.6710E-05	77.41
210	1.4742E-05	74.55
225	1.3349E-05	72.40
240	1.2189E-05	69.65
255	1.0756E-05	68.29
270	9.9999E-06	66.33
285	9.2701E-06	64.89
300	8.5890E-06	63.01

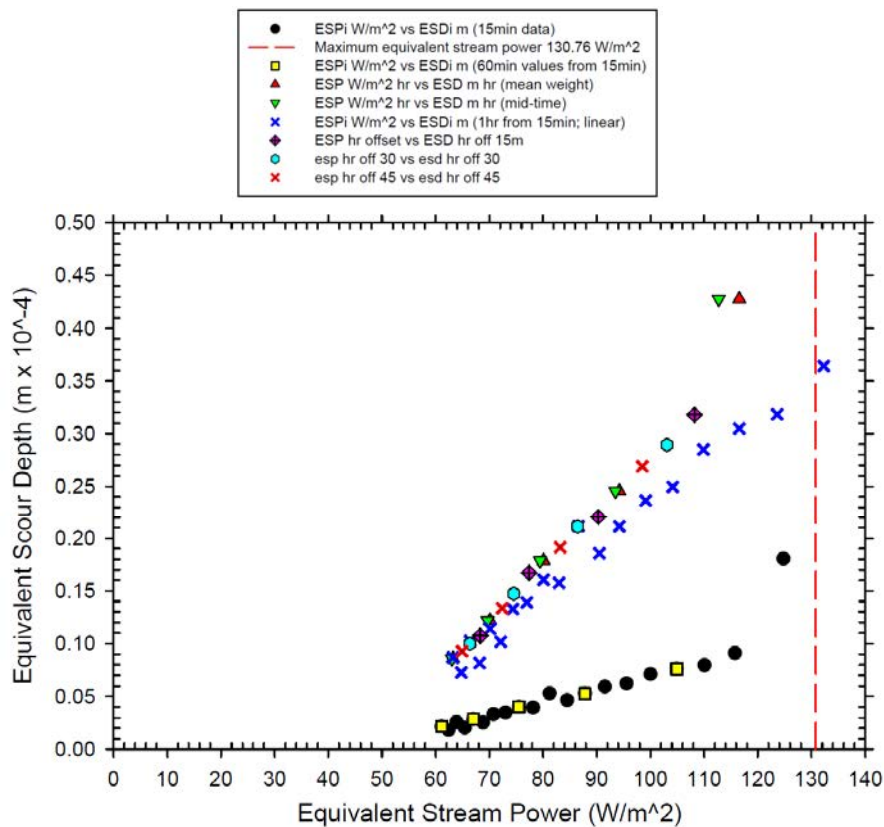


Figure 6.3: Various presentations of the equivalent scour depth versus equivalent stream power.

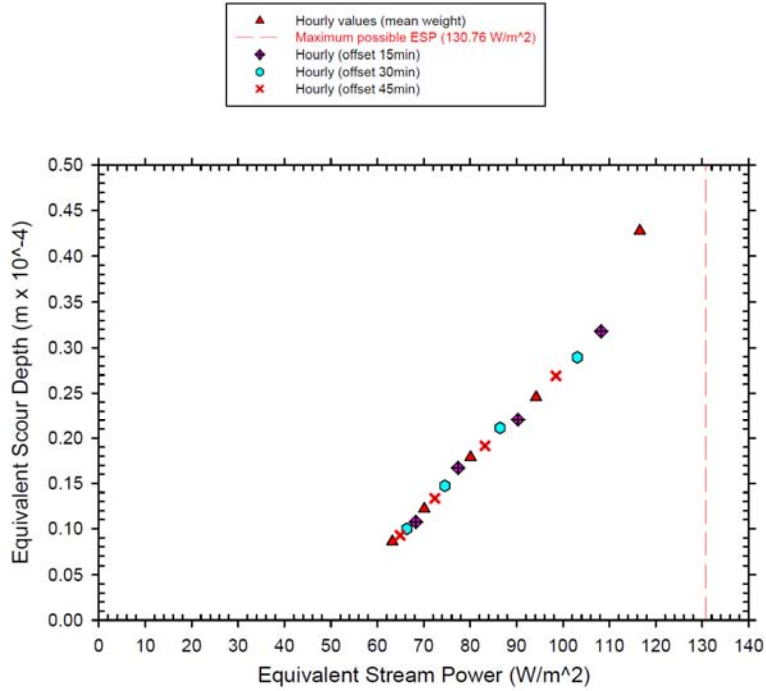


Figure 6.4: The equivalent hourly scour depth versus equivalent hourly stream power for the Wisconsin River sandstone based on the mean weight.

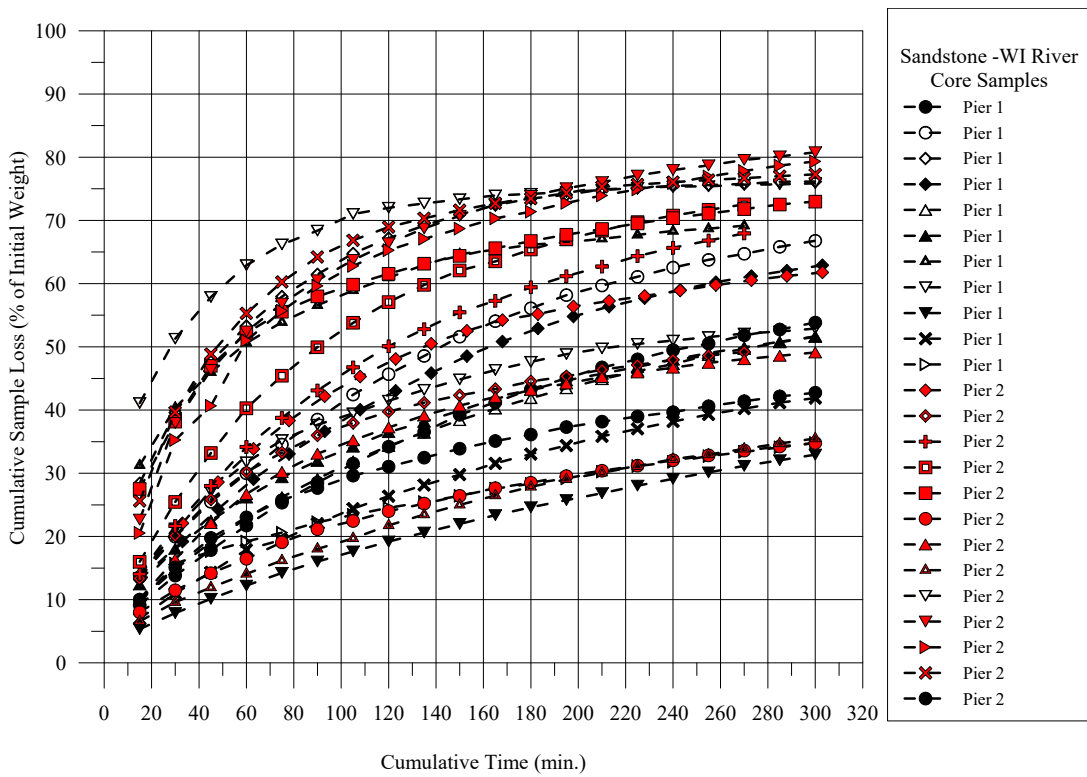


Figure 6.5: Cumulative sample loss versus cumulative test time for core sandstone samples from the Wisconsin River.

When the cumulative sample loss as percent of the initial mass is plotted against the cumulative test time on a natural logarithmic scale, the slope of the line represents the abrasion number. Data from the first four test runs were omitted from the calculations for the abrasion number. These results show a nearly linear relationship for the majority of the samples tested, which is in agreement with the observations of Dickenson and Baillie (1999). Figure 6.6 shows the cumulative sample loss as percentage of the initial mass versus natural log of cumulative test time for sandstone core specimens from the Wisconsin River. The slope of the line represents the abrasion number, which varies from 17.76 to 24.84 for the specimens presented in Figure 6.6. Large abrasion numbers result when rock fragments degrade/abrade very quickly in the modified slake durability test, and low abrasion numbers are exhibited by more durable rock which did not show significant abrasion (Keaton et al. 2012).

Figures 6.7 and 6.8 show the equivalent hourly scour depth versus equivalent hourly stream power for sandstone samples from the Wisconsin River. The geotechnical scour number for the tested samples is also shown in the figures. The geotechnical scour number is obtained by fitting a line of the test point in the equivalent hourly scour depth versus equivalent hourly stream power plot that passes through the origin i.e. $ESD = GSN \times ESP$. Moreover, a linear ($ESD = a \times ESP + b$) or power law curve ($ESD = c \times ESP^d$) can be used to obtain the intercept with the equivalent hourly stream power axis to provide the threshold of equivalent hourly stream power that is required to initiate the scour of degradable rock.

In Figure 6.7, data from the first data point was included in the calculations of the geotechnical scour number. In this case and for the data shown in Figure 6.7 (a), the geotechnical scour number varies between 2.99×10^{-7} and $4.66 \times 10^{-7} \text{ m}[\text{W} \cdot \text{m}^{-2}]^{-1}$, with coefficients of variation ranging from 0.77 to 0.96. Inspection of Figure 6.7 (a) indicates that the data can be better represented by a linear or power function rather than a linear function passing through the origin. In addition, when the linear function is used to represent the data without forcing the line to pass through the origin, the threshold of the equivalent hourly stream power required to initiate the scour is calculated as shown in Figure 6.7 (b). In this case the threshold of equivalent hourly stream power ranges between 36 and 49.1 W/m^2 . This indicates that a minimum stream power threshold must be exceeded to initiate the abrasion of the sandstone. Figure 6.7 (c) depicts the data with power function regression, with coefficients of determination varying from 0.92 to 0.99.

In Figure 6.8, data from the first data point was excluded from calculation of the geotechnical scour number, as explained earlier. For the data shown in Figure 6.8, the geotechnical scour number ranges from 2.78×10^{-7} to $3.68 \times 10^{-7} \text{ m}[\text{W} \cdot \text{m}^{-2}]^{-1}$. In addition, when the linear function is used to represent the data without forcing the line to pass through the origin, a threshold of the equivalent hourly stream power required to initiate the scour is calculated (Figure 6.8). In this case the threshold of equivalent hourly stream power ranges between 33.9 and 42.7 W/m^2 .

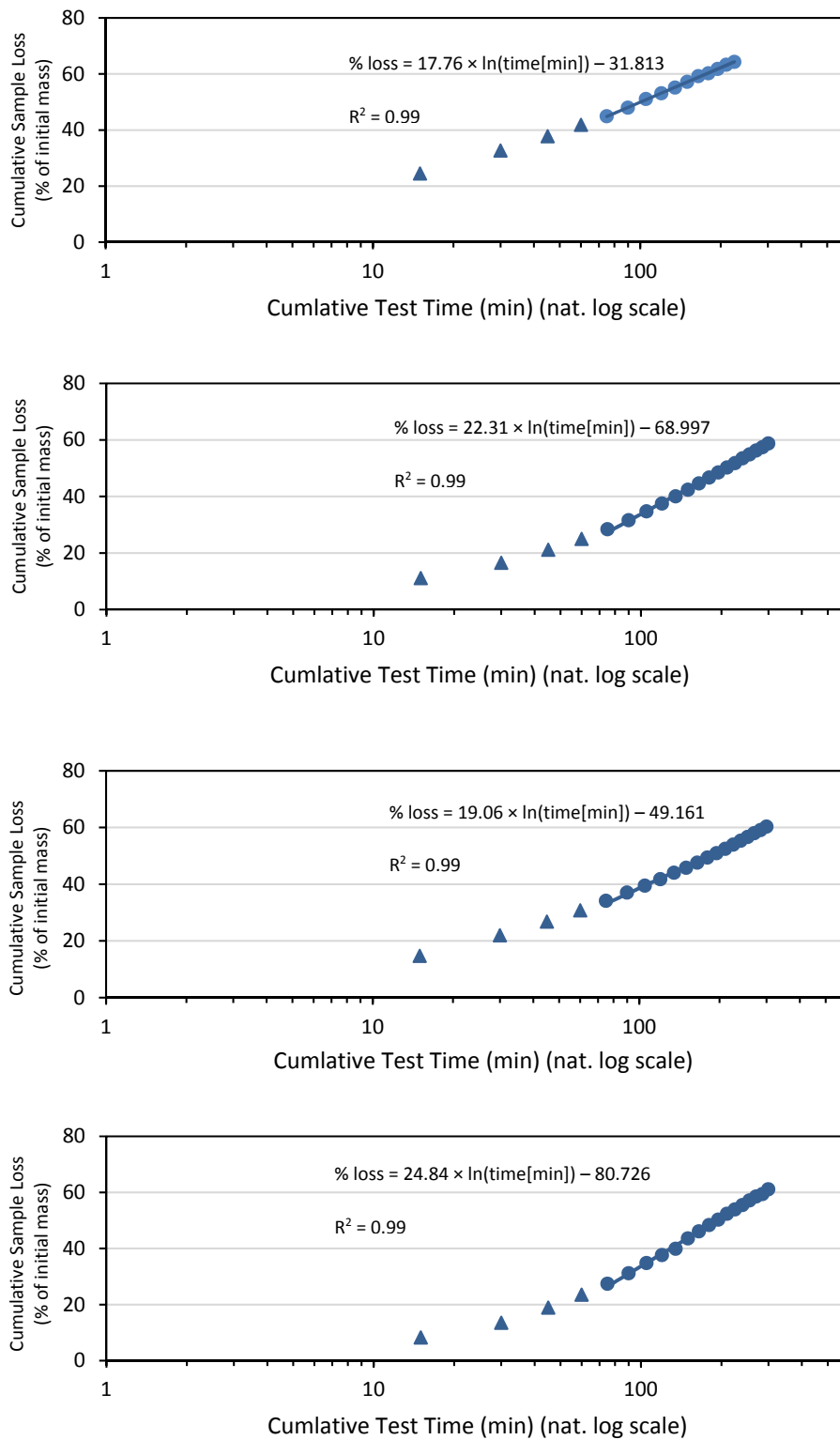
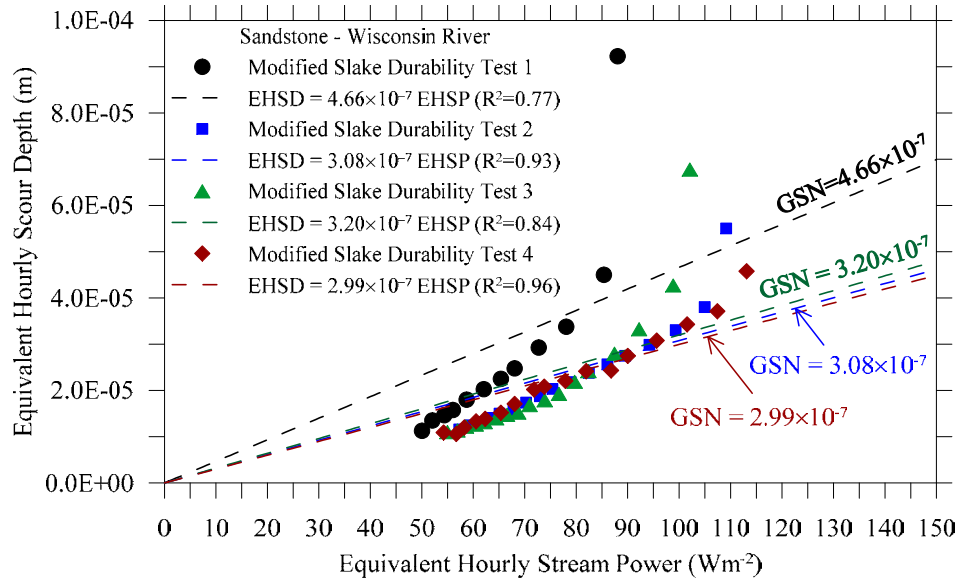
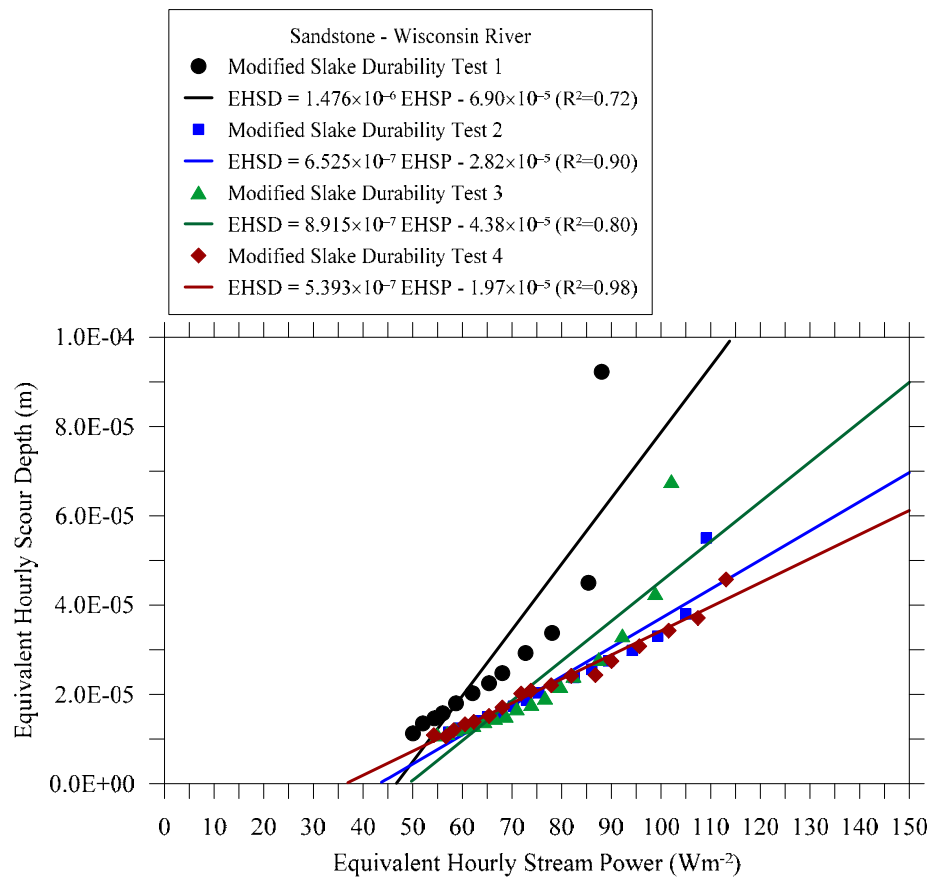


Figure 6.6: Cumulative sample loss versus cumulative test time in natural logarithmic scale for core sandstone samples from the Wisconsin River.



(a) Linear function passing through the origin



(b) Linear function

Figure 6.7: Equivalent hourly scour depth versus equivalent hourly stream power for sandstone samples from the Wisconsin River with the first point of data included.

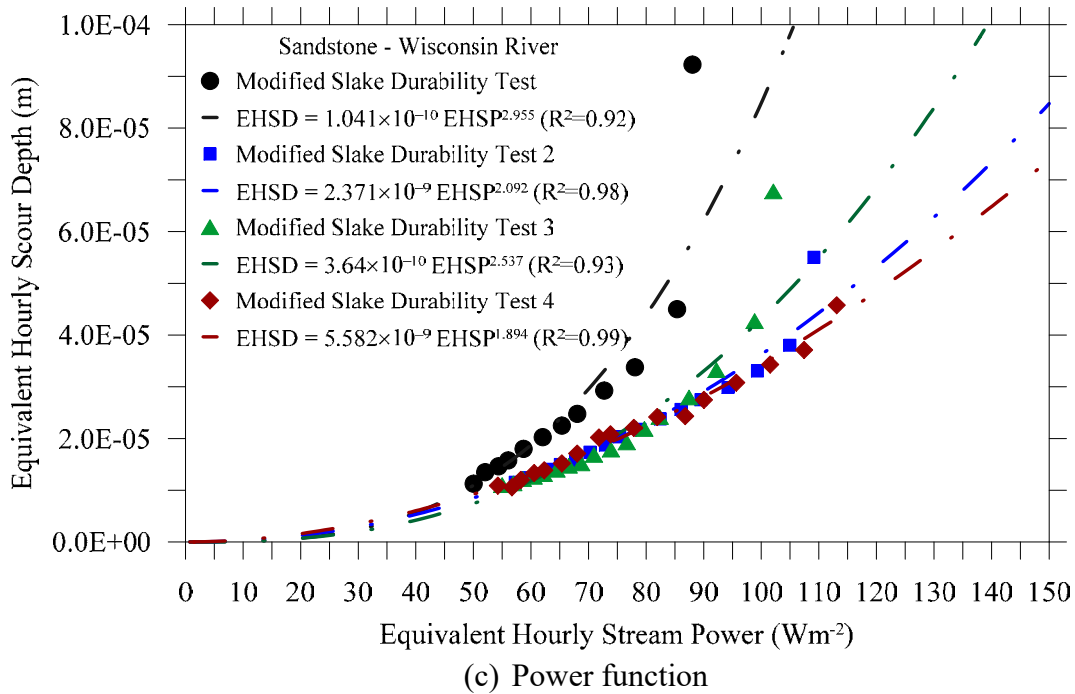


Figure 6.7 (cont.): Equivalent hourly scour depth versus equivalent hourly stream power for sandstone samples from the Wisconsin River with the first point of data included.

Tables 6.3 and 6.4 summarize the geotechnical scour number values for sandstone core and hand-picked samples from Wisconsin River with and without the first data point from the modified slake durability test. Inspection of Table 6.3 shows that the geotechnical scour number for Wisconsin River sandstone ranges between 1.14×10^{-7} and $7.31 \times 10^{-7} \text{ m}[\text{W} \cdot \text{m}^{-2}]^{-1}$ with thresholds of equivalent hourly stream power ranging between 8.1 and 84.38 W/m^2 . Examination of Table 6.4 indicates that the geotechnical scour number for Wisconsin River sandstone ranges between 9.49×10^{-8} and $5.29 \times 10^{-7} \text{ m}[\text{W} \cdot \text{m}^{-2}]^{-1}$ with thresholds of equivalent hourly stream power ranging between 9 and 80.6 W/m^2 .

Figure 6.9 shows the representation of durable and degradable rocks based on the modified slake durability tests conducted on claystone, siltstone, sandstone, and limestone as presented by Keaton (2013). Analysis of modified slake durability test results for Wisconsin River sandstone showed a wide range of geotechnical scour numbers indicating that some specimens abraded rapidly while other specimens degraded at a slower rate. For example, sandstone specimens with geotechnical number greater than $5.0 \times 10^{-7} \text{ m}[\text{W} \cdot \text{m}^{-2}]^{-1}$ abraded rapidly, which is consistent with Keaton's (2013) designation of degradable rocks show in Figure 6.9. Sandstone core specimen #39 with $\text{GSN} = 6.54 \times 10^{-7} \text{ m}[\text{W} \cdot \text{m}^{-2}]^{-1}$ and EHSP threshold of $27.34 \text{ W} \cdot \text{m}^{-2}$ to initiate abrasion is classified as rapidly degrading rock. Such characterization of this rock with the abrasion number of 17.14 is also consistent with the classification of hard to weak sandstone by Dickenson and Baillie (1999) based on the abrasion number range.

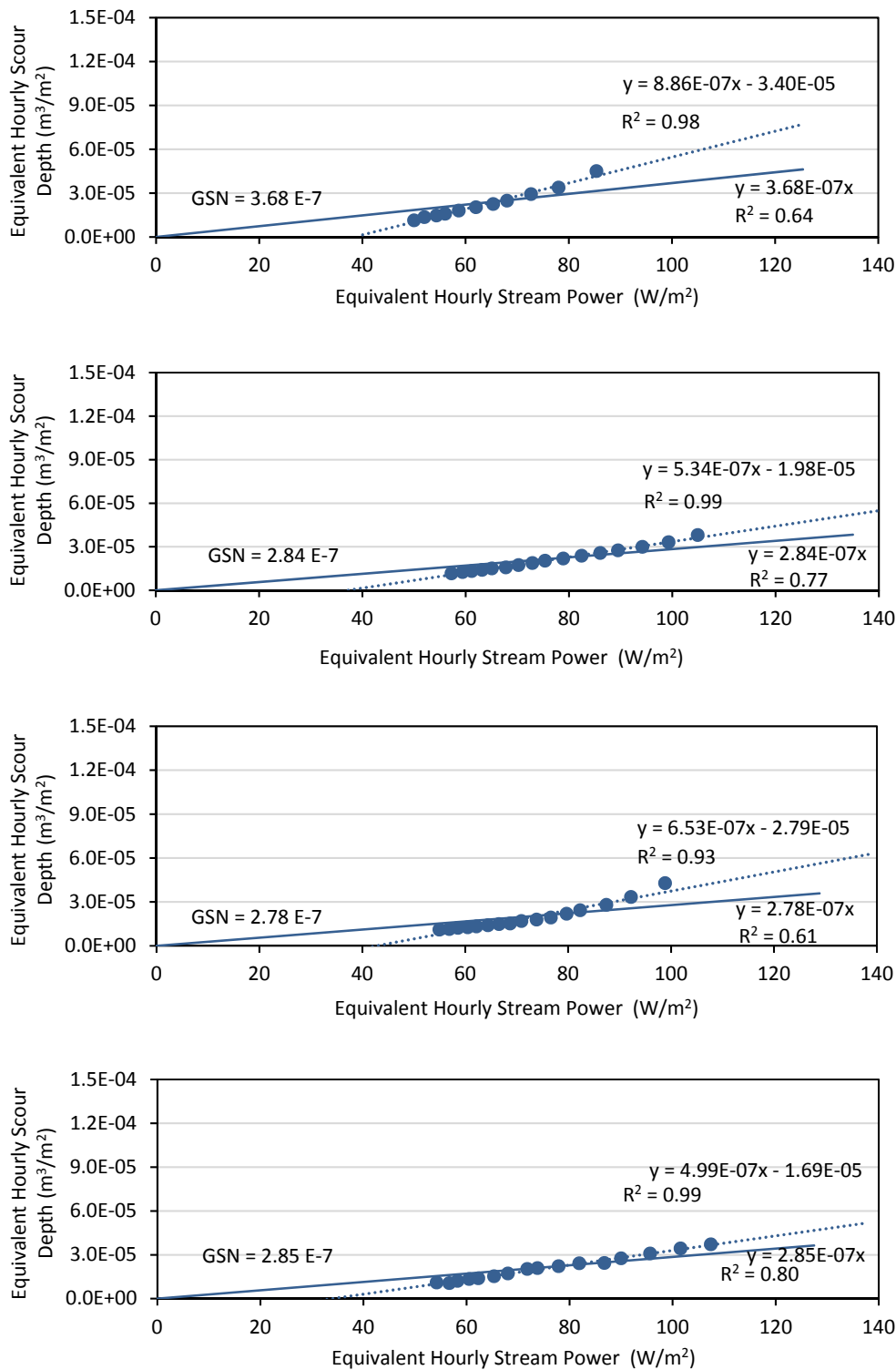


Figure 6.8: Equivalent hourly scour depth versus equivalent hourly stream power for sandstone samples from the Wisconsin River with the first point of data neglected.

Table 6.3: Geotechnical scour number as well as threshold of equivalent hourly stream power for sandstone samples from the Wisconsin River (with the first point of test data considered in the calculations).

Row #	Sample Type	Number of Test Cycles	Geotechnical Scour Number								Threshold of equivalent hourly stream power intercept (W/m ²)
			$ESD = GSN \times ESP$			$ESD = a \times ESP + b$					
			GSN (zero intercept) (m[W·m ⁻²] ⁻¹)	Standard Error of Estimate (m)	SSR	r ²	Standard Error of Estimate (m)	SSR	a (m)	b (m[W·m ⁻²] ⁻¹)	
1	Hand	10	4.993959E-07	2.03E-05	2.05E-09	0.77	1.19E-05	7.08E-10	1.987628E-06	1.179772E-04	59.36
2	Hand	15	7.265362E-07	3.18E-05	1.01E-08	0.69	2.09E-05	4.35E-09	2.858815E-06	9.978904E-05	34.91
3	Hand	15	4.661431E-07	1.85E-05	3.44E-09	0.72	1.23E-05	1.52E-09	1.476303E-06	6.889073E-05	46.66
4	Hand	20	3.080092E-07	6.99E-06	7.33E-10	0.90	3.71E-06	2.06E-10	6.525171E-07	2.819808E-05	43.21
5	Hand	20	3.199519E-07	1.11E-05	1.84E-09	0.80	6.74E-06	6.82E-10	8.915286E-07	4.382467E-05	49.16
6	Hand	20	2.994550E-07	4.96E-06	3.69E-10	0.98	1.57E-06	3.69E-11	5.392628E-07	1.968742E-05	36.51
7	Hand	20	2.621026E-07	4.06E-06	2.48E-10	0.95	1.91E-06	5.47E-11	4.576392E-07	1.682654E-05	36.77
8	Hand	20	3.797891E-07	1.19E-05	2.12E-09	0.79	7.72E-06	8.95E-10	9.081736E-07	3.483915E-05	38.36
9	Hand	20	5.586156E-07	2.68E-05	1.08E-08	0.86	8.86E-06	1.18E-09	1.270421E-06	3.825399E-05	30.11
10	Hand	20	3.549066E-07	9.18E-06	1.26E-09	0.86	5.41E-06	4.38E-10	7.627552E-07	2.904339E-05	38.08
11	Hand	20	4.142213E-07	9.86E-06	1.46E-09	0.89	5.55E-06	4.63E-10	8.330888E-07	2.787594E-05	33.46
12	Hand	20	2.864231E-07	1.50E-05	3.37E-09	0.87	6.71E-06	6.75E-10	1.202176E-06	6.866140E-05	57.11
13	Hand	20	1.944024E-07	6.42E-06	6.17E-10	0.19	6.41E-06	6.16E-10	2.132416E-07	1.726362E-06	8.10
14	Hand	20	3.284049E-07	1.78E-05	4.73E-09	0.77	9.97E-06	1.49E-09	1.530097E-06	7.550743E-05	49.35
15	Hand	20	7.307819E-07	2.24E-05	7.54E-09	0.67	1.66E-05	4.15E-09	1.796710E-06	4.184350E-05	23.29
16	Hand	20	4.075896E-07	1.33E-05	2.65E-09	0.91	5.85E-06	5.14E-10	1.096565E-06	4.422761E-05	40.33
17	Hand	20	4.066969E-07	1.25E-05	2.33E-09	0.87	6.66E-06	6.65E-10	1.008789E-06	3.891731E-05	38.58
18	Hand	20	2.702007E-07	6.99E-06	7.32E-10	0.78	4.86E-06	3.54E-10	5.758728E-07	2.454784E-05	42.63
19	Hand	20	3.060868E-07	7.79E-06	9.10E-10	0.89	4.10E-06	2.52E-10	6.798529E-07	2.887371E-05	42.47
20	Core	20	2.456043E-07	5.84E-06	5.12E-10	0.96	1.90E-06	5.42E-11	5.797360E-07	2.868839E-05	49.49
21	Core	20	3.661437E-07	7.60E-06	8.66E-10	0.95	3.09E-06	1.43E-10	7.138623E-07	2.547718E-05	35.69
22	Core	20	5.998114E-07	1.97E-05	5.85E-09	0.90	8.65E-06	1.12E-09	1.668967E-06	5.330319E-05	31.94

Table 6.3 (Cont.): Geotechnical scour number as well as threshold of equivalent hourly stream power for sandstone samples from the Wisconsin River (with the first point of test data considered in the calculations).

Row #	Sample Type	Number of Test Cycles	Geotechnical Scour Number								Threshold of equivalent hourly stream power intercept (W/m ²)
			$ESD = GSN \times ESP$			$ESD = a \times ESP + b$					
			GSN (zero intercept) (m[W·m ⁻²] ⁻¹)	Standard Error of Estimate (m)	SSR	r ²	Standard Error of Estimate (m)	SSR	a (m)	b (m[W·m ⁻²] ⁻¹)	
23	Core	20	3.276418E-07	8.05E-06	9.73E-10	0.94	3.36E-06	1.69E-10	7.228770E-07	2.997341E-05	41.46
24	Core	20	2.288556E-07	7.10E-06	7.55E-10	0.93	2.71E-06	1.11E-10	6.677160E-07	3.779082E-05	56.60
25	Core	20	2.249837E-07	9.22E-06	1.28E-09	0.87	4.27E-06	2.74E-10	8.266992E-07	5.025189E-05	60.79
26	Core	20	1.679643E-07	9.33E-06	1.30E-09	0.89	3.71E-06	2.07E-10	9.480291E-07	7.053782E-05	74.40
27	Core	20	3.395231E-07	1.29E-05	2.48E-09	0.97	3.13E-06	1.47E-10	1.084910E-06	5.344946E-05	49.27
28	Core	20	2.353940E-07	1.32E-05	2.28E-09	0.92	4.43E-06	2.55E-10	1.277752E-06	8.582630E-05	67.17
29	Core	20	4.486898E-07	2.14E-05	5.93E-09	0.79	1.20E-05	1.86E-09	1.837315E-06	7.777454E-05	42.33
30	Core	20	4.241032E-07	9.43E-06	1.16E-09	0.96	3.42E-06	1.52E-10	8.710539E-07	3.200213E-05	36.74
31	Core	20	5.168848E-07	1.22E-05	1.93E-09	0.97	3.72E-06	1.80E-10	1.081961E-06	3.666645E-05	33.89
32	Core	20	4.867273E-07	2.09E-05	6.14E-09	0.83	1.09E-05	1.68E-09	1.744952E-06	6.926045E-05	39.69
33	Core	20	1.273983E-07	6.39E-06	5.71E-10	0.89	2.46E-06	8.46E-11	7.784295E-07	6.486467E-05	83.33
34	Core	20	2.290802E-07	1.14E-05	1.81E-09	0.97	2.50E-06	8.76E-11	1.063990E-06	7.060306E-05	66.36
35	Core	20	2.485169E-07	1.34E-05	2.69E-09	0.92	4.63E-06	3.22E-10	1.200430E-06	7.433991E-05	61.93
36	Core	20	1.292141E-07	4.28E-06	2.75E-10	0.89	1.86E-06	5.21E-11	4.953762E-07	3.695375E-05	74.60
37	Core	20	1.177716E-07	3.37E-06	1.71E-10	0.88	1.56E-06	3.65E-11	4.219525E-07	3.167845E-05	75.08
38	Core	20	5.704430E-07	2.68E-05	1.08E-08	0.81	1.39E-05	2.88E-09	2.704234E-06	9.016766E-05	33.34
39	Core	20	6.546934E-07	1.70E-05	4.34E-09	0.89	8.95E-06	1.20E-09	1.410494E-06	3.856928E-05	27.34
40	Core	20	1.665670E-07	5.48E-06	4.50E-10	0.90	2.38E-06	8.52E-11	5.597710E-07	3.752972E-05	67.04
41	Core	20	1.135871E-07	7.60E-06	8.67E-10	0.60	5.22E-06	4.08E-10	8.288874E-07	6.994332E-05	84.38
42	Core	20	6.317173E-07	1.72E-05	4.43E-09	0.92	7.67E-06	8.84E-10	1.434487E-06	4.277498E-05	29.82
43	Core	20	6.439590E-07	2.10E-05	6.61E-09	0.93	7.62E-06	8.71E-10	1.814840E-06	5.715328E-05	31.49

Table 6.4: Geotechnical scour number as well as threshold of equivalent hourly stream power for sandstone samples from the Wisconsin River (with the first point of test data neglected in the calculations).

Row #	Sample Type	Number of Test Cycles	Geotechnical Scour Number								Threshold of equivalent hourly stream power intercept (W/m ²)
			$ESD = GSN \times ESP$			$ESD = a \times ESP + b$					
			GSN (zero intercept) (m[W·m ⁻²] ⁻¹)	Standard Error of Estimate (m)	SSR	r ²	Standard Error of Estimate (m)	SSR	a (m)	b (m[W·m ⁻²] ⁻¹)	
1	Hand	10	3.968362E-07	6.21E-06	1.93E-10	0.99	9.35E-07	4.37E-12	1.113834E-06	5.492481E-05	49.31
2	Hand	15	4.583757E-07	9.70E-06	9.40E-10	0.96	2.75E-06	7.58E-11	1.486900E-06	4.571017E-05	30.74
3	Hand	15	3.684911E-07	6.12E-06	3.74E-10	0.98	1.50E-06	2.25E-11	8.861443E-07	3.401438E-05	38.38
4	Hand	20	2.840421E-07	3.81E-06	2.18E-10	0.99	6.58E-07	6.49E-12	5.337477E-07	1.983312E-05	37.16
5	Hand	20	2.782676E-07	5.54E-06	4.60E-10	0.93	2.39E-06	8.57E-11	6.533396E-07	2.791581E-05	42.73
6	Hand	20	2.854425E-07	3.73E-06	2.08E-10	0.99	7.78E-07	9.08E-12	4.992587E-07	1.693537E-05	33.92
7	Hand	20	2.504210E-07	2.73E-06	1.12E-10	0.98	9.56E-07	1.37E-11	4.087208E-07	1.322551E-05	32.36
8	Hand	20	3.199803E-07	4.95E-06	3.68E-10	0.98	1.30E-06	2.53E-11	6.440165E-07	2.051504E-05	31.85
9	Hand	20	4.500575E-07	7.62E-06	8.72E-10	0.99	1.30E-06	2.55E-11	9.454807E-07	2.498719E-05	26.43
10	Hand	20	3.145374E-07	4.61E-06	3.19E-10	0.98	1.34E-06	2.71E-11	5.944214E-07	1.916099E-05	32.23
11	Hand	20	3.655787E-07	5.20E-06	4.05E-10	0.98	1.44E-06	3.11E-11	6.650067E-07	1.899309E-05	28.56
12	Hand	20	2.342039E-07	1.00E-05	1.51E-09	0.83	5.14E-06	3.96E-10	9.758428E-07	5.352913E-05	54.85
13	Hand	20	1.890994E-07	6.19E-06	5.74E-10	0.13	6.95E-06	7.25E-10	1.720411E-07	1.542459E-06	8.97
14	Hand	20	2.429012E-07	8.06E-06	9.76E-10	0.96	2.02E-06	6.12E-11	1.005420E-06	4.637316E-05	46.12
15	Hand	20	4.865736E-07	6.08E-06	5.55E-10	0.98	1.63E-06	3.99E-11	9.868074E-07	1.830741E-05	18.55
16	Hand	20	3.434315E-07	7.83E-06	9.19E-10	0.99	1.09E-06	1.78E-11	8.774403E-07	3.266782E-05	37.23
17	Hand	20	3.437346E-07	6.47E-06	6.29E-10	0.98	1.67E-06	4.19E-11	7.687887E-07	2.619647E-05	34.07
18	Hand	20	2.438413E-07	2.76E-06	1.14E-10	0.97	1.10E-06	1.82E-11	4.190656E-07	1.367955E-05	32.64
19	Hand	20	2.771362E-07	4.38E-06	2.88E-10	0.98	1.15E-06	1.98E-11	5.517733E-07	2.049911E-05	37.15
20	Core	20	2.299466E-07	4.15E-06	2.58E-10	1.00	4.00E-07	2.41E-12	5.162324E-07	2.391351E-05	46.32
21	Core	20	3.370275E-07	5.00E-06	3.75E-10	0.99	7.44E-07	8.31E-12	6.242703E-07	2.015564E-05	32.29
22	Core	20	4.572237E-07	1.12E-05	1.88E-09	1.00	1.04E-06	1.61E-11	1.287130E-06	3.859157E-05	29.98

Table 6.4 (Cont.): Geotechnical scour number as well as threshold of equivalent hourly stream power for sandstone samples from the Wisconsin River (with the first point of test data neglected in the calculations).

Row #	Sample Type	Number of Test Cycles	Geotechnical Scour Number								Threshold of equivalent hourly stream power intercept (W/m ²)
			$ESD = GSN \times ESP$			$ESD = a \times ESP + b$					
			GSN (zero intercept) (m[W·m ⁻²] ⁻¹)	Standard Error of Estimate (m)	SSR	r ²	Standard Error of Estimate (m)	SSR	a (m)	b (m[W·m ⁻²] ⁻¹)	
23	Core	20	2.983494E-07	5.12E-06	3.93E-10	1.00	5.27E-07	4.16E-12	6.168080E-07	2.325177E-05	37.70
24	Core	20	2.091112E-07	4.69E-06	3.30E-10	0.99	7.86E-07	9.27E-12	5.666321E-07	3.002095E-05	52.98
25	Core	20	1.968434E-07	5.43E-06	4.43E-10	0.97	1.30E-06	2.54E-11	6.483369E-07	3.681234E-05	56.78
26	Core	20	1.444170E-07	5.97E-06	5.34E-10	0.94	1.75E-06	4.60E-11	7.593275E-07	5.460388E-05	71.91
27	Core	20	2.950132E-07	9.39E-06	1.32E-09	0.99	1.00E-06	1.51E-11	9.656831E-07	4.614402E-05	47.78
28	Core	20	1.947192E-07	8.47E-06	9.32E-10	0.97	1.79E-06	4.18E-11	1.039649E-06	6.780826E-05	65.22
29	Core	20	3.189502E-07	9.19E-06	1.10E-09	0.99	1.29E-06	2.18E-11	1.186760E-06	4.655445E-05	39.23
30	Core	20	3.848394E-07	6.26E-06	5.09E-10	1.00	8.43E-07	9.24E-12	7.603657E-07	2.557190E-05	33.63
31	Core	20	4.590663E-07	8.54E-06	9.48E-10	0.99	1.18E-06	1.82E-11	9.606364E-07	3.053372E-05	31.78
32	Core	20	3.566464E-07	1.04E-05	1.51E-09	0.93	3.60E-06	1.82E-10	1.208060E-06	4.449302E-05	36.83
33	Core	20	1.133340E-07	4.10E-06	2.35E-10	0.96	9.49E-07	1.26E-11	6.273808E-07	5.056298E-05	80.59
34	Core	20	1.991867E-07	8.35E-06	9.75E-10	0.99	1.16E-06	1.90E-11	9.506286E-07	6.186853E-05	65.08
35	Core	20	2.065630E-07	8.84E-06	1.17E-09	0.97	1.93E-06	5.57E-11	9.894745E-07	5.946216E-05	60.09
36	Core	20	1.199647E-07	2.70E-06	1.09E-10	0.98	4.81E-07	3.48E-12	4.052605E-07	2.842381E-05	70.14
37	Core	20	1.107051E-07	2.08E-06	6.48E-11	0.97	4.95E-07	3.67E-12	3.426502E-07	2.387702E-05	69.68
38	Core	20	3.447511E-07	1.14E-05	1.96E-09	1.00	9.78E-07	1.43E-11	1.688868E-06	5.380467E-05	31.86
39	Core	20	5.295297E-07	9.56E-06	1.37E-09	0.97	2.77E-06	1.15E-10	1.104133E-06	2.725366E-05	24.68
40	Core	20	1.532875E-07	3.41E-06	1.74E-10	0.99	5.63E-07	4.76E-12	4.585690E-07	2.863671E-05	62.45
41	Core	20	9.493763E-08	2.85E-03	1.22E-04	0.78	1.85E-06	5.13E-11	5.110361E-07	4.031638E-05	78.89
42	Core	20	5.210933E-07	1.10E-05	1.83E-09	0.96	3.54E-06	1.87E-10	1.183650E-06	3.285232E-05	27.76
43	Core	20	4.928685E-07	1.32E-05	2.60E-09	0.99	1.79E-06	4.82E-11	1.472033E-06	4.430478E-05	30.10

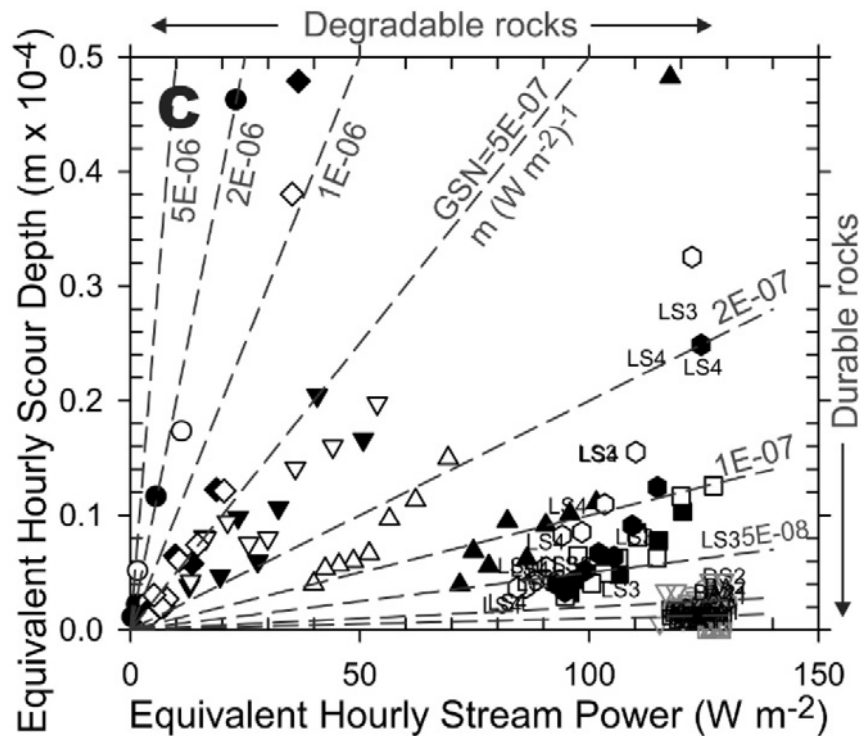


Figure 6.9: Degradable and durable rock characterization based on modified slake durability test (Keaton 2013).

It should be noted that sandstone of the Wisconsin River is considered a degradable rock based on the modified slake durability test, but the actual scour depth calculations depend on the stream power of the Wisconsin River and the gravel/bedload cover around the bridge foundation. Without the analyses of the actual flow data for the river near of the bridge foundation, the modified slake durability test results cannot be used to estimate scour of rock. Such analysis is presented in detail in Chapter 7.

Table 6.5 presents the abrasion number values for sandstone core and hand-picked samples from the Wisconsin River from the modified slake durability test. The abrasion number is obtained by fitting a line to the cumulative loss of specimen as percent of initial mass versus the cumulative test time in natural logarithmic scale i.e. $CSL = \beta \ln(t) + b$. Inspection of Table 6.5 shows that the abrasion number for Wisconsin River sandstone ranges between 6.24 and 24.84. Dickenson and Baillie (1999) found the range of abrasion numbers for their sandstone samples to be from 10-20, with a lower abrasion number value indicating more abrasion resistance.

The modified slake durability test results on the Red Cedar River and Spring Brook sandstone are in general similar to those of the Wisconsin River sandstone. These results are presented in Appendix B.

Table 6.5: The abrasion number values for sandstone core and hand-picked samples from the Wisconsin River from the modified slake durability test.

Row #	Sample Type	Number of Test Cycles	Abrasion Number: $CSL = \beta \ln(t) + b$				
			β	b	r^2	Standard Error of Estimate	SSR
1	Hand	10	16.57	-29.26	1.00	0.14	0.08
2	Hand	15	10.78	17.82	0.99	0.38	1.30
3	Hand	15	17.75	-31.81	1.00	0.18	0.29
4	Hand	20	22.31	-69.00	1.00	0.40	2.30
5	Hand	20	19.05	-49.16	1.00	0.50	3.54
6	Hand	20	24.84	80.73	1.00	0.45	2.88
7	Hand	20	24.39	-82.39	1.00	0.65	5.86
8	Hand	20	20.20	-45.49	1.00	0.36	1.78
9	Hand	20	17.95	-23.05	0.99	0.88	10.92
10	Hand	20	22.17	-59.13	1.00	0.41	2.31
11	Hand	20	22.66	-57.01	1.00	0.55	4.30
12	Hand	20	14.21	-23.22	0.99	0.59	4.88
13	Hand	20	23.53	-84.64	1.00	0.69	6.58
14	Hand	20	12.10	-4.25	0.99	0.44	2.68
15	Hand	20	13.35	9.53	0.99	0.68	6.42
16	Hand	20	17.82	-31.67	0.99	0.64	5.76
17	Hand	20	19.15	-38.67	1.00	0.24	0.84
18	Hand	20	21.93	-66.26	0.99	0.72	7.22
19	Hand	20	22.00	-63.44	1.00	0.36	1.82
20	Core	20	21.11	-66.47	1.00	0.30	1.23
21	Core	20	23.77	-67.92	1.00	0.51	3.59
22	Core	20	12.88	4.90	0.94	1.48	30.76
23	Core	20	22.68	-65.77	1.00	0.46	3.01
24	Core	20	18.61	-54.65	1.00	0.21	0.59
25	Core	20	16.34	-41.63	1.00	0.20	0.57
26	Core	20	12.41	-28.21	1.00	0.16	0.35
27	Core	20	16.87	-33.53	0.99	0.89	11.11
28	Core	20	12.22	-19.02	1.00	0.18	0.44
29	Core	20	11.73	4.50	0.97	0.78	8.50
30	Core	20	22.86	-59.53	1.00	0.27	0.98
31	Core	20	21.01	-44.10	0.99	0.62	5.40
32	Core	20	12.62	1.16	1.00	0.06	0.05
33	Core	20	11.44	-30.63	1.00	0.21	0.63
34	Core	20	13.66	-28.18	1.00	0.39	2.10

Table 6.5 (Cont.): The abrasion number values for sandstone core and hand-picked samples from the Wisconsin River from the modified slake durability test.

Row #	Sample Type	Number of Test Cycles	Abrasion Number: $CSL = \beta \ln(t) + b$				
			β	b	r^2	Standard Error of Estimate	SSR
35	Core	20	13.20	-21.49	0.99	0.50	3.56
36	Core	20	14.39	-46.80	1.00	0.32	1.48
37	Core	20	13.76	-46.33	0.99	0.58	4.64
38	Core	20	6.24	41.21	0.91	0.87	10.71
39	Core	20	17.14	-15.94	0.99	0.71	7.14
40	Core	20	16.54	-52.584	1.00	0.31	1.37
41	Core	20	10.27	-24.47	0.99	0.47	3.05
42	Core	20	16.50	-14.35	1.00	0.46	2.95
43	Core	20	11.55	12.78	0.96	1.04	15.05

6.2 Modified Slake Durability Test Results of Dolostone and Gneiss

Modified slake durability tests were conducted on dolostone from Fox River and Manitowoc River as well as on gneiss from Black River. Figures 6.10 and 6.11 show pictures of dolostone core specimens (Fox River) and hand-picked gneiss (Black River) at various times during the modified slake durability test, respectively.

The results of modified slake durability tests on Fox River dolostone are presented in Figure 6.12 and plotted as equivalent hourly scour depth versus equivalent hourly stream power neglecting initial test data point. Figure 6.13 shows the results of modified slake durability tests on Black River gneiss. In both figures, the geotechnical scour number as well as the stream power threshold are obtained from the slope and intercept.

Figure 6.14 depicts the relationship between cumulative sample loss and cumulative test time for dolostone samples from Fox River and for gneiss from Black River. The total sample losses for these rocks are small compared with sandstone. Table 6.6 presents the geotechnical scour number for dolostone samples from Fox River, which ranges between 1.64×10^{-9} and 6.53×10^{-9} ($m[W \cdot m^{-2}]^{-1}$). This range characterizes such rock within the durable rock range based on Keaton (2013). The geotechnical scour number for Black River gneiss samples is presented in Table 6.7 and varies between 5.39×10^{-9} and 7.39×10^{-9} ($m[W \cdot m^{-2}]^{-1}$). Tables 6.8 summarizes the abrasion number for dolostone samples from Fox River, which varies between 0.85 and 3.33, while Table 6.9 presents the abrasion number for gneiss samples from Black River with a range from 2.63 to 3.44, which clearly classifies these rocks under the category of basalt and very hard rocks according to Dickenson and Baillie (1999).



Figure 6.10: Dolostone specimens (core samples) from the Fox River at various stages of the continuous abrasion test (modified slake durability test).



Figure 6.11: Gneiss specimens (hand-picked samples) from the Black River at various stages of the continuous abrasion test (modified slake durability test).

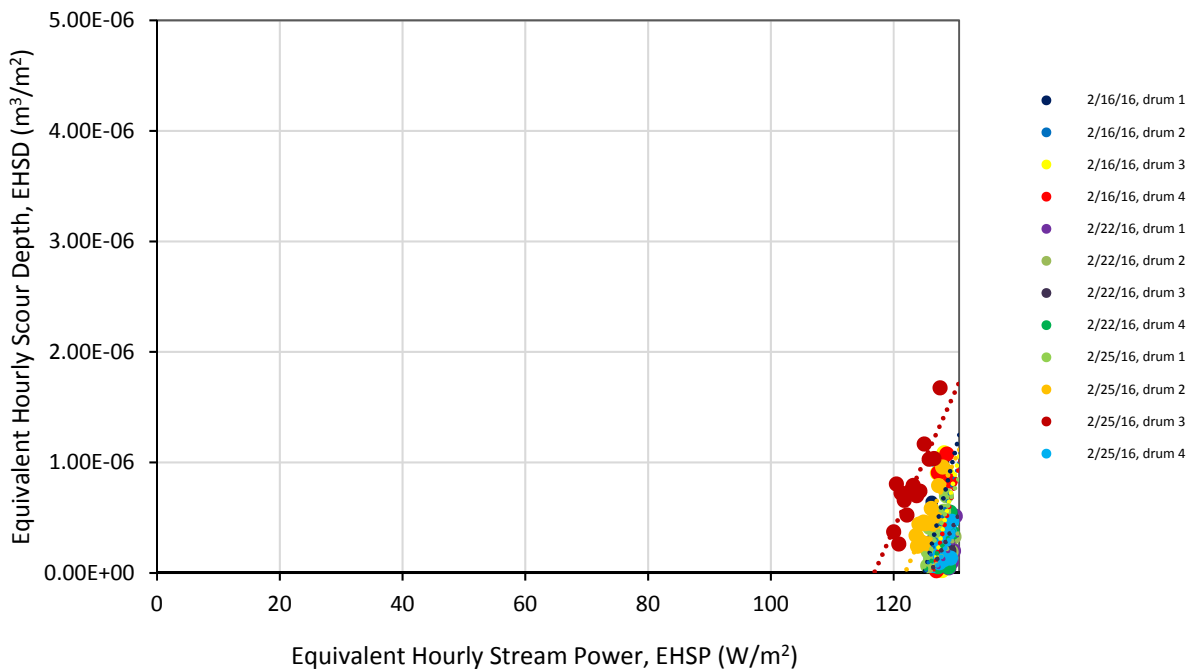
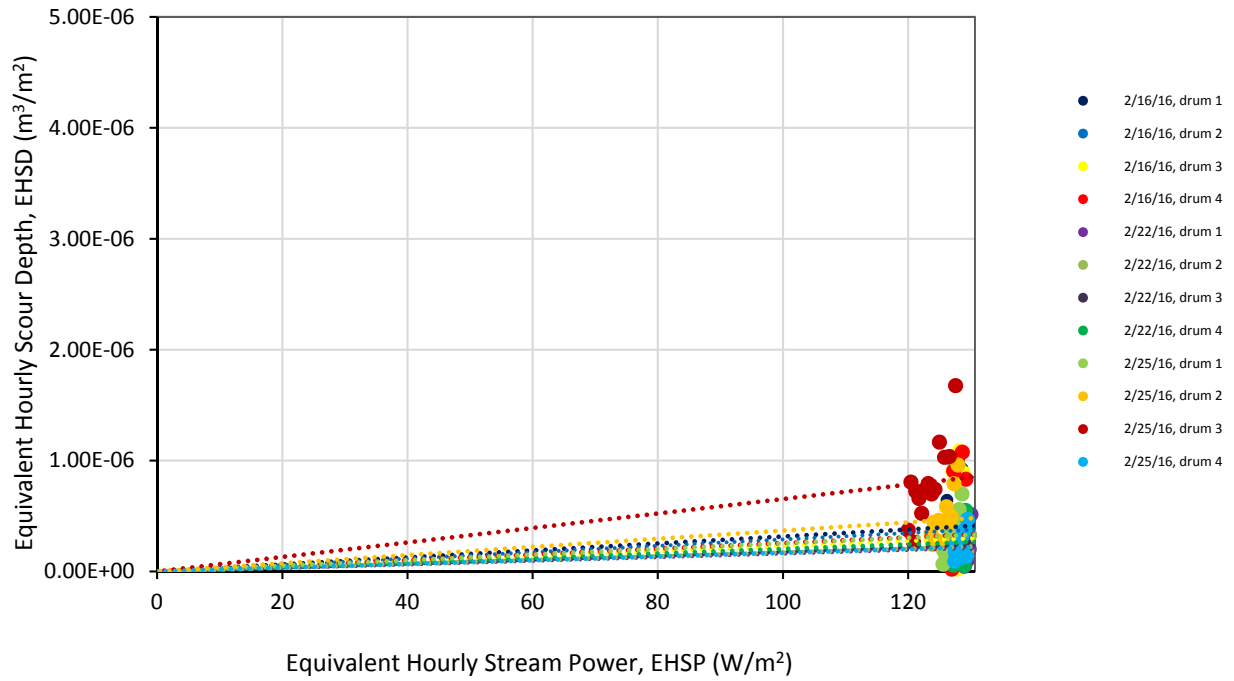


Figure 6.12: Results of modified slake durability test plotted as equivalent hourly scour depth versus equivalent hourly stream power for the Fox River dolostone core specimens (neglecting initial data point).

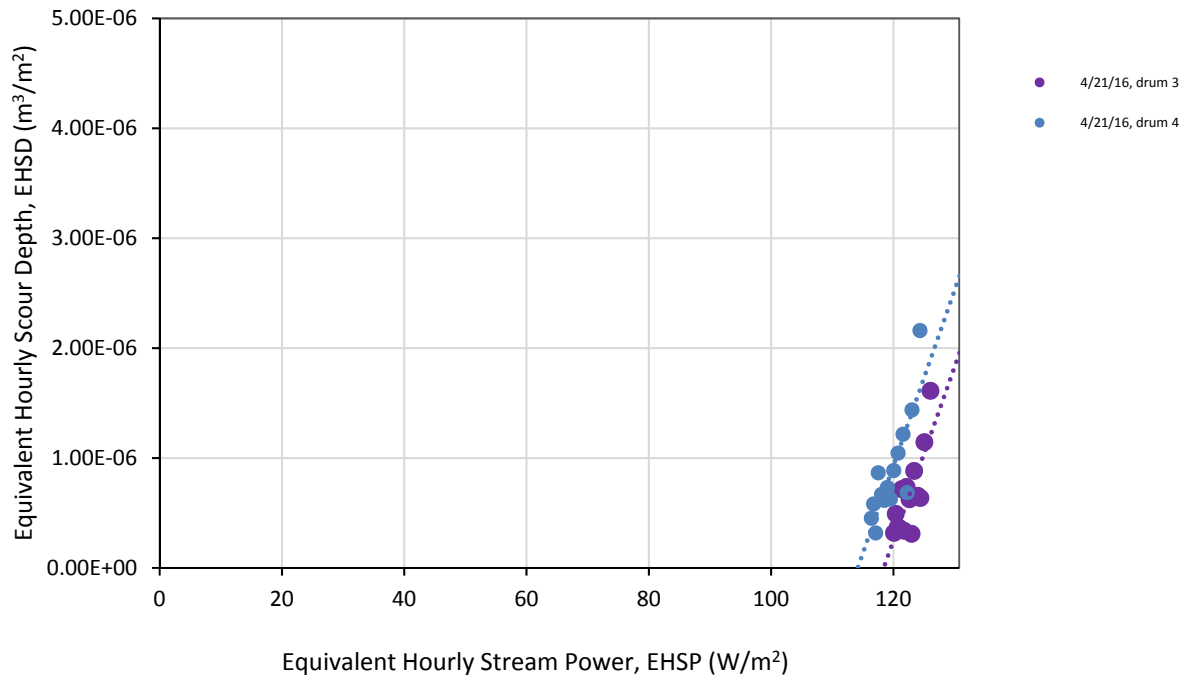
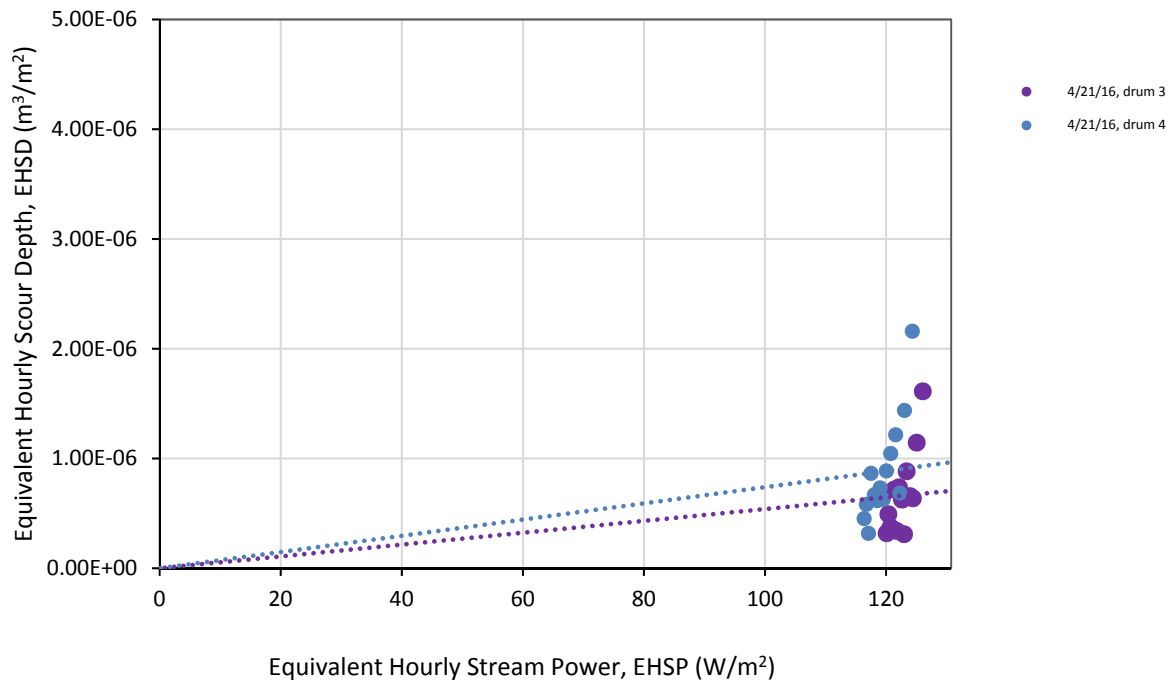
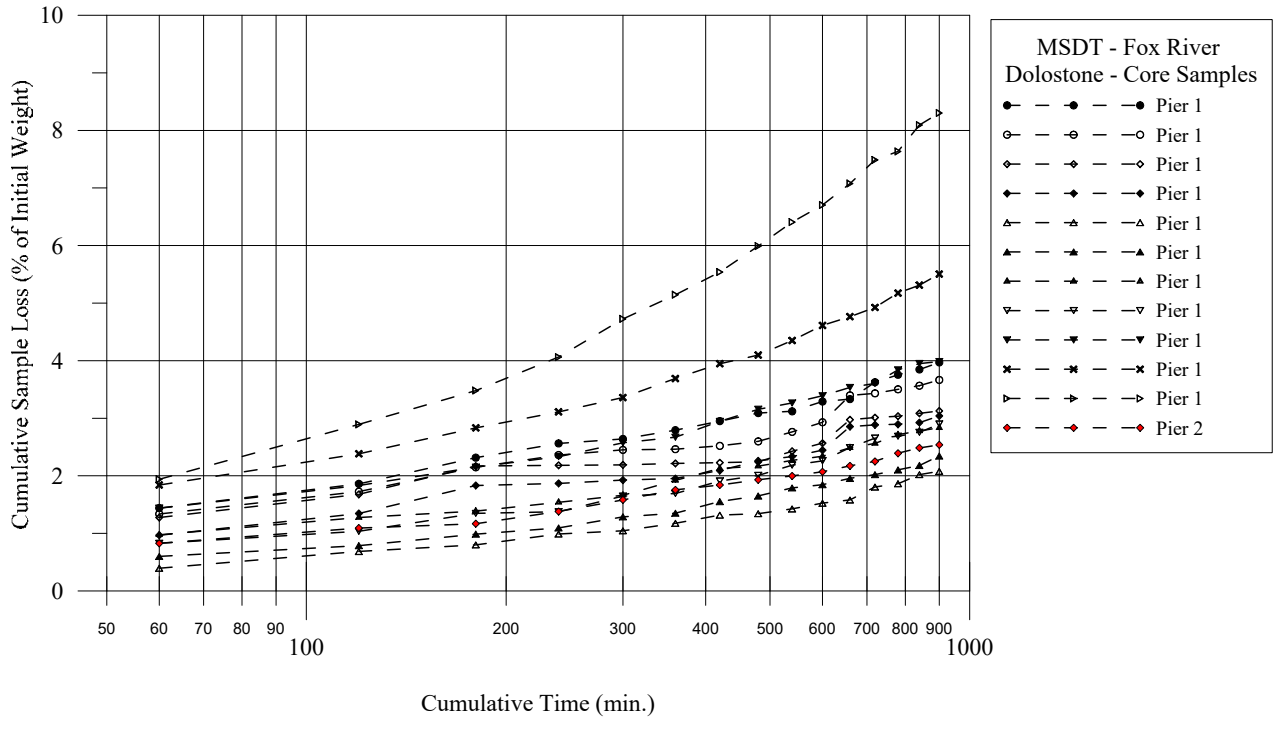
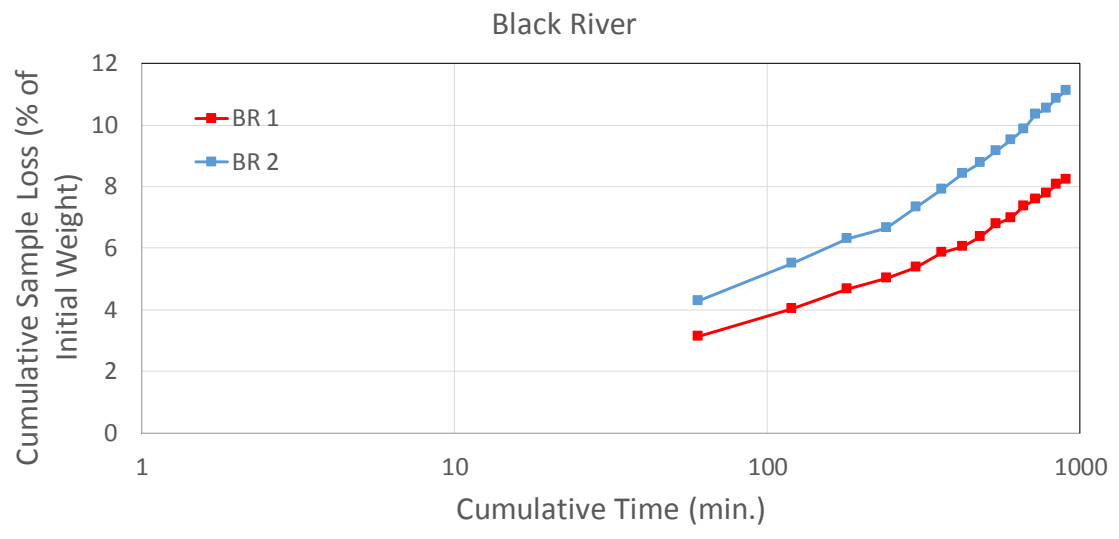


Figure 6.13: Results of modified slake durability test plotted as equivalent hourly scour depth versus equivalent hourly stream power for the Black River gneiss hand-picked specimens (neglecting initial data point).



(a) Dolomite



(b) Gneiss

Figure 6.14: Cumulative sample loss for dolostone and gneiss.

Table 6.6: Geotechnical scour number for dolostone samples from the Fox River.

Sample Type	Number of Test Cycles	Geotechnical Scour Number								Threshold of equivalent hourly stream power intercept (W/m ²)
		$ESD = GSN \times ESP$			$ESD = a \times ESP + b$					
		GSN (zero intercept) (m[W·m ⁻²] ⁻¹)	Standard Error of Estimate (m)	SSR	r ²	Standard Error of Estimate (m)	SSR	a (m)	b (m[W·m ⁻²] ⁻¹)	
Core	15	3.15E-09	2.96E-07	1.05E-12	0.43	2.24E-07	6.02E-13	2.21E-07	-2.76E-05	125.04
Core	15	2.89E-09	3.46E-07	1.44E-12	0.20	3.11E-07	1.16E-12	1.80E-07	-2.25E-05	125.14
Core	15	2.29E-09	3.96E-07	1.88E-12	0.17	3.62E-07	1.57E-12	2.46E-07	-3.10E-05	126.38
Core	15	2.56E-09	3.63E-07	1.58E-12	0.21	3.23E-07	1.25E-12	2.21E-07	-2.79E-05	126.33
Core	15	1.64E-09	1.38E-07	2.29E-13	0.17	1.27E-07	1.92E-13	9.15E-08	-1.16E-05	126.69
Core	15	1.71E-09	1.00E-07	1.21E-13	0.27	8.65E-08	8.98E-14	7.80E-08	-9.82E-06	125.89
Core	15	1.83E-09	1.41E-07	2.37E-13	0.36	1.13E-07	1.54E-13	1.15E-07	-1.44E-05	125.99
Core	15	2.04E-09	1.68E-07	3.37E-13	0.14	1.56E-07	2.93E-13	7.59E-08	-9.47E-06	124.72
Core	15	2.53E-09	1.85E-07	4.11E-13	0.57	1.23E-07	1.82E-13	1.42E-07	-1.77E-05	124.59
Core	15	3.68E-09	2.08E-07	5.21E-13	0.68	1.21E-07	1.75E-13	1.26E-07	-1.54E-05	121.85
Core	15	6.53E-09	3.52E-07	1.49E-12	0.70	1.99E-07	4.73E-13	1.25E-07	-1.45E-05	116.83
Core	15	1.68E-09	1.20E-07	1.72E-13	0.43	9.06E-08	9.84E-14	1.20E-07	-1.52E-05	126.56

Table 6.7: Geotechnical scour number for Gneiss samples from the Black River.

Sample Type	Number of Test Cycles	Geotechnical Scour Number								Threshold of equivalent hourly stream power intercept (W/m ²)
		$ESD = GSN \times ESP$			$ESD = a \times ESP + b$					
		GSN (zero intercept) (m[W·m ⁻²] ⁻¹)	Standard Error of Estimate (m)	SSR	r ²	Standard Error of Estimate (m)	SSR	a (m)	b (m[W·m ⁻²] ⁻¹)	
Hand	15	5.39E-09	3.64E-07	1.59E-12	0.63	2.27E-07	6.19E-13	1.58E-07	-1.87E-05	118.41
Hand	15	7.39E-09	4.65E-07	2.60E-12	0.69	2.66E-07	8.48E-13	1.59E-07	-1.82E-05	114.16

Table 6.8: Abrasion number for dolostone samples from the Fox River.

Sample Type	Number of Test Cycles	Abrasion Number: $CSL = \beta \ln(t) + b$				
		β	b	r^2	Standard Error of Estimate	SSR
Core	15	1.21	-4.35	0.96	0.09	0.08
Core	15	1.30	-5.20	0.90	0.16	0.24
Core	15	1.04	-2.53	0.87	0.15	0.20
Core	15	1.14	-4.75	0.94	0.11	0.10
Core	15	0.93	-4.33	0.95	0.08	0.06
Core	15	0.94	-4.13	0.99	0.04	0.02
Core	15	1.02	-4.14	0.99	0.05	0.02
Core	15	1.21	-5.38	0.98	0.07	0.05
Core	15	1.35	-5.23	0.99	0.05	0.03
Core	15	1.93	-7.72	0.99	0.07	0.04
Core	15	3.33	-14.47	0.99	0.12	0.13
Core	15	0.85	-3.29	0.98	0.05	0.02

Table 6.9: Abrasion number for Gneiss samples from the Black River.

Sample Type	Number of Test Cycles	Abrasion Number: $CSL = \beta \ln(t) + b$				
		β	b	r^2	Standard Error of Estimate	SSR
Hand	15	2.63	-9.72	0.96	0.09	0.08
Hand	15	3.44	-12.36	0.98	0.09	0.08

6.3 Eau Claire River Granite

Figure 6.15 depicts a picture of granite sample from coring at Eau Claire River. The appearance of the samples suggests that the rock has undergone significant weathering. The samples were heavily jointed, and appeared to be bonded by clay particles, likely kaolinite (a byproduct of chemical weathering of feldspar-bearing rock such as granite).



Figure 6.15: Intact rock from core samples (note heavy, erratic jointing)

Few core pieces were suitable for the modified slake durability test, as the specified mass of a single sample piece is required to be 40 -60 grams (ASTM D4644). Two samples of rock for the modified slake durability test, prepared in accordance with ASTM D4644, are shown in Figure 6.16.

Unweathered granite is a durable and hard rock, and is expected to show only small losses in the modified slake durability test. Several processes occur as granite becomes weathered. Feldspar is hydrolyzed into kaolinite and sodium or potassium ions, biotite and amphibole are hydrolyzed into clay minerals and undergo oxidation to form iron oxides, while quartz resists weathering and is carried away from the granite as sand grains. The sample pieces fragmented heavily after a single 1-hour test cycle due to the heavily jointed nature of the samples. Figure 6.17 shows the samples before and after the first modified slake durability test run.

Granite type rock, as mentioned previously, tends to be very tough and durable. For this reason, hour-long test cycles were chosen for the modified slake durability test. Figure 6.17 shows the sample degradation through the test. It can be seen that the larger pieces continue to break down into smaller pieces throughout the test procedure. This rapid degradation was not reflected in the measured mass losses, as the fragments tended to remain within the drum. As a

result, the geotechnical scour number calculated from the test data suggests that the sample is durable rock. Regression statistics for the samples are shown in Tables 6.10 and 6.11.



Figure 6.16: Samples of rock for use in modified slake durability test procedure.



(a)



(b)



(c)



(d)

Figure 6.17: Samples before first test cycle [(a) and (b)], and after first cycle [(c) and (d)]

Table 6.10: Geotechnical scour number for granite samples from the Eau Claire River.

Sample Type	Number of Test Cycles	Geotechnical Scour Number								Threshold of equivalent hourly stream power intercept (W/m ²)
		$ESD = GSN \times ESP$			$ESD = a \times ESP + b$					
		GSN (zero intercept) (m[W·m ⁻²] ⁻¹)	Standard Error of Estimate (m)	SSR	r ²	Standard Error of Estimate (m)	SSR	a (m)	b (m[W·m ⁻²] ⁻¹)	
Core	15	2.53E-08	1.19908E-06	1.73E-11	0.91	4.128E-07	2.04E-12	1.73E-07	-1.54E-05	89.02
Core	15	2.65E-08	1.69025E-06	3.43E-11	0.88	6.391E-07	4.90E-12	2.52E-07	-2.22E-05	88.06
Core	20	1.14E-08	7.04614E-07	8.44E-12	0.83	2.989E-07	1.52E-12	2.30E-07	-1.56E-05	67.73
Core	20	9.82E-09	6.22034E-07	6.58E-12	0.76	3.187E-07	1.73E-12	2.05E-07	-1.54E-05	74.79

Table 6.11: Abrasion number for granite samples from the Eau Claire River.

Sample Type	Number of Test Cycles	Abrasion Number: $CSL = \beta \ln(t) + b$				
		β	b	r ²	Standard Error of Estimate	SSR
Core	15	9.71	-38.17	1.00	0.08	0.05
Core	15	7.98	-22.93	1.00	0.58	3.05
Core	20	2.91	31.44	0.99	0.10	0.15
Core	20	3.05	25.08	1.00	0.09	0.10

The geotechnical scour number calculated for the samples ranges between 9.82×10^{-9} and $2.65 \times 10^{-8} \text{ m} \cdot [\text{W} \cdot \text{m}^{-2}]^{-1}$. Judging solely from this parameter, the rock would be deemed as durable within the applied stream power of the modified slake durability test. While the rock material itself is durable with respect to the forces of flowing water, it is clearly susceptible to the quarrying and plucking modes of scour. Abrasion numbers for the samples vary from 2.91 to 9.71, which is less than 10, a value common to durable rock such as basalt or hard sandstone (Dickenson and Baillie, 1999).

The modified slake durability test was conducted on bulk core samples, which included the argillaceous material present in the cores. While this type of material is not suited for the slake durability test, the test was conducted to determine the durability of the bulk sample material rather than the more durable material that lies within the core. The sample disintegrated very rapidly (Figure 6.18) after soaking and showed high losses/breakdown in the first test cycle of the test, but showed very small rates of loss after the first cycle. This is due to the “washing

away” of fine-grained soil particles and fragments of rock smaller than 2 millimeters. Once this material was removed, the samples showed mass losses similar to the prepared core samples previously tested. Table 6.12 shows the regression statistics for the bulk core samples. As was the case with the previous samples tested, statistical analysis of the test data yielded results consistent with those of durable rock.

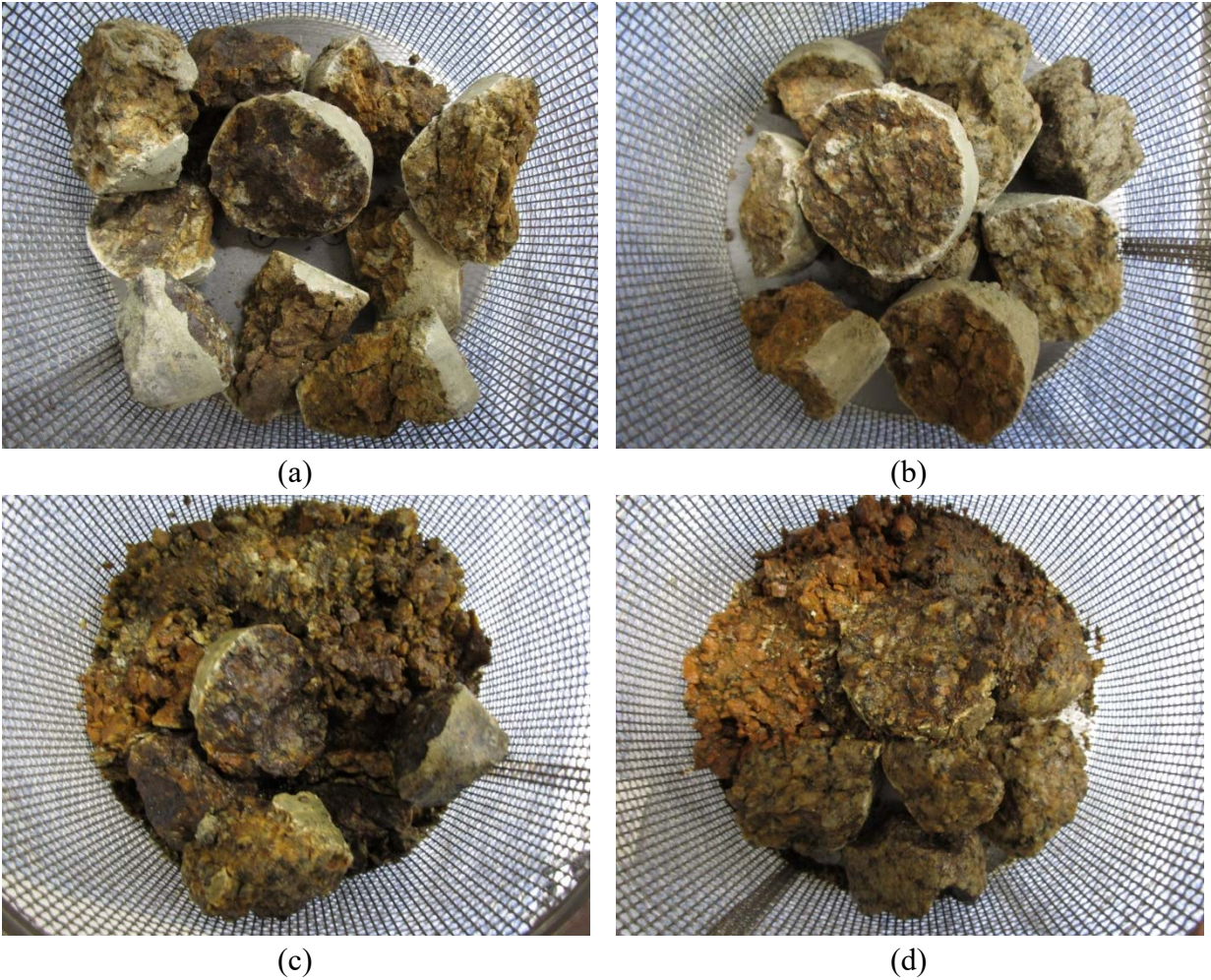


Figure 6.18: Core samples used in test; prior to immersion in water [(a) and (b)], and after soaking in water [(c) and (d)]

Table 6.12: Geotechnical scour numbers and abrasion numbers for Bulk Core Samples

n	GSN	SEE	SSR	r ²	SEE	SSR	a	b	β	b	r ²	SEE	SSR
20	1.14×10 ⁻⁸	7.05×10 ⁻⁷	8.44×10 ⁻¹²	0.83	2.99×10 ⁻⁷	1.52×10 ⁻¹²	2.30×10 ⁻⁷	-1.56×10 ⁻⁵	2.91	31.44	0.994	0.104	0.151
20	9.82×10 ⁻⁹	6.22×10 ⁻⁷	6.58×10 ⁻¹²	0.76	3.19×10 ⁻⁷	1.73×10 ⁻¹²	2.05×10 ⁻⁷	-1.54×10 ⁻⁵	3.05	25.08	0.996	0.086	0.102

As shown in Table 6.12, the abrasion numbers for the tested samples were of the same magnitude for extremely durable rock such as basalt.

Judging from the appearance and the behavior of the whole core samples, the highly fractured and weathered granite appears to be highly susceptible to the quarrying/plucking modes of scour. However, with respect to the slake durability procedure, the samples were found to perform as very durable rock. This highlights the fact that the modified slake durability test is appropriate only when assessing a geomaterial's susceptibility to the abrasion or grain scale (smaller than 2 mm) plucking modes of scour. In order to determine the response of the material with respect to quarrying/plucking to an applied stream power, a method to assess the degree of fracturing is necessary. A sieve analysis of a cycled sample could potentially provide information of the fracturing of the sample in the form of a grain size distribution. By correlating this information with the total cumulative stream power expended into the sample during the test, we can estimate how a given material will degrade when exposed to a certain stream power not only with respect to abrasion and grain-scale plucking, but also to quarrying and plucking on any scale as well. However, breaking up the sample into its constituent particles does not require that the sample be cycled through the test; this could be achieved by any means. Moreover, durable samples of rock will show insignificant losses during the test, irrespective of the length of the cycles. The equivalent scour depth vs. equivalent stream power graph of durable rock samples is characterized by erratic losses, while soft, weak rock samples show a more predictable trend.

The assumed stream power used in the modified slake durability test, as derived by Keaton et al. (2012), is not representative of in-situ stream power experienced by the rock mass. Quarrying and plucking are hydraulic processes, primarily dependent on shear stress and pressure fluctuations in the flow. The slake durability test subjects a sample to abrasion both from the wire basket and other sample pieces, with relatively insignificant hydraulic forces imparted to the sample. However, the sample's performance in the test may show how the rock degrades when exposed to impact, specifically the size distribution of the pieces left from the test procedure. As smaller pieces of rock are more likely to be carried off by hydraulic forces, a sample that degrades into smaller pieces will be less resistant to the forces that cause scour. With properties of the rock sample, such as density, a minimum scour threshold can be inferred from the size distribution of the spent sample from the modified slake durability test using a proper hydraulic loading parameter such as stream power. Hence, a sieve analysis of the spent rock material from the modified slake durability test could provide information about the quarrying resistance of that particular rock formation.

While the modified slake durability test was primarily developed to assess the abrasion and grain-scale plucking resistance of rock (Dickenson and Baillie, 1999; Keaton et al. 2012), it can provide useful information as to the performance of the material with respect to macro-scale plucking as well. This is important, as quarrying and plucking may be the dominant mode of rock scour for given geologic and hydraulic conditions, especially for weathered durable rock types.

For rock samples such as the ones tested in this study, that are composed of gravel sized particles surrounded by fine grained soil, scour could be a significant problem. Briaud et al. (2004) show that scour depths as calculated per the methods of HEC-18 are similar for both fine grained and coarse grained soils, differing in the amount of time to achieve those scour depths.

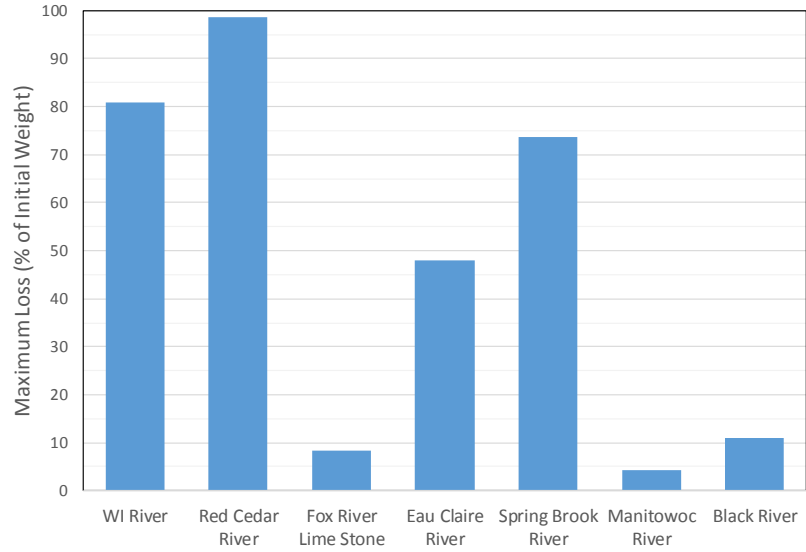
Keaton (2013) describes weathering of rock as an indirect mode of scour. The rock mass is prepared for scour by weathering processes, which degrade the sample into smaller pieces that can easily be carried off by water in a flow. From the condition of the samples tested in this study, it can be inferred that a significant degree of weathering had occurred. Weathering of the rock will result in the formation of fine grained clay particles, which will eventually undergo progressive scour. As the fine grained soils are carried away, the gravel sized pieces can be plucked and carried when the threshold stream power is exceeded. This scenario could result in significant scour depths in a major flood event.

6.4 Evaluation of Modified Slake Durability Test Results for Investigated Bedrock

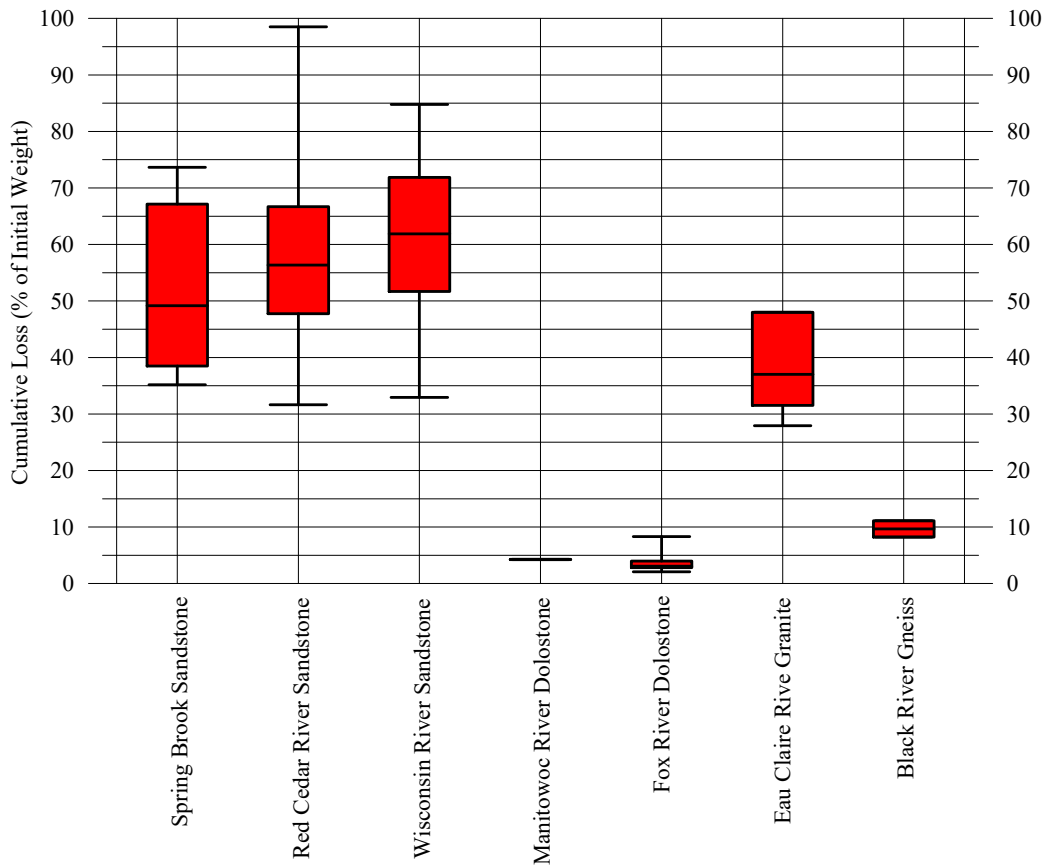
Figure 6.19 depicts a box-whisker plot for comparison of total specimen weight loss as a percentage of initial specimen weight for all investigated rocks resulted from the modified slake durability test. Inspection of the figure demonstrates that sandstone (Red Cedar River, Wisconsin River, and Spring Brook) exhibited the most weight loss with a minimum specimen weight loss of more than 33% and a maximum weight loss of 98%. Granite from Eau Claire River exhibited significant weight loss as well with a range from 28% to 48%. Dolostone specimens from Fox and Manitowoc Rivers exhibited the lowest weight loss with a minimum of 2% and a maximum of 8%. Black River gneiss weight loss varies between 8% and 11% of the initial specimen weight. The sandstone is considered among the weakest within the tested group, with the highest weight losses.

The summary results of the modified slake durability test on representative specimens of the investigated rocks are presented in terms of equivalent hourly scour depth versus the effective hourly stream power in Figure 6.20. The geotechnical scour number for all rock specimens was calculated and presented earlier in this chapter (a) with the initial data point considered in the analysis and (b) with the initial data point neglected in the analysis – only for sandstone specimens. Significant percentage of sandstone specimens from the Wisconsin River, the Red Cedar River and Spring Brook possessed geotechnical scour numbers that are high, and if the actual river flow conditions result in high stream powers, such degradable rock could exhibit significant scour in the field. As noted above, the geotechnical scour number is the slope of the ESD_i vs. ESP_i regression line, which is forced to a zero intercept (Keaton, 2012). The design scour depth is then simply the product of the geotechnical scour number and the expected cumulative stream power for the cross section, that is:

$$y_s = GSN * \Omega \quad (6.1)$$



(a) Maximum weight loss for the investigated bedrocks



(b) Maximum and minimum weight loss for the investigated bedrocks

Figure 6.19: Comparison of bedrock specimen loss as a percent of the initial weight of the specimen obtained from modified slake durability test for all bedrock samples at the investigated bridge sites.

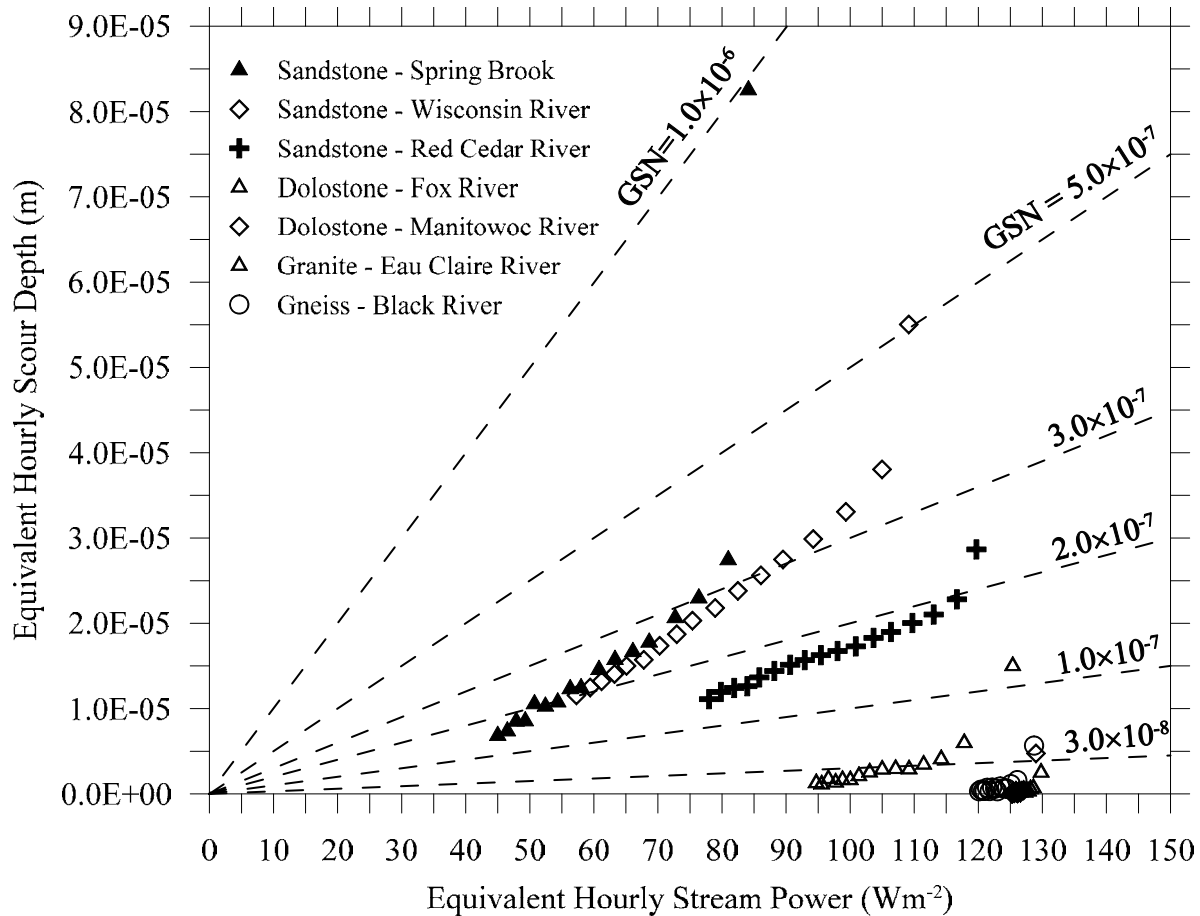


Figure 6.20: Results of modified slake durability tests for representative rock specimens obtained from the investigated bridge sites (initial data point neglected).

Assuming a bridge site with cumulative annual stream power of $500 \text{ kW/m}^2 \cdot \text{yr}$ and a remaining bridge service life of 15 years (assumed values taken from Keaton, 2013), the total design scour depth as predicted by the Keaton (2013) model, for the most scour susceptible material tested, would be:

$$1.495 \times 10^{-7} \text{ m} \cdot (\text{W} \cdot \text{m}^2)^{-1} \times 500 \text{ kW} \cdot \text{m}^{-2} \cdot \text{yr}^{-1} \times \left| \frac{10^3 \text{ W}}{1 \text{ kW}} \right| \times 15 \text{ yr} = 1.12 \text{ m}$$

This simple approach to calculating design scour depth provides an alternative to that from the empirical scour number, which requires existing scour depth data. Keaton (2013) notes that additional research into the applications of the geotechnical scour number is necessary, specifically flume tests (which ideally degrade the sample solely by means of hydraulic energy dissipation) and continuous abrasion tests (which degrade the sample by means of mechanical energy) on identical samples to develop a correlation between the two methods.

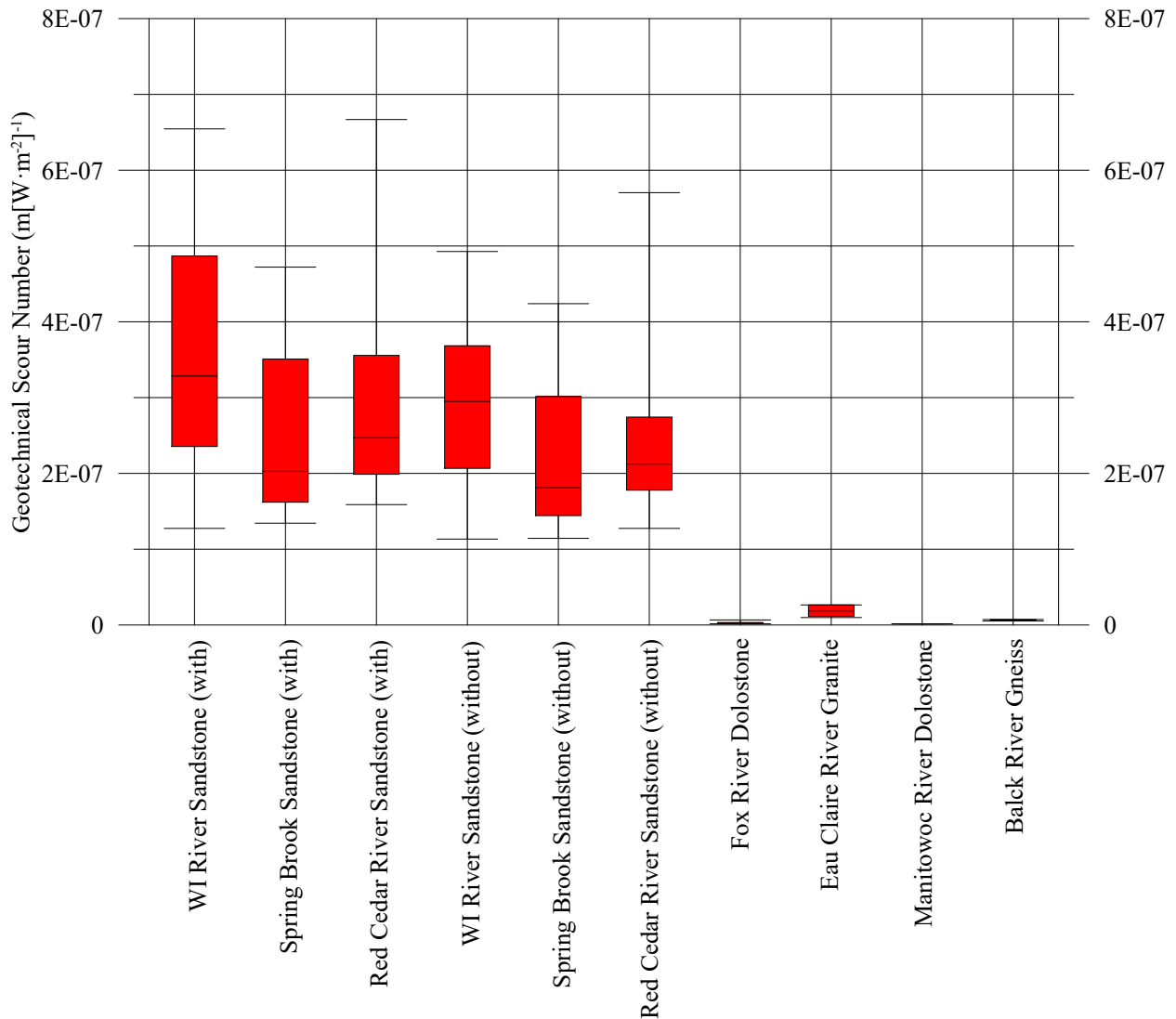


Figure 6.21: Geotechnical scour number for all investigated rocks – (95 percentile), including with and without initial data points.

The dimensions of the geotechnical scour number are length per unit stream power. In this analysis, the GSN parameters carry the units of $\text{m} \cdot (\text{W}/\text{m}^2)^{-1}$. However, for hydraulic design in the United States, English Imperial units are commonly used. The GSN can be converted to the English Imperial unit of $\text{ft} \cdot (\text{ft} \cdot \text{lb}/\text{s} \cdot \text{ft}^2)^{-1}$ as follows:

$$\begin{aligned}
 1 \frac{\text{m} \cdot \text{m}^2}{\text{W}} &= 1 \frac{\text{s} \cdot \text{m} \cdot \text{m}^2}{\text{N} \cdot \text{m}} = 1 \frac{\text{s} \cdot \text{m} \cdot \text{m}}{\text{N}} \times \left| \frac{4.4482 \text{ N}}{1 \text{ lb}} \right| \times \left| \frac{1 \text{ ft}}{0.3048 \text{ m}} \right|^2 = 47.88 \frac{\text{s} \cdot \text{ft} \cdot \text{ft}}{\text{lb}} \\
 &\approx 47.88 \text{ ft} \cdot \left(\frac{\text{ft} \cdot \text{lb}}{\text{s} \cdot \text{ft}^2} \right)^{-1}
 \end{aligned}$$

Rock scour is a rock-water interaction phenomenon (Keaton et al. 2012); therefore, the stream power is an important factor in initiating/starting rock scour. From the modified slake durability test results, the threshold values of the equivalent hourly stream power required to initiate scour of the investigated rock types are calculated and presented in Figure 6.22. Inspection of the figure shows that a minimum of 1.72, 8.97, and 27.53 (W/m^2) equivalent hourly stream power needed to initiate scour of sandstone from Red Cedar River, Wisconsin River, and Spring Brook, respectively. On the other hand, higher values of minimum equivalent hourly stream power are calculated for all other investigated rocks. For example, the minimum equivalent hourly stream power required to initiate scour for Eau Claire granite is 67.73 (W/m^2), which is considered a very high value for the actual river water flow/stream power.

Based on Dickenson and Baillie (1999) continuous abrasion test study on 31 rock specimens, abrasion numbers ranging from 1 to 10 were obtained for basalts and very hard rocks, from 10 to 20 for determined for hard to weak sandstones, and from 20 to 30 or more were obtained for soft siltstones and shales. The maximum and minimum abrasion number values for investigated rocks are presented in Figure 6.23. Examination of the figure demonstrates that majority of the sandstone specimens possesses abrasion numbers between 10 and 20, putting them in the category of hard to weak sandstones. There is a small number of sandstone specimens with abrasion numbers larger than 20, which characterizes them within the category of soft siltstones and shales.

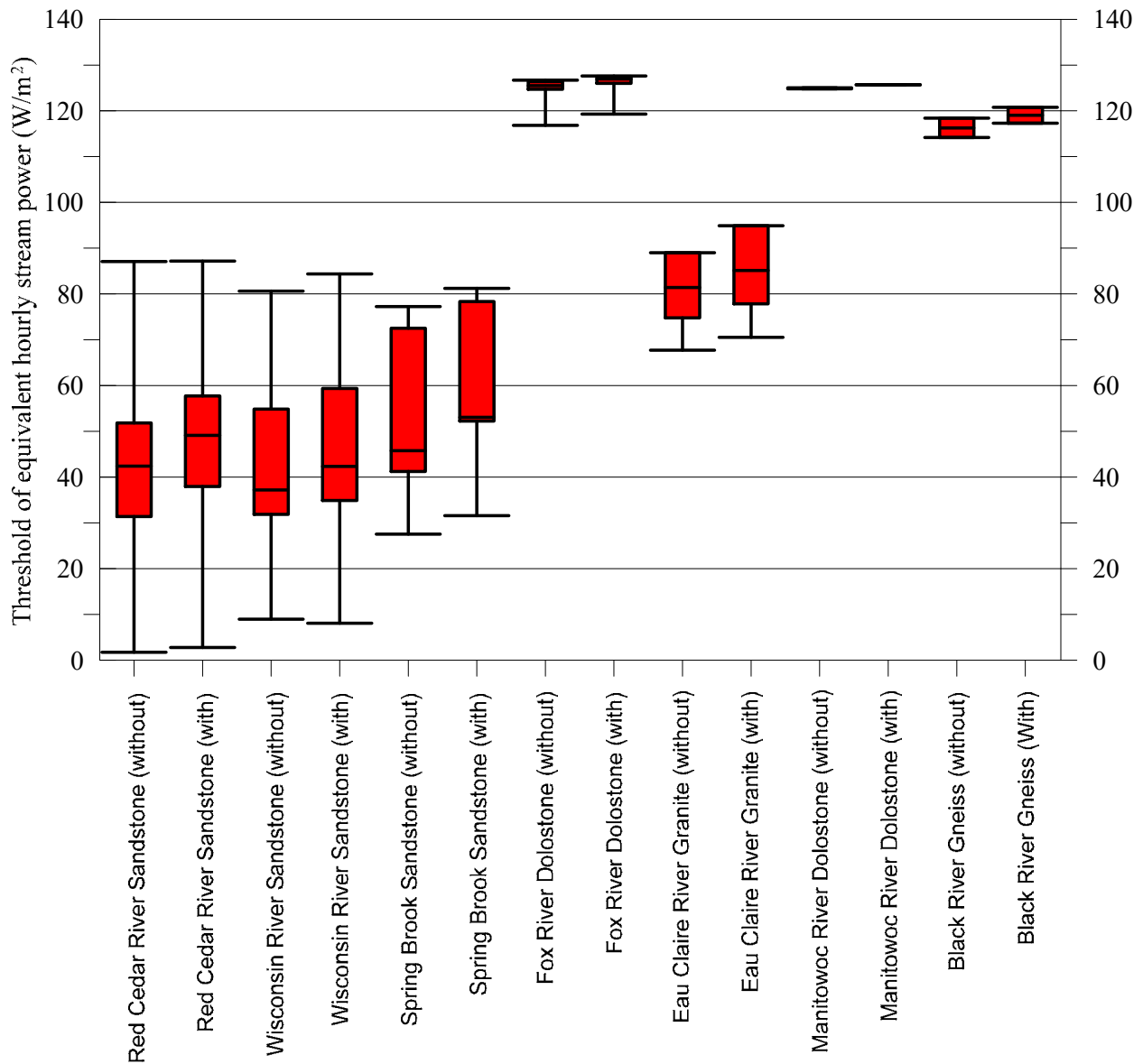


Figure 6.22: Threshold values of equivalent hourly stream power required to initiate scour of the investigated rock types obtained from the modified slake durability test (minimum, median and maximum values), including values calculated with the without considering initial data points.

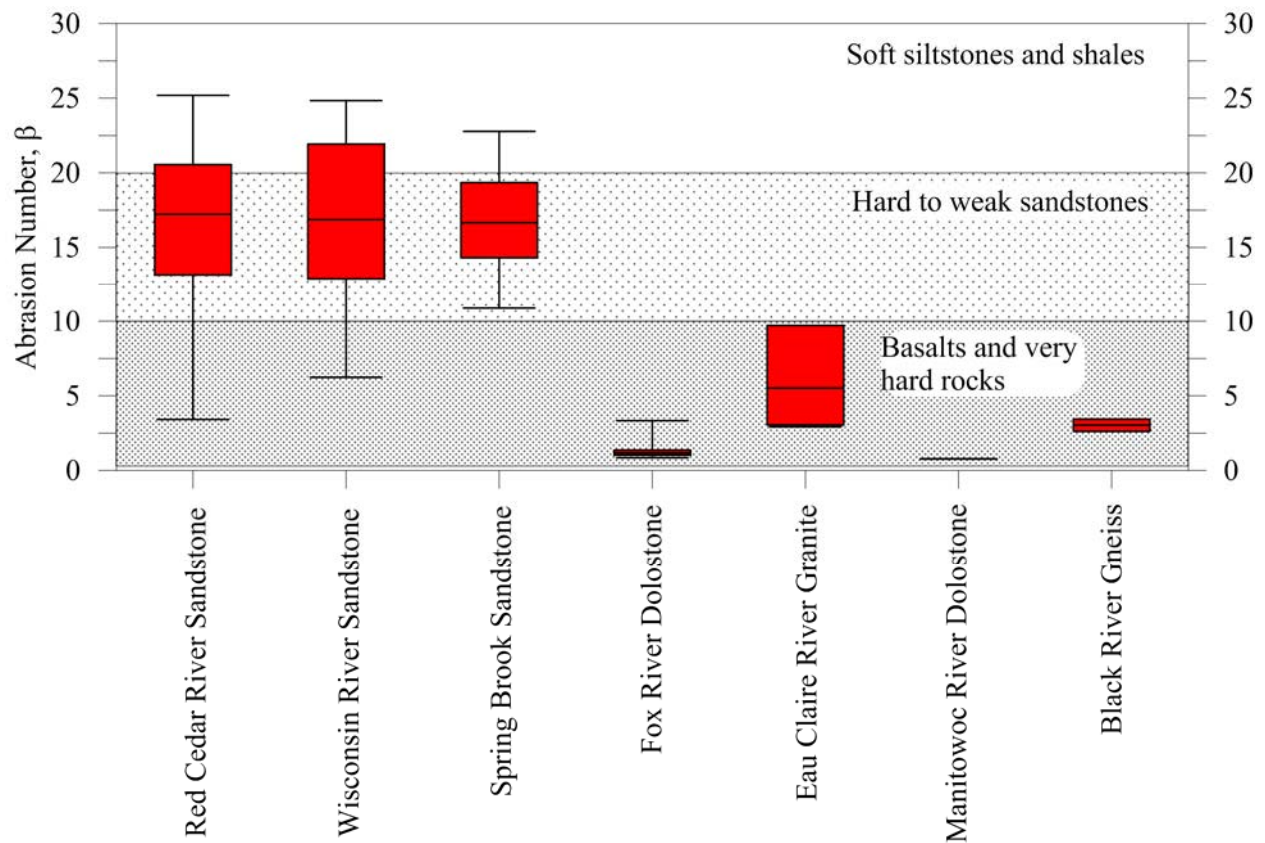


Figure 6.23: Box-Whisker plot shows extreme values, median, lower quartile, and upper quartile abrasion number values for investigated rocks with the rock durability classification based on Dickenson and Baillie (1999).

Chapter 7

Hydraulic Modeling Analysis

In this project, we focus on rock scour at bridges due to abrasion, which is a progressive, grain-scale erosion of degradable rock materials in response to water flow. The stream power of river flow has been considered as the most appropriate loading parameter. This chapter presents the rock scour analysis of six study sites, where hydrological data are available and geotechnical scour numbers of sample rocks were obtained through the modified slake durability test. The stream power based on the local flow and shear around bridge piers is calculated through a hydraulic simulation model with varying river discharge. The annual average scour depth both at the river bed and near the bridge piers is estimated from daily stream flow data, and the long term scour depths are predicted based on the flood frequency analysis.

7.1 Selected Bridge Sites for Scour Analysis

In this project, six bridges are selected across the state of Wisconsin for rock scour analysis, where hydrological data are available. In order to provide necessary data for bridge hydraulic modeling, field surveys using echo sounder system are conducted to obtain at least six river bed cross sections at each project location: three upstream and three downstream sections that are about one and two bridge lengths away from the structure, and two cross-sections of both faces of the bridge. Bridge structure details, including the bridge length, width, deck elevation and thickness, and distribution and size of piers and abutments, are obtained from technical drawings available through WisDOT. Table 7.1 lists the description, locations and names of these bridges, along with the identification number of nearby USGS stream stations.

7.2 Hydrological Data Analysis

The list of all USGS streamflow stations can be from the site <http://waterdata.usgs.gov/wi/nwis/current?type=flow>. An automatic web data program has been developed in Matlab to extract streamflow data automatically from USGS stations that are nearest to the selected bridge sites. Data extracted include historical daily flow time series, annual peak flows, and the field measurements data.

Figure 7.1 shows the historical daily flow and annual peak values recorded at the six stations. The figure also indicates the estimated flood flow rates of 10, 100 and 500 year events according to the flood frequency analysis described in this chapter. The daily flow data combined with hydraulic modeling of flow through bridges are used to calculate the cumulative stream power both at the river bed and around the bridge piers.

Table 7.1: List of selected project sites for bridge scour analysis

Site name	Description	Site location (Latitude, Longitude)	ID of the nearest USGS stream stations
US10-BR	U.S. Highway 10 across the Black River at Neillsville, WI	(44.552237, -90.608225)	05381000
STH13-WR	State Trunk Highway 13 across the Wisconsin River	(43.627674, -89.780925)	05404000
I43-MR	Interstate I-43 across the Manitowoc River	(44.109028, -87.713360)	04085427
US51-ECR	U.S. Highway 51 across the Eau Claire River	(44.916381, -89.611671)	05397500
STH47-FR	State Trunk Highway 47 across the Fox River	(44.253000, -88.415464)	04084445
I94-RCR	Interstate I-94 across the Red Cedar River	(44.907990, -91.897348)	05369000

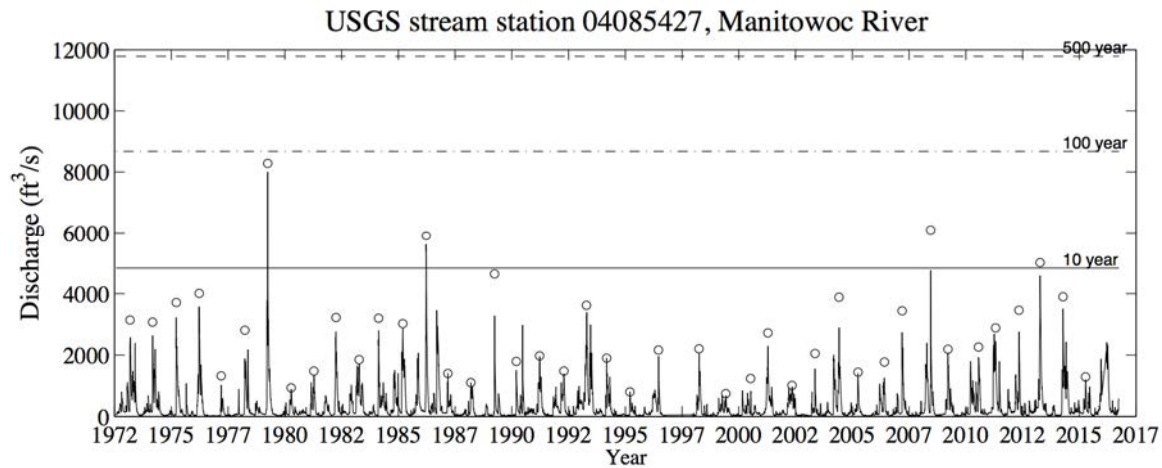


Figure 7.1: Daily stream flow rates (vertical lines) and annual peak flow rates (circles) recorded by USGS stream flow stations near the six bridge sites. Flood flow of 10, 100 and 500 year events are estimated from frequency analysis based on the annual peak flow series of each site.

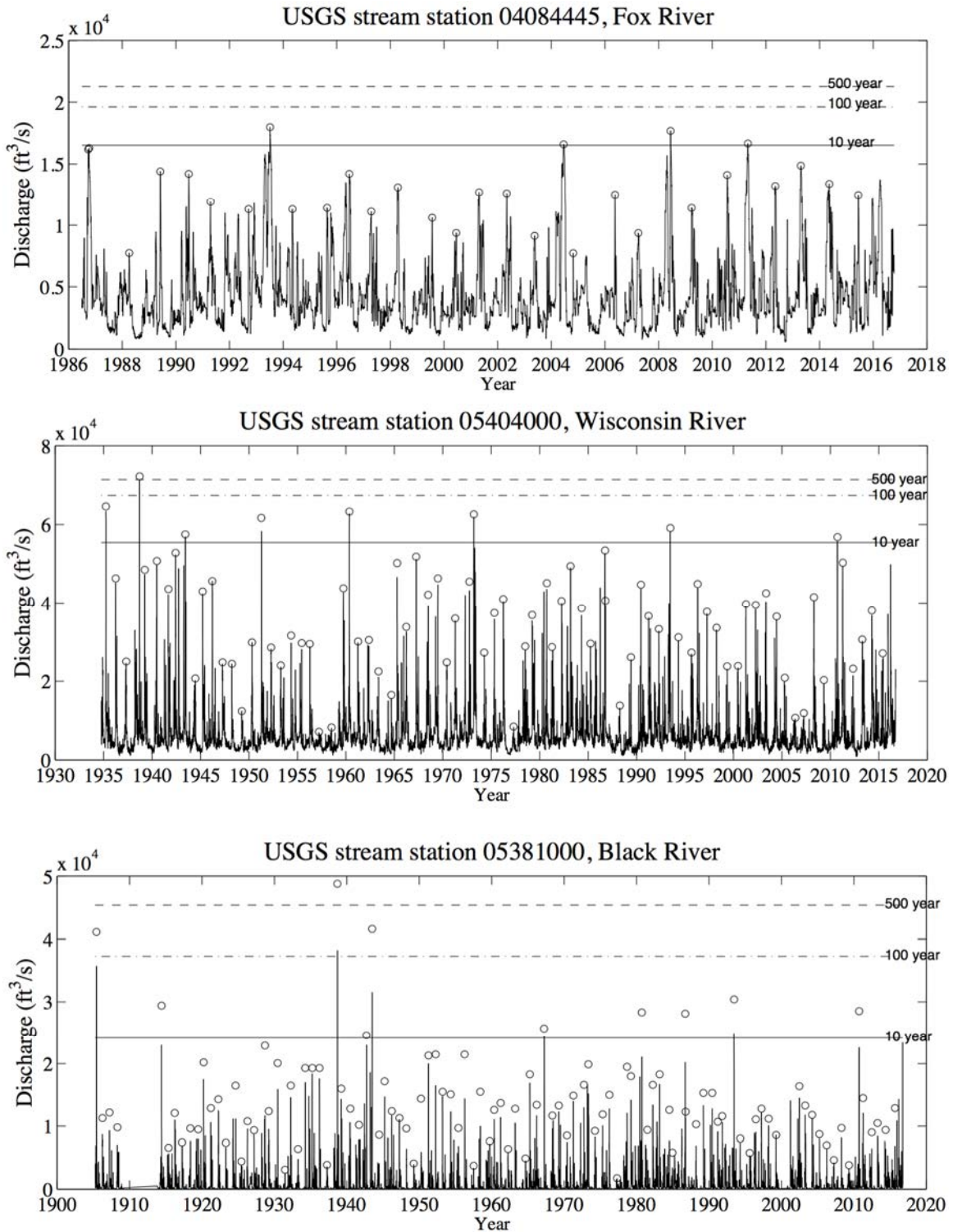


Figure 7.1 (cont.): Daily stream flow rates (vertical lines) and annual peak flow rates (circles) recorded by USGS stream flow stations near the six bridge sites. Flood flow of 10, 100 and 500 year events are estimated from frequency analysis based on the annual peak flow series of each site.

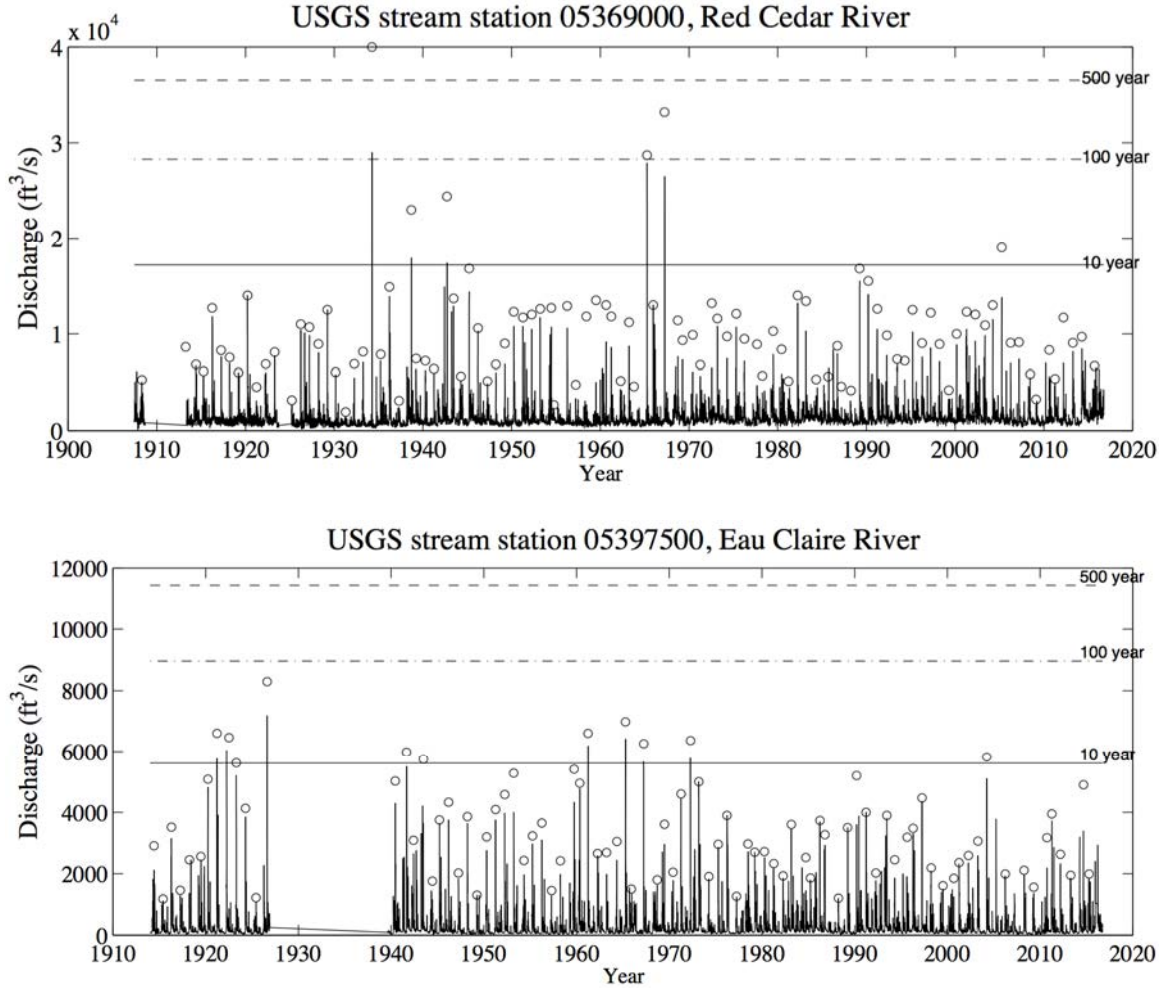


Figure 7.1 (cont.): Daily stream flow rates (vertical lines) and annual peak flow rates (circles) recorded by USGS stream flow stations near the six bridge sites. Flood flow of 10, 100 and 500 year events are estimated from frequency analysis based on the annual peak flow series of each site.

The probability-weighted approach has been used to predict the long-term rock erosion depth based on the return period (recurrence interval) of flood events. Similarly, we can estimate the annual effective stream power with the flood frequency analysis, which can be easily converted to an annual erosion depth following the scour number approach.

Annual peak flow data are used for flood frequency analysis. The magnitude of flood (Q_T) of a given return period (T) can be estimated from the frequency factor method, assuming a log-Pearson type III probability distribution. Given a series of annual peak flows in n years, Q_1, Q_2, \dots, Q_n , we can construct the 10-based logarithmic series: $y_i = \log_{10} Q_i$, ($i = 1, 2, \dots, n$). Denoting μ_Y , σ_Y , and G_S as the sample mean, sample standard deviation and sample skewness of

the series y_i , the magnitude Q_T of a T year event can be estimated using the frequency factor method, i.e.,

$$\log_{10} Q_T = \mu_Y + K(T, G_s)\sigma_Y \quad (7.1)$$

where K is the frequency factor as a function of the return period T and the skewness G_s , which can be calculated using the Kite's equation:

$$K = z + (z^2 - 1)k + \frac{1}{3}(z^3 - 6z)k^2 - (z^2 - 1)k^3 + zk^4 + \frac{1}{3}k^5 \quad (7.2)$$

where $k = \frac{G_s}{6}$, $z = \Phi^{-1}\left(1 - \frac{1}{T}\right)$ and Φ^{-1} is the inverse function of the cumulative distribution function (CDF) of a standard normal distribution, Φ .

In order to test the goodness of fit of the assumed log-Pearson Type III distribution, the sorted annual peak series (log-transformed) are plotted against the K -factor, which is calculated based on the return period estimated through the empirical Weibull formula, i.e.,

$$T_m = \frac{n+1}{m} \quad (7.3)$$

where m is the rank of the flow rate among the sorted annual peak series. The test results are shown in Figure 7.2. A linear trend of $y_m \equiv \log_{10} Q_m \sim K(T_m)$ for a majority portion of the peak flow series suggests that the assumed log-Pearson distribution is a good probability model for flood frequency analysis.

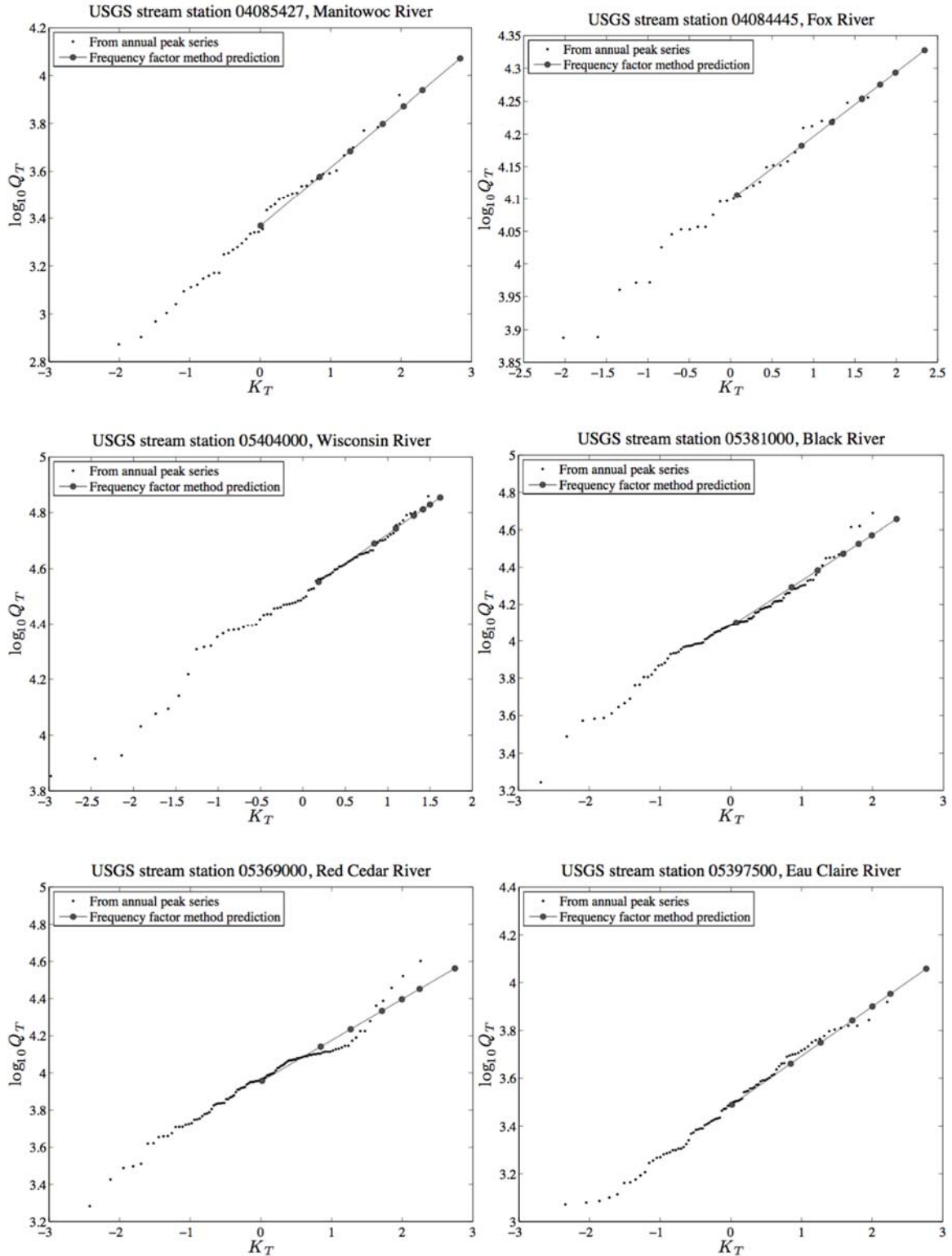


Figure 7.2: Tests of the goodness of fit of a log-Pearson Type III distribution with the annual peak flow series recorded at the selected USGS stream stations.

Flood flow discharge corresponding to return period $T = 2, 5, 10, 25, 50, 100,$ and 500 years are calculated with Equation (7.1) and these values are shown in Figure 7.2. They are listed in Table 7.2 for the six river stations as well.

Table 7.2: Flood flow rates (in cubic feet per second, cfs) with occurrence interval of $T = 2, 5, 10, 25, 50, 100,$ and 500 years.

River station	Return period T (years)						
	2	5	10	25	50	100	500
Manitowoc River	2,337	3,770	4,883	6,290	7,452	8,675	11,784
Fox River	12,765	15,214	16,526	17,933	18,839	19,649	21,262
Wisconsin River	35,664	49,013	55,433	61,450	64,778	67,363	71,399
Black River	12,653	19,645	24,166	29,647	33,540	37,264	45,391
Red Cedar River	9,069	13,841	17,177	21,540	24,881	28,286	36,527
Eau Claire River	3,084	4,580	5,609	6,941	7,951	8,976	11,434

Meanwhile the average duration of a T year event, D_T , can be estimated by analyzing the daily flow time series. A T year event is defined as a consecutive daily flow series that is higher than Q_T . All these events are identified from the daily flow series and their durations are averaged as an estimate for D_T . A power-law relation is applied to fit the relation between the duration and the return period,

$$D_T = aT^b \tag{7.4}$$

and the best-fitted parameters a and b are used to calculate D_T for any given recurrence interval T following this power law function. This analysis for the six river stations is presented in Figure 7.3. The empirical power law relations with the best fitted parameters are also shown in this figure.

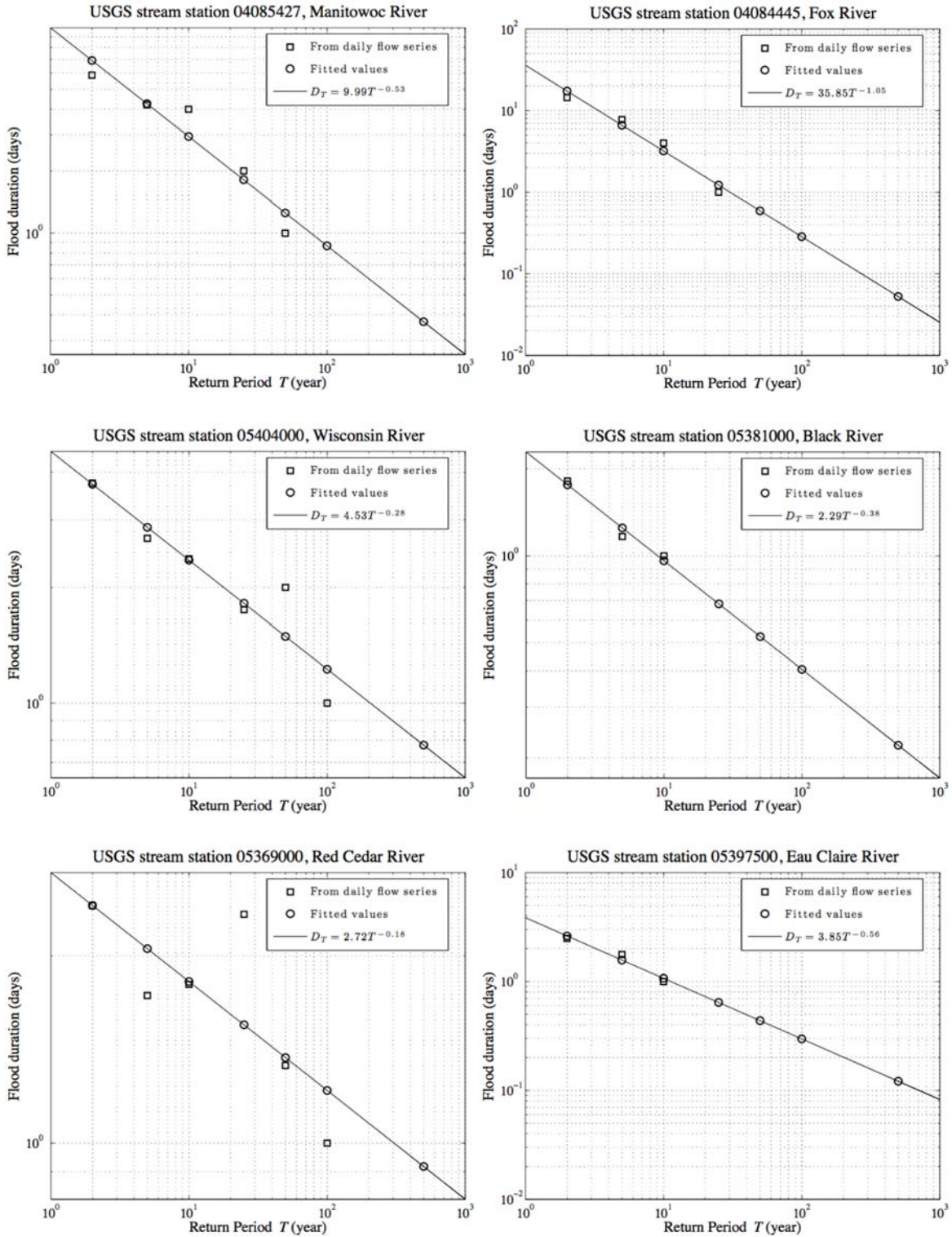


Figure 7.3: Relation between the average event duration to the flood recurrence interval (return period) at the selected USGS stream stations.

Flood magnitude for $T = 2, 5, 10, 25, 50, 100$ and 500 years are calculated and converted to a stream power following rating relations. These stream power values are then multiplied by the estimated average duration D_T to represent the cumulative power of a T year event.

7.3 Hydraulic Modeling

The purpose of hydraulic modeling is to determine the stream power P , which can be expressed in terms of the shear stress τ and the representative flow velocity V , i.e.,

$$P = \tau V \quad (7.5)$$

where both the representative velocity and shear stress can be the cross-sectional averaged value, if the long-term scour across the entire river cross-section is considered; alternatively they can be the local maximum stream-tube velocity around the pier or abutment if the local scour is concerned.

HEC-RAS software (Army Corps of Engineers) is applied for the hydraulic modeling. With the hydrological data available from the nearby USGS stream station, river discharges representing different recurrence intervals are applied in the model to determine the local velocity and shear stresses at the bridge, both along the river bed and around the bridge structures. Field surveys over several cross sections upstream and downstream of the bridge and immediately at the both faces of the bridge are imported into HEC-RAS. Bridge structures, including the bridge orientation (with respect to the river streamline), the length, width, thickness and elevation of the bridge deck, and the type of piers and their locations and width, are also reconstructed in the model for hydraulic calculations. Figure 7.4 shows an example of river cross-sections surveyed at site US10-BR (US highway 10 across the Black River).

Since flows at the downstream end of the bridges at all selected sites are subcritical, the boundary condition is set at the downstream cross-section, with a normal depth condition. Steady flows are simulated with specified discharge rates, ranging from the base flow to extreme flood flow conditions (return period $T = 2, 5, 10, 25, 50, 100$, and 500 years). Figure 7.5 presents a sample simulation results for site US10-BR, which shows the river bed topography and water surface profiles for the 10, 100 and 500-year flood flow conditions.



Figure 7.4: River cross-sections survey for river bed topography at site US10-BR.

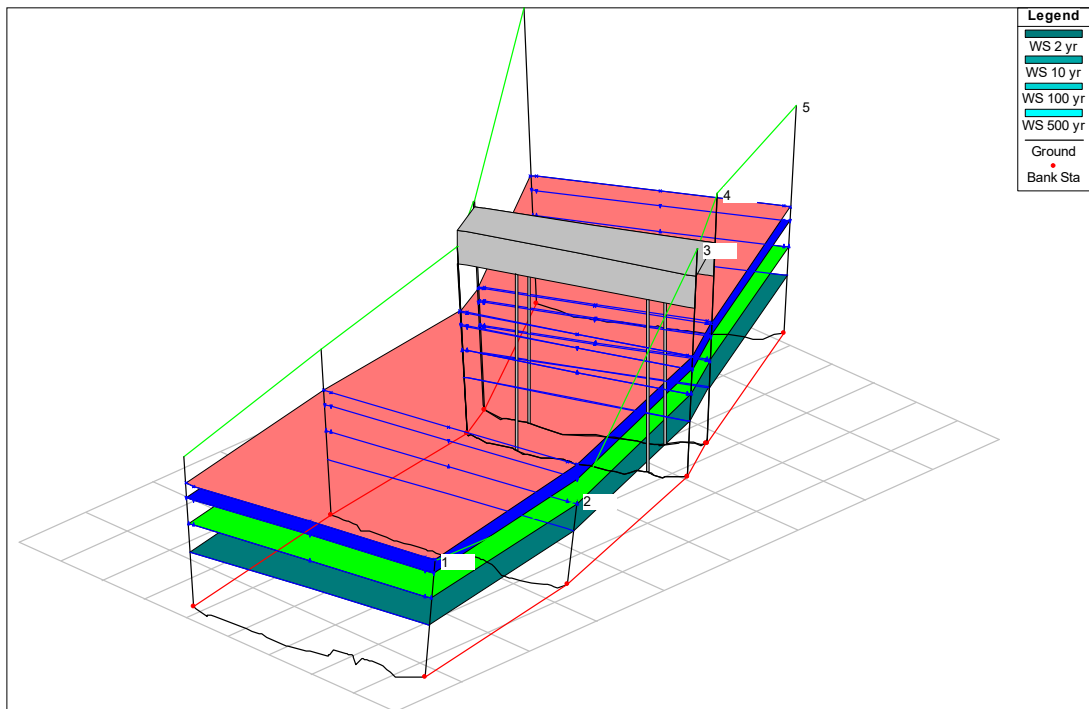


Figure 7.5: Sample hydraulic simulation result for site US10-BR with HEC-RAS.

The output of the HEC-RAS simulation includes the average velocity, river bed shear stress, water surface elevation, flow area and wetted perimeter at every cross sections. It also reports the local velocity and shear stress around bridge piers. In this study, simulation results are applied to reconstruct a rating curve that relates the stream power to the river discharge, which then can be applied for scour estimation and prediction. It should be noted that local velocity and shear stress around each bridge piers and abutments for one site are nearly the same for all the six project sites. Therefore, the average stream power over all the piers is reported here, and used for the following scour analysis.

Figure 7.6 shows the rating relation based on HEC-RAS simulation results. It appears that a power-law function can well describe the relation between the simulated stream power and river discharge, i.e.,

$$P = \alpha Q^\beta \quad (7.6)$$

A least-square regression is applied to establish an empirical relation, which will be used in the following bridge scour calculation. The best-fitted parameters α and β are also shown in the legend of Figure 7.6. It appears that for most of these selected project sites, the exponents β are between 1.2 and 1.4. However, the site of the I-94 bridge over the Red Cedar River is an exception, where $\beta = 2.13$ and 2.17 for the river bed and bridge piers, respectively. In addition, for the site of US-10 across the Black River, $\beta = 0.97$ for the river bed below the bridge.

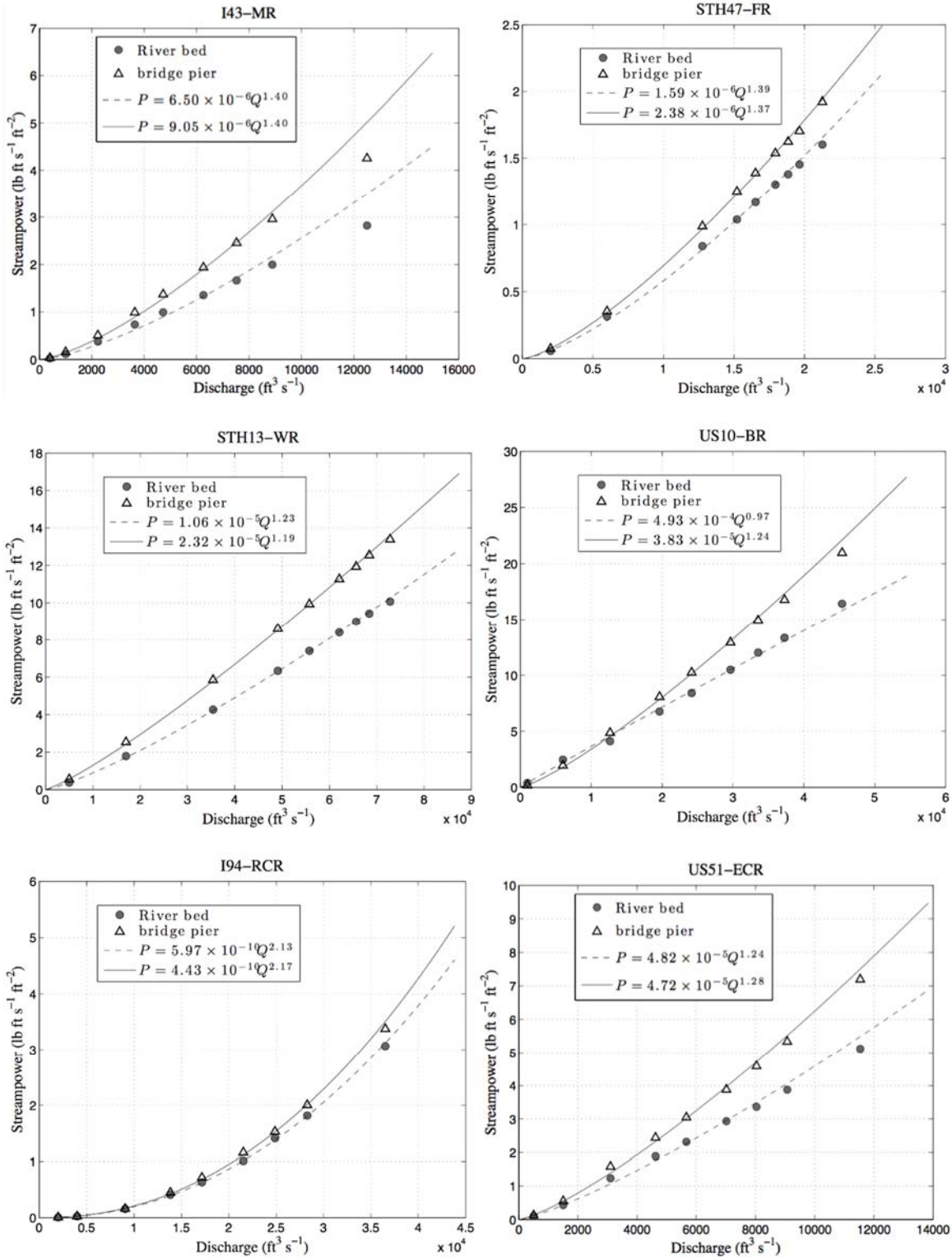


Figure 7.6: Rating curves between the stream power and the river discharge reconstructed from HEC-RAS simulation results.

7.4 Bridge Scour Estimation

7.4.1 Standard method

Rock scour around bridge structures is estimated and presented in terms of the annual average scour depth, which depends on the annual average stream power over river bed foundations and around the bridge piers. The geotechnical scour number obtained from laboratory testing is applied to relate the scour depths to the stream power.

The daily flow data from USGS stations combined with the rating relations from HEC-RAS simulations are used to estimate the annual stream power in the past. Figure 7.7 shows the time series of daily stream power at the six bridge sites. Here only the stream power over the river bed is presented, and the range of data is selected such that there is no gap (missing data) in the continuous measurement.

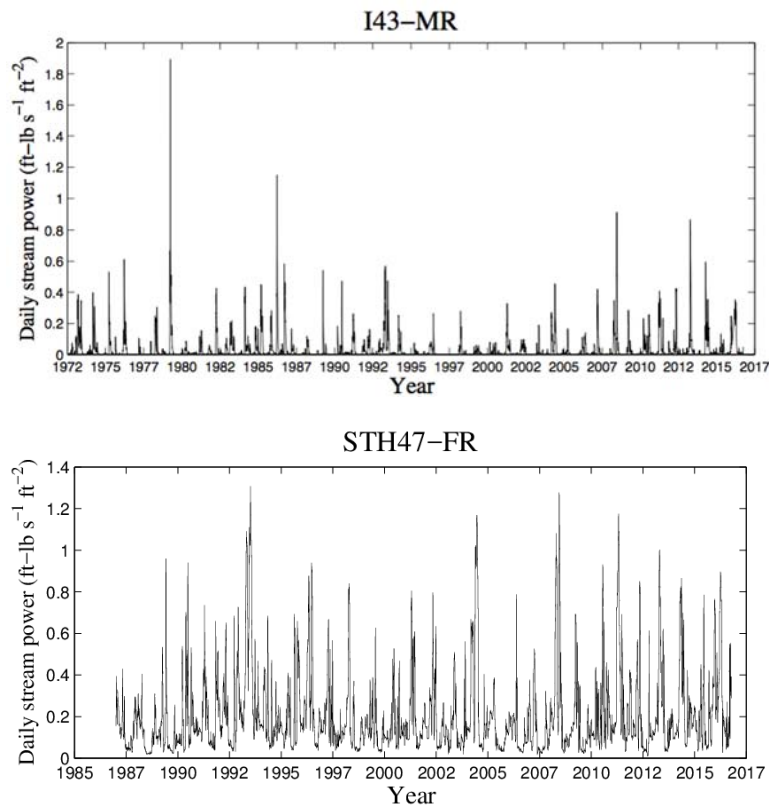


Figure 7.7: Time series of daily stream power over the river bed at all six project sites, calculated from USGS daily stream flow and power-discharge rating relations.

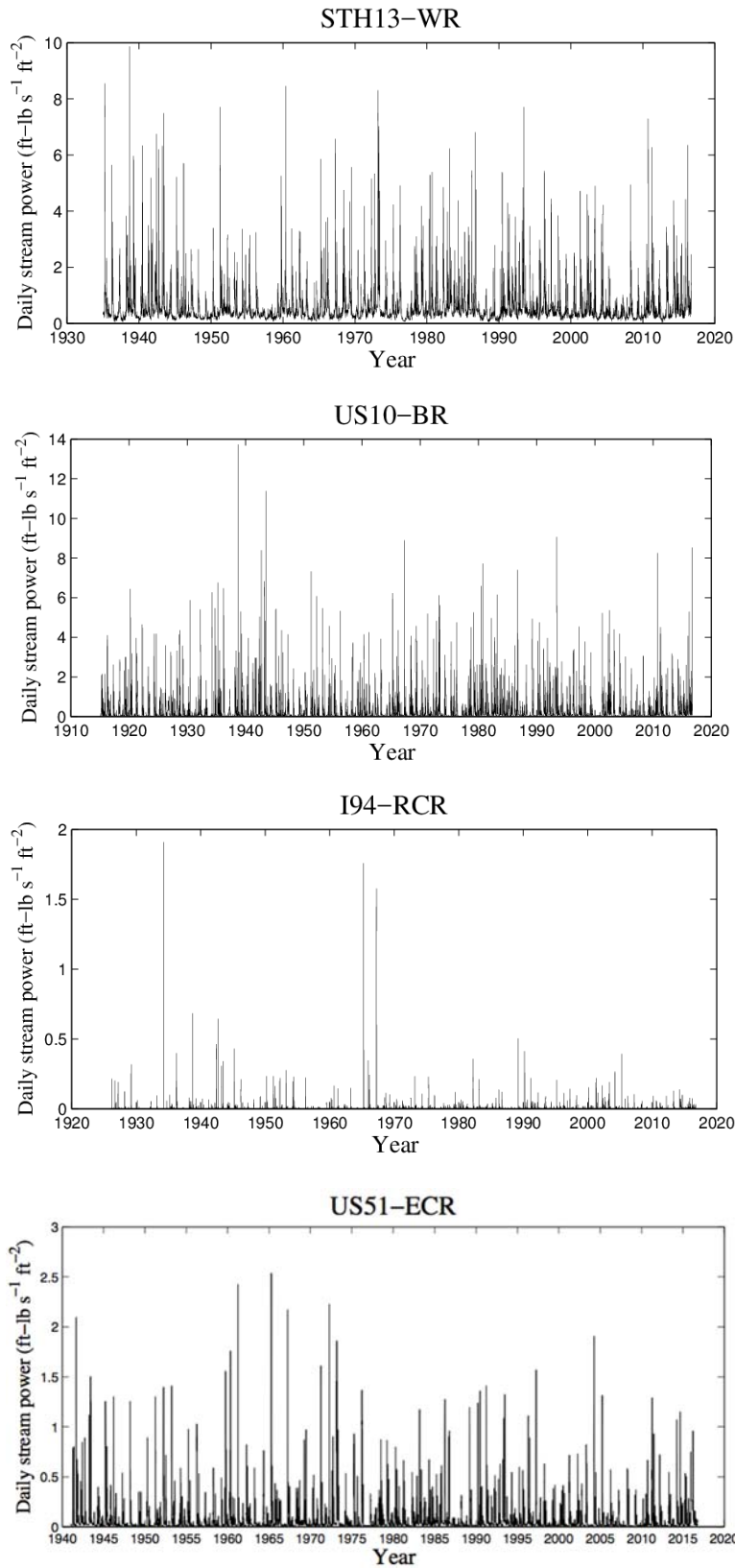


Figure 7.7 (cont.): Time series of daily stream power over the river bed at all six project sites, calculated from USGS daily stream flow and power-discharge rating relations.

In order to estimate the mean daily stream power, cumulative stream power is plotted against time. A linear regression is applied to the data, and the slope of the linear fit is considered as the average daily stream power. This value times 365 (days/year) and 86,400 (seconds/day) will be the total work done by the stream flow in one year over one squared foot of river bottom. However, in the following analysis, we will keep the unit of stream power as [lb-ft s⁻¹ ft⁻²] for convenience. We denote the annual mean stream power from this cumulative power analysis as $\bar{\Omega}$, i.e., the slope of the linear regression. The cumulative stream power distributions both over the river bed and around the bridge pier, as well as the linear fitting slopes (with intercept forced to zero) for all six sites are presented in Figure 7.8.

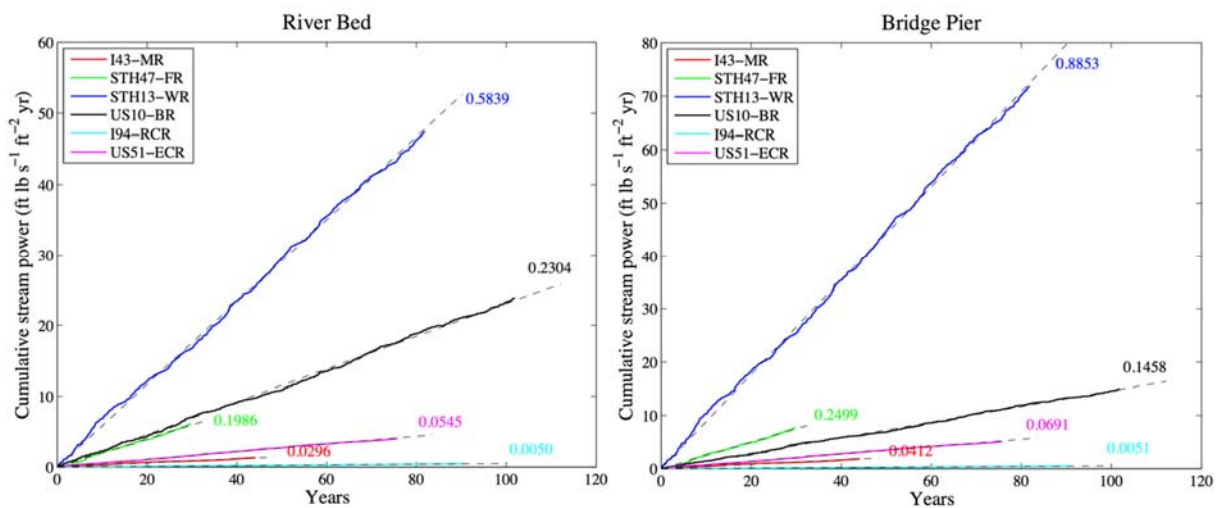


Figure 7.8: Cumulative stream power over the river bed under the bridge and around bridge piers at the six project sites. Dashed lines are linear regression of the cumulative stream power, and the numbers represents the slope of the linear regression, i.e., the annual average stream power, $\bar{\Omega}$, over the period of stream flow observation.

Considering the effects of sediment erosion and deposition, part of the rock foundation may not be directly subject to the shear stress of stream flow due to the protection of sediment deposition. Therefore, rock scour occurs only when a threshold hydraulic condition is exceeded. Here we may assume the “channel-forming” flow as the critical condition for the start of rock scouring. While there is no general parameterization, a 1 to 2-year flow has been widely accepted as the “channel-forming” flow condition. In order to account for this condition, we can estimate the effective mean annual stream power base on a threshold condition, i.e., plot the cumulative power of the flow with a threshold of the 2-year flow magnitude, with the slope of a linear regression is denoted as $\bar{\Omega}_2$. The cumulative stream power with this threshold and the corresponding linear regression analyses for all projects sites are shown in Figure 7.9. Comparing Figure 7.9 with Figure 7.8, it can be shown that annual average stream powers with

the “channel-forming” threshold are typically one order of magnitude smaller than those without the threshold.

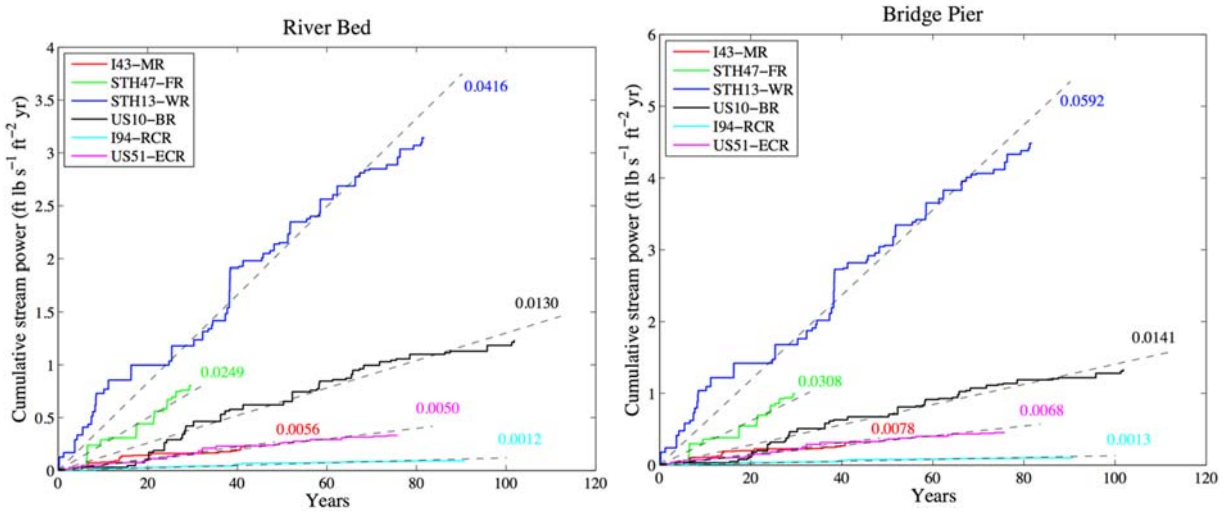


Figure 7.9: Cumulative stream power with a 2-year flow threshold (“channel-forming”) at the six project sites. Dashed lines are linear regressions of the cumulative stream power, and the numbers represents the slope of the linear regressions, i.e., the annual average stream power, $\overline{\Omega}_2$, over the period of stream flow observation.

Geotechnical scour numbers of sample rocks from the modified slake durability analysis are denoted as K_S . These numbers are first averaged over all samples at each project site. They are also converted to the English units, i.e., from $[m (W m^{-2})^{-1}]$ to $[ft (lb-ft s^{-1} ft^{-2})^{-1}]$, by multiplying the conversion factor 47.88. The estimated annual scour depth (y_S - without threshold, or y_{S2} - with threshold) can be simply calculated as

$$y_S = 24 \cdot 365 K_S \overline{\Omega} \quad \text{and} \quad y_{S2} = 24 \cdot 365 K_S \overline{\Omega}_2 \quad (7.7)$$

Following this calculation, the mean annual scour depth of the rock foundation and around bridge piers at all six project sites can be obtained.

7.4.2. Long-term rock scour based on flood frequency analysis

The probability-weighted approach has been used to predict the long-term rock erosion depth based on the return period (recurrence interval) of flood events. The annual effective stream power can be estimated with the flood frequency analysis, which can be easily converted to an annual erosion depth in light of the scour number approach.

Flood magnitude for $T = 2, 5, 10, 25, 50, 100$ and 500 years can be converted to a stream power following rating relations, i.e., Figure 7.6. These stream power values are then multiplied by the estimated average duration D_T to represent the cumulative power of a T year event, following the empirical relations shown in Figure 7.3. The calculation result is interpreted as the cumulated flood event stream power, and it is plotted against the recurrence probability (i.e., $1/T$) to represent its probability distribution of a given year (cf. Figure 7.10). The annual cumulative stream power ($\overline{\Omega}_{SF}$, where the subscript F denotes “frequency-weighted”) can be calculated with the following probability-weighted equation:

$$\overline{\Omega}_{SF} = \int \Omega_T dP_T \quad (7.8)$$

where Ω_T is the cumulative stream power of a T year event and $P_T = 1/T$ is the corresponding probability of the occurrence of a T year event for any given year. Eventually, the long term annual rock scour depth can be estimated as:

$$y_{SF} = 24K_S \overline{\Omega}_{SF} \quad (7.9)$$

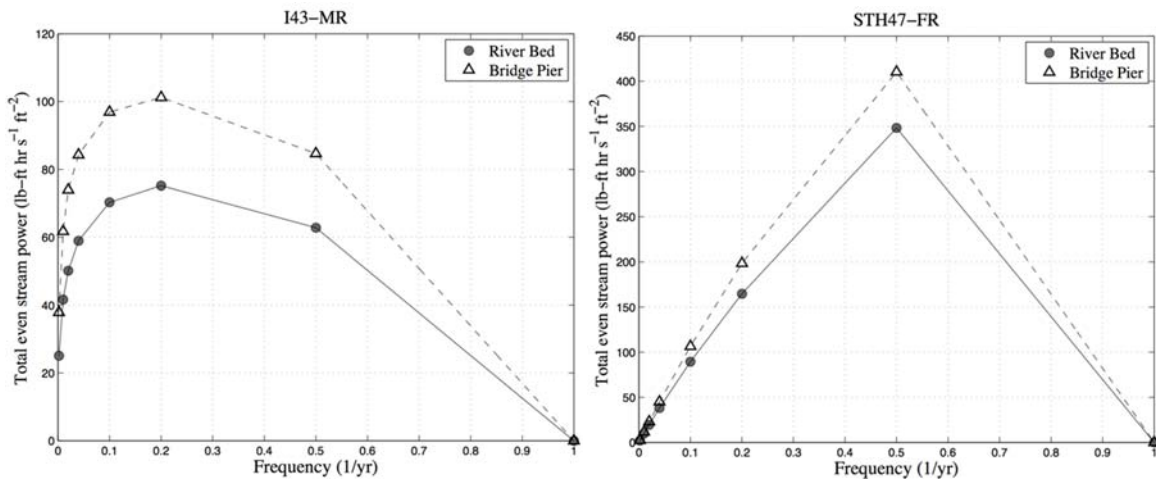


Figure 7.10: Probability distribution of the cumulative stream power over a flood event for all six project sites.

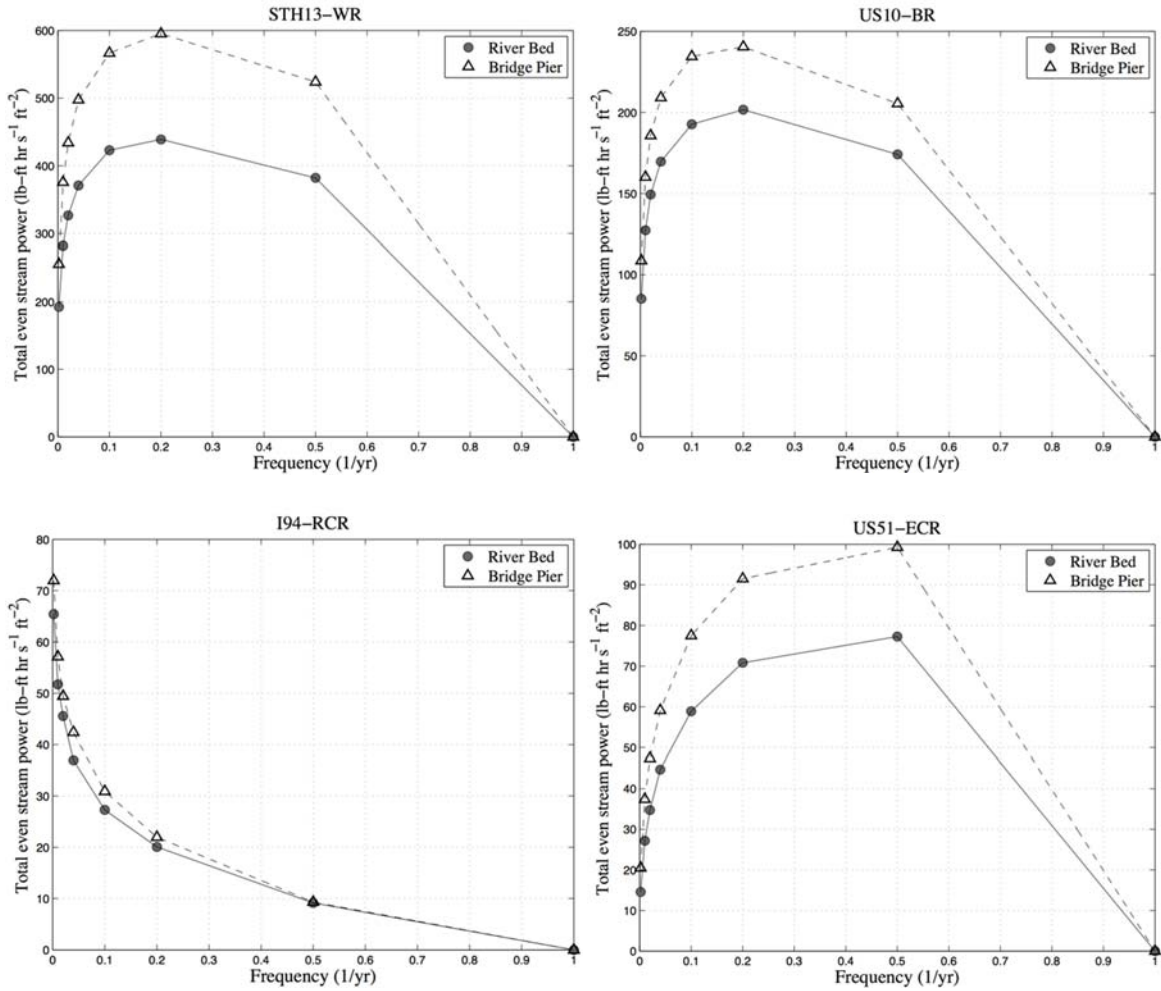


Figure 7.10 (cont.): Probability distribution of the cumulative stream power over a flood event for all six project sites.

In summary, the annual average stream power with and without “channel-forming” threshold ($\bar{\Omega}$ and $\bar{\Omega}_2$), and the average event cumulated stream power ($\bar{\Omega}_F$) estimated from the flood frequency analysis are listed in Table 7.3. For the purpose of comparison, $\bar{\Omega}_F$ is divided by 365×24 hours to be dimensionally consistent with $\bar{\Omega}$ and $\bar{\Omega}_2$. The estimated scour depths over a period of 50 years are also presented in Table 7.4 for all six bridge sites.

Table 7.3: Annual average stream power with and without “channel-forming” threshold ($\bar{\Omega}$ and $\bar{\Omega}_2$), and the long term average stream power from flood frequency analysis ($\bar{\Omega}_F/365/24$). (Note stream power units are: [ft-lb s⁻¹ ft⁻²])

Site name	$\bar{\Omega}$		$\bar{\Omega}_2$		$\bar{\Omega}_F$	
	River bed	Bridge pier	River bed	Bridge pier	River bed	Bridge pier
I43-MR	0.0296	0.0412	0.0056	0.0078	0.0056	0.0077
STH47-FR	0.1986	0.2499	0.0249	0.0308	0.0207	0.0245
STH13-WR	0.5839	0.8853	0.0416	0.0592	0.0340	0.0462
US10-BR	0.2304	0.1458	0.0130	0.0141	0.0155	0.0185
I94-RCR	0.0050	0.0051	0.0012	0.0013	0.0015	0.0016
US51-ECR	0.0545	0.0691	0.0050	0.0068	0.0060	0.0077

7.4.3. Effects of the critical stream power for rock scour

As demonstrated in the geotechnical analysis, the equivalent scour depth ~ stream power relation obtained in the modified slake durability test seems to be better correlated if a threshold stream power is considered, i.e.,

$$y_s = K_s(\Omega - \Omega_{crit}) \quad (7.10)$$

where Ω_{crit} is a critical stream power for the initiation of rock erosion. By explicitly including the critical condition, the estimated scour number K_S is generally several times greater than that obtained by forcing a zero intercept for the linear regression (e.g., $\Omega_{crit} = 0$).

The scour depth considering this critical effect is denoted as \bar{y}_S , which is calculated based on geotechnical test of each sample and the time series of daily stream power. Then the averaged scour depth for each test site is reported.

In addition, the effect of sediment shielding can be included such that rock scour can occur only if the stream power is greater than the critical value and the covering sediment are also resuspended under channel-forming conditions. Thus, the scour depth is

$$\bar{y}_{S2} = \begin{cases} K_s(\Omega - \Omega_{crit}) & \text{if } \Omega > \Omega_{crit} \text{ and } Q > Q_2 \\ 0 & \text{otherwise} \end{cases} \quad (7.11)$$

7.4.4 Annual scour depth at all test sites

Averaged annual rock scour depths on the river bed and around bridge piers at all six study sites are calculated following the five different methods described in 7.4.1 - 7.4.4. They are denoted as y_s , y_{s2} , y_{SF} , \bar{y}_s , and \bar{y}_{s2} , i.e., scour depth with the standard scour number method, standard method with “channel-forming” criteria, flood frequency method, scour number method with critical stream power, and scour number method with both “channel-forming” and critical stream power thresholds. Comparisons of estimated scour depths at the six sites are shown in Figure 7.11.

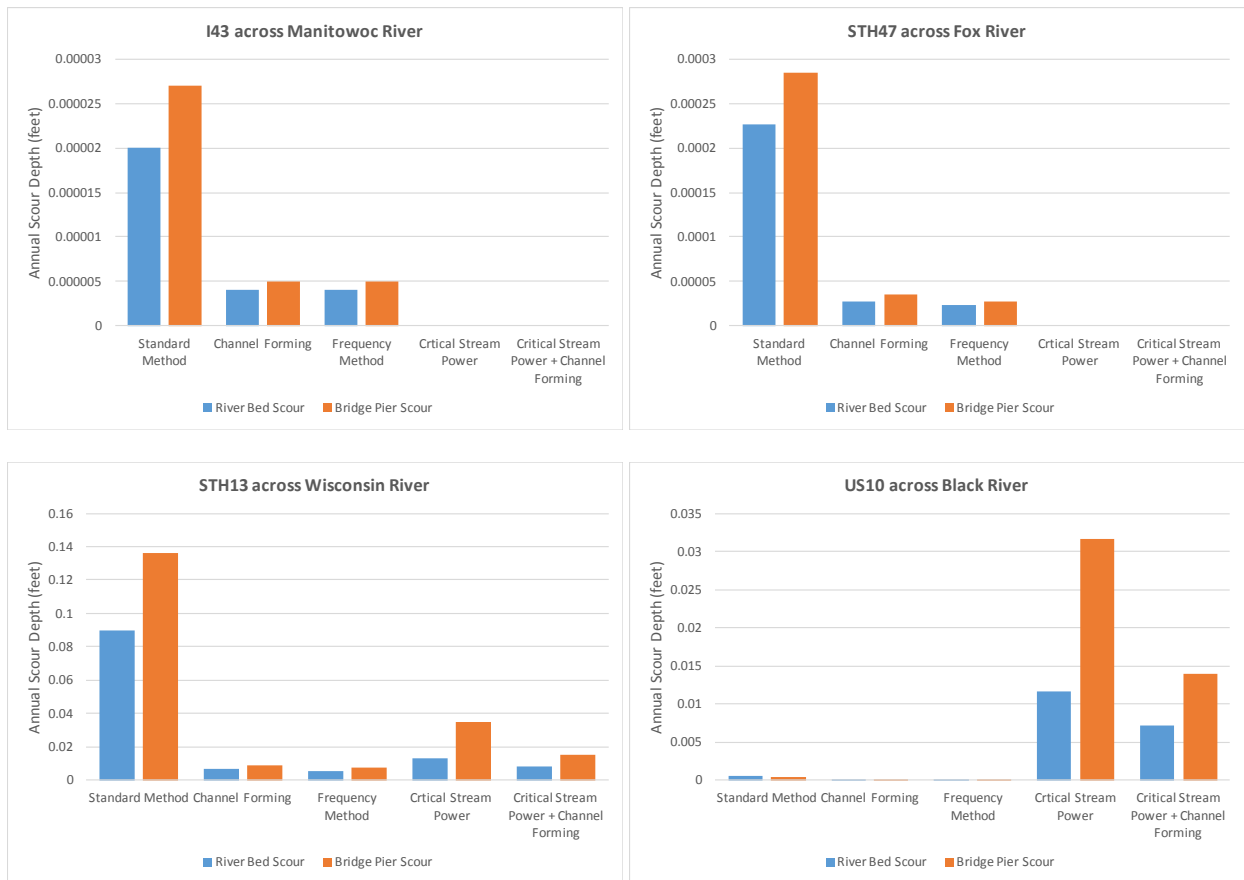


Figure 7.11: Estimated annual average scour depths on the rock foundation and around bridge piers with different methods

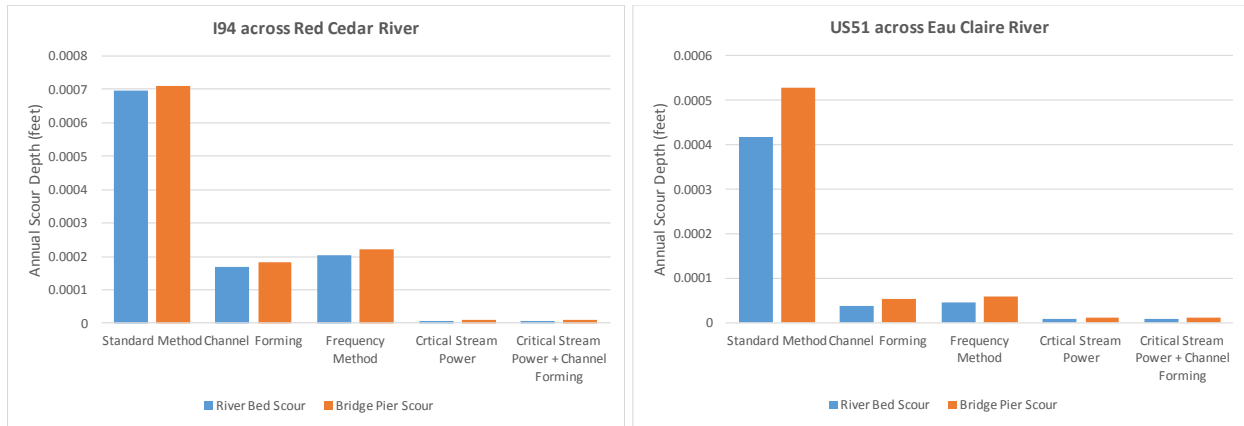


Figure 7.11 (cont.): Estimated annual average scour depths on the rock foundation and around bridge piers with different methods.

Considering that most bridges have a designed service period of 75 years, estimated total scour depths over 75 years for all six test sites are presented in Table 7.4, where estimated scour greater than 0.1 ft is considered as significant and marked in **bold**.

Table 7.4: Estimated average rock scour depths over a 75-year period. (Scour depth unit: [ft])

Site name	$75y_S$		$75y_{S2}$		$75y_{SF}$		$75\bar{y}_S$		$75\bar{y}_{S2}$	
	River bed	Bridge pier	River bed	Bridge pier						
I43-MR	0.0015	0.0020	0.0003	0.0003	0.0003	0.0004	0.0000	0.0000	0.0000	0.0000
STH47-FR	0.0170	0.0213	0.0021	0.0026	0.0018	0.0021	0.0000	0.0000	0.0000	0.0000
STH13-WR	7.7342	10.210	0.4798	0.6827	0.3917	0.5331	0.9594	2.6195	0.5985	1.1603
US10-BR	0.0452	0.0286	0.0026	0.0028	0.0031	0.0036	0.8717	2.3720	0.5390	1.0427
I94-RCR	0.0524	0.0534	0.0126	0.0136	0.0152	0.0166	0.0006	0.0008	0.0006	0.0008
US51-ECR	0.0313	0.0397	0.0029	0.0039	0.0035	0.0044	0.0006	0.0008	0.0006	0.0008

7.5 Summary and Discussion

As demonstrated by the hydraulic modeling and analysis on six sample bridge sites, the estimated annual scour depths of investigated rocks on both the river bed foundation and around bridge piers are typically small to negligible except for two bridge sites on the Wisconsin River and Black River. When using continuous stream power without the threshold of a “channel-forming” condition, the predicted 75-year scour depths at STH13-WR are 7.7 and 10.2 ft on the river bed and around the bridge pier, respectively (see table 7.4). These numbers are likely

overpredictions considering the sediment deposition that covers the channel bed. Scour depths with flood frequency analysis are generally close to that of the cumulative stream power from daily flow series with “channel-forming” threshold conditions. Both are significantly smaller than the depths predicted without the threshold condition. In addition, most modified slake durability test results suggest that effective scour does not occur until a critical shearing condition is met. For the case of STH13-WR, the estimated scour depth with this critical stream power condition is also significantly smaller than that predicted from the standard method, while it is slightly greater than that predicted from the standard method with “channel-forming” threshold.

Results from the site of US10 across the Black River are an exception. While the scour depth with the standard method is predicted to be insignificant, it is much higher when the critical stream power method is adopted (see Table 7.4). Modified slake durability tests showed that scour numbers with critical condition included are on average 25 times greater than those without the critical condition. However, only two samples from this site were collected and analyzed; thus, greater uncertainties are expected and the results should be interpreted with some reservation.

Scour depth estimated with continuous stream flow data can be applied to erosion of rock foundations without sediment deposition, e.g., on the steep side slope of the river channel, or the exposed pier footing. For rock foundations covered by sediments, scour prediction with “channel-forming” thresholds is more relevant.

7.6 Proposed New Guidelines for WisDOT Bridge Bedrock Scour Analysis

The procedure and results described in this research can serve as an addition to the standard bridge scour analysis, i.e., document HEC-18, which is generally applied for sand-bed channels. Additional efforts involved for degradable bedrock scour include hydrological and hydraulic analysis presented in this chapter, e.g., flood frequency analysis, hydraulic modeling, estimating flow duration, and calculating stream power. Typical geotechnical investigation needed for conventional bridge scour analysis should be sufficient for implementing the rock scour procedures, with the additional efforts of collecting channel bed rock samples and performing the modified slake durability tests. The integration of the rock scour procedure to the conventional bridge scour method has been proposed by Keaton et al. (2012), which is shown in Figure 7.12.

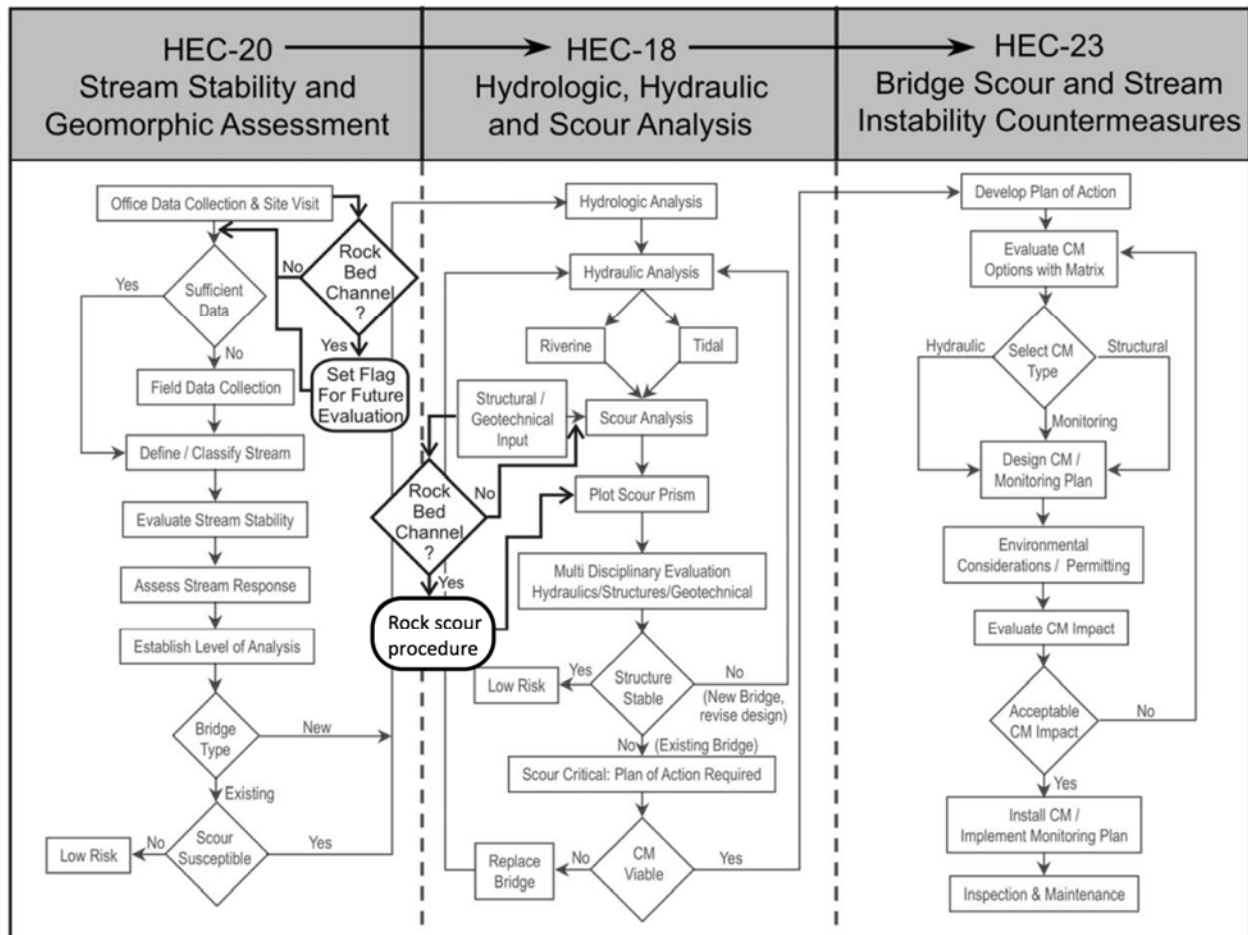


Figure 7.12. Conceptual relationship of this rock scour research with HEC-18, HEC-20, and HEC-23, adapted from Keaton et al. (2012).

For WisDOT, we suggest that the new procedures for degradable rock scour analysis be integrated into the existing document, i.e., the *WisDOT Bridge Manual* (Chapter 8 – *Hydraulics*). Scour analysis in the *Bridge Manual* generally follows the HEC-18 method. Conventionally, it is considered that bridges shall be designed to withstand the effects of scour from a super-flood, e.g., a flood exceeding the 100-year level, without failing (see Section 8.3.1.6 in the *Bridge Manual*). For degradable bedrock foundations, scour would occur progressively even under normal flow conditions. Therefore, daily flow data are necessary for the updated rock scour analysis. Revised design procedures are summarized below:

1. **Hydrologic analysis:** This task can be integrated into section 8.2 of the *Bridge Manual*. For degradable bedrock scour analysis, daily flow data must be acquired from available sources, such as those obtained from nearby USGS stream stations. Daily flow series are used to develop discharge, flow duration, mean velocity, and/or depth for the typical range of flood events with recurrence intervals of 2, 5, 10, 25, 50, 100 and 500 years.

Detailed procedures have been demonstrated in section 7.2 of this report. For an existing or designed bridge site without nearby stream data, hydrological models may be adopted to simulate flow rates at the specified recurrence intervals.

2. **Geological characterization and sample collection:** Field surveying should be conducted to describe the rock material (rock type, grain size, consistency, etc.). Existence of overfall and headcut conditions should also be described and documented. If possible, the amount and type of bedload and channel armor materials shall be described and reported. Bedrock samples can be collected through coring at various locations along the flood plain cross section. This procedure can be coordinated with routine investigation for bridge foundations. Intact bulk samples representing the bank and streambed rocks can also be collected. Samples collected onsite need to be prepared for laboratory testing following the procedures described in Chapters 2 and 6 of this report.
3. **Develop channel cross sections and profiles:** These tasks are identical to those in the standard bridge hydraulic analysis. Methods presented in the *Bridge Manual* apply equally well to bed rock scour analysis, i.e., section 8.3.2.1 ~ 8.3.2.4. Specifically, hydraulic parameters, including the hydraulic stream slope, profiles of selected floodplain cross-sections, and Manning's n values, need to be determined through field surveying activities.
4. **Laboratory testing:** The purpose of this task is to determine the geotechnical scour number through the modified slake durability test on collected core and intact rock samples. Laboratory procedures have been described in detail in Chapter 2 of this report. These procedures can be integrated into the *Bridge Manual* as a separate subsection in section 8.3.2 ("Design Procedures"). Specific attention should be paid to examine if a significant threshold exists for the initiation of rock scour processes. The threshold condition can be converted to an equivalent critical stream power for the subsequent scour analysis.
5. **Hydraulic modeling:** The hydraulic modeling methodology is generally consistent with that described in section 8.3.2.5 of the *Bridge Manual*. All models recommended by the manual, i.e., HEC-RAS, WSPRO and HY8, can be applied for bed rock scour analysis. However, additional parameters including the shear stress (τ) and stream power ($P = \tau V$) should be reported from these models for the subsequent rock scour calculations. Model simulations should be conducted to analyze hydraulic parameters under extreme flow conditions with recurrence intervals of 2, 5, 10, 25, 50, 100, and 500 years. A regression analysis can be applied to the simulated stream power ~ discharge relation for scour calculations based on the cumulative stream power method. These additional considerations can be integrated as a separate subsection in 8.3.2 of the *Bridge Manual*.

6. **Scour depth evaluation:** Subsection 8.3.2.7 of the *Bridge Manual* describes several models that can be applied to scour evaluation, including methods for live bed and clear water scour, long-term aggradation and degradation, contraction scour, and local scour at bridge piers and abutments. Additional equations can be integrated into this subsection for the consideration of degradable rock scour. Geotechnical scour numbers determined from rock samples can be applied here for scour depth estimations. These equations include:

- (a) the standard method based on available daily flow data, with or without channel-forming condition (Equation (7.7) in this report);
- (b) the flood frequency method (Equations (7.8) and (7.9) in this report);
- (c) cumulative stream power with critical erosion condition, with and without channel-forming condition (Equations (7.10) and (7.11) in this report).

Methods (a) and (c) are suitable for existing bridges with detailed hydrological data availability, e.g., the daily flow data. Estimated annual scour depth can be extrapolated for prediction of future erosion of the bridge's remaining life. Method (b) can be used for bridge design where general flood frequency data exists for the design stream site, while daily flow data is not necessary. Selection of these methods depends on the geological characteristics of the design bridge site, e.g., bedload and armor layer conditions, and the type and erodibility of bedrocks, which can be determined through site surveying (i.e., task 2) and the results of laboratory tests (i.e., task 4) described in the revised guideline.

Chapter 8

Conclusions

This research evaluates the scour potential of bedrocks supporting Wisconsin DOT bridge foundations. Ten highway bridges were selected for this study, of which seven are supported by shallow foundations, and five were built on sandstone in rivers/streams. The remaining bridges are supported by foundations on degradable granite, gneiss, and dolostone. The research study included modified slake durability tests on core and hand-picked rock specimens obtained from streams/river of seven bridge sites (10 bridge structures), field work that included site visits and geologic characterization of bedrocks, hydrographic bottom channel surveys, and hydraulic modeling and analysis to estimate scour depth of bedrocks on both the river bed and around bridge piers.

Based on the analysis of the modified slake durability test results, the sandstone exhibited significant mass loss during the continuous abrasion test. The geotechnical scour numbers and the abrasion numbers were calculated for the investigated rock specimens, which provided higher values for the sandstone compared with the other investigated rock types. This indicates that under high stream powers such degradable rock (i.e., sandstone) is more susceptible to higher scour rates compared with the other investigated rock types. It should be noted that the scour is water-rock interaction phenomenon; while the effective stream powers applied to these specimens in the modified slake durability test are high, the bedrocks that support bridge foundations in a river may not be subjected to these extreme stream power values and therefore they may degrade/abrade at a slower rate.

The hydraulic modeling and analysis presented the details of the rock scour prediction at each bridge site based on stream flow data collected/analyzed from gauge stations near the investigated project sites and the results of the modified slake durability tests.

The hydraulic modeling and analysis on six bridge sites demonstrated that the estimated annual scour depths of the investigated rocks on both the river bed foundations and around bridge piers are typically small to negligible except for two bridge sites on the Wisconsin River and the Black River. When using continuous stream power without the threshold of a “channel-forming” condition, the 75-year scour depths at STH13-WR are estimated as 7.7 and 10.2 ft on the river bed and around the bridge pier, respectively (see Table 7.4). These numbers likely overpredict scour considering the sediment deposition that covers the channel bed. Scour depths with flood frequency analysis are generally close to that of the cumulative stream power from daily flow series with “channel-forming” threshold conditions. Both of them are significantly smaller than values predicted without the threshold condition. In addition, most modified slake durability test results suggest that effective scour does not occur until a critical shearing condition is met. For the case of STH13-WR, the estimated scour depth with this critical stream

power condition is also significantly smaller than the depth predicted from the standard method, while it is slightly greater than that from the standard method with “channel-forming” threshold.

Results from the site of US-10 across the Black River are an exception. While the scour depth with the standard method is predicted to be insignificant, it is much higher when the critical stream power method is adopted (see Table 7.4). Modified slake durability tests showed that geotechnical scour numbers with critical condition included are on average 25 times greater than those without the critical condition. However, only two samples from this site were collected and analyzed; thus, greater uncertainties are expected and the results should be interpreted with some caution.

Scour depth estimated with continuous stream flow data can be applied to abrasion of rock foundations without sediment deposition, e.g., on the steep side slope of the river channel, or the exposed pier footing. For rock foundations covered by sediments, scour prediction with a “channel-forming” thresholds is more relevant.

The procedure and results described in this research can serve as an addition to the standard bridge scour analysis, i.e., document HEC-18, which is generally applied for sand-bed channels. Additional efforts involved for rock bed scour include hydrological and hydraulic analyses presented in Chapter 7, including flood frequency analysis, hydraulic modeling, estimating flow duration, and calculating stream power. Typical geotechnical investigation needed for conventional bridge scour analysis should be sufficient for implementing the rock scour procedures, with the additional efforts of collecting channel bed rock samples and performing the modified slake durability tests.

The integration of the rock scour procedure into the conventional bridge scour evaluation method proposed by Keaton et al. (2012), which is shown in Figure 7.12. Section 7.6, presented “New Guidelines for Bridge Bedrock Scour Analysis” that incorporates the results of this research project into rock scour analysis for design of bridge foundation.

References

1. ASTM D1586, 2011, Standard Test Method for Standard Penetration Test (SPT) and Split-Barrel Sampling of Soils: American Society for Testing and Materials Procedure D1586-11.
2. ASTM D4644, 2008, Standard Test Method for Slake Durability of Shales and Similar Weak Rocks: American Society for Testing and Materials Procedure D4644-08.
3. ASTM D2216, 2010, Standard Test Methods for Laboratory Determination of Water (Moisture) Content of Soil and Rock by Mass: American Society for Testing and Materials Procedure D2216-10.
4. ASTM C88, 2005, Standard Test Method for Soundness of Aggregates by Use of Sodium Sulfate or Magnesium Sulfate: American Society for Testing and Materials Procedure C88-05.
5. ASTM C131, 2006, Standard Test Method for Resistance to Degradation of Small-Size Coarse Aggregate by Abrasion and Impact in the Los Angeles Machine: American Society for Testing and Materials Procedure C131-06.
6. ASTM C131/C131M, 2014, Standard Test Method for Resistance to Degradation of Small-Size Coarse Aggregate by Abrasion and Impact in the Los Angeles Machine: American Society for Testing and Materials Procedure C131M-14.
7. Annandale, G. W., 1995, Erodibility: *Journal of Hydraulic Research*, vol. 33, 471–494.
8. Annandale, G. W., Wittler, R. J., Ruff, J. F., and Lewis, T. M., 1998, Prototype Validation of Erodibility Index for Scour in Granular Media: ASCE Conference on Water Resources, Memphis, TN.
9. Annandale, G. W., 2000, Prediction of Scour at Bridge Pier Foundations Founded on Rock and Other Earth Materials: *Transportation Research Record: Journal of the Transportation Research Board*, No. 1696, 67–70.
10. Annandale, G. W., 2001, Reservoir conservation and sediment management, Water week 2001 Water Bank Group, Washington, DC.
11. Annandale, G. W., 2006, *Scour Technology*, New York, McGraw-Hill
12. Annandale, G. W., 2007, Current state-of-the-art Rock Scouring Technology, in Biscontin, G. ed., *Geotechnics of Soil Erosion: Proceedings of Geo-Denver 2007*, February 18–21, 2007, Denver, Colorado, American Society of Civil Engineers Geotechnical Special Publication No. 167, 1–12.

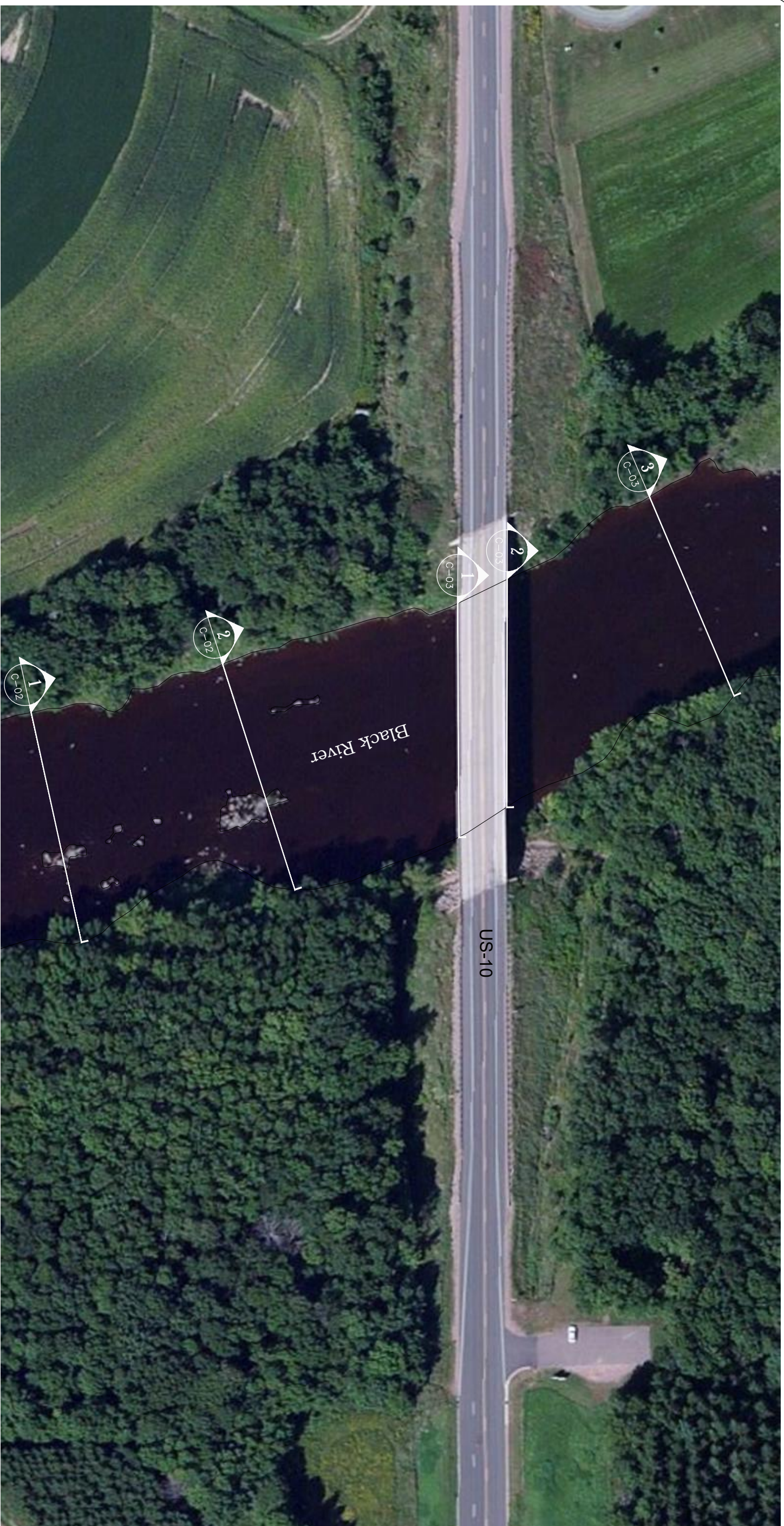
13. Anderson, R.S., 1986, Erosion profiles due to particles entrained by wind: Application of an eolian sediment transport model: Geological Society of America Bulletin 97, 1270-1278.
14. Arndt, R. E. A., 1981, Cavitation in fluid machinery and hydraulic structures. Annual Review of Fluid Mechanics. Vol. 13, 273-328.
15. Barnes, H. L., 1956, Cavitation as a Geological Agent: American Journal of Science, vol. 254, 493–505.
16. Bollaert, E. F. R., 2002, Transient Water Pressures in Joints and Formation of Rock Scour due to High-Velocity Jet Impact: PhD Thesis N°2548, Ecole Polytechnique Fédérale de Lausanne, Switzerland.
17. Bollaert, E. F. R., 2010, Numerical Modeling of Scour at Bridge Foundations on Rock, in Burns, S. E., Bhatia, S. K., Avila, C. M. C., and Hunt, B. E., eds., Scour and Erosion: Proceedings of the Fifth International Conference on Scour and Erosion, November 7–10, 2010, San Francisco, American Society of Civil Engineers Geotechnical Special Publication No. 210, 767–776.
18. Briaud, J.-L., Govindasamy, A. V., Kim, D., Gardoni, P., Olivera, F., Chen, H.- C., Mathewson, C., Elsbury, K., 2009, Simplified Method For Estimating Scour at bridges: Technical Report, Texas Transportation Institute, Texas A&M University System, College Station, Texas, Report No. FHWA-TX-09/0-5505-1.
19. Briaud, J.-L., Chen, H-C., Li, Y., and Nurtjahyo, P., 2004a, SRICOS-EFA Method for Complex Piers in Fine- Grained Soils: Journal of Geotechnical and Geoenvironmental Engineering, vol. 130, no. 11, 1180–1191.
20. Briaud, J.-L., Chen, H-C., Li, Y., Nurtjahyo, P., and Wang, J., 2004b, Pier and Contraction Scour in Cohesive Soils: Washington, DC, Transportation Research Board, National Cooperative Highway Research Program, Report 516.
21. Brown, B. A., 1988, Bedrock Geology of Wisconsin, West-Central Sheet: University of Wisconsin-Extension Geological and Natural History Survey, Madison, Wisconsin.
22. Brown, B. A., 2005, Preliminary Bedrock Geologic Map of Outagamie County, Wisconsin: University of Wisconsin-Extension Geological and Natural History Survey, Madison, Wisconsin.
23. Clayton, L. and Attig, J. W., 1990, Geology of Sauk County, Wisconsin: University of Wisconsin-Extension, Geological and Natural History Survey, Madison, Wisconsin.

24. Costa, J. E., and O'Connor, J. E., 1995, Geomorphically Effective Floods, in Natural and Anthropogenic Influences in Fluvial Geomorphology—Wolman Volume: Costa, J. E., Miller, A. J., Potter, K. W., and Wilcock, P. R., eds., Washington, D.C., American Geophysical Union Geophysical Monograph 89, 45–56.
25. Deere, D.U., 1963, Technical Description of Rock Cores for Engineering Purposes, Rock Mechanics and Engineering Geology, vol. 1, No. 1, 16-22.
26. Dickenson, S. E., and Baillie, M. W., 1999, Predicting Scour in Weak Rock of the Oregon Coast Range: unpublished research report, Department of Civil, Construction, and Environmental Engineering, Oregon State University, Corvallis, OR, Final Report SPR 382, Oregon Department of Transportation and Report No. FHWA-OR-RD-00-04.
27. Dott, Jr., R.H., Attig, J.W., 2004, Roadside geology of Wisconsin: Mountain Press Publishing Company; 1st ed., ISBN-13: 978-0878424924.
28. Emmerling, R., 1973, The Instantaneous of the Wall Pressure under a Turbulent Boundary Layer Flow, Max-Planck-Institiut fur Stromungsforschung, Report No.9.
29. Franklin, J.A., Chandra, C., 1972, The slake durability test: International Journal of Rock Mechanics and Mining Sciences, 325– 341
30. FHWA, 1991a, Scourability of Rock Formations: U.S. Department of Transportation, Federal Highway Administration Memorandum HNG-31, July 19, 1991, included in Appendix M of Richardson and Davis, 2001.
31. Hancock, G. S., Anderson, R. S., and Whipple, K. X., 1998, Beyond Power: Bedrock Incision Process and Form, in Tinkler, K. J., and Wohl, E. E., eds., Rivers Over Rock: Fluvial Processes in Bedrock Channels: American Geophysical Union, Geophysical Monograph 107, 35–60.
32. Hinze, J.D., 1975, Turbulence, 2nd ed. McGraw-Hill, New York.
33. Howard, A., and Kerby, G., 1983, Channel changes in badlands: Geological Society of America Bulletin, vol. 94, 739–752.
34. Kirsten, H. A. D., 1982, A Classification System for Excavation in Natural Materials: Civil Engineer in South Africa, vol. 24, no. 7, 293–308.
35. Kirsten, H. A. D., 1988, Case Histories of Groundmass Characterization for Excavatability, in Kirkaldie, L., ed., Rock Classification Systems for Engineering Purposes: ASTM STP 984, ASTM, Philadelphia, PA, 102–120.

36. Keaton, J. R., Mishra, S. K., and Clopper, E. P., 2012, Scour at Bridge Foundations on Rock. National Research Council (U.S.) National Cooperative Highway Research Program and American Association of State Highway and Transportation Officials. Transportation Research Board. Washington, D.C
37. Keaton, J. R., 2013, Estimating Erodible Rock Durability and Geotechnical Parameters for Scour Analysis: Environmental and Engineering Geoscience, vol. 19, No. 4, 319-343.
38. Keaton, J. R., and Mishra, S. K., 2010, Modified Slake Durability Test for Erodible Rock Material, in Burns, S. E., Bhatia, S. K., Avila, C. M. C., and Hunt, B. E., eds., Scour and Erosion: Proceedings of the Fifth International Conference on Scour and Erosion, November 7–10, 2010, San Francisco, American Society of Civil Engineers Geotechnical Special Publication No. 210, 743–748.
39. La Berge, G. L. and Myers, P. E., 1983, Precambrian Geology of Marathon County, Wisconsin: University of Wisconsin-Extension, Geological and Natural History Survey, Madison, Wisconsin.
40. Mishra, S. K., Keaton, J. R., Clopper, P. E., and Lagasse, P. F., 2010, Hydraulic Loading for Bridges Founded on Erodible Rock, in Burns, S. E., Bhatia, S. K., Avila, C. M. C., and Hunt, B. E., eds., Scour and Erosion: Proceedings of the Fifth International Conference on Scour and Erosion, November 7–10, 2010, San Francisco, American Society of Civil Engineers Geotechnical Special Publication No. 210, 734–742.
41. Morgenstern, N.R., and Eigenbrod, K.D., 1974, Classification of argillaceous soils and rocks: American Society of Civil Engineers J. Geotech. Eng. Div., vol. 100, GT10, 1137-1155.
42. Mudrey, Jr., M. G., Brown, B. A., Greenberg, J. k., 1982, Bedrock Geology Map of Wisconsin: University of Wisconsin-Extension Geological and Natural History Survey, Madison, Wisconsin.
43. Nickmann, M., Spaun, G. and Thuro, K., 2006, Engineering geological classification of weak rocks. In: Proc. 10th International IAEG Congress 2006, Nottingham: Paper number 492, IAEG London.
44. NRCS, 2001, Field Procedures Guide for the Headcut Erodibility Index: Chapter 52, Part 628, National Engineering Handbook, U.S. Department of Agriculture Natural Resources Conservation Service, 210-VINEH, rev; available online at <http://policy.nrcs.usda.gov/OpenNonWebContent.aspx?content=18379.wba> , accessed December 2009.

45. Richardson, E.V., Harrison, L. J., Richardson, J. R., and Davis, S. R., 1993, Evaluation of scour at bridges. HEC-18 Federal Highway Administration, Washington, D.C. Available from the National Technical Information Service, Springfield, Virginia 22161.
46. Richardson, E. V., and Davis, S. R., 2001, Hydraulic Engineering Circular No. 18: Evaluating Scour at Bridges, 4th ed, Federal Highway Administration, NHI 01-001.
47. Sklar, L., and Dietrich, W. E., 1997, The influence of downstream variations in sediment supply and transport capacity on bedrock channel longitudinal profiles [abs.]: *Eos* (Transactions, American Geophysical Union), vol. 78, no. 46 suppl., p. F299
48. Shields, A., 1936, Application of Similarity Principles, and Turbulence Research to Bed-Load Movement, California Institute of Technology, Pasadena, CA (translated from German).
49. Schlichting, H., and Gersten, K., 2000, *Boundary Layer Theory*: 8th ed, New York, Springer.
50. Tinkler, K. J., and Parish, J., 1998, Recent Adjustments to the Long Profile of Cooksville Creek, and Urbanized Bedrock Channel in Mississauga, Ontario, in Tinkler, K. J., and Wohl, E. E., eds., *Rivers Over Rock: Fluvial Processes in Bedrock Channels*: Washington, D.C., American Geophysical Union Geophysical Monograph 107, 167–187.
51. Whipple, K. X., and Tucker, G. E., 1999, Dynamics of bedrock channels in active orogens: Implications for height limits of mountain ranges, landscape response timescales, and research needs: *Journal of Geophysical Research*, vol. 104, 17661–17674
52. Wood, L. E. and Deo, P., 1975, A suggested system for classifying shale materials for embankments: *Bulletin Association Engineering Geologists*, vol. 12, No. 1, 39–55.

Appendix A – Bottom Channel Hydrographic Surveys



GENERAL NOTES:

1. The hydrographic survey was completed on September 15, 2015 by Collins Engineers, Inc.
2. Soundings were obtained using a continuously recording fathometer operating at 200KHZ and linked to a WAAS capable GPS receiver.
3. Base map information shown on this drawing shall be considered approximate.

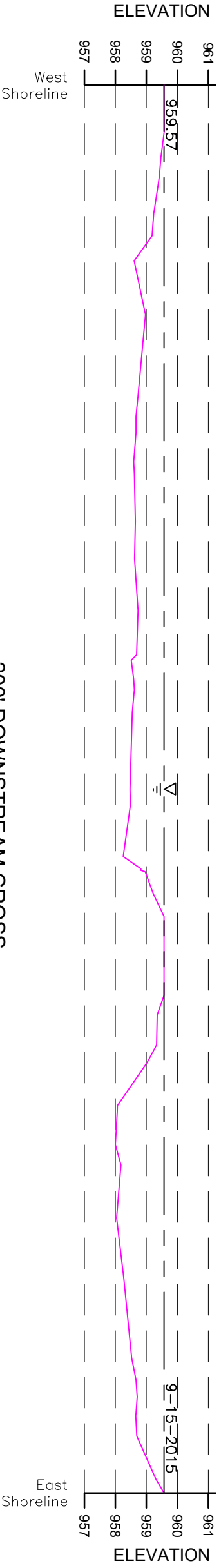
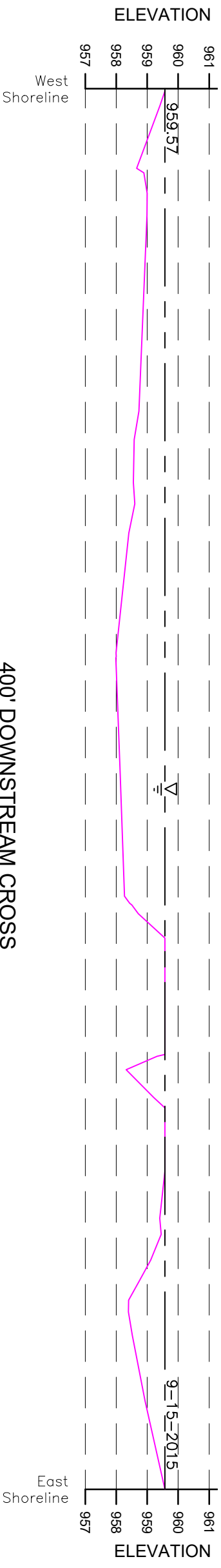
STRUCTURE NOTES:

1. The measured waterline elevation was 959.57 feet on the survey date of 9-15-2015.
2. The waterline was measured 0.80 feet below the top of the footing of Pier 1.
3. Access to the site was via a jon boat at the site

COLLINS ENGINEERS
 2033 W. Howard Ave
 Milwaukee, WI 53095
 Phone: 414-282-6905

WHRP-Predicting Scour of Bedrock Structure Overall
Structure B-10-131
 Neillsville, WI

CEI PROJECT 61-9236
INSPECTED BY: CSH
DRAWN BY: CSH
CHECKED BY: SJM
DATE: 9-15-2015
SHEET NO: C-01



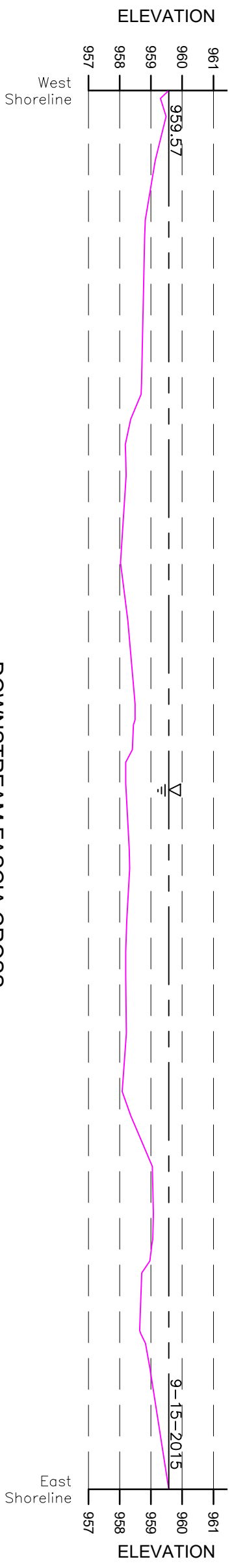
NOTE: Vertical scale multiplied by a factor of 5 for clarity.

COLLINS ENGINEERS
 2033 W. Howard Ave
 Milwaukee, WI 53095
 Phone: 414-282-6905

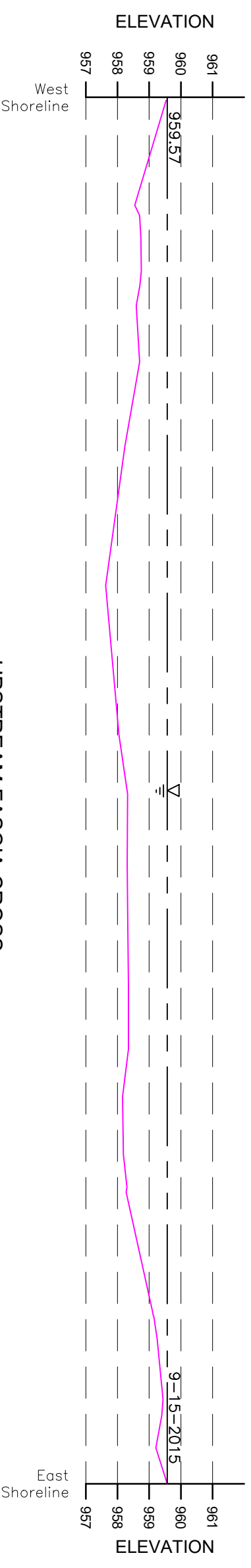


**WHRP-Predicting Scour of Bedrock
 Downstream Cross Sections
 Structure B-10-131**
 Neillsville, WI

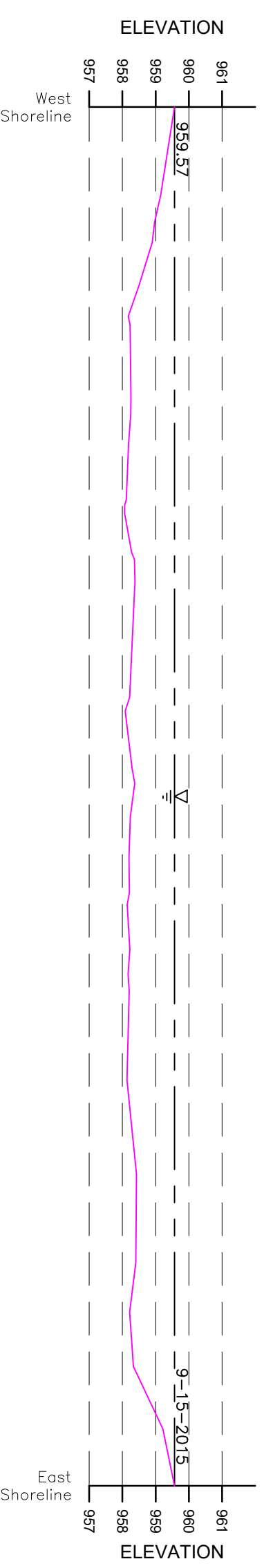
CEI PROJECT
 61-9236
 INSPECTED BY:
 CSH
 DRAWN BY:
 CSH
 CHECKED BY:
 SJM
 DATE:
 9-15-2015
 SHEET NO:
C-02



1
 DOWNSTREAM FASCIA CROSS
 SECTION - LOOKING NORTH
 SCALE: 1" = 20'



2
 UPSTREAM FASCIA CROSS
 SECTION - LOOKING NORTH
 SCALE: 1" = 20'



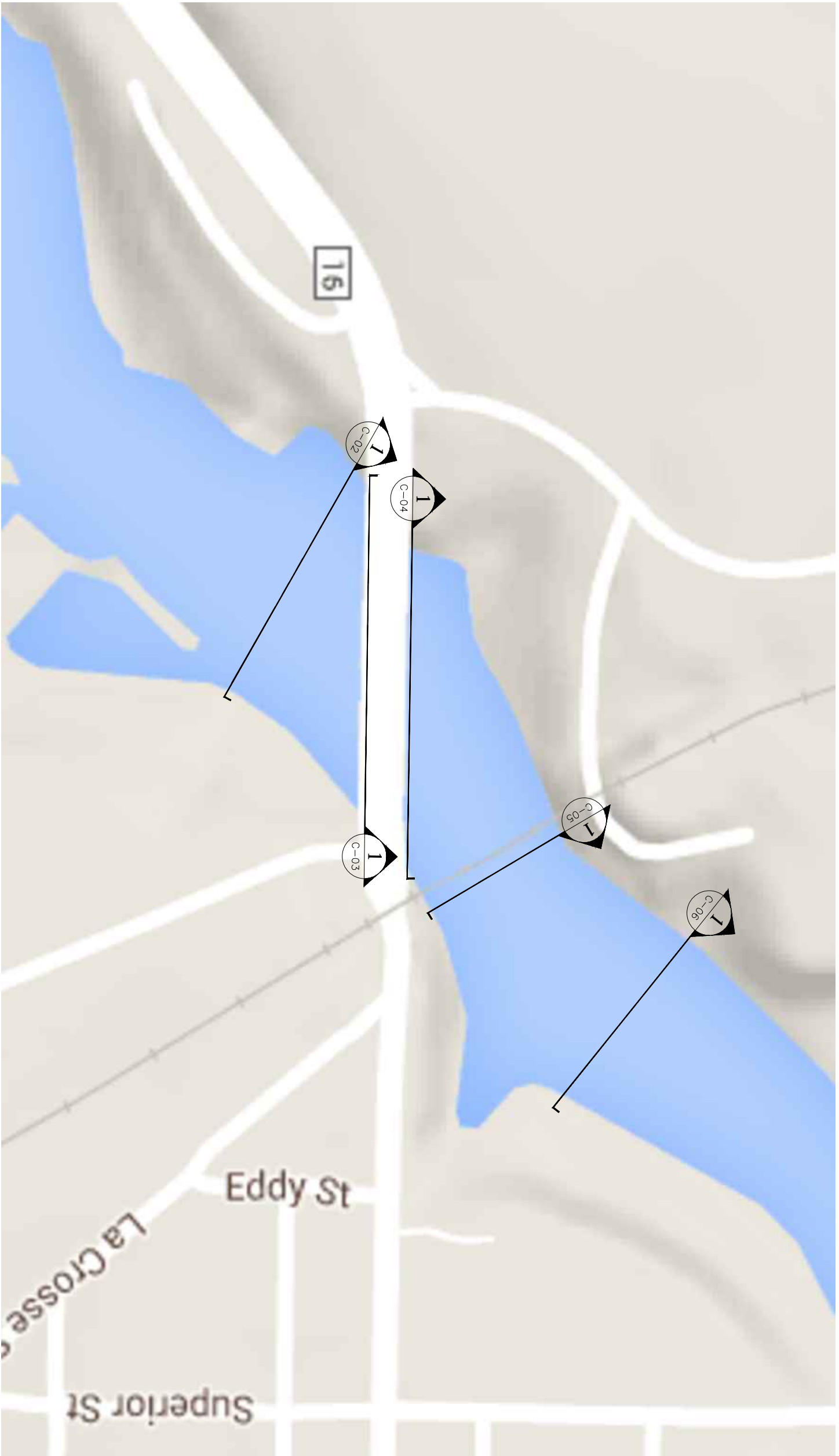
3
 200' UPSTREAM CROSS
 SECTION - LOOKING NORTH
 SCALE: 1" = 20'

NOTE: Vertical scale multiplied by a factor of 5 for clarity.

COLLINS ENGINEERS^{PC}
 2033 W. Howard Ave
 Milwaukee, WI 53095
 Phone: 414-282-6905

**WHRP-Predicting Scour of Bedrock
 Cross Sections
 Structure B-10-131**
 Neillsville, WI

CEI PROJECT 61-9236
INSPECTED BY: CSH
DRAWN BY: CSH
CHECKED BY: SJM
DATE: 9-15-2015
SHEET NO: C-03



STRUCTURE OVERALL
 SCALE: 1" = 200'

GENERAL NOTES:

1. The hydrographic survey was completed on September 11, 2015 by Collins Engineers, Inc.
2. Soundings were obtained using a continuously recording fathometer operating at 200KHZ and linked to a WAAS capable GPS receiver.
3. Base map information shown on this drawing shall be considered approximate.

STRUCTURE NOTES:

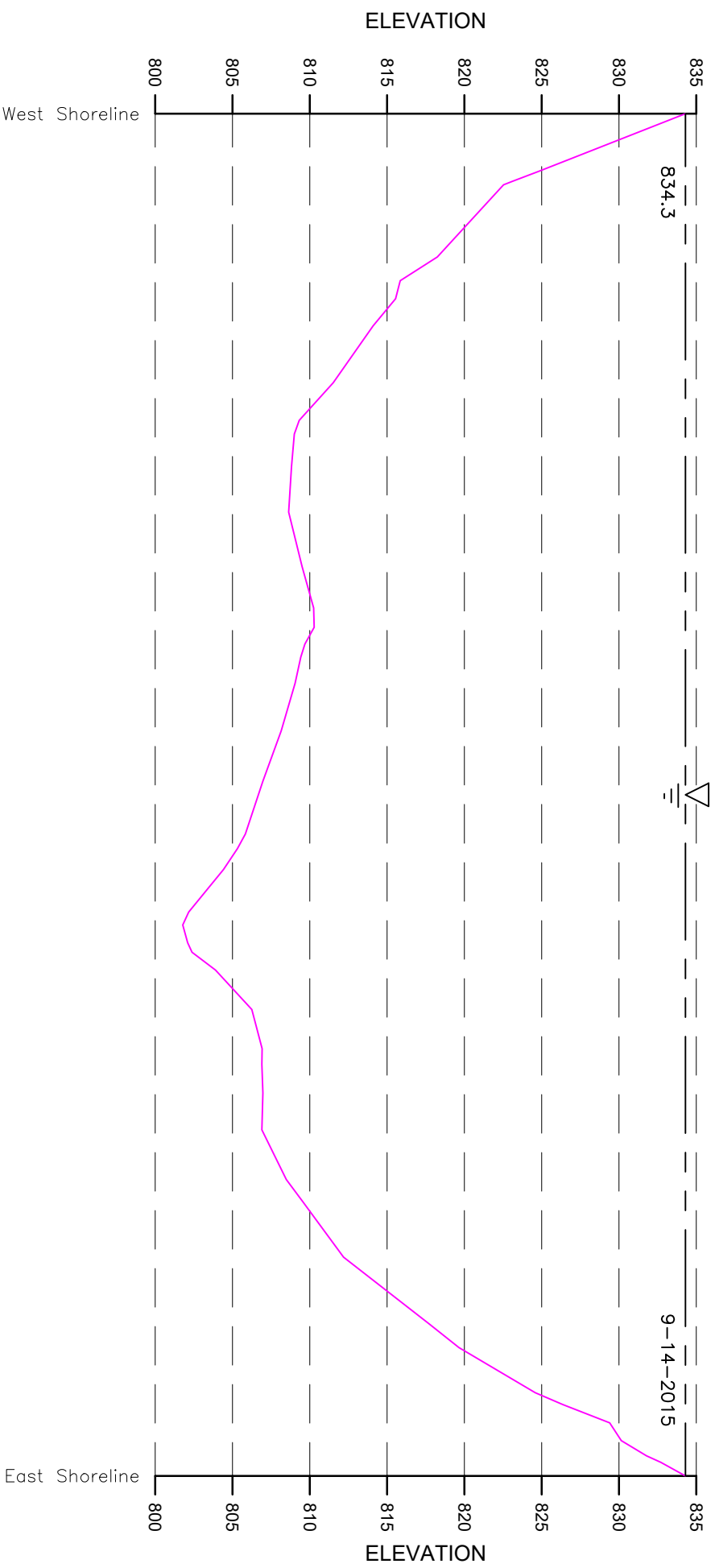
1. The measured waterline elevation was 534.3 feet on the survey date of 9-15-2015.
2. The waterline was measured 15.7 feet below the joint between the pier shaft and pier cap of Pier 1 of B-11-104.
3. Access to the site was via a boat launch 0.5 miles NE of the bridge. GPS Coordinates: N43°38'03.16", W89°46'20.60"

COLLINS ENGINEERS
 455 Sherman St.
 Suite 160
 Denver, CO 80203
 Phone: 303-447-9300

UWM
WHRP

WHRP-Predicting Scour of Bedrock Structure Overall
Structure B-11-001/104
 Wisconsin Dells, WI

CEI PROJECT
 61-9236
 INSPECTED BY:
 CSH
 DRAWN BY:
 CSH
 CHECKED BY:
 RAF
 DATE:
 9-14-2015
 SHEET NO:
C-01



1
180' DOWNSTREAM CROSS SECTION - LOOKING NORTHEAST
 HORIZONTAL SCALE: 1" = 50'

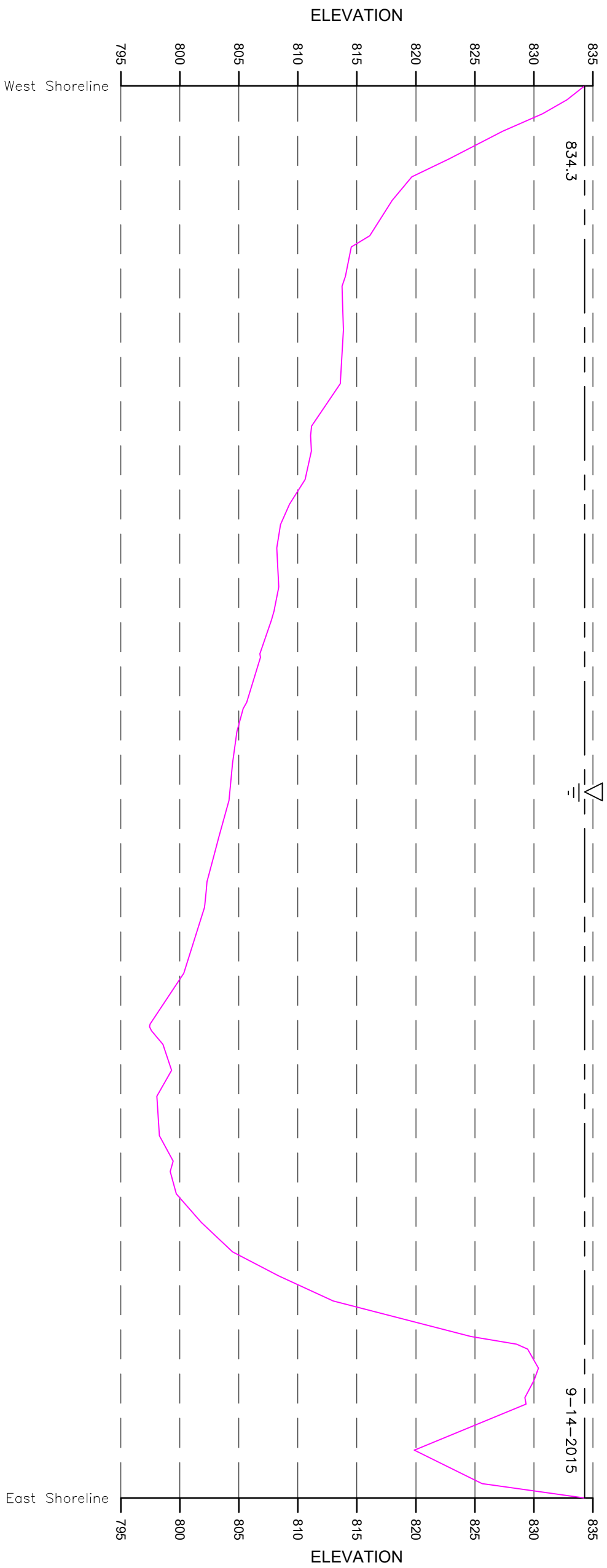
NOTE: Vertical scale multiplied by a factor of 5 for clarity.

COLLINS ENGINEERS
 455 Sherman St.
 Suite 160
 Denver, CO 80203
 Phone: 303-447-9300



WHRP-Predicting Scour of Bedrock
180' Downstream Cross Section
Structure B-11-001/104
 Wisconsin Dells, WI

CEI PROJECT
 61-9236
 INSPECTED BY:
 CSH
 DRAWN BY:
 CSH
 CHECKED BY:
 RAF
 DATE:
 9-14-2015
 SHEET NO:
C-01



1
DOWNSTREAM FASCIA CROSS SECTION - LOOKING NORTH
 HORIZONTAL SCALE: 1" = 50'

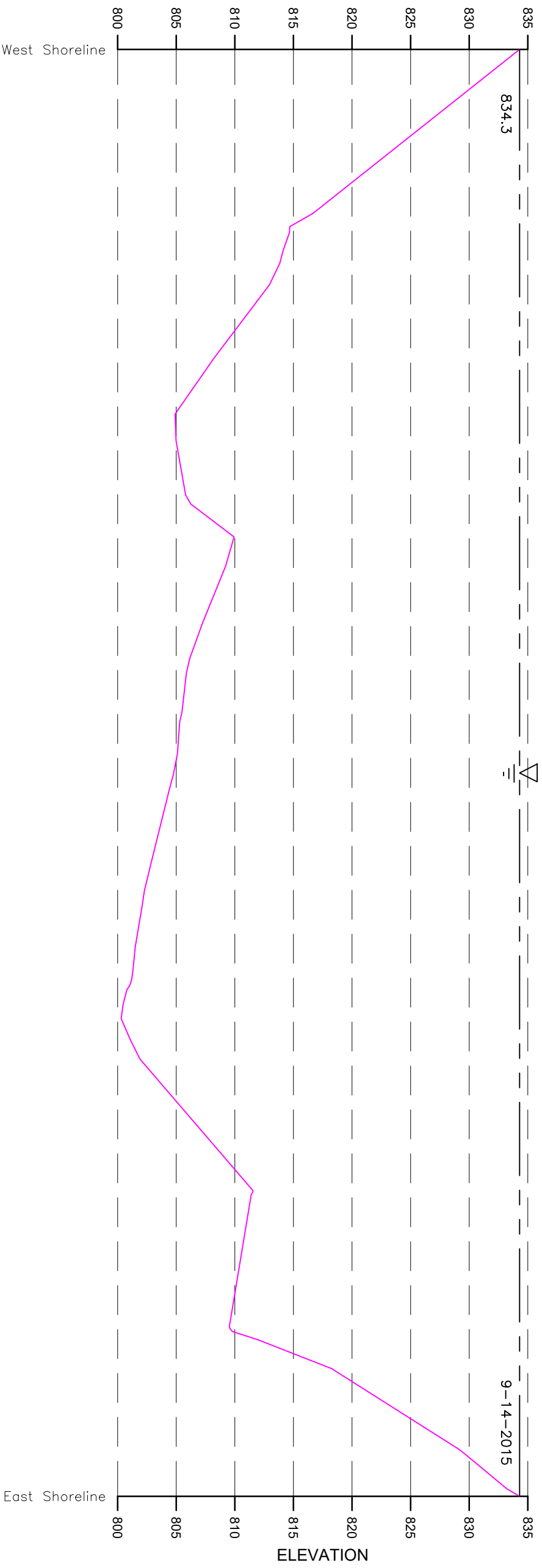
NOTE: Vertical scale multiplied by a factor of 5 for clarity.

COLLINS ENGINEERS
 455 Sherman St.
 Suite 160
 Denver, CO 80203
 Phone: 303-447-9300

UWM
WHRP

WHRP-Predicting Scour of Bedrock Downstream Fascia Cross Section Structure B-11-001/104
 Wisconsin Dells, WI

CEI PROJECT 61-9236
INSPECTED BY: CSH
DRAWN BY: CSH
CHECKED BY: RAF
DATE: 9-14-2015
SHEET NO: C-02



1
 UPSTREAM FASCIA CROSS
 SECTION - LOOKING NORTH
 HORIZONTAL SCALE: 1" = 50'

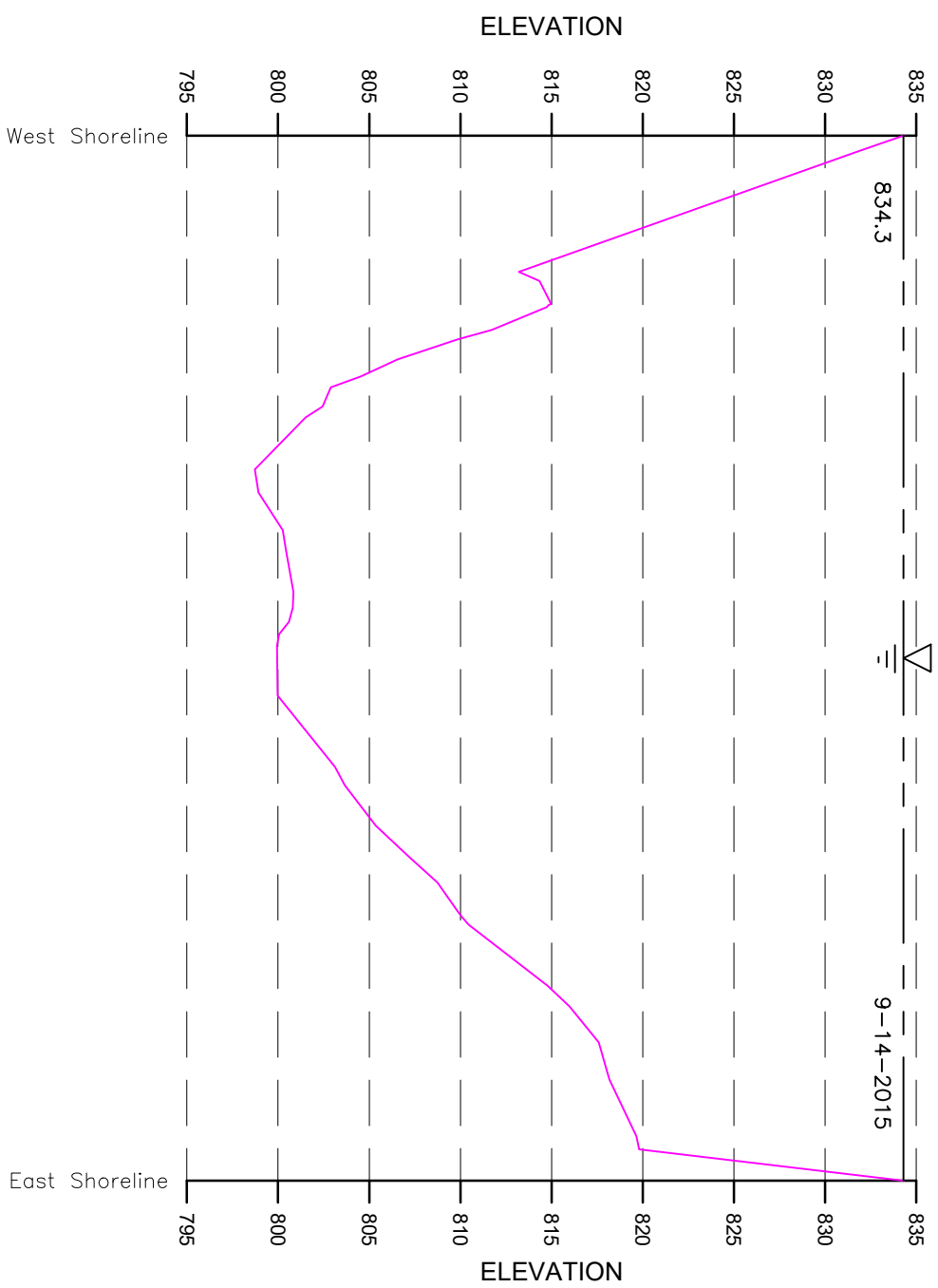
NOTE: Vertical scale multiplied by a factor of 5 for clarity.

COLLINS ENGINEERS
 455 Sherman St.
 Suite 160
 Denver, CO 80203
 Phone: 303-447-9300



**WHRP-Predicting Scour of Bedrock
 Upstream Fascia Cross Section
 Structure B-11-001/104**
 Wisconsin Dells, WI

CEI PROJECT 61-9236
INSPECTED BY: CSH
DRAWN BY: CSH
CHECKED BY: RAF
DATE: 9-14-2015
SHEET NO: C-03



1
345' UPSTREAM CROSS SECTION - LOOKING NORTHEAST
 HORIZONTAL SCALE: 1" = 50'

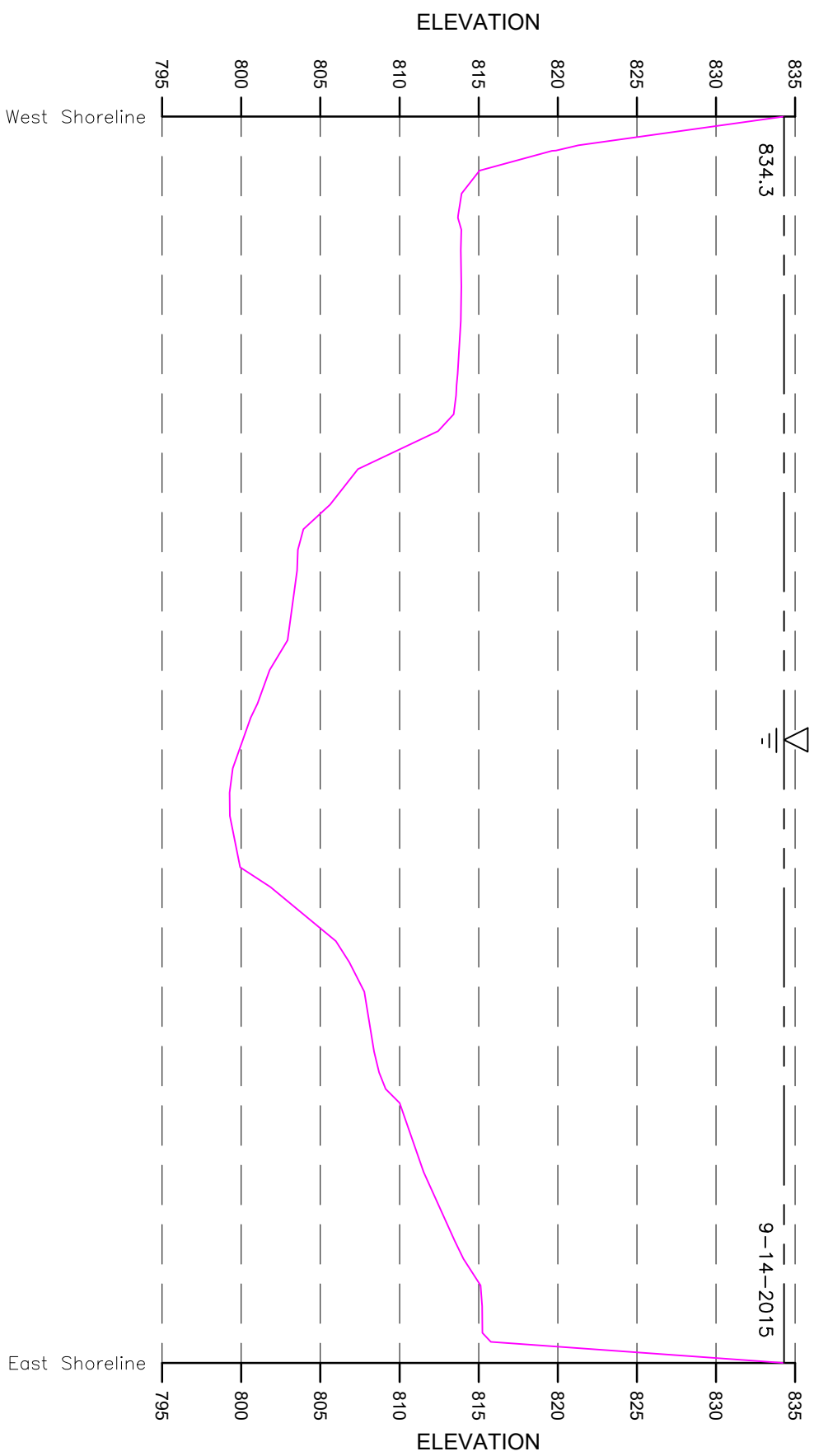
NOTE: Vertical scale multiplied by a factor of 5 for clarity.

COLLINS ENGINEERS
 455 Sherman St.
 Suite 160
 Denver, CO 80203
 Phone: 303-447-9300



WHRP-Predicting Scour of Bedrock
345' Upstream Cross Section
Structure B-11-001/104
 Wisconsin Dells, WI

CEI PROJECT
 61-9236
 INSPECTED BY:
 CSH
 DRAWN BY:
 CSH
 CHECKED BY:
 RAF
 DATE:
 9-14-2015
 SHEET NO:
C-04



1
650' UPSTREAM CROSS SECTION - LOOKING NORTHEAST
 HORIZONTAL SCALE: 1" = 50'

NOTE: Vertical scale multiplied by a factor of 5 for clarity.

COLLINS ENGINEERS
 455 Sherman St.
 Suite 160
 Denver, CO 80203
 Phone: 303-447-9300



WHRP-Predicting Scour of Bedrock
650' Upstream Cross Section
Structure B-11-001/104
 Wisconsin Dells, WI

CEI PROJECT 61-9236
INSPECTED BY: CSH
DRAWN BY: CSH
CHECKED BY: RAF
DATE: 9-14-2015
SHEET NO: C-05



GENERAL NOTES:

1. The hydrographic survey was completed on September 15, 2015 by Collins Engineers, Inc.
2. Soundings were obtained using a continuously recording fathometer operating at 200KHz and linked to a WAAS capable GPS receiver.
3. Base map information shown on this drawing shall be considered approximate.



STRUCTURE NOTES:

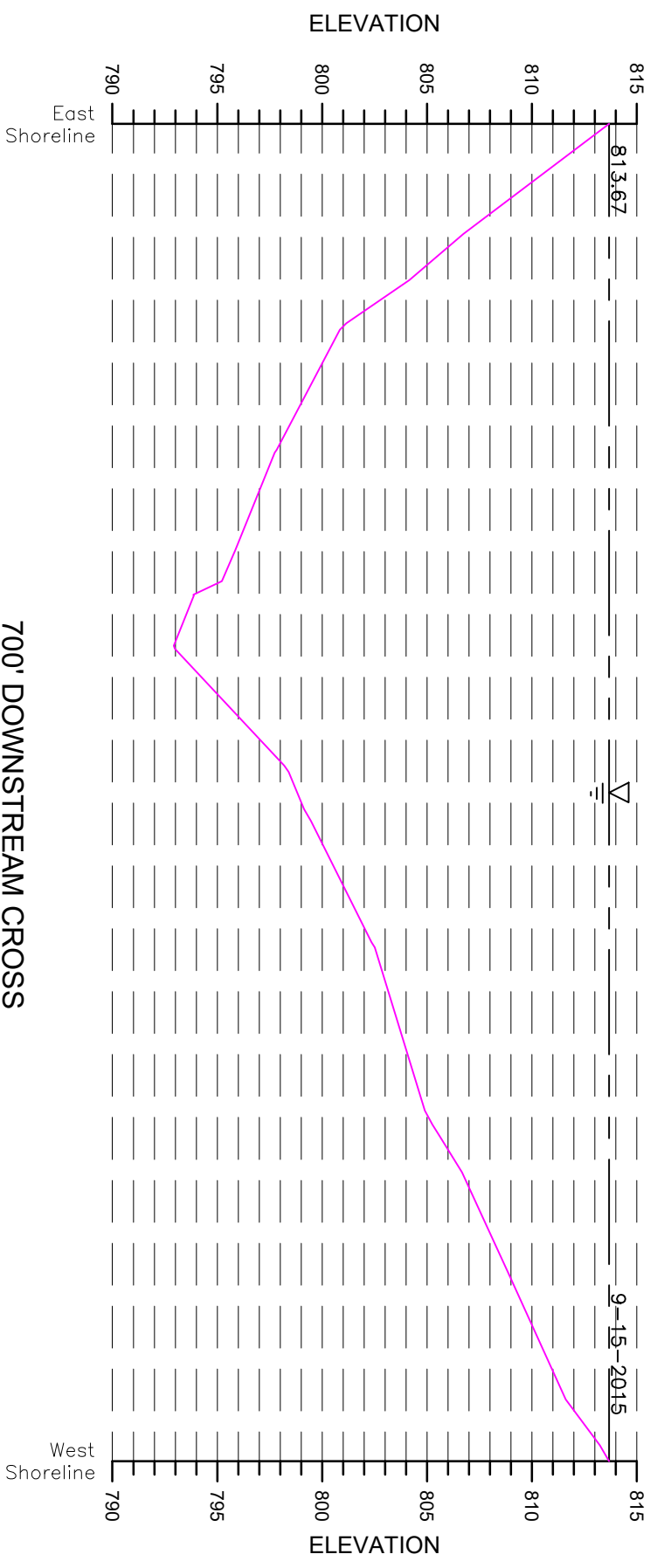
1. The measured waterline elevation was 813.67 feet on the survey date of 9-15-2015.
2. The waterline was measured 2.3 feet below the construction joint on column 1 of Pier 2.
3. Access to the site was via a boat launch SW of the bridge in Wakanda Park. GPS coordinates: N44°54'03.7", W91°54'49.26"

CEL PROJECT	01-9236
INSPECTED BY:	CSH
DRAWN BY:	CSH
CHECKED BY:	SJM
DATE:	9-15-2015
SHEET NO:	C-01

**WHRP-Predicting Scour of Bedrock
Structure Overall
Structure B-17-208\209**
Menomonee, WI



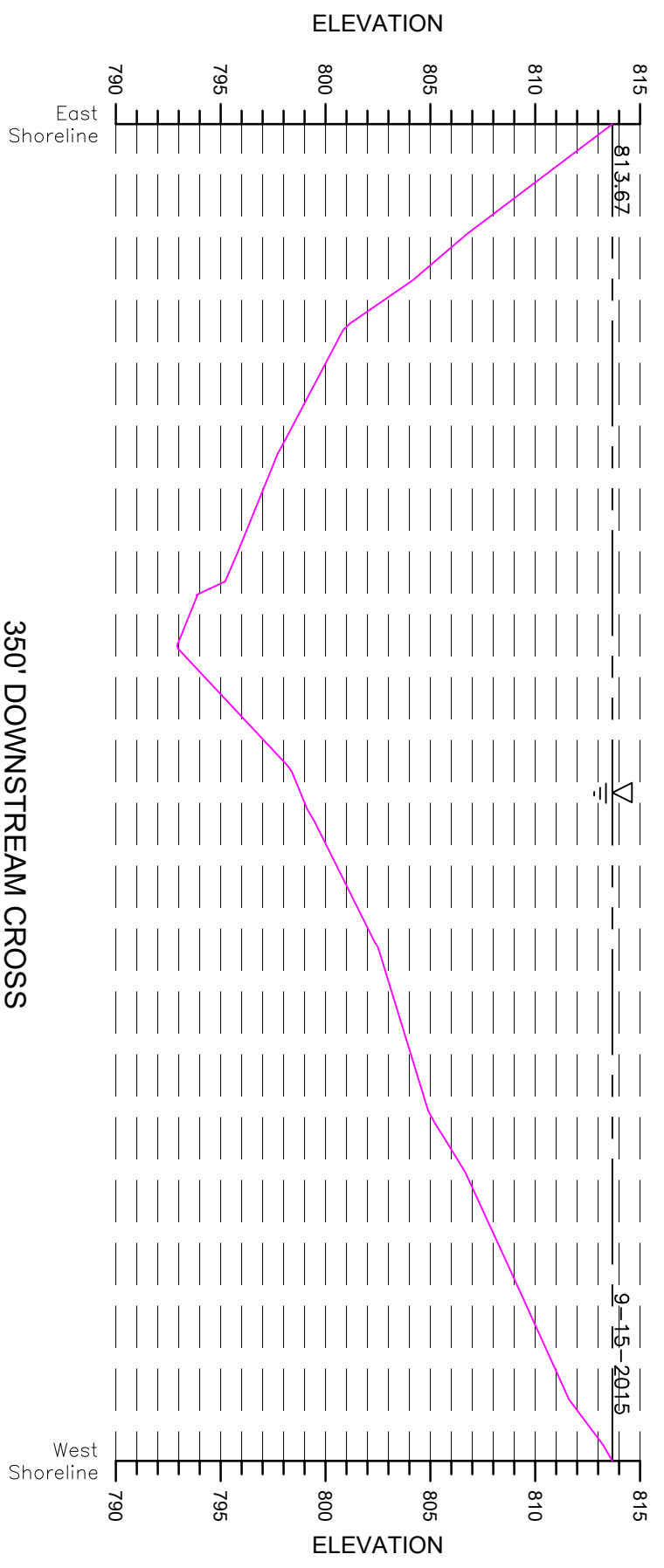
COLLINS ENGINEERS
2033 W. Howard Ave
Milwaukee, WI 53095
Phone: 414-282-6905



1

700' DOWNSTREAM CROSS
SECTION - LOOKING SOUTH

SCALE: 1" = 40'



2

350' DOWNSTREAM CROSS
SECTION - LOOKING SOUTH

SCALE: 1" = 40'



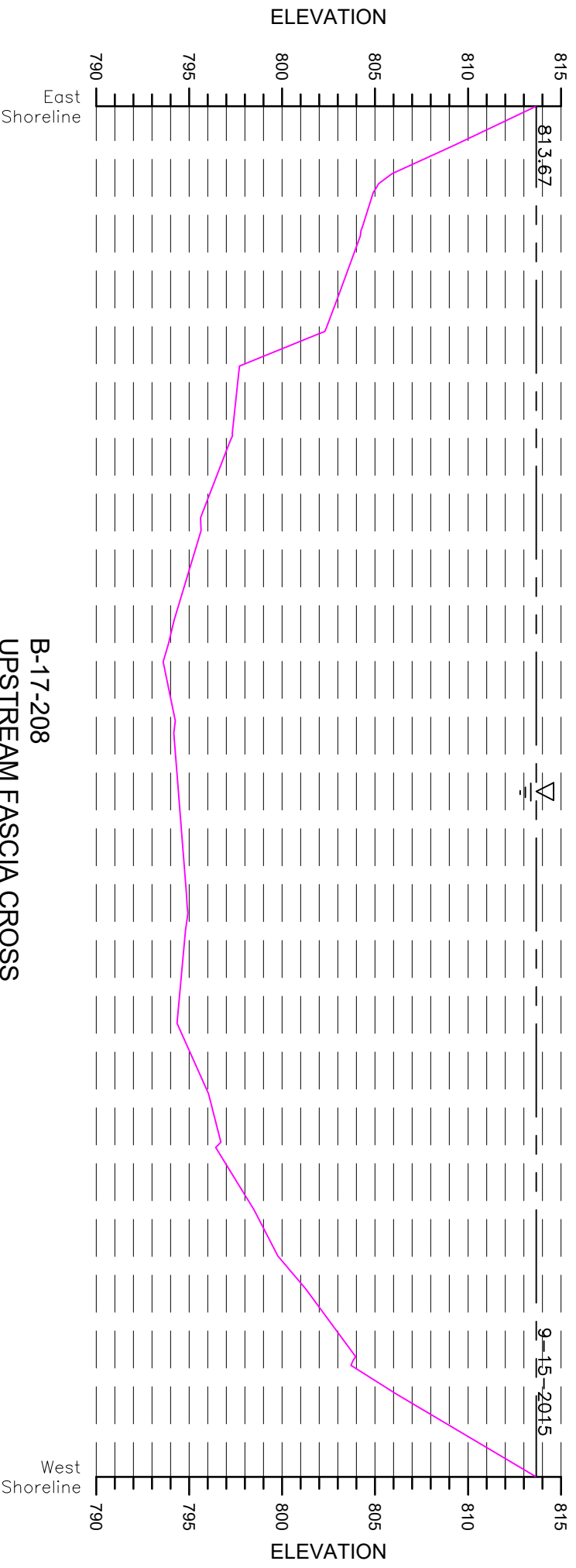
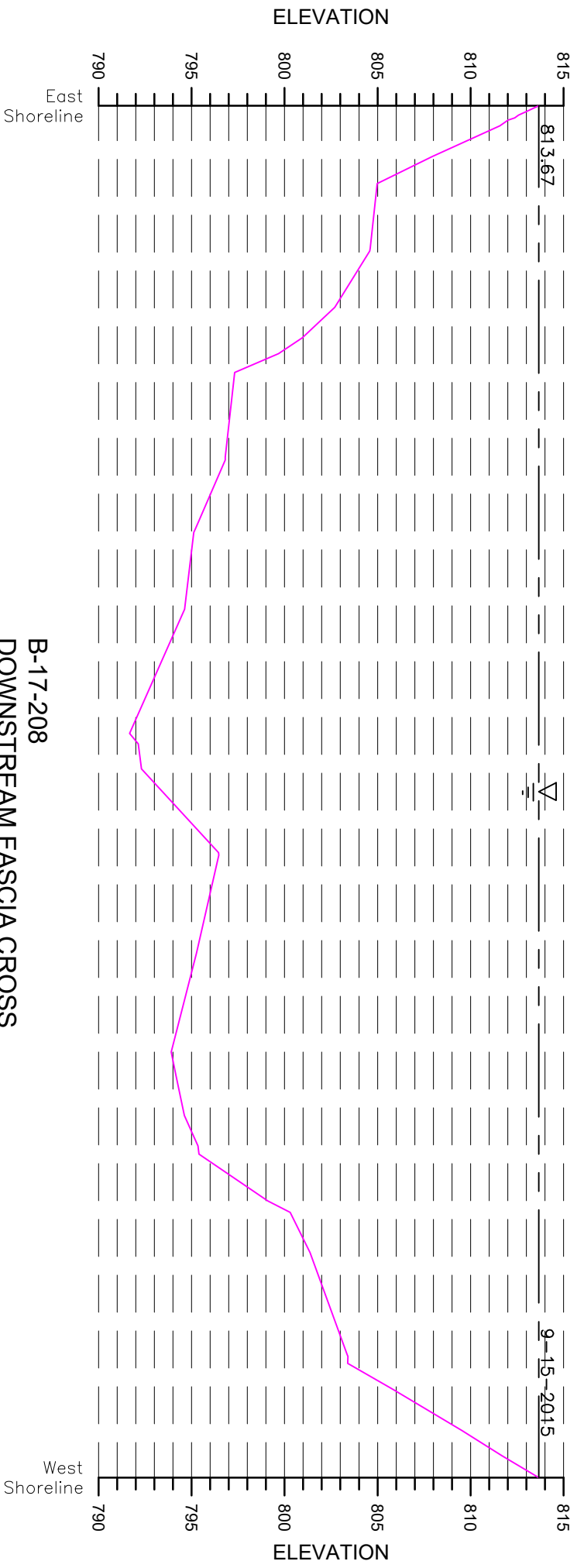
NOTE: Vertical scale multiplied by a factor of 5 for clarity.

COLLINS ENGINEERS
2033 W. Howard Ave
Milwaukee, WI 53095
Phone: 414-282-6905

**WHRP-Predicting Scour of Bedrock
Downstream Cross Sections
Structure B-17-208/209**
Menomonee, WI

CEI PROJECT 61-9236
INSPECTED BY: CSH
DRAWN BY: CSH
CHECKED BY: SJM
DATE: 9-15-2015
SHEET NO: C-02

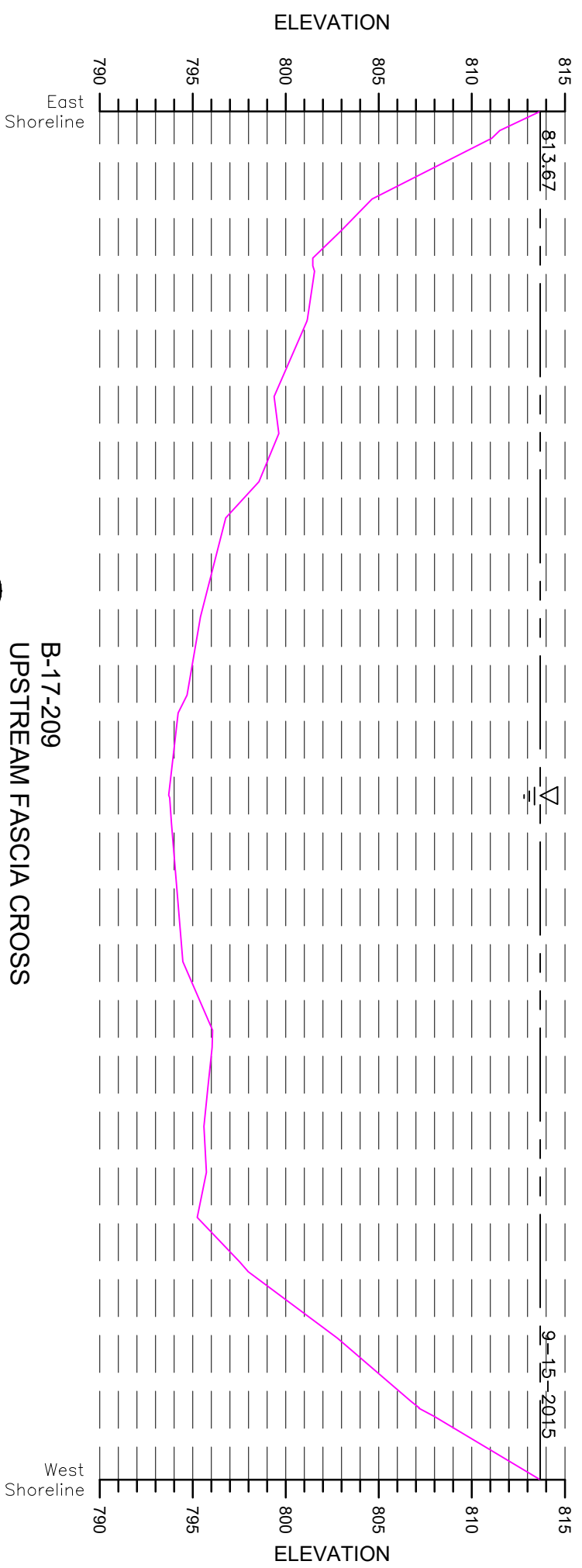
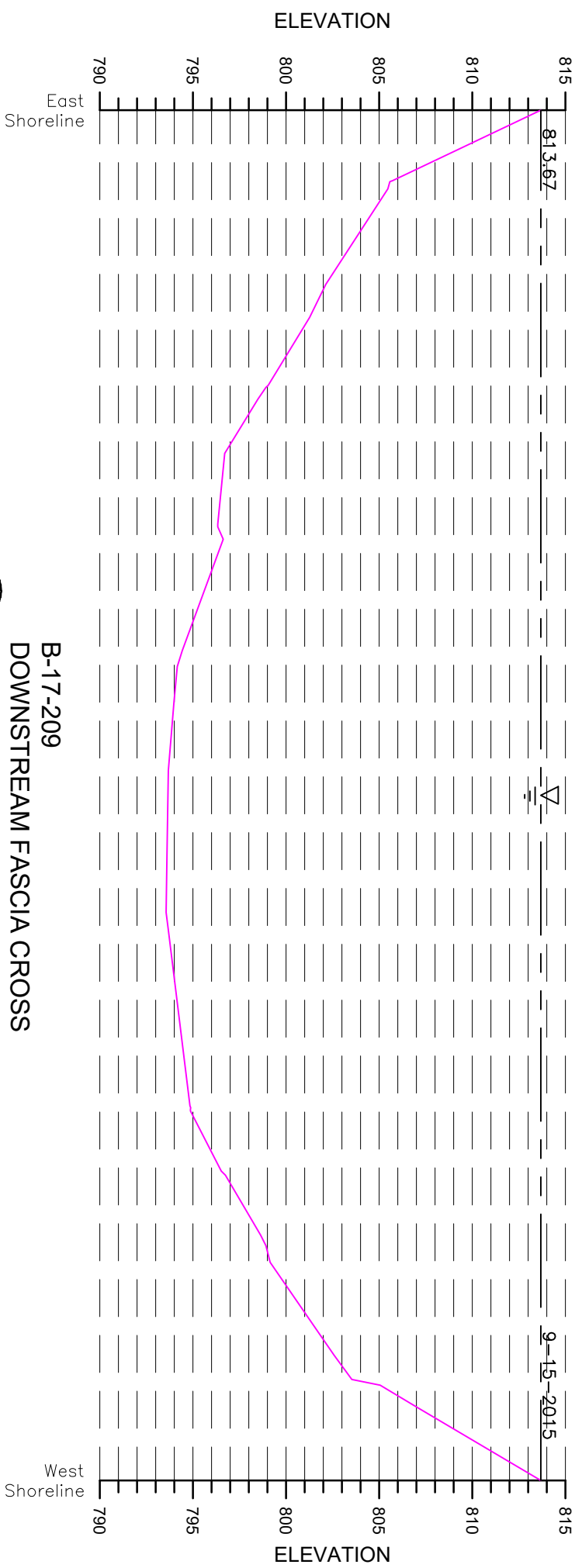
NOTE: Vertical scale multiplied by a factor of 5 for clarity.



COLLINS ENGINEERS^{PC}
2033 W. Howard Ave
Milwaukee, WI 53095
Phone: 414-282-6905

**WHRP-Predicting Scour of Bedrock
B-17-208 Fascia Cross Sections
Structure B-17-208/209**
Menomonee, WI

CEI PROJECT 61-9236
INSPECTED BY: CSH
DRAWN BY: CSH
CHECKED BY: SJM
DATE: 9-15-2015
SHEET NO: C-03



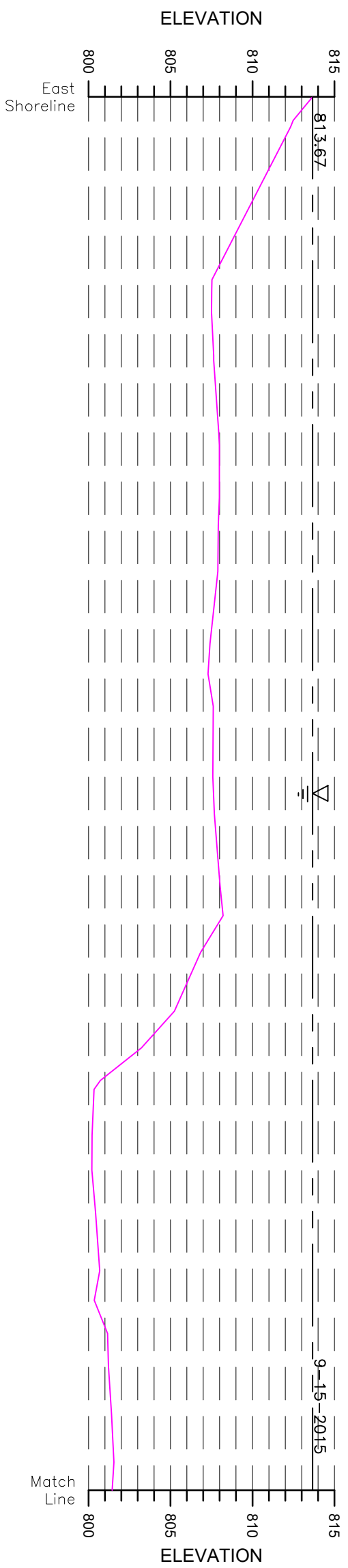
NOTE: Vertical scale multiplied by a factor of 5 for clarity.

COLLINS ENGINEERS
 2033 W. Howard Ave
 Milwaukee, WI 53095
 Phone: 414-282-6905

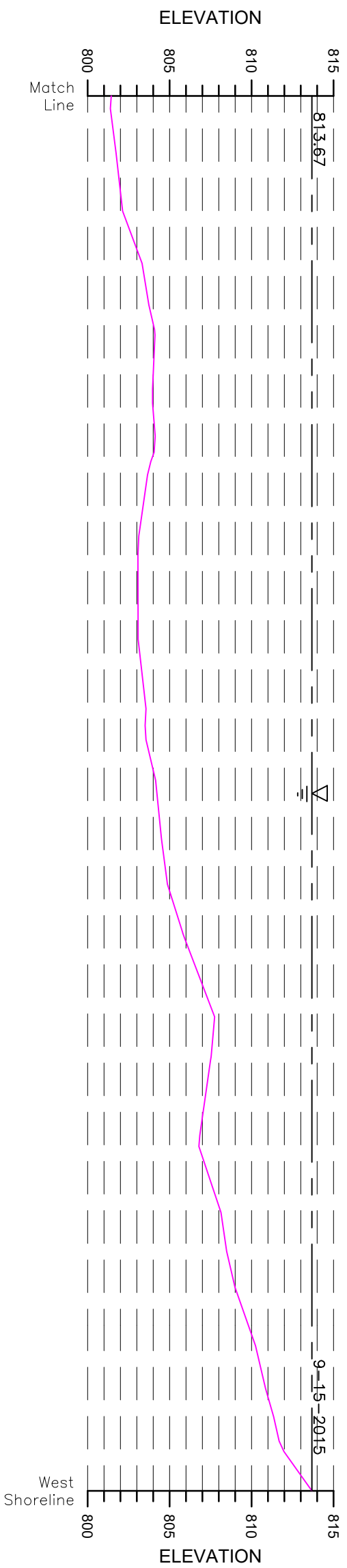


**WHRP-Predicting Scour of Bedrock
 B-17-209 Fascia Cross Sections
 Structure B-17-208/209**
 Menomonee, WI

CEI PROJECT
 61-9236
 INSPECTED BY:
 CSH
 DRAWN BY:
 CSH
 CHECKED BY:
 SJM
 DATE:
 9-15-2015
 SHEET NO:
C-04



1
 350' UPSTREAM CROSS
 SECTION - LOOKING SOUTH
 SCALE: 1" = 40'



2
 350' UPSTREAM CROSS
 SECTION - LOOKING SOUTH
 SCALE: 1" = 40'

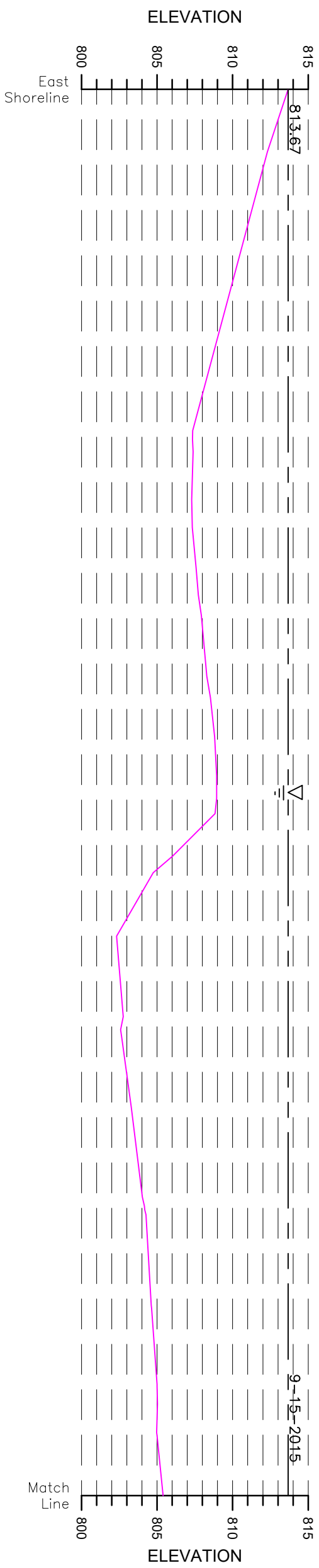
NOTE: Vertical scale multiplied by a factor of 5 for clarity.

COLLINS ENGINEERS
 2033 W. Howard Ave
 Milwaukee, WI 53095
 Phone: 414-282-6905

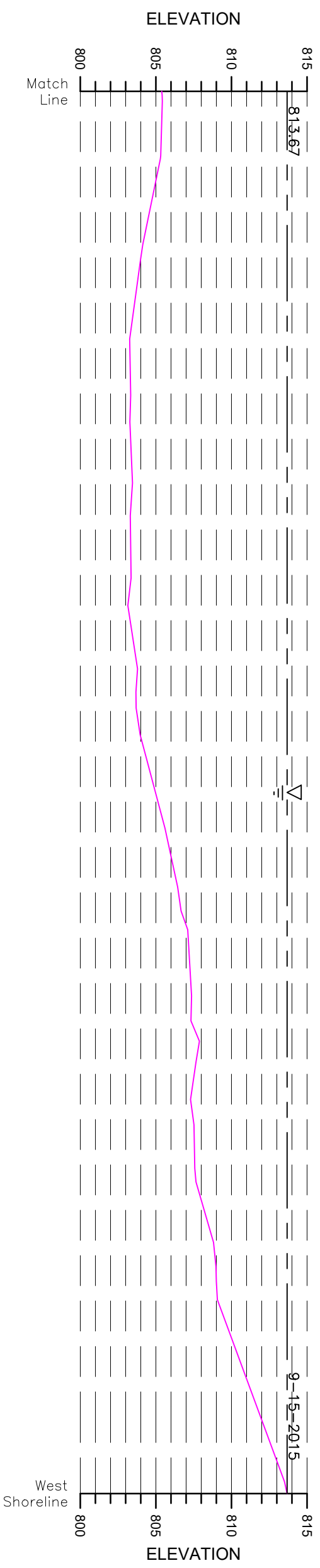
UWM
WHRP

WHRP-Predicting Scour of Bedrock
350' Upstream Cross Section
Structure B-17-208/209
 Menomonee, WI

CEI PROJECT 61-9236
INSPECTED BY: CSH
DRAWN BY: CSH
CHECKED BY: SJM
DATE: 9-15-2015
SHEET NO: C-05



1
 700' UPSTREAM CROSS
 SECTION - LOOKING SOUTH
 SCALE: 1" = 40'



2
 700' UPSTREAM CROSS
 SECTION - LOOKING SOUTH
 SCALE: 1" = 40'

NOTE: Vertical scale multiplied by a factor of 5 for clarity.

COLLINS ENGINEERS
 2033 W. Howard Ave
 Milwaukee, WI 53095
 Phone: 414-282-6905

UWM
WHRP

WHRP-Predicting Scour of Bedrock
700' Upstream Cross Section
Structure B-17-208/209
 Menomonee, WI

CEI PROJECT	61-9236
INSPECTED BY:	CSH
DRAWN BY:	CSH
CHECKED BY:	SJM
DATE:	9-15-2015
SHEET NO:	C-07



GENERAL NOTES:

1. The sounding plan was completed on September 17th, 2015 by Collins Engineers, Inc.
2. Soundings were obtained using a survey rod.
3. Base map information shown on this drawing shall be considered approximate.



STRUCTURE NOTES:

1. The measured waterline elevation was 464.68 feet on the survey date of 9-17-2015.
2. The waterline was measured 0.7 feet below the top of the foundation of Pier 2 (B-36-72) at the upstream nose.
3. Access to the site was via the roadway of the structure.

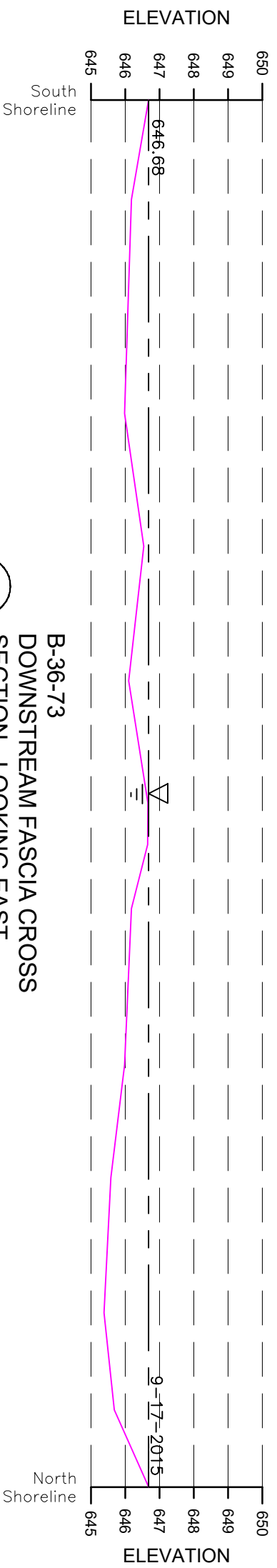
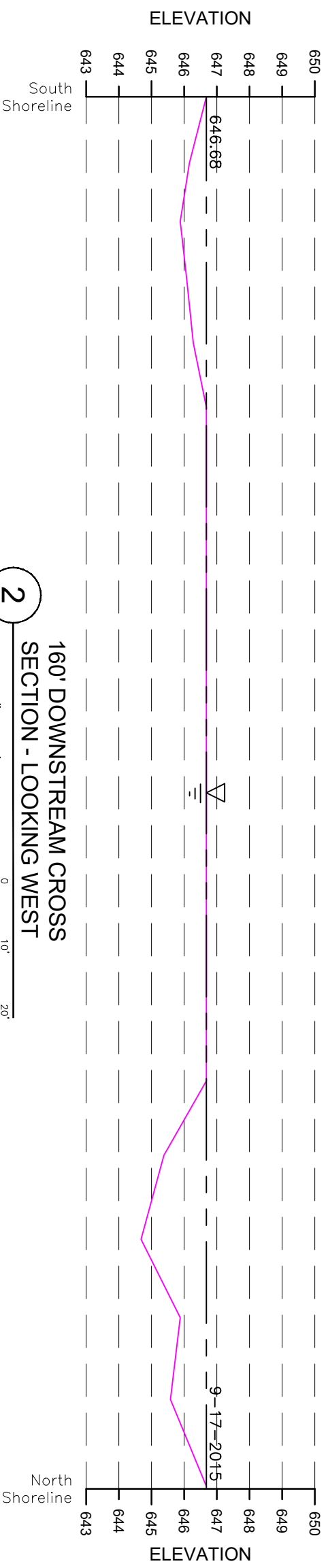
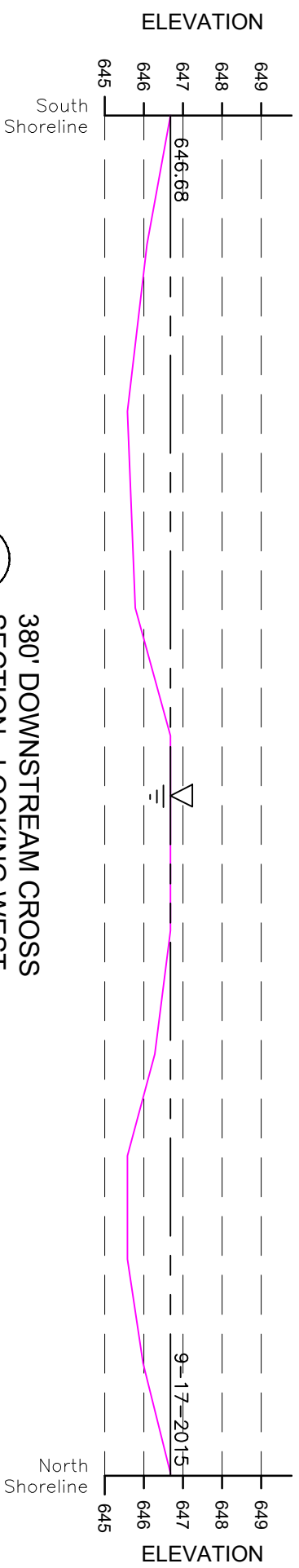
G:\V236-UWM ROCK SCOUR STUDY\CAD\BASE FILES\B-36-72_73.DWG 02/11/2016 02:33:56 PM

CEI PROJECT 01-9236
INSPECTED BY: CSH
DRAWN BY: CSH
CHECKED BY: SJM
DATE: 9-17-2015
SHEET NO: C-01

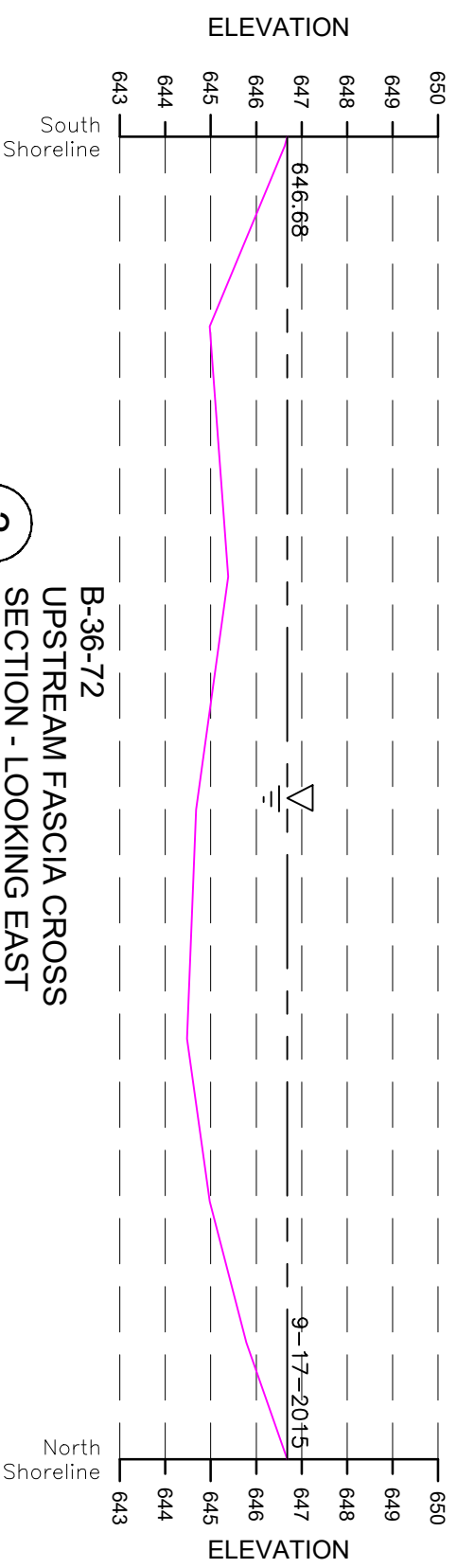
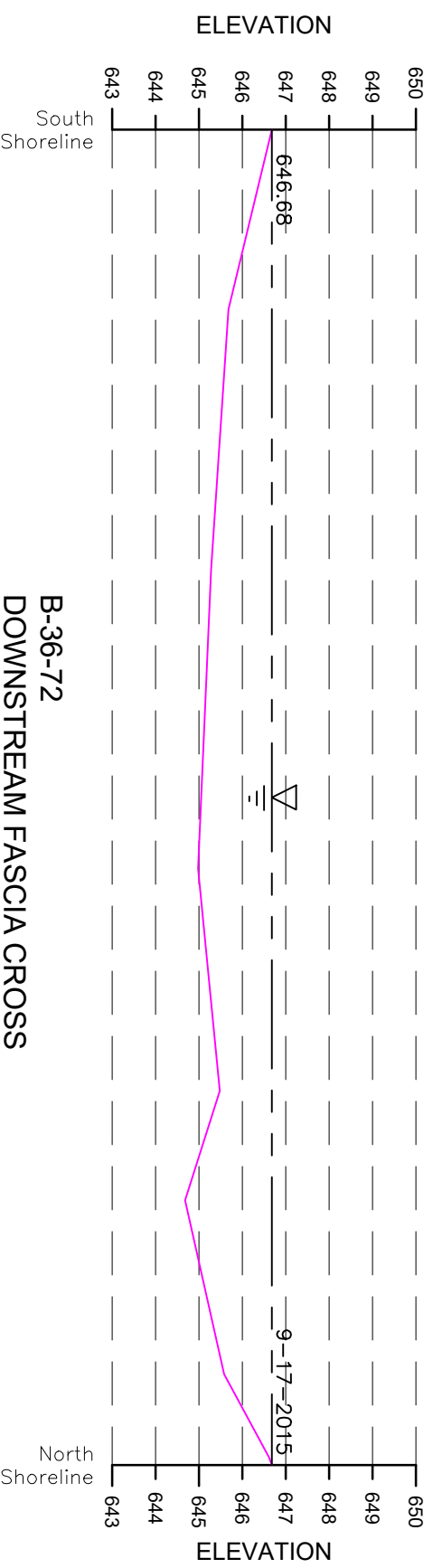
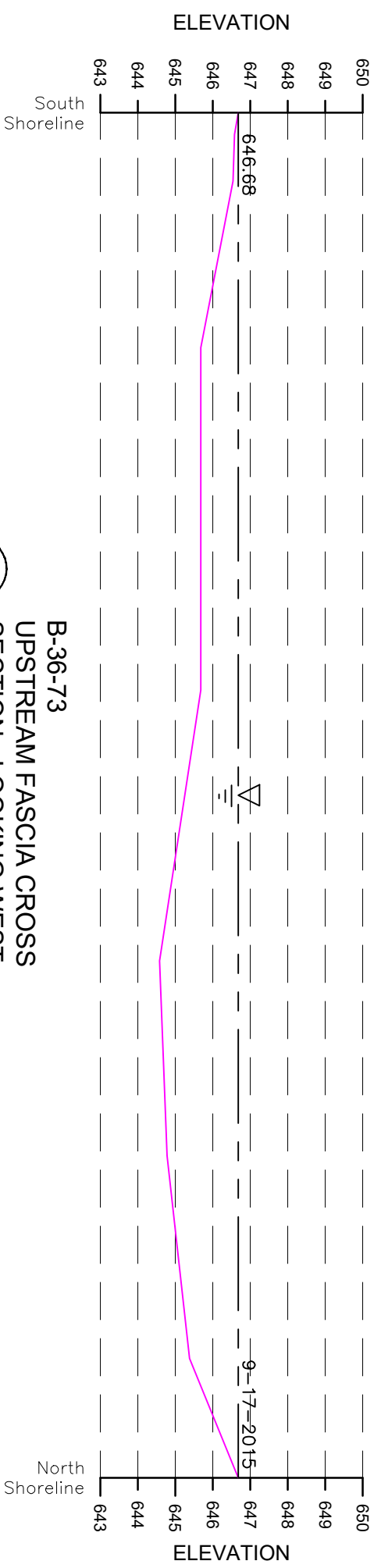
**WHRP-Predicting Scour of Bedrock
Structure Overall
Structure B-36-72\73**
 Manitowoc, WI



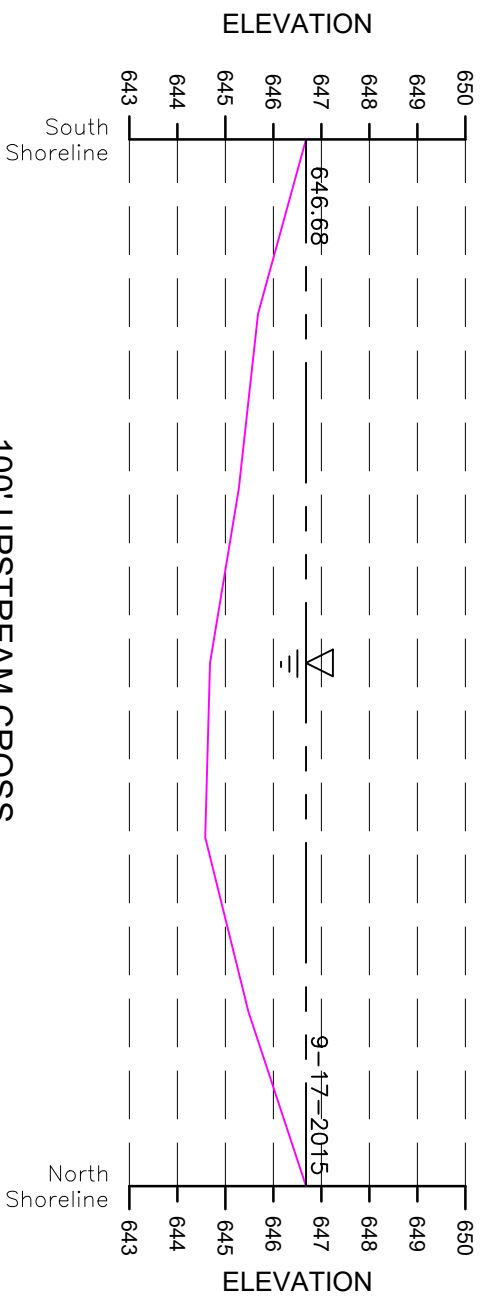
COLLINS ENGINEERS
 2033 W. Howard Ave
 Milwaukee, WI 53095
 Phone: 414-282-6905



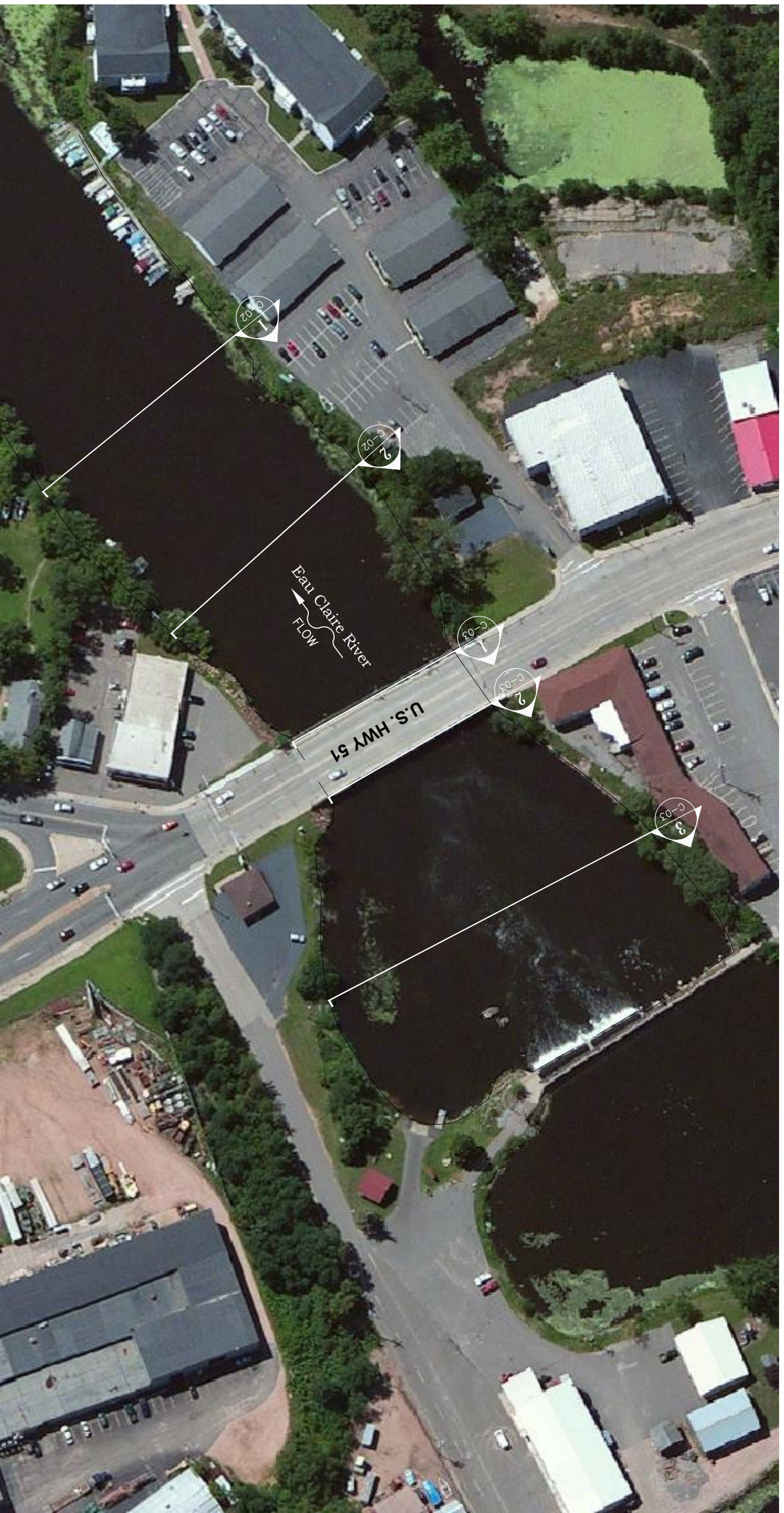
NOTE: Vertical scale multiplied by a factor of 5 for clarity.



NOTE: Vertical scale multiplied by a factor of 5 for clarity.

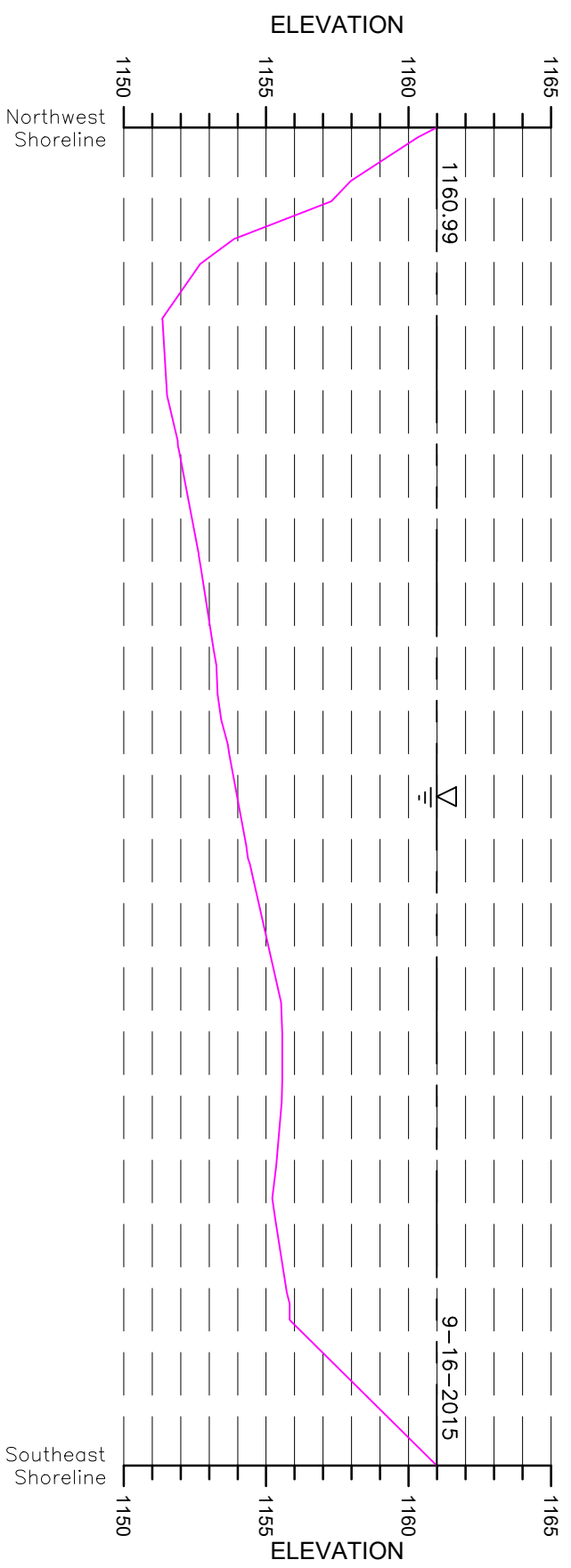


NOTE: Vertical scale multiplied by a factor of 5 for clarity.



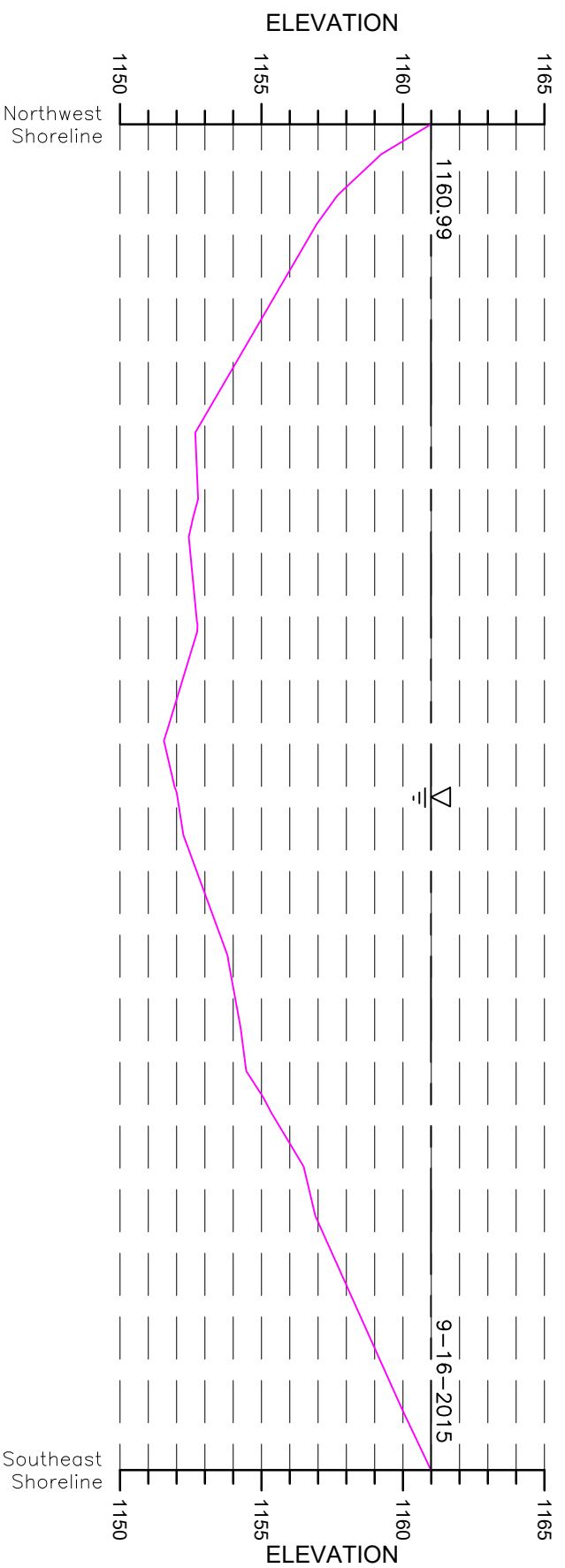
- GENERAL NOTES:**
1. The hydrographic survey was completed on September 16, 2015 by Collins Engineers, Inc.
 2. Soundings were obtained using a continuously recording fathometer operating at 200KHZ and linked to a WAAS capable GPS receiver.
 3. Base map information shown on this drawing shall be considered approximate.

- STRUCTURE NOTES:**
1. The measured waterline elevation was 1160.99 feet on the survey date of 9-16-2015.
 2. The waterline was measured 4.1 feet below the top of Pier 1 at the downstream nose.
 3. Access to the site was via a boat launch NE of the bridge. GPS coordinates: N44°54'58.74", W89°36'36.28"



1

350' DOWNSTREAM CROSS SECTION - LOOKING NORTHEAST

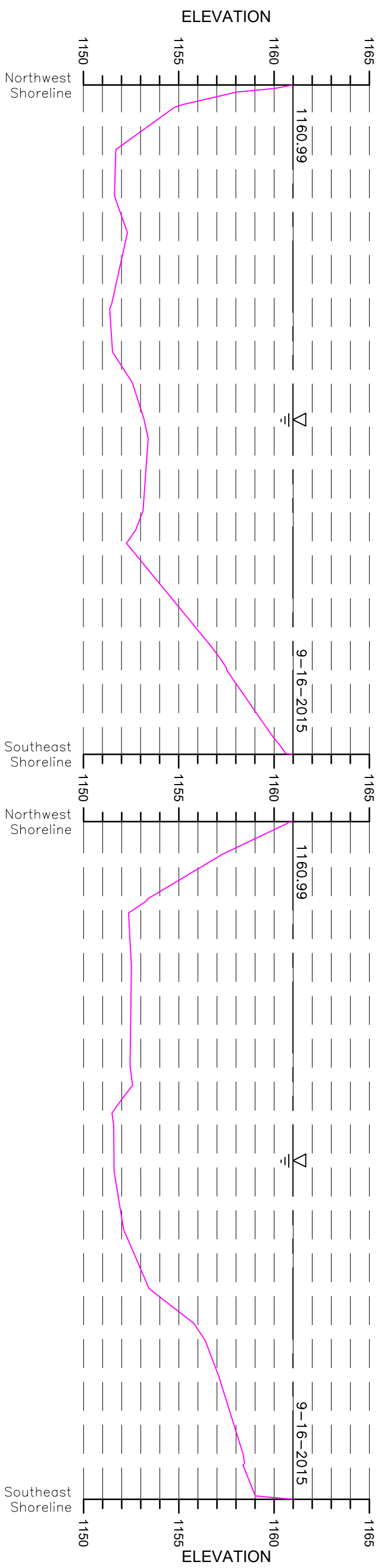


2

175' DOWNSTREAM CROSS SECTION - LOOKING NORTHEAST



NOTE: Vertical scale multiplied by a factor of 5 for clarity.



1

DOWNSTREAM FASCIA CROSS SECTION - LOOKING NORTHEAST

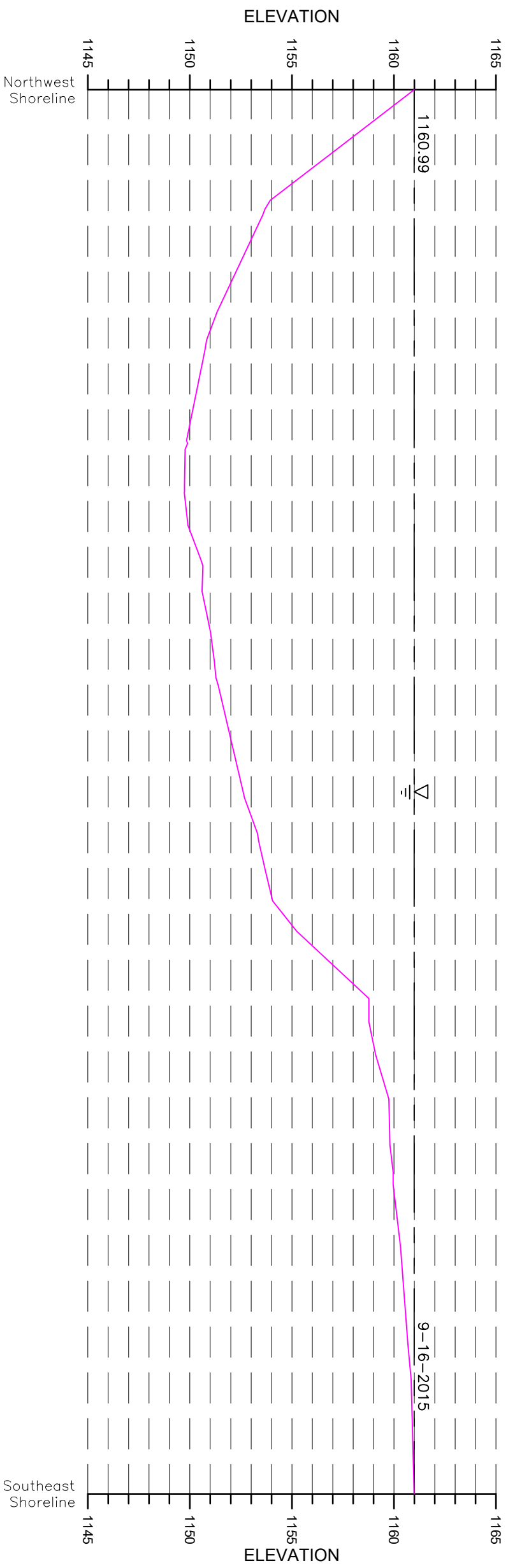
SCALE: 1" = 30'



2

UPSTREAM FASCIA CROSS SECTION - LOOKING NORTHEAST

SCALE: 1" = 30'



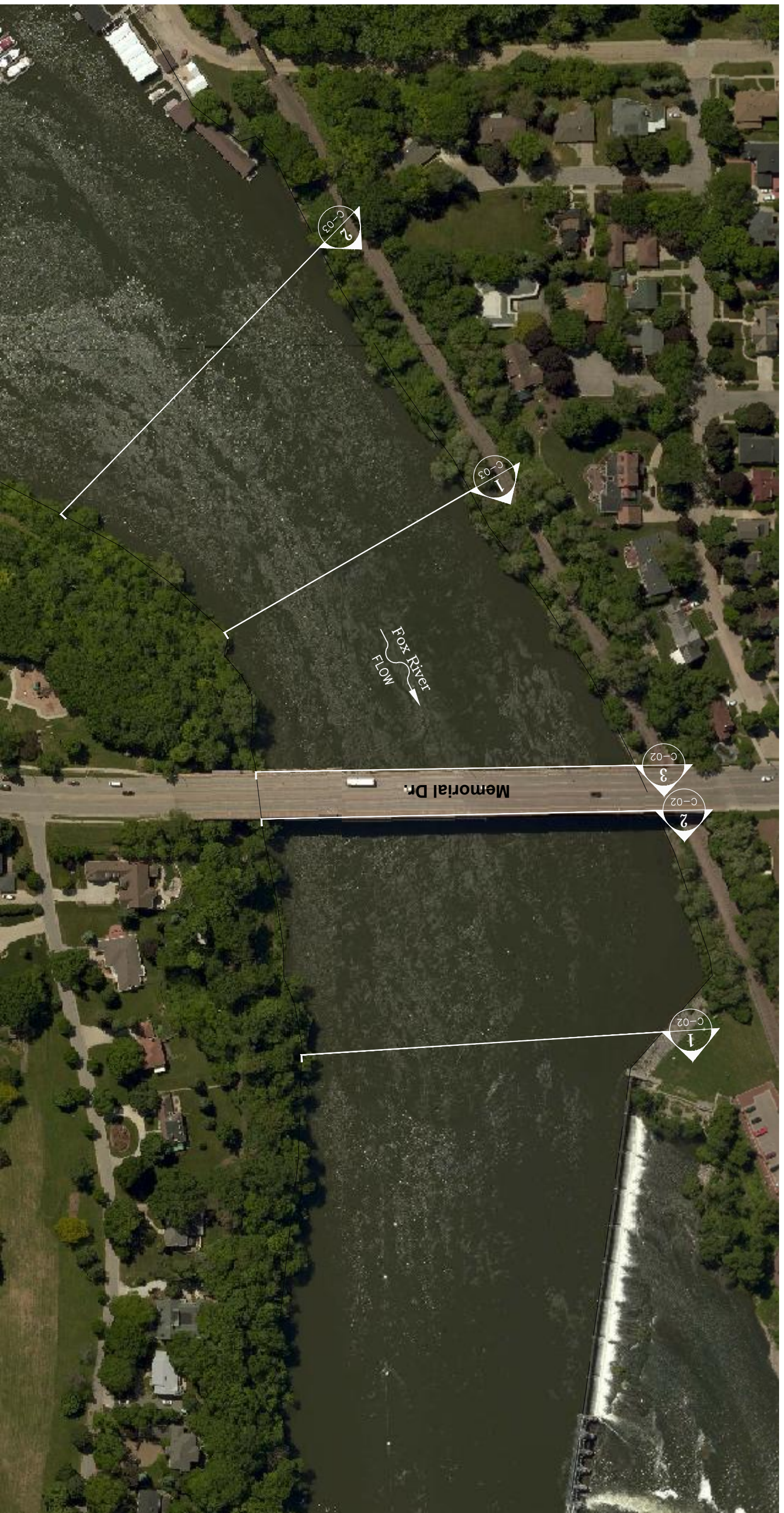
3

175' UPSTREAM CROSS SECTION - LOOKING NORTHEAST

SCALE: 1" = 30'



NOTE: Vertical scale multiplied by a factor of 5 for clarity.



- GENERAL NOTES:**
1. The hydrographic survey was completed on September 16, 2015 by Collins Engineers, Inc.
 2. Soundings were obtained using a continuously recording fathometer operating at 200KHZ and linked to a WAAS capable GPS receiver.
 3. Base map information shown on this drawing shall be considered approximate.

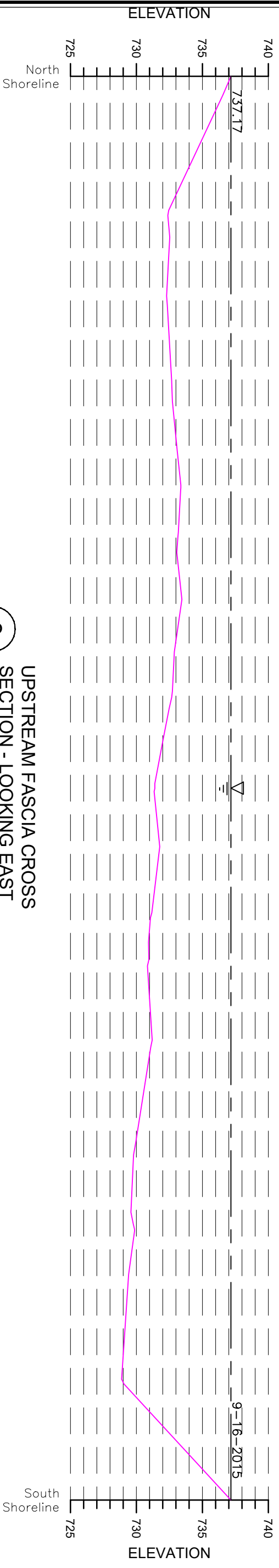
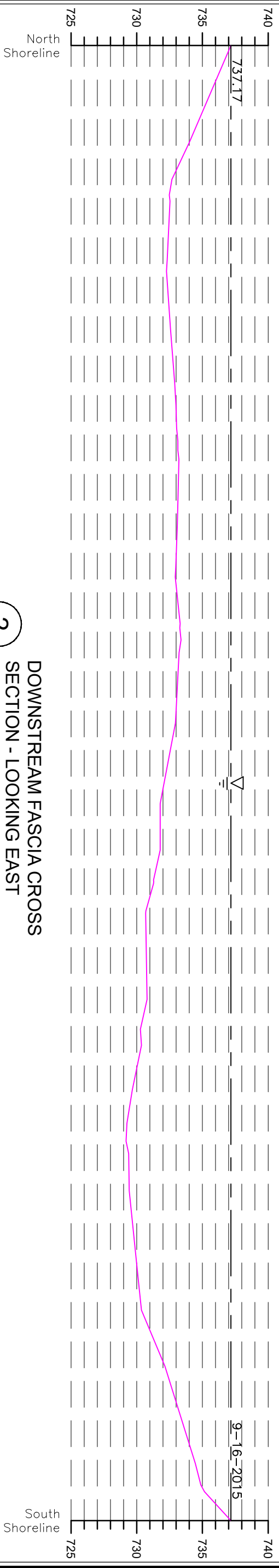
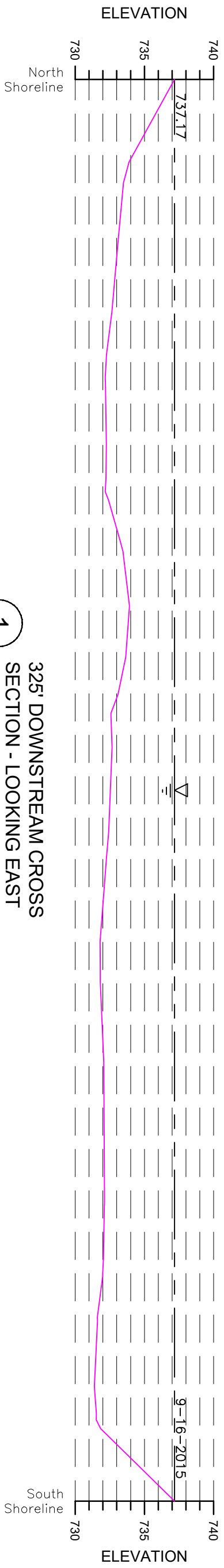
- STRUCTURE NOTES:**
1. The measured waterline elevation was 737.17 feet on the survey date of 9-16-2015.
 2. The waterline was measured 2.8 feet below the top of the base of Pier 2 at the downstream nose.
 3. Access to the site was via a boat launch 0.3 miles SW of the bridge. GPS coordinates: N44°15'00.87", W88°25'14.64"

COLLINS ENGINEERS
 2033 W. Howard Ave
 Milwaukee, WI 53095
 Phone: 414-282-6905

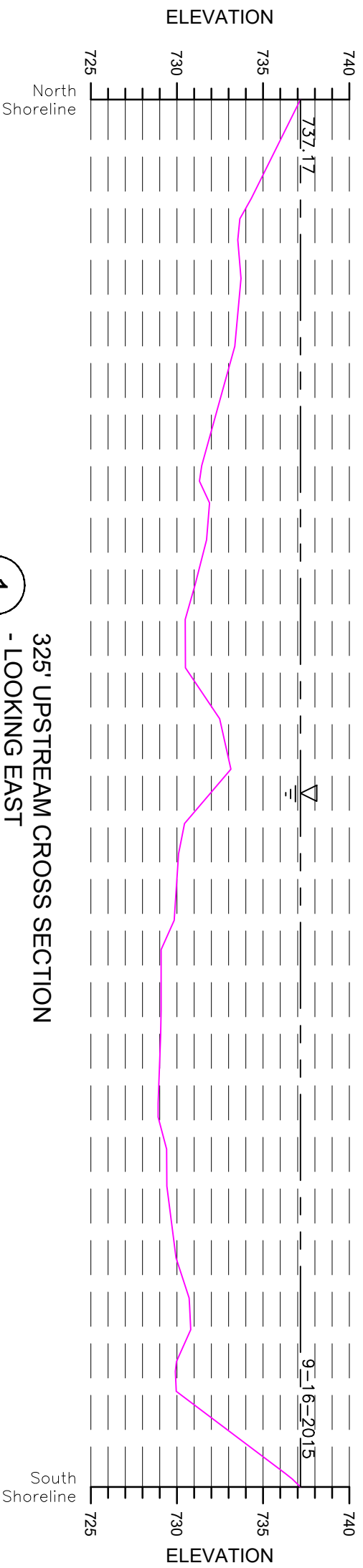


**WHRP-Predicting Scour of Bedrock
 Structure Overall
 Structure B-44-98**
 Appleton, WI

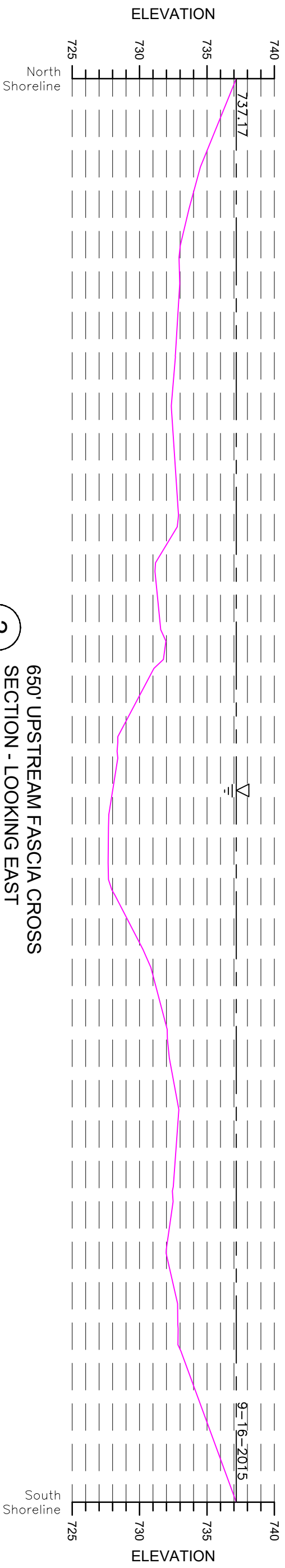
CEI PROJECT 61-9236
INSPECTED BY: CSH
DRAWN BY: CSH
CHECKED BY: SJM
DATE: 9-16-2015
SHEET NO: C-01



NOTE: Vertical scale multiplied by a factor of 5 for clarity.



1
325' UPSTREAM CROSS SECTION
- LOOKING EAST
SCALE: 1" = 40'



2
650' UPSTREAM FASCIA CROSS
SECTION - LOOKING EAST
SCALE: 1" = 40'

NOTE: Vertical scale multiplied by a factor of 5 for clarity.



GENERAL NOTES:

1. The hydrographic survey was completed on September 14, 2015 by Collins Engineers, Inc.
2. Soundings were obtained using a continuously recording fathometer operating at 200KHZ and linked to a WAAS capable GPS receiver.
3. Base map information shown on this drawing shall be considered approximate.

STRUCTURE NOTES:

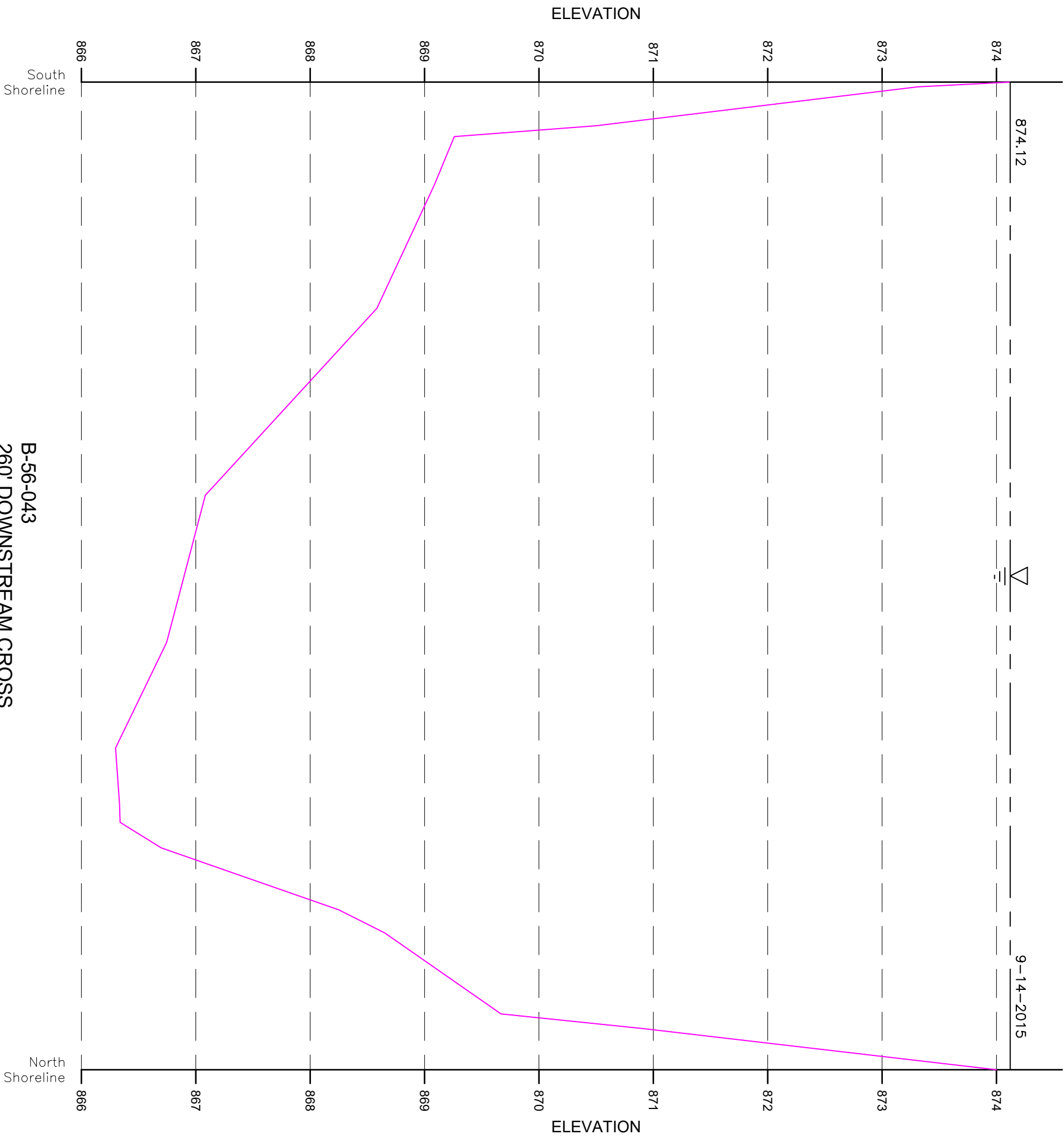
1. The measured waterline elevation was 874.12 feet on the survey date of 9-15-2015.
2. The waterline was measured 12 feet below the top of the 2nd column from the west of Pier 1 of B-56-42.
3. Access to the site was via a jon boat at the site.

COLLINS ENGINEERS
 2033 W. Howard Ave
 Milwaukee, WI 53095
 Phone: 414-282-6905

WHRP-Predicting Scour of Bedrock Structure Overall
Structure B-56-42/43
 Wisconsin Dells, WI

CEI PROJECT 61-9236
INSPECTED BY: CSH
DRAWN BY: CSH
CHECKED BY: SJM
DATE: 9-14-2015
SHEET NO: C-01

NOTE: Vertical scale multiplied by a factor of 5 for clarity.

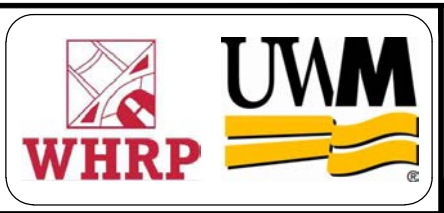


1
 B-56-043
 260' DOWNSTREAM CROSS
 SECTION - LOOKING WEST
 HORIZONTAL SCALE: 1" = 5'

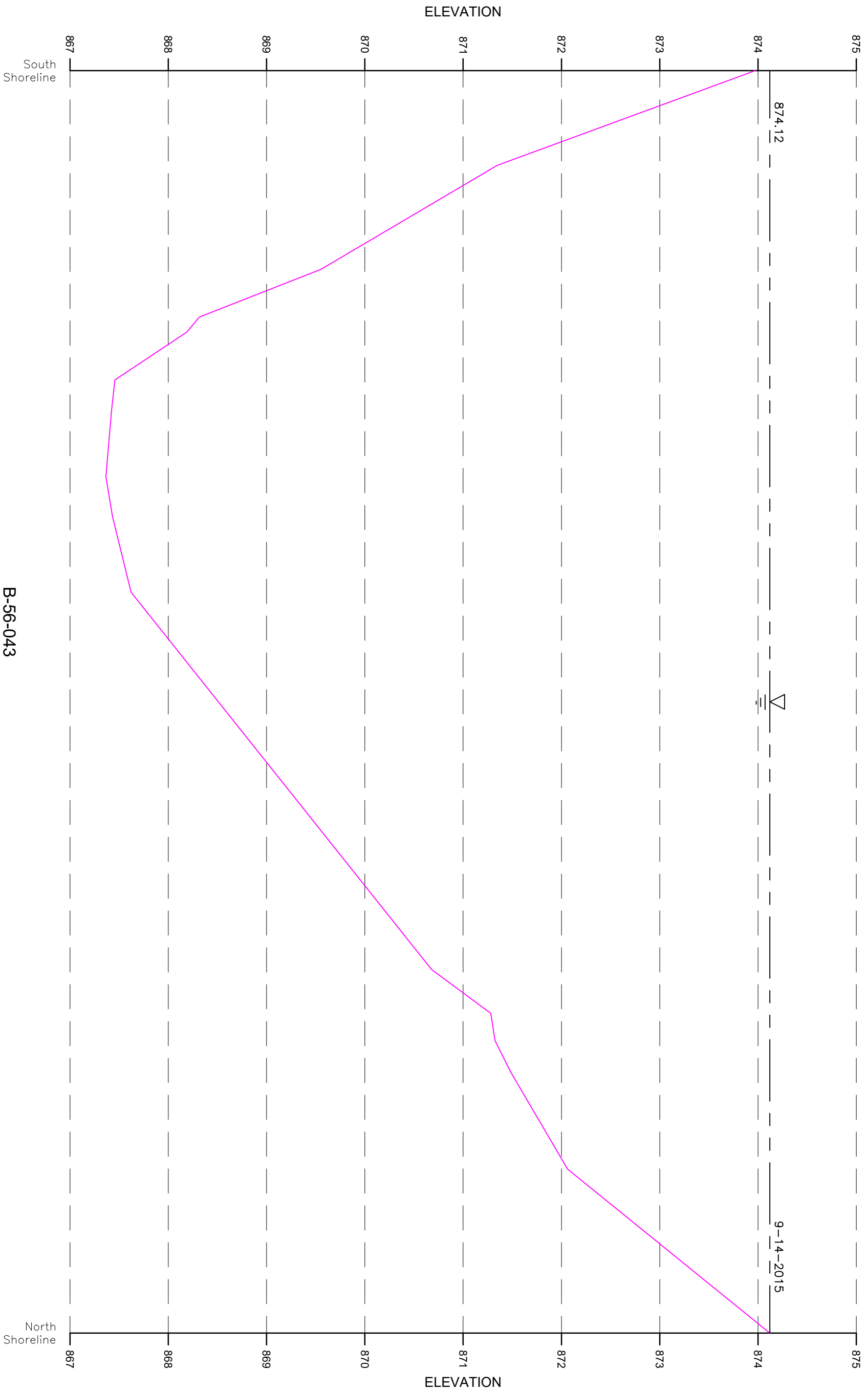


CEI PROJECT 61-9236
INSPECTED BY: CSH
DRAWN BY: CSH
CHECKED BY: SJM
DATE: 9-14-2015
SHEET NO: C-02

**WHRP-Predicting Scour of Bedrock
 260' Downstream Cross Section
 Structure B-56-42/43**
 Wisconsin Dells, WI



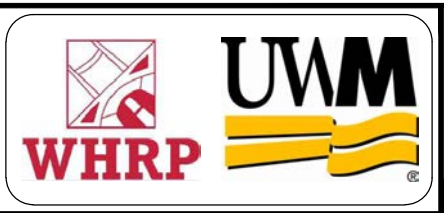
COLLINS ENGINEERS
 2033 W. Howard Ave
 Milwaukee, WI 53095
 Phone: 414-282-6905



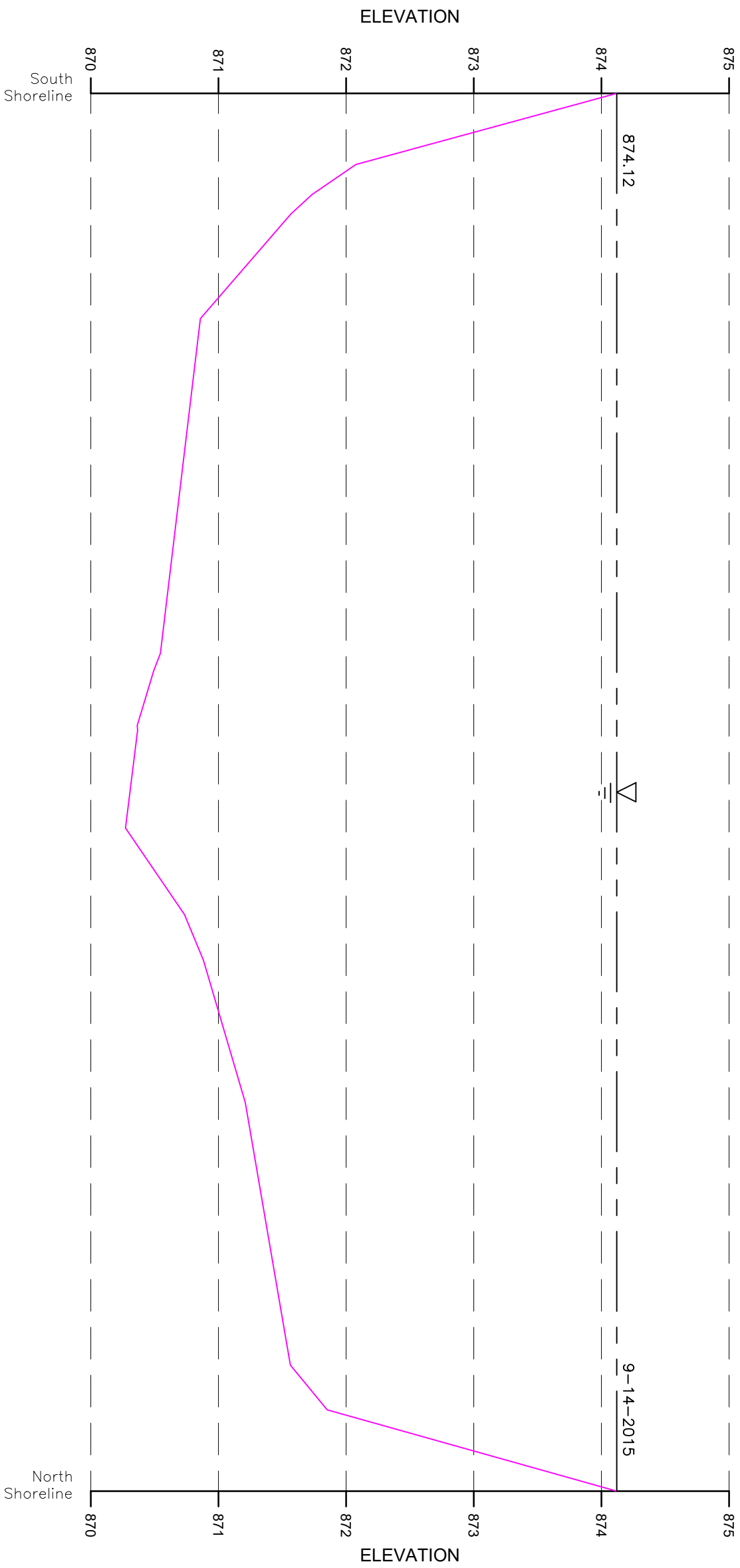
1
 B-56-043
 130' DOWNSTREAM CROSS
 SECTION - LOOKING WEST
 HORIZONTAL SCALE: 1" = 5'

CEI PROJECT 61-9236
INSPECTED BY: CSH
DRAWN BY: CSH
CHECKED BY: RAF
DATE: 9-14-2015
SHEET NO: C-03

**WHRP-Predicting Scour of Bedrock
 130' Downstream Cross Section
 Structure B-56-42/43**
 Wisconsin Dells, WI



COLLINS ENGINEERS^{PC}
 2033 W. Howard Ave
 Milwaukee, WI 53095
 Phone: 414-282-6905



1
 B-56-043
 DOWNSTREAM FASCIA CROSS
 SECTION - LOOKING WEST
 HORIZONTAL SCALE: 1" = 5'

NOTE: Vertical scale multiplied by a factor of 5 for clarity.

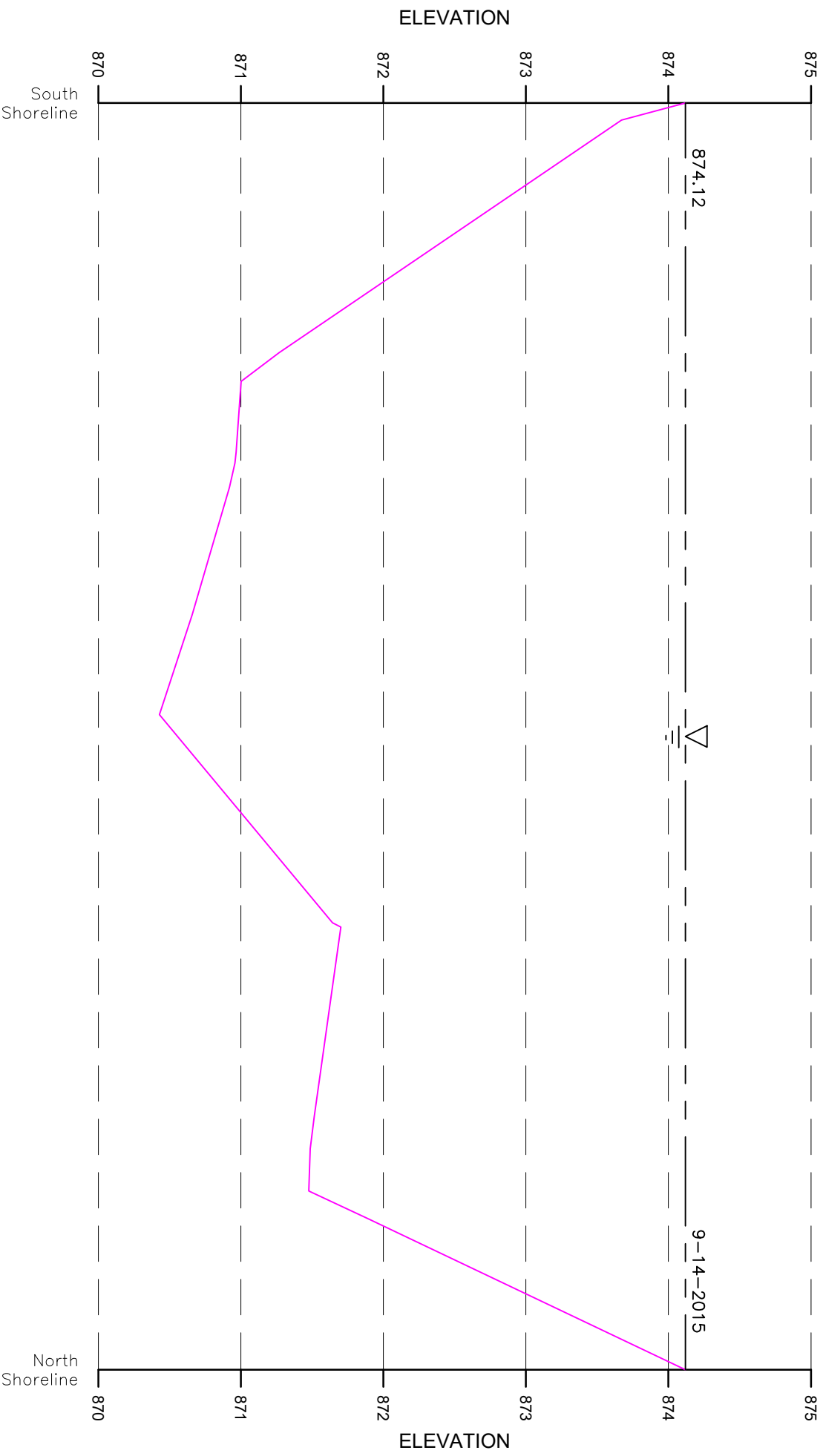
G:\9236 - UWM ROCK SCOUR STUDY\CAD\BASE FILES\B-56-42_43.DWG 10/27/2015 11:26:00 AM

COLLINS ENGINEERS
 2033 W. Howard Ave
 Milwaukee, WI 53095
 Phone: 414-282-6905



**WHRP-Predicting Scour of Bedrock
 Downstream Fascia Cross Section
 Structure B-56-42/43**
 Wisconsin Dells, WI

CEI PROJECT 61-9236
INSPECTED BY: CSH
DRAWN BY: CSH
CHECKED BY: SJM
DATE: 9-14-2015
SHEET NO: C-04



1
 B-56-043
 UPSTREAM FASCIA CROSS
 SECTION - LOOKING WEST
 HORIZONTAL SCALE: 1" = 5'

NOTE: Vertical scale multiplied by a factor of 5 for clarity.

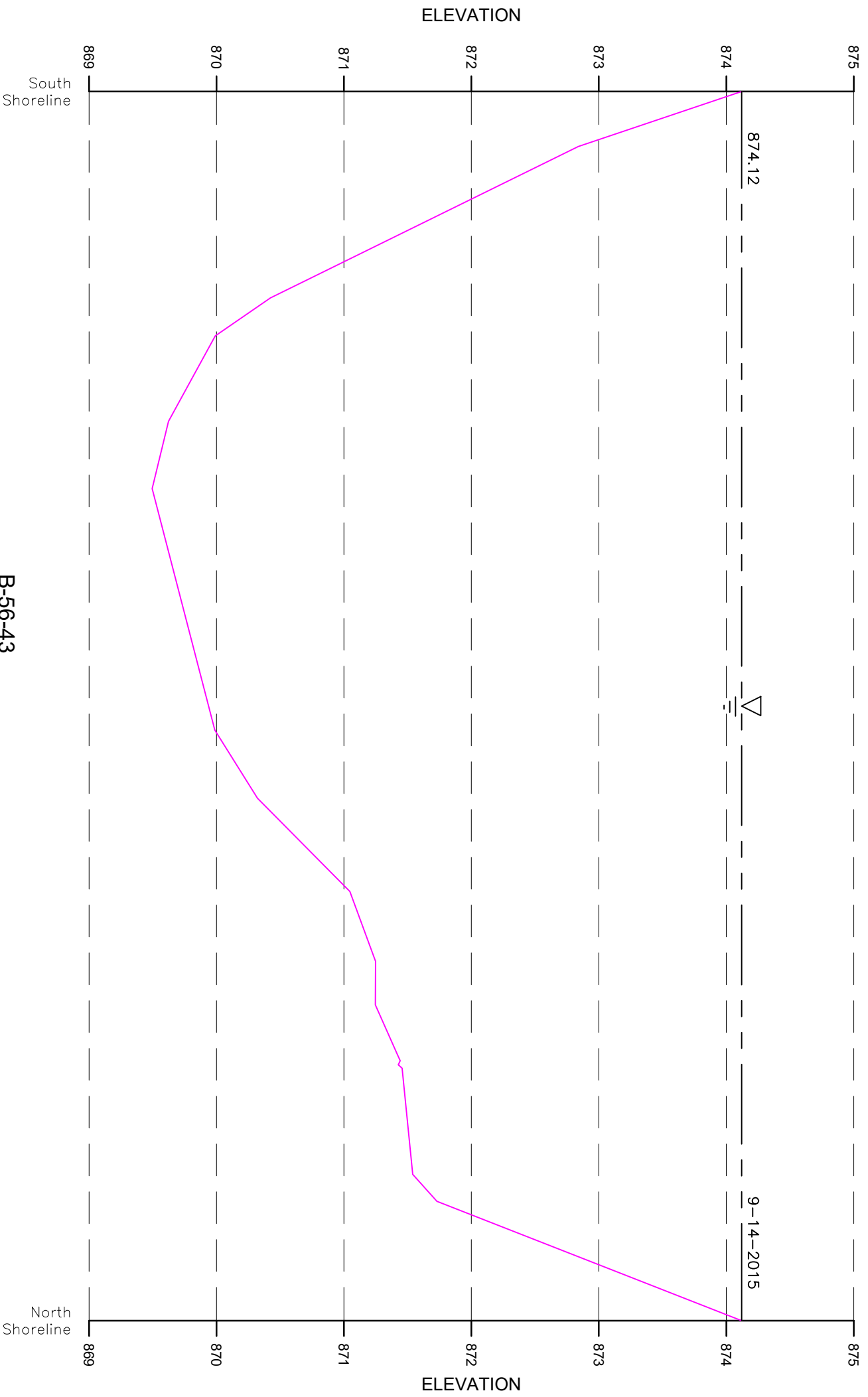
G:\9236 - UWM ROCK SCOUR STUDY\CAD\BASE FILES\B-56-42_43.DWG 10/27/2015 11:25:35 AM

COLLINS ENGINEERS
 2033 W. Howard Ave
 Milwaukee, WI 53095
 Phone: 414-282-6905



**WHRP-Predicting Scour of Bedrock
 Upstream Fascia Cross Section
 Structure B-56-42/43**
 Wisconsin Dells, WI

CEI PROJECT 61-9236
INSPECTED BY: CSH
DRAWN BY: CSH
CHECKED BY: SJM
DATE: 9-14-2015
SHEET NO: C-05



B-56-43
70' UPSTREAM CROSS
SECTION - LOOKING WEST

1
 HORIZONTAL SCALE: 1" = 5'

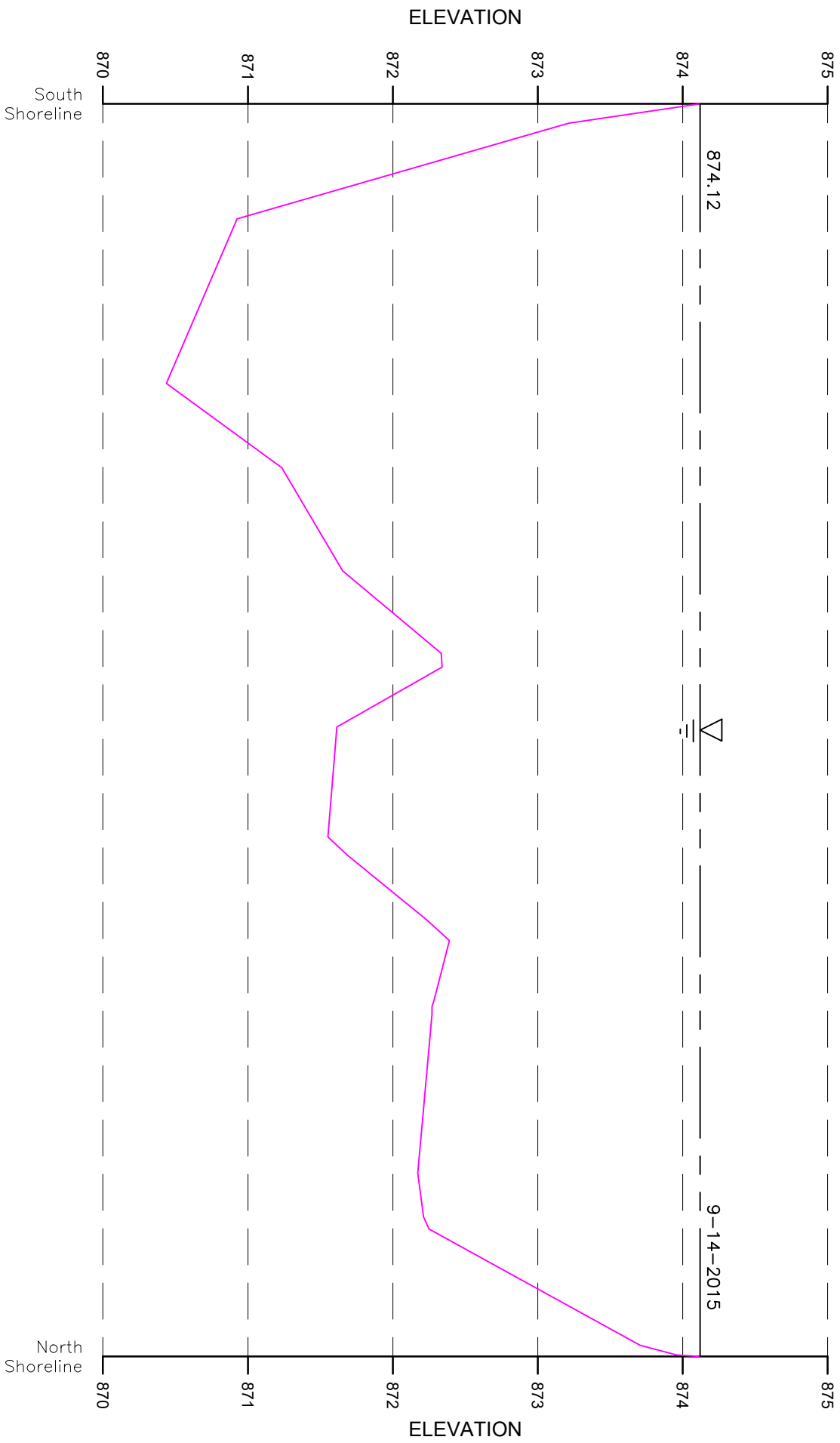
NOTE: Vertical scale multiplied by a factor of 5 for clarity.

COLLINS ENGINEERS
 2033 W. Howard Ave
 Milwaukee, WI 53095
 Phone: 414-282-6905



WHRP-Predicting Scour of Bedrock
70' Upstream Cross Section
Structure B-56-42/43
 Wisconsin Dells, WI

CEI PROJECT
 61-9236
 INSPECTED BY:
 CSH
 DRAWN BY:
 CSH
 CHECKED BY:
 SJM
 DATE:
 9-14-2015
 SHEET NO:
C-06



1
 B-56-42
 DOWNSTREAM FASCIA CROSS
 SECTION - LOOKING WEST
 HORIZONTAL SCALE: 1" = 5'

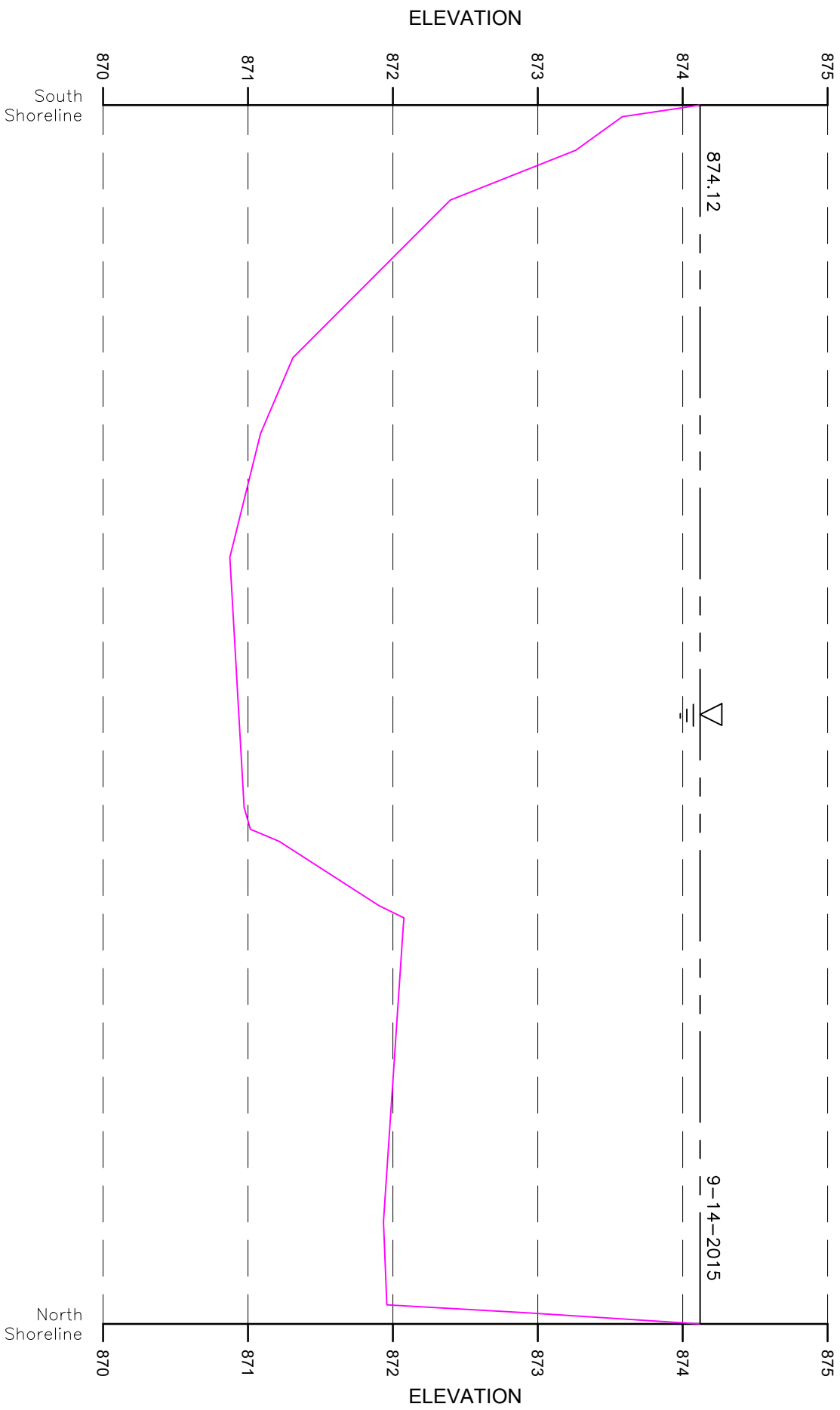
NOTE: Vertical scale multiplied by a factor of 5 for clarity.

COLLINS ENGINEERS
 2033 W. Howard Ave
 Milwaukee, WI 53095
 Phone: 414-282-6905



**WHRP-Predicting Scour of Bedrock
 Downstream Fascia Cross Section
 Structure B-56-42/43**
 Wisconsin Dells, WI

CEI PROJECT
 61-9236
 INSPECTED BY:
 CSH
 DRAWN BY:
 CSH
 CHECKED BY:
 SJM
 DATE:
 9-14-2015
 SHEET NO:
C-07



1

B-56-42
UPSTREAM FASCIA CROSS
SECTION - LOOKING WEST

HORIZONTAL SCALE: 1" = 5'

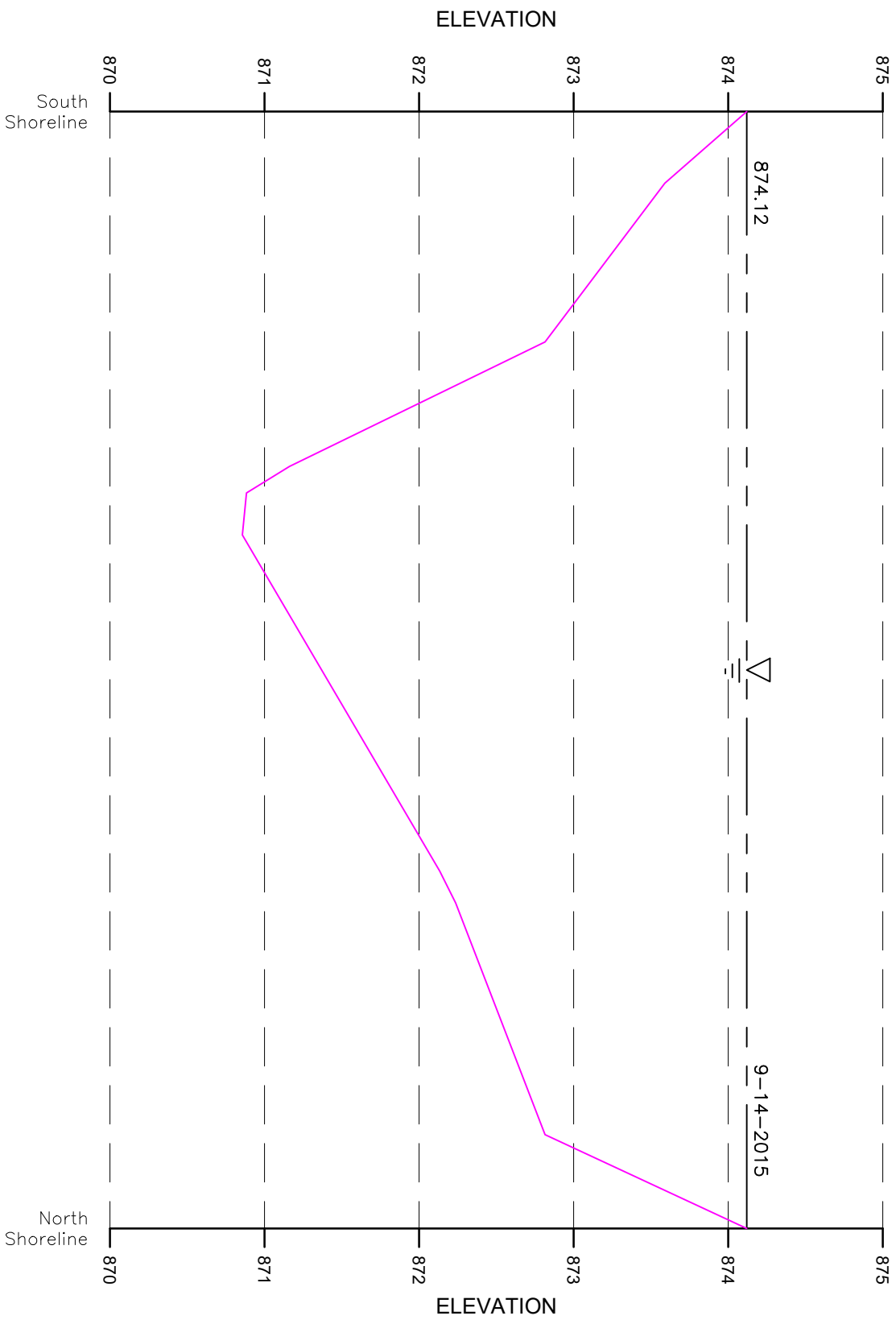
NOTE: Vertical scale multiplied by a factor of 5 for clarity.

COLLINS ENGINEERS
 2033 W. Howard Ave
 Milwaukee, WI 53095
 Phone: 414-282-6905



WHRP-Predicting Scour of Bedrock
Upstream Fascia Cross Section
Structure B-56-42/43
 Wisconsin Dells, WI

CEI PROJECT
 61-9236
 INSPECTED BY:
 CSH
 DRAWN BY:
 CSH
 CHECKED BY:
 SJM
 DATE:
 9-14-2015
 SHEET NO:
C-08



1
 B-56-42
 50' UPSTREAM CROSS
 SECTION - LOOKING WEST
 HORIZONTAL SCALE: 1" = 5'

NOTE: Vertical scale multiplied by a factor of 5 for clarity.

COLLINS ENGINEERS
 2033 W. Howard Ave
 Milwaukee, WI 53095
 Phone: 414-282-6905



WHRP-Predicting Scour of Bedrock
50' Upstream Cross Section
Structure B-56-42/43
 Wisconsin Dells, WI

CEI PROJECT
 61-9236
 INSPECTED BY:
 CSH
 DRAWN BY:
 CSH
 CHECKED BY:
 SJM
 DATE:
 9-14-2015
 SHEET NO:
C-09

Appendix B – Modified Slake Durability Test Results

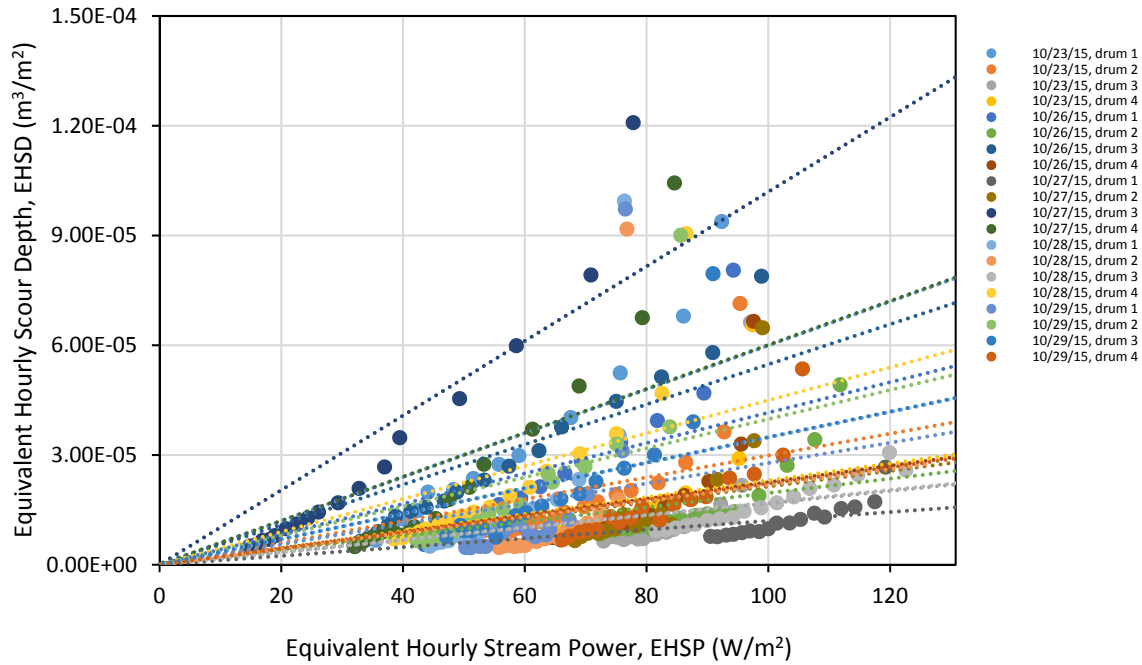


Figure B-1: Results of modified slake durability test plotted as equivalent hourly scour depth and equivalent hourly stream power for Red Cedar River (neglecting initial data point)

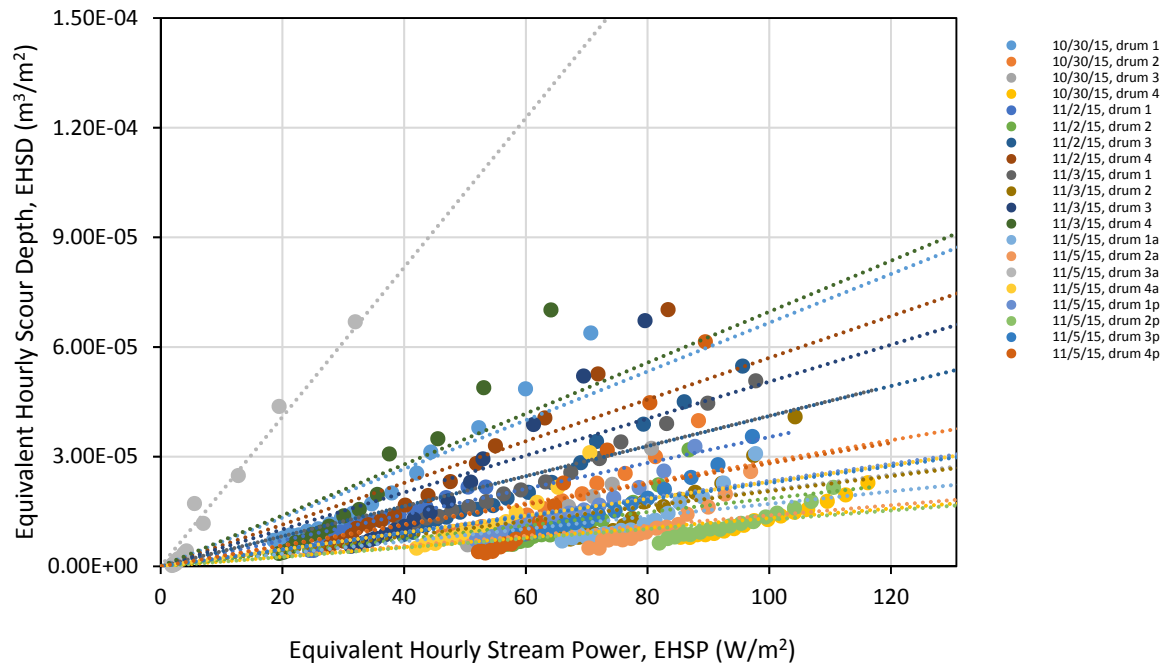


Figure B-2: Results of modified slake durability test plotted as equivalent hourly scour depth and equivalent hourly stream power for Red Cedar River (neglecting initial data point)

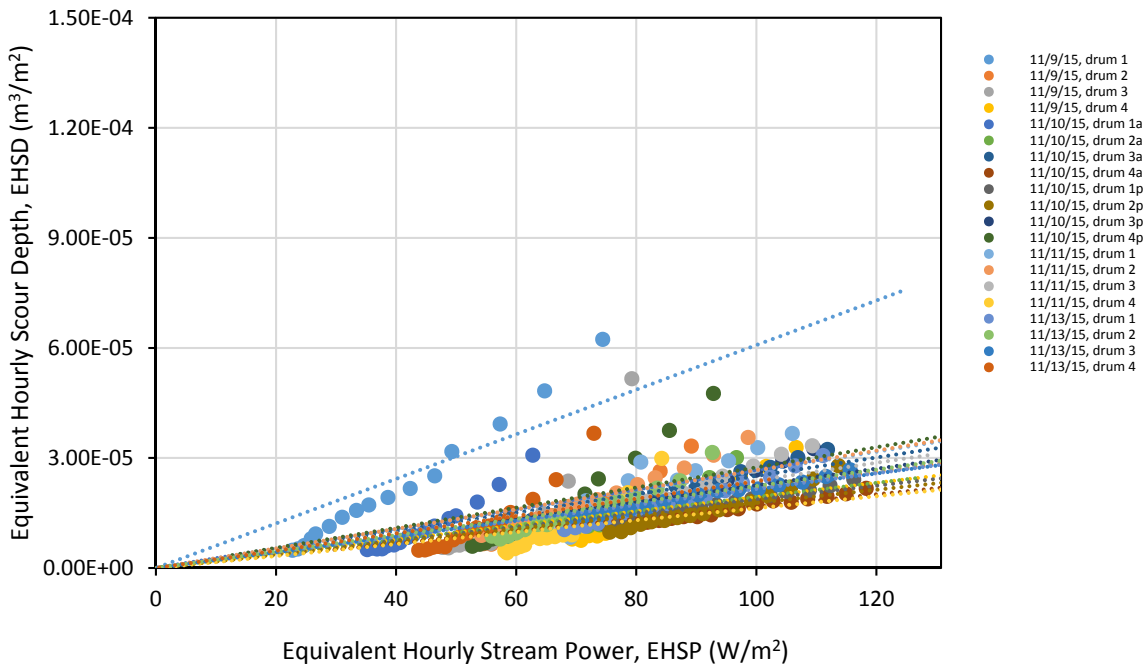


Figure B-3: Results of modified slake durability test plotted as equivalent hourly scour depth and equivalent hourly stream power for Red Cedar River (neglecting initial data point)

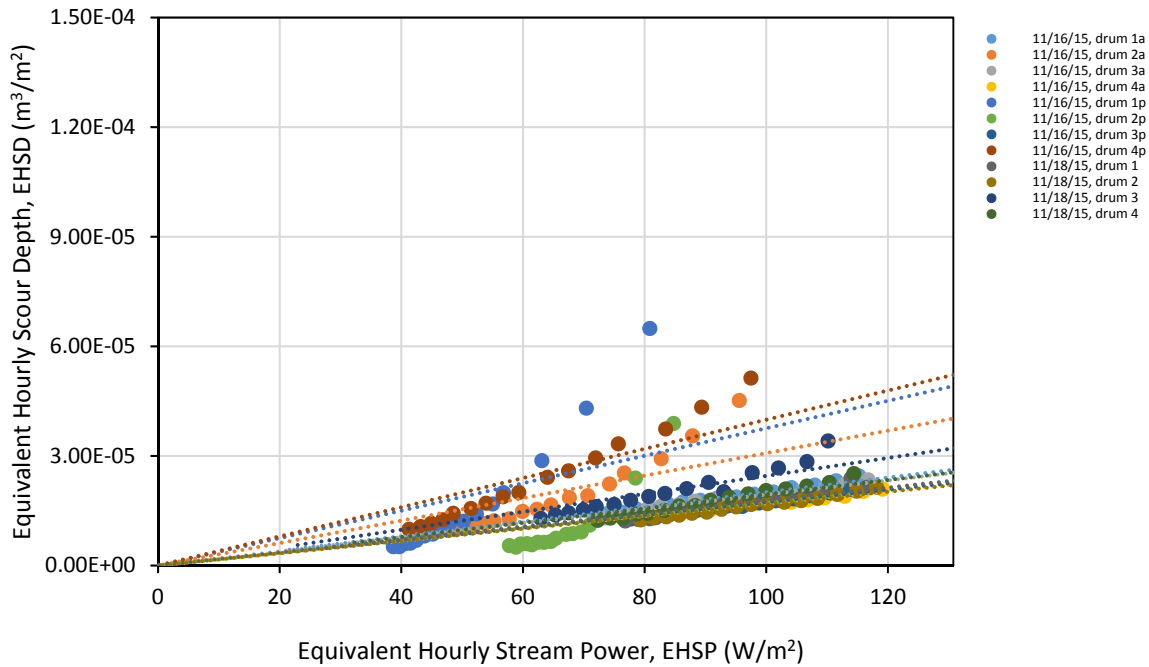


Figure B-4: Results of modified slake durability test plotted as equivalent hourly scour depth and equivalent hourly stream power for Red Cedar River (neglecting initial data point)

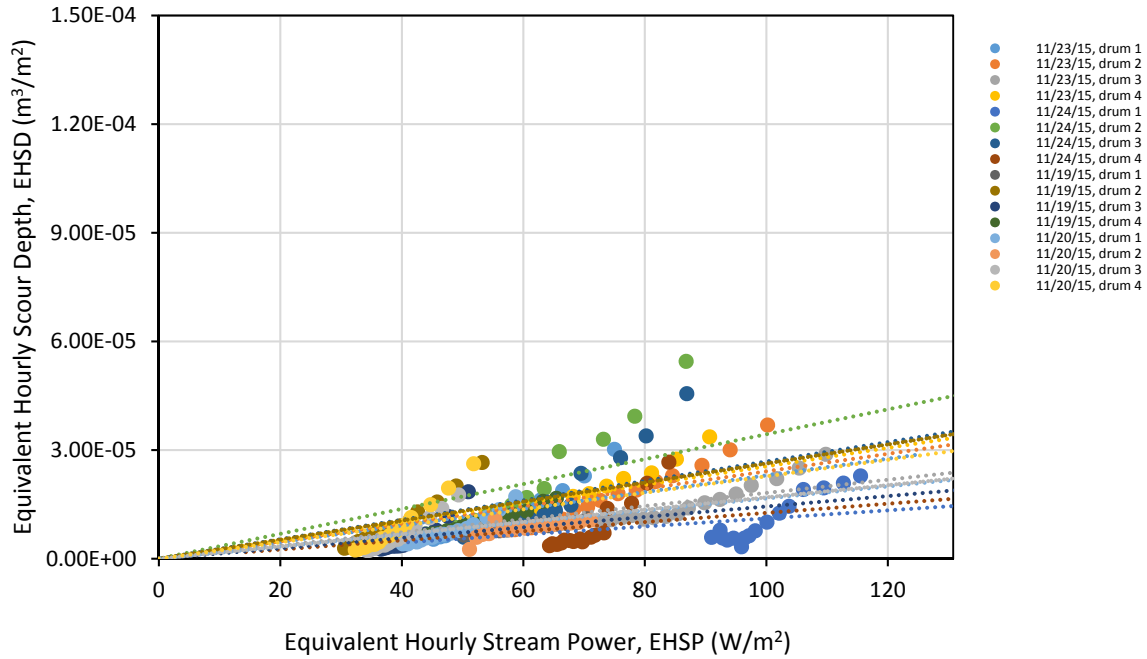


Figure B-5: Results of modified slake durability test plotted as equivalent hourly scour depth and equivalent hourly stream power for Red Cedar River (neglecting initial data point)

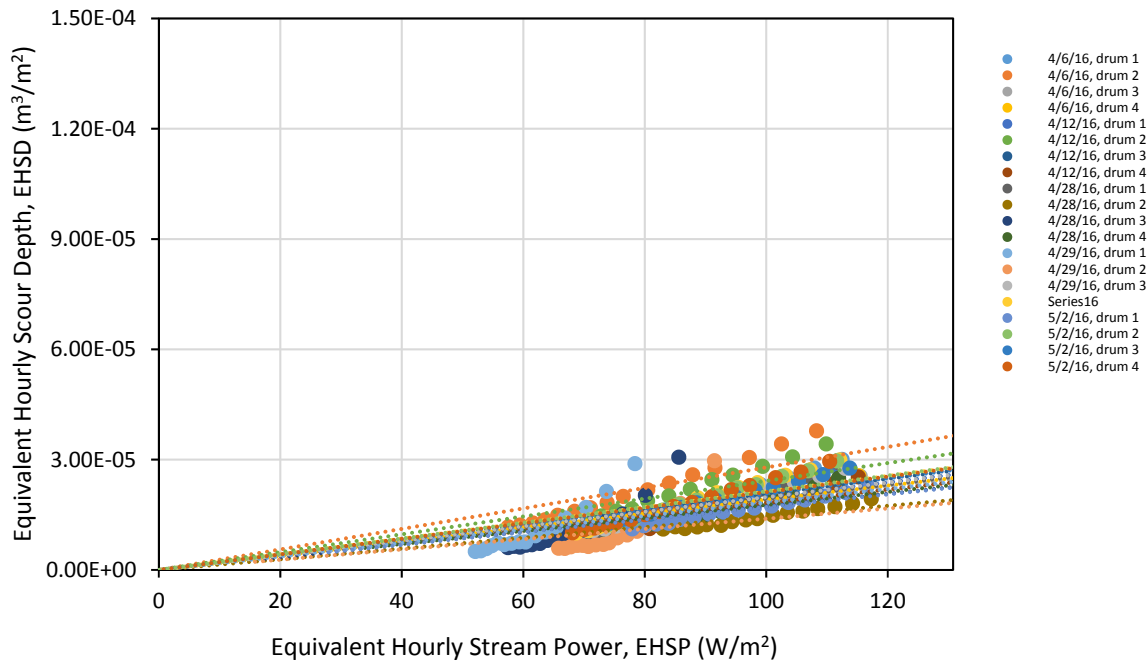


Figure B-6: Results of modified slake durability test plotted as equivalent hourly scour depth and equivalent hourly stream power for Red Cedar River (neglecting initial data point)

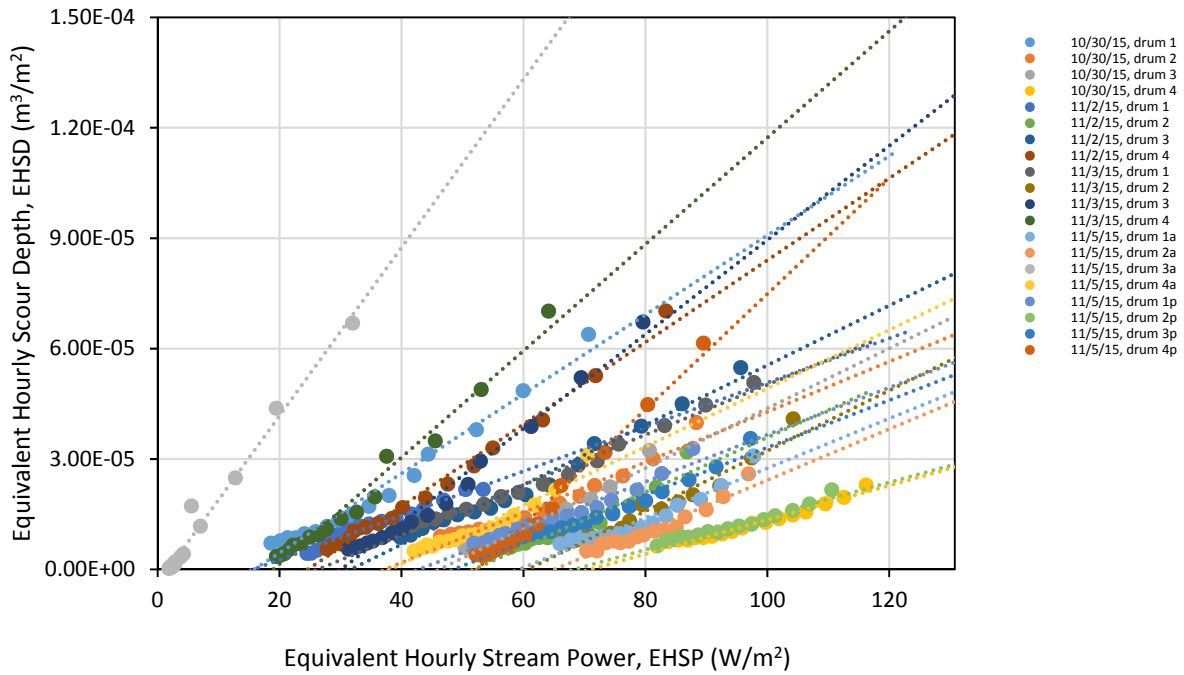


Figure B-7: Results of modified slake durability test plotted as equivalent hourly scour depth and equivalent hourly stream power for Red Cedar River (neglecting initial data point)

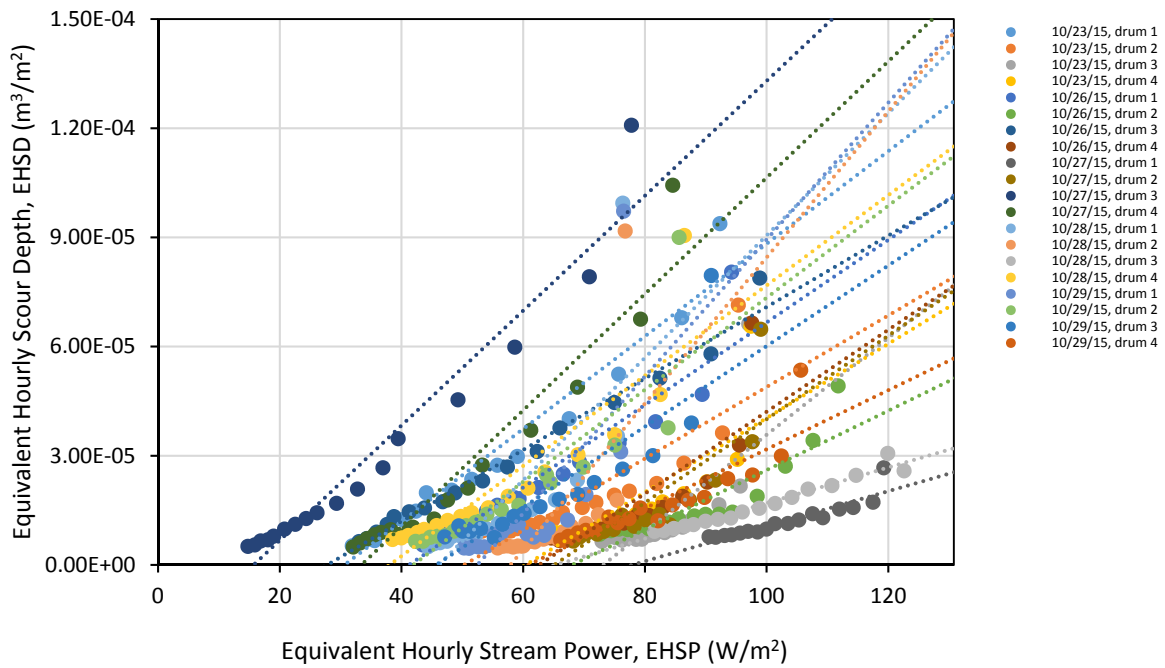


Figure B-8: Results of modified slake durability test plotted as equivalent hourly scour depth and equivalent hourly stream power for Red Cedar River (neglecting initial data point)

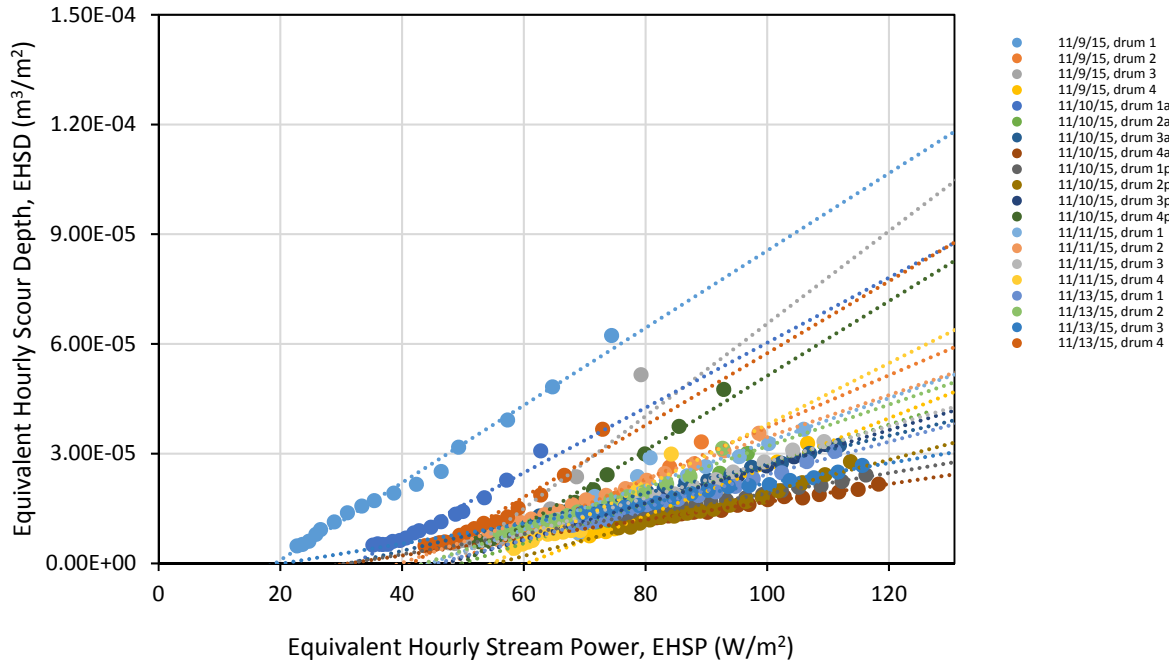


Figure B-9: Results of modified slake durability test plotted as equivalent hourly scour depth and equivalent hourly stream power for Red Cedar River (neglecting initial data point)

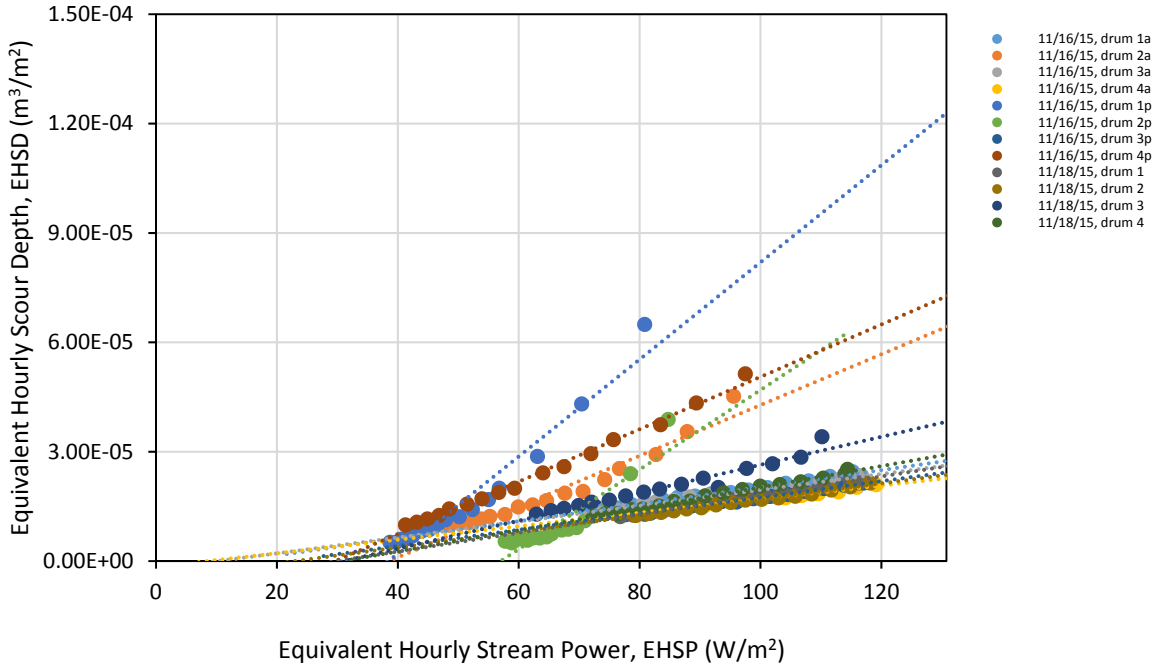


Figure B-10: Results of modified slake durability test plotted as equivalent hourly scour depth and equivalent hourly stream power for Red Cedar River (neglecting initial data point)

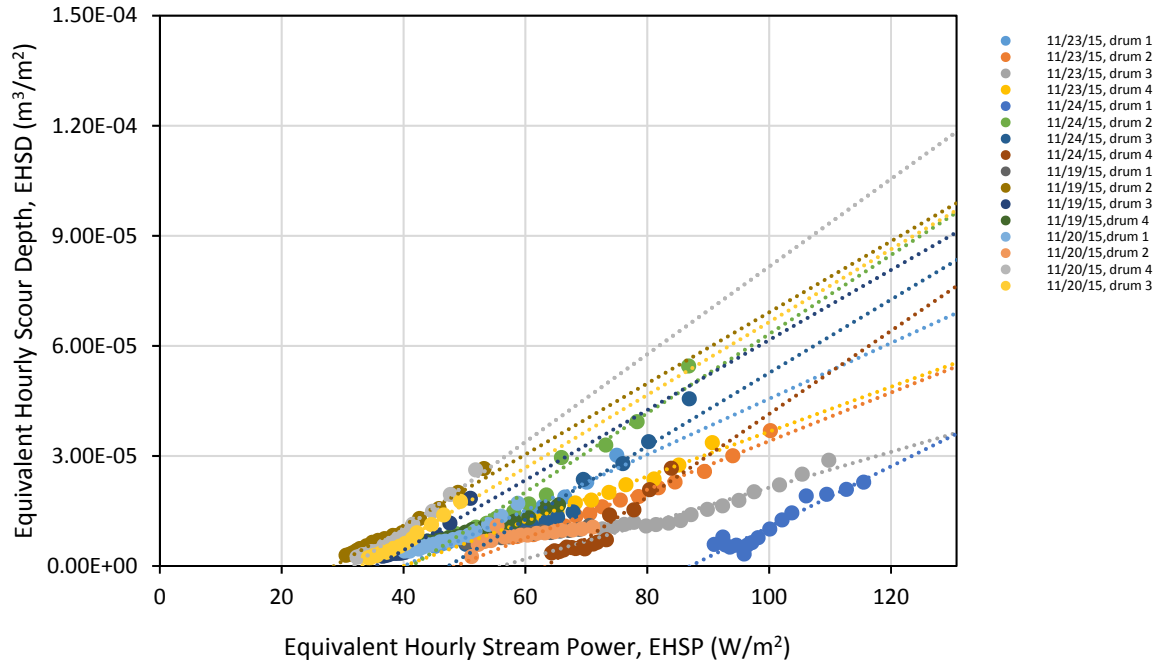


Figure B-11: Results of modified slake durability test plotted as equivalent hourly scour depth and equivalent hourly stream power for Red Cedar River (neglecting initial data point)

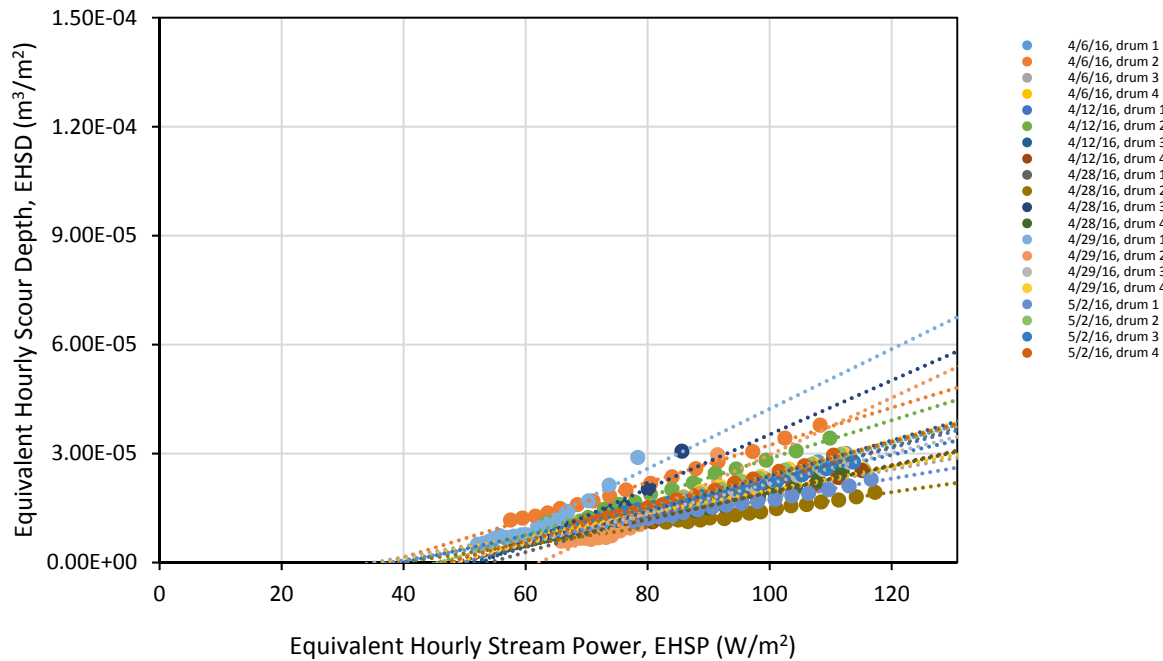


Figure B-12: Results of modified slake durability test plotted as equivalent hourly scour depth and equivalent hourly stream power for Red Cedar River (neglecting initial data point)

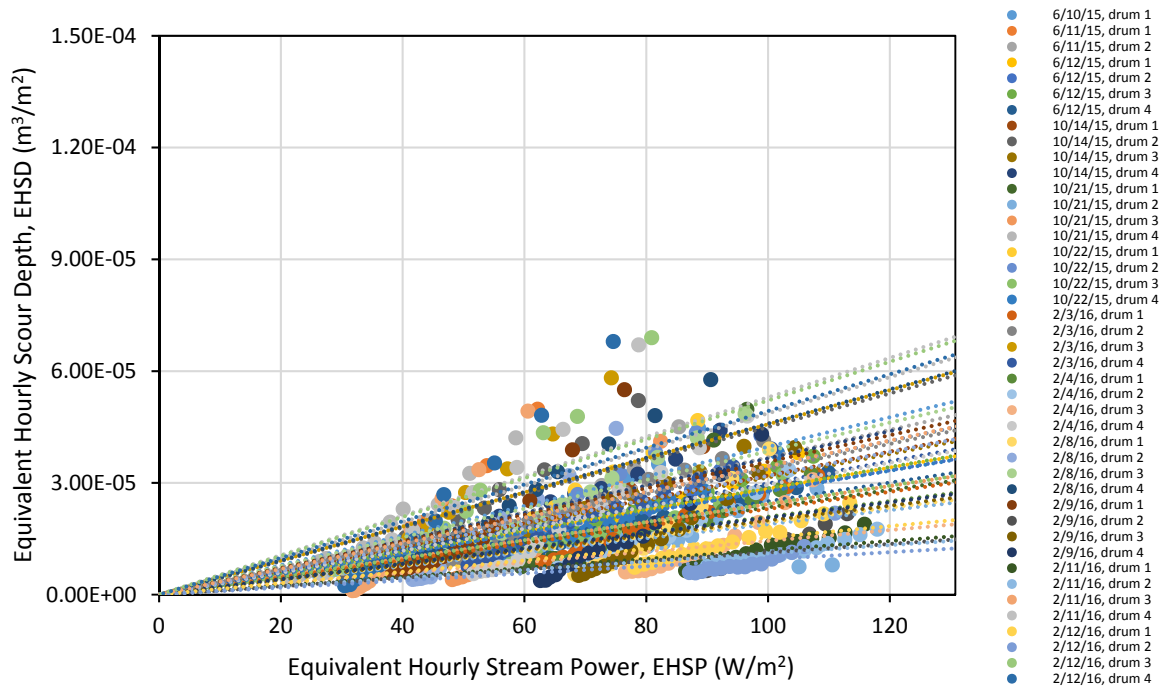


Figure B-13: Results of modified slake durability test plotted as equivalent hourly scour depth and equivalent hourly stream power for Wisconsin River (neglecting initial data point)

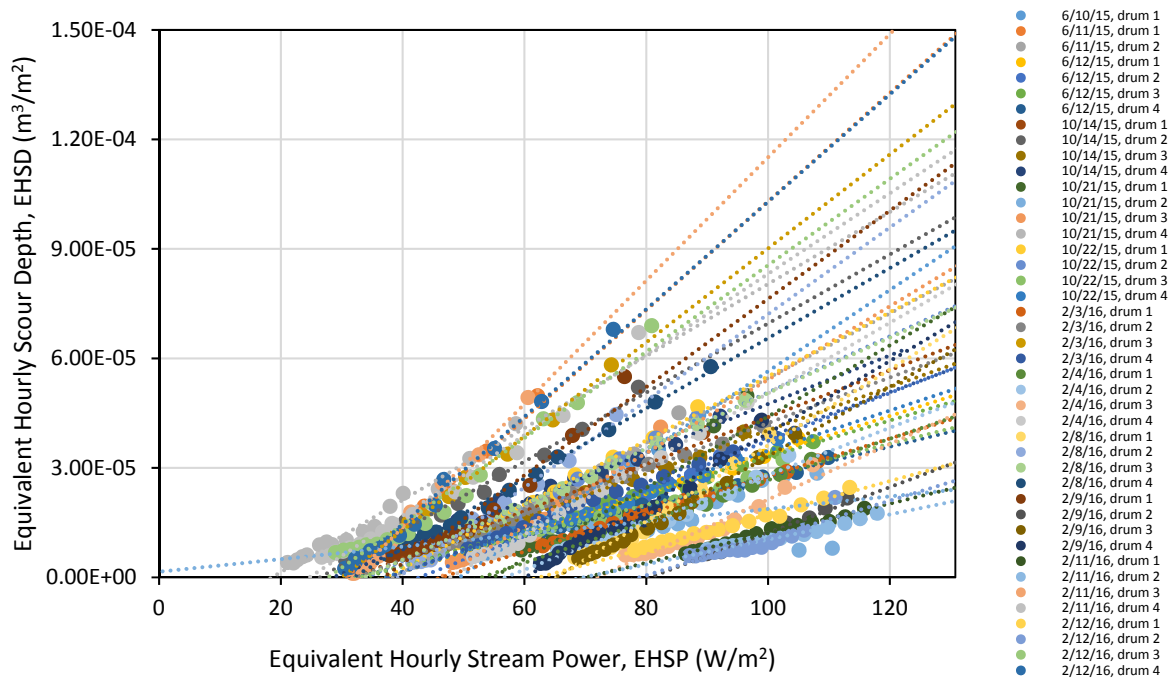


Figure B-14: Results of modified slake durability test plotted as equivalent hourly scour depth and equivalent hourly stream power for Red Cedar River (neglecting initial data point)

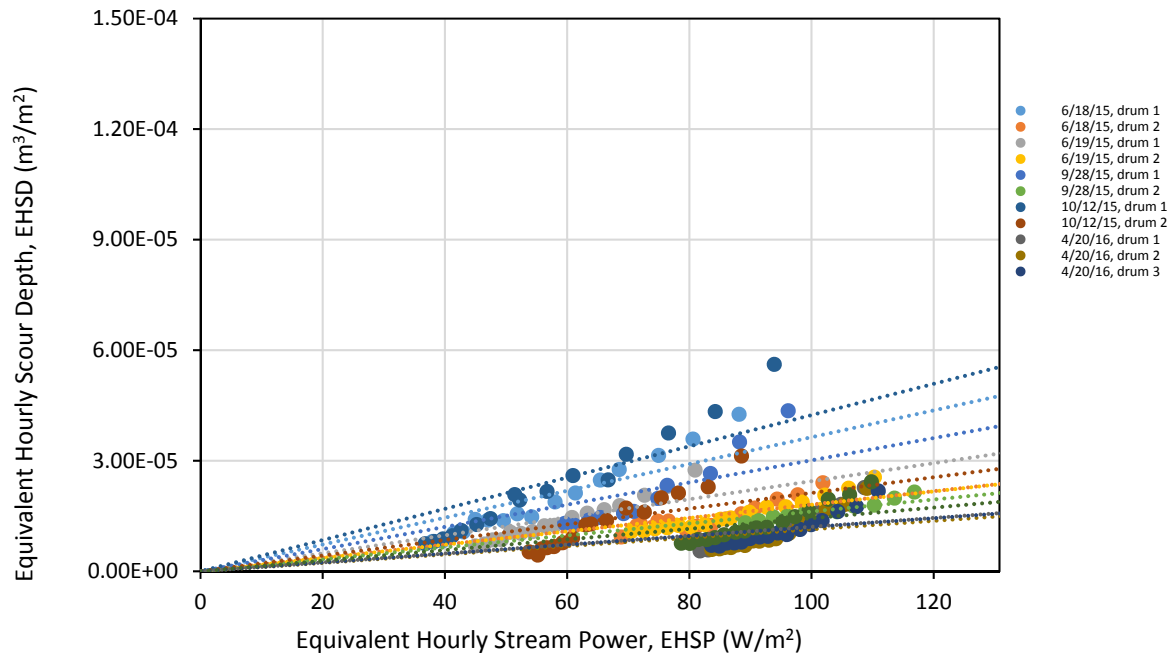


Figure B-15: Results of modified slake durability test plotted as equivalent hourly scour depth and equivalent hourly stream power for Spring Brook (neglecting initial data point)

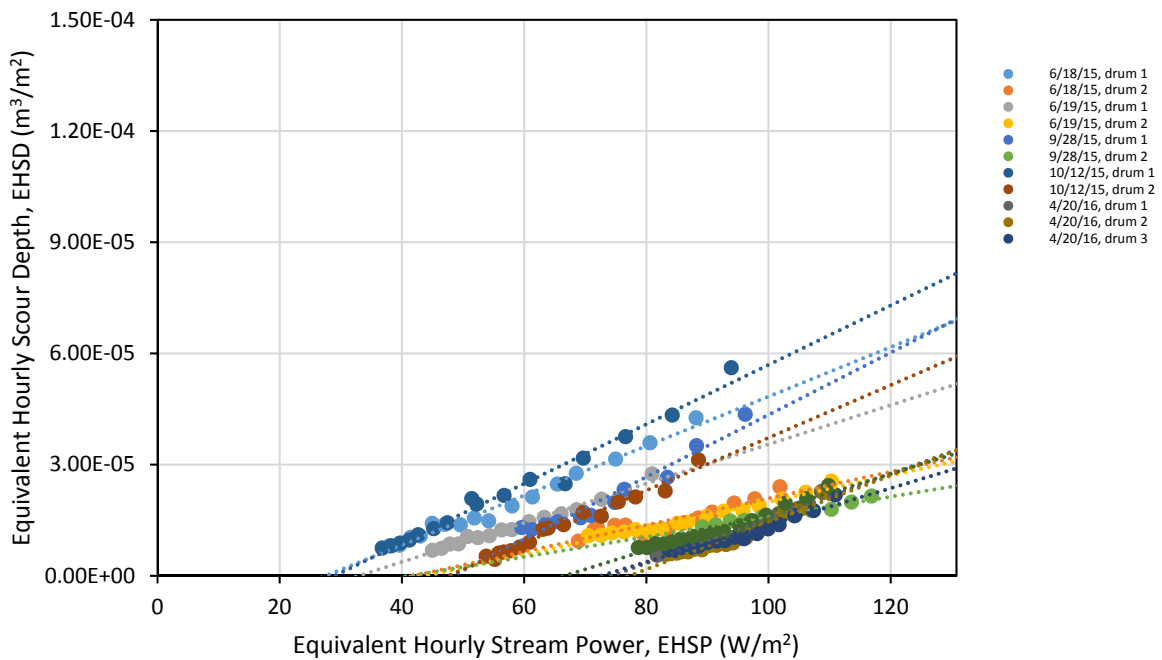


Figure B-16: Results of modified slake durability test plotted as equivalent hourly scour depth and equivalent hourly stream power for spring brook (neglecting initial data point)

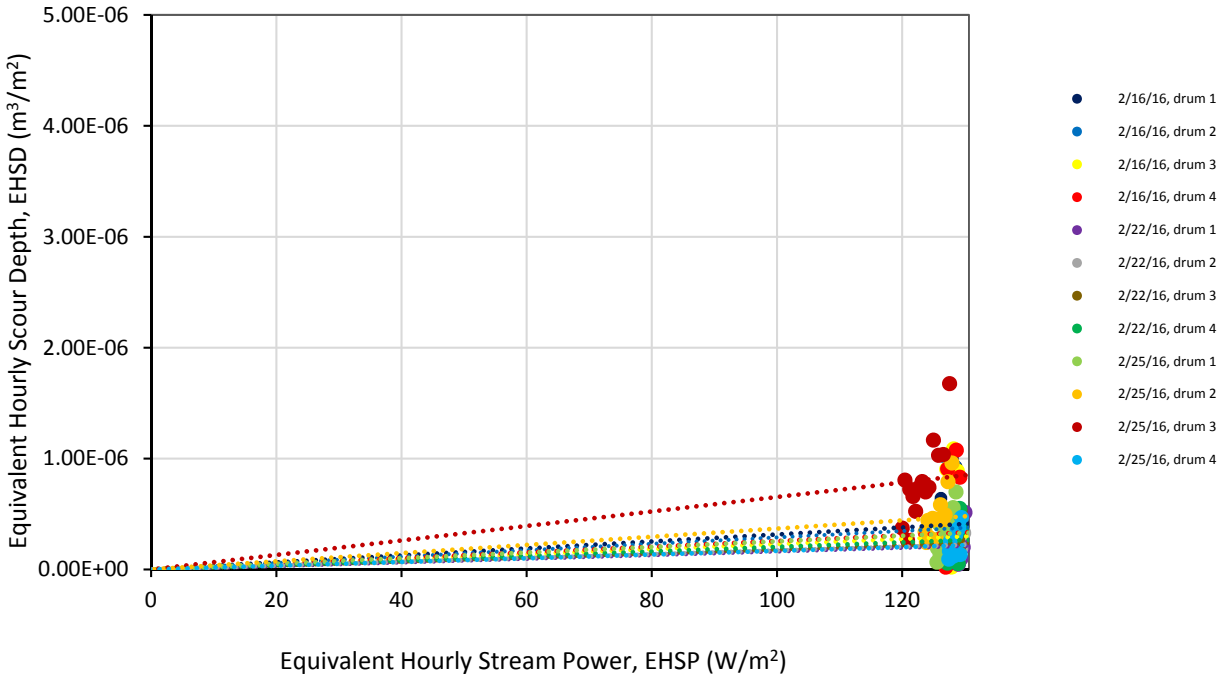


Figure B-17: Results of modified slake durability test plotted as equivalent hourly scour depth and equivalent hourly stream power for Fox River (neglecting initial data point)

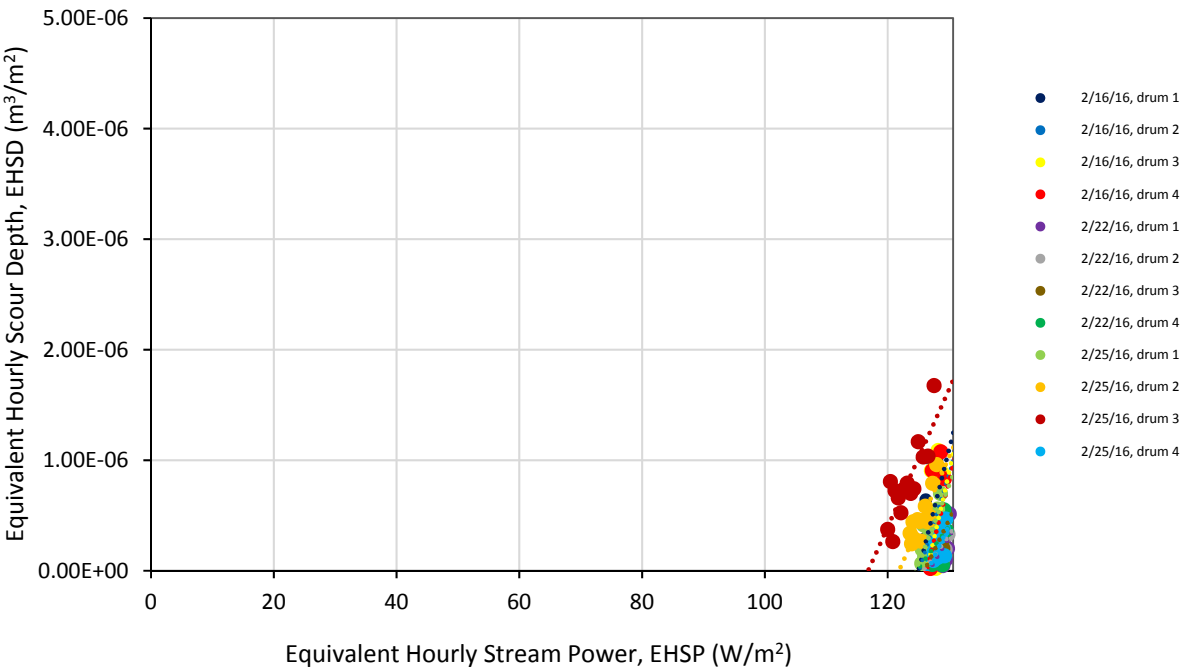


Figure B-18: Results of modified slake durability test plotted as equivalent hourly scour depth and equivalent hourly stream power for Fox River (neglecting initial data point)

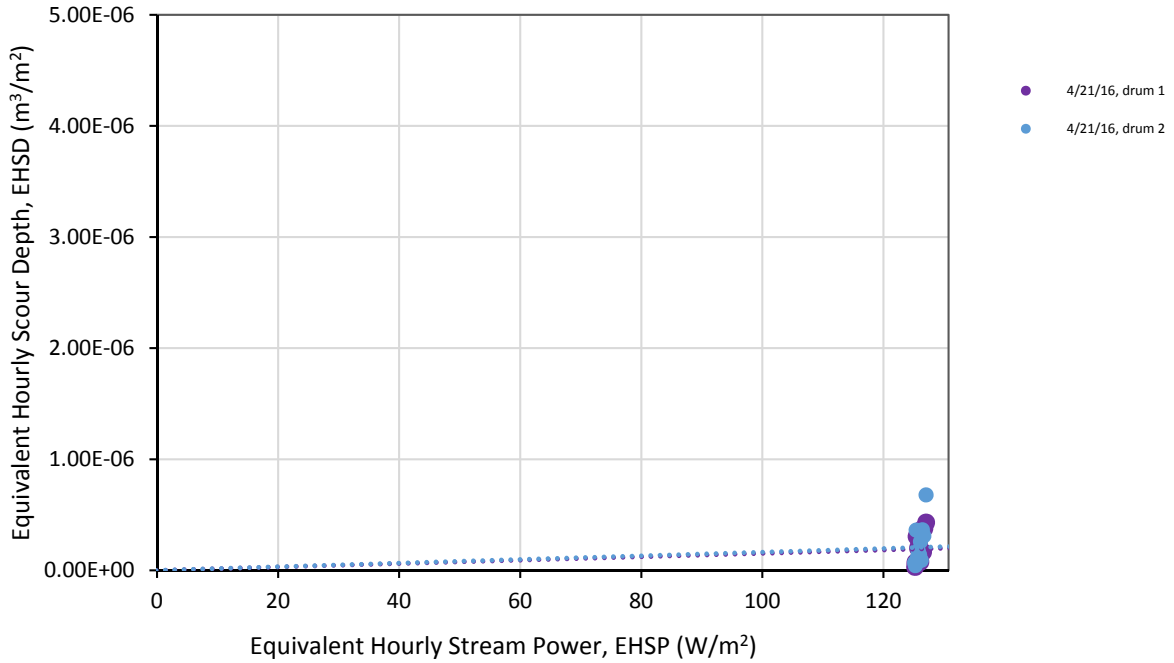


Figure B-19: Results of modified slake durability test plotted as equivalent hourly scour depth and equivalent hourly stream power for Manitowoc River (neglecting initial data point)

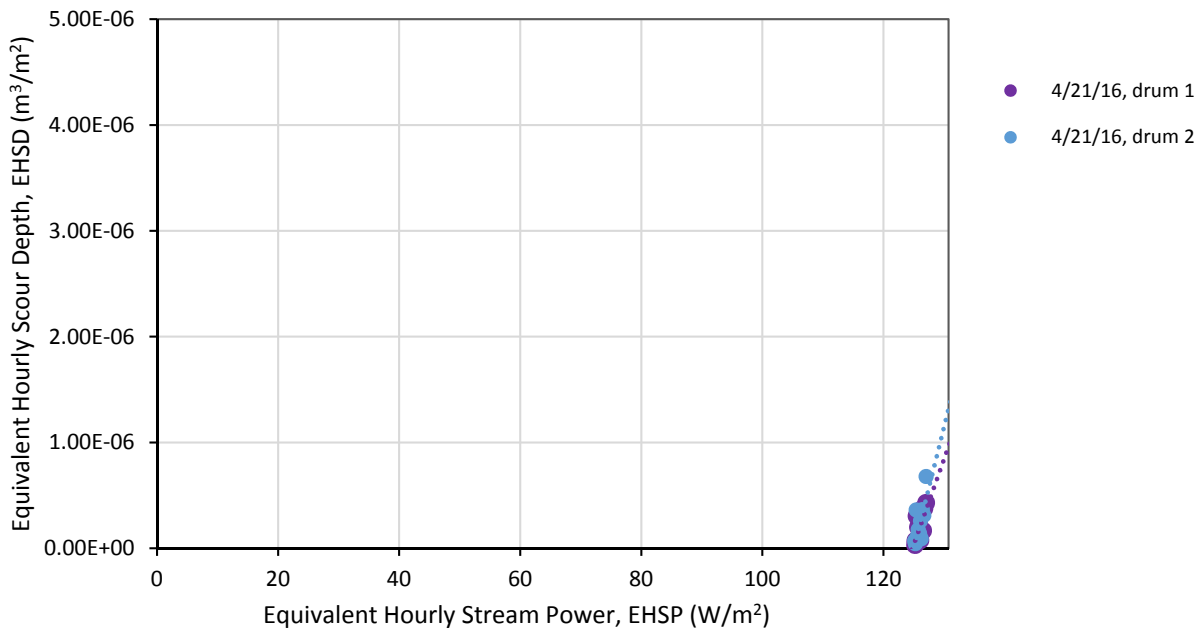


figure b-20: results of modified slake durability test plotted as equivalent hourly scour depth and equivalent hourly stream power for Manitowoc River (neglecting initial data point)

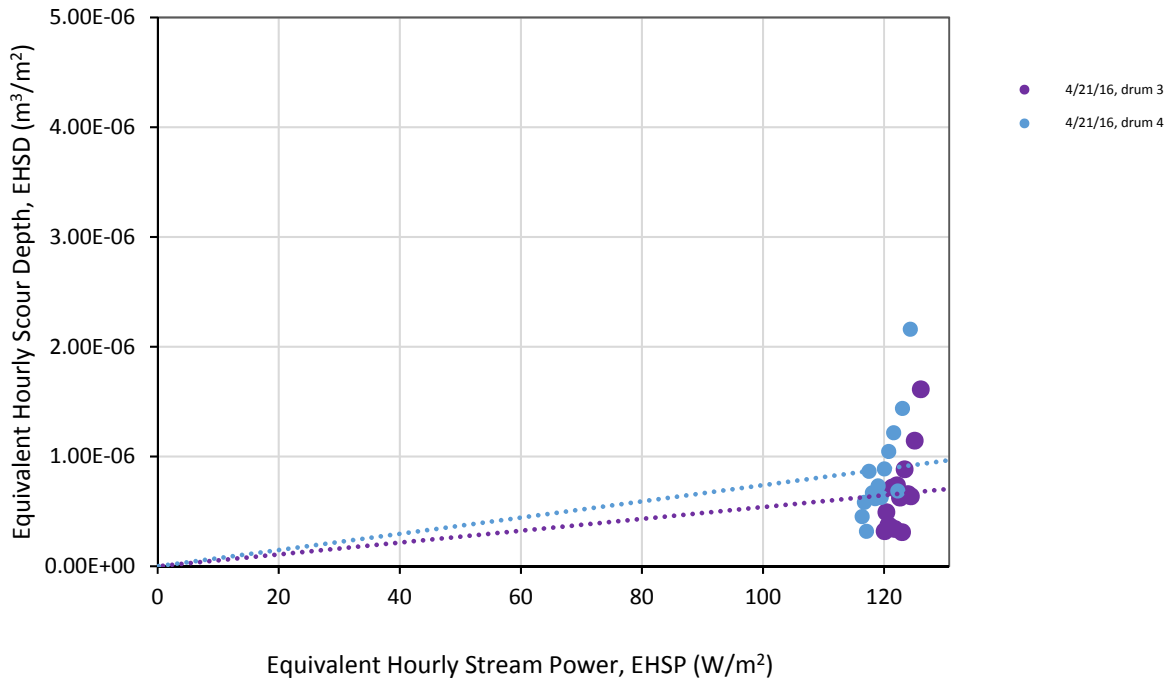


Figure B-21: Results of modified slake durability test plotted as equivalent hourly scour depth and equivalent hourly stream power for Black River (neglecting initial data point)

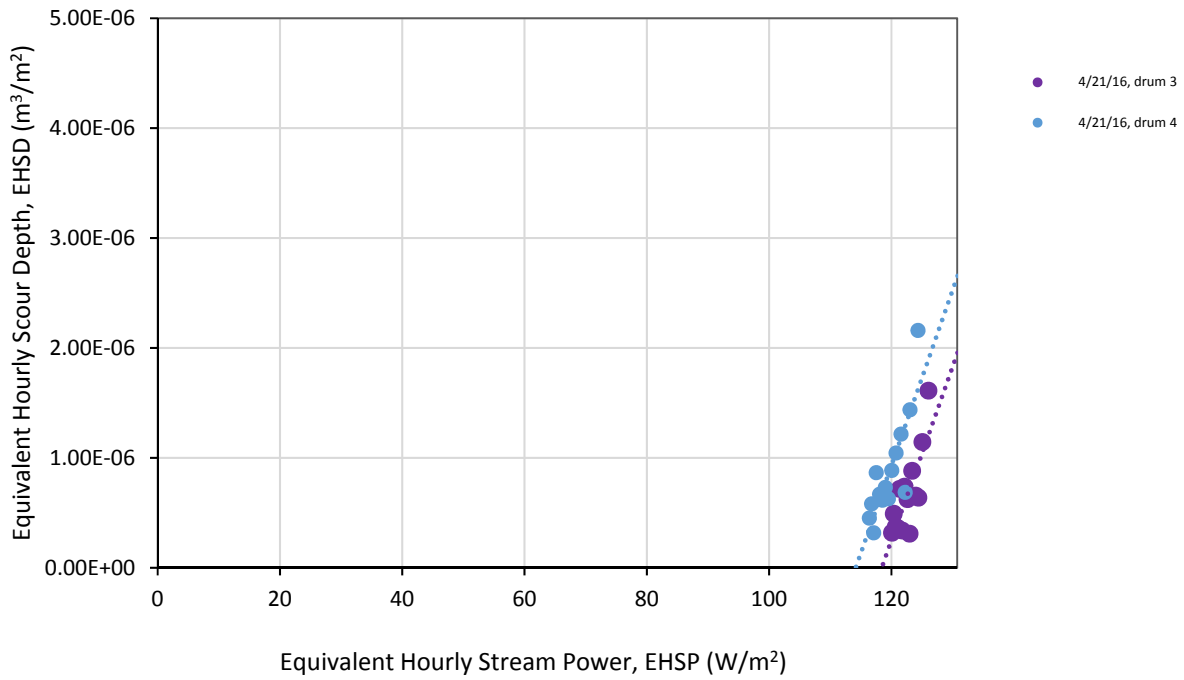


Figure B-22: Results of modified slake durability test plotted as equivalent hourly scour depth and equivalent hourly stream power for Back River (neglecting initial data point)

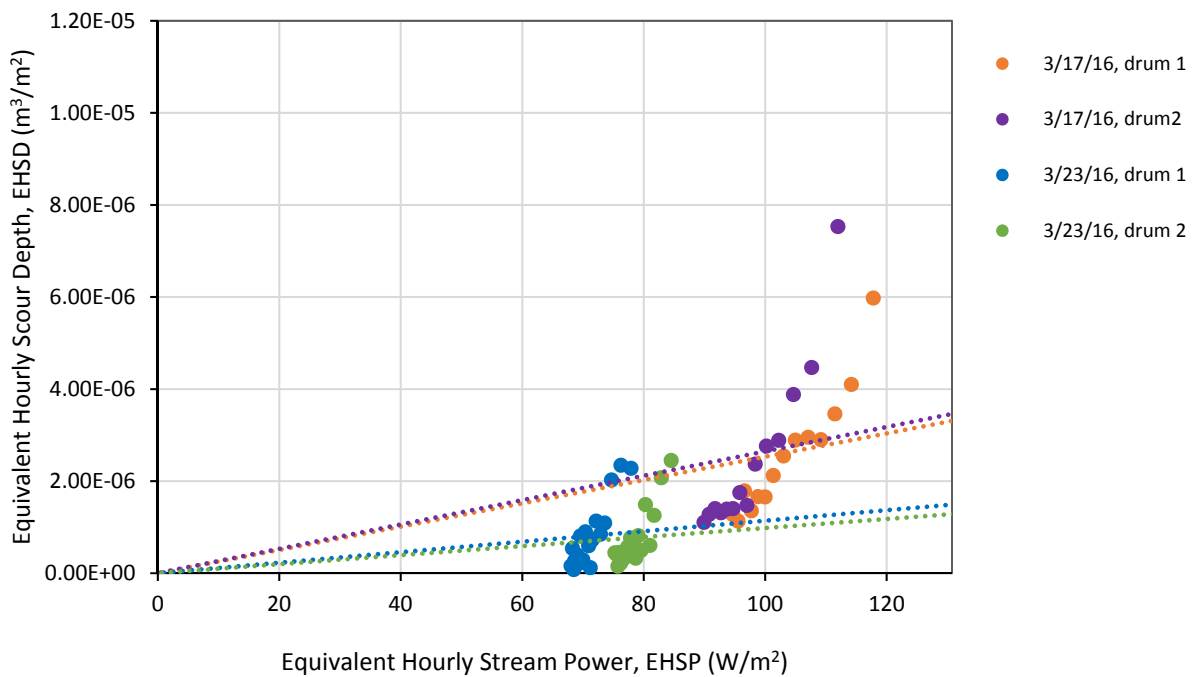


Figure B-23: Results of modified slake durability test plotted as equivalent hourly scour depth and equivalent hourly stream power for Eau Claire River (neglecting initial data point)

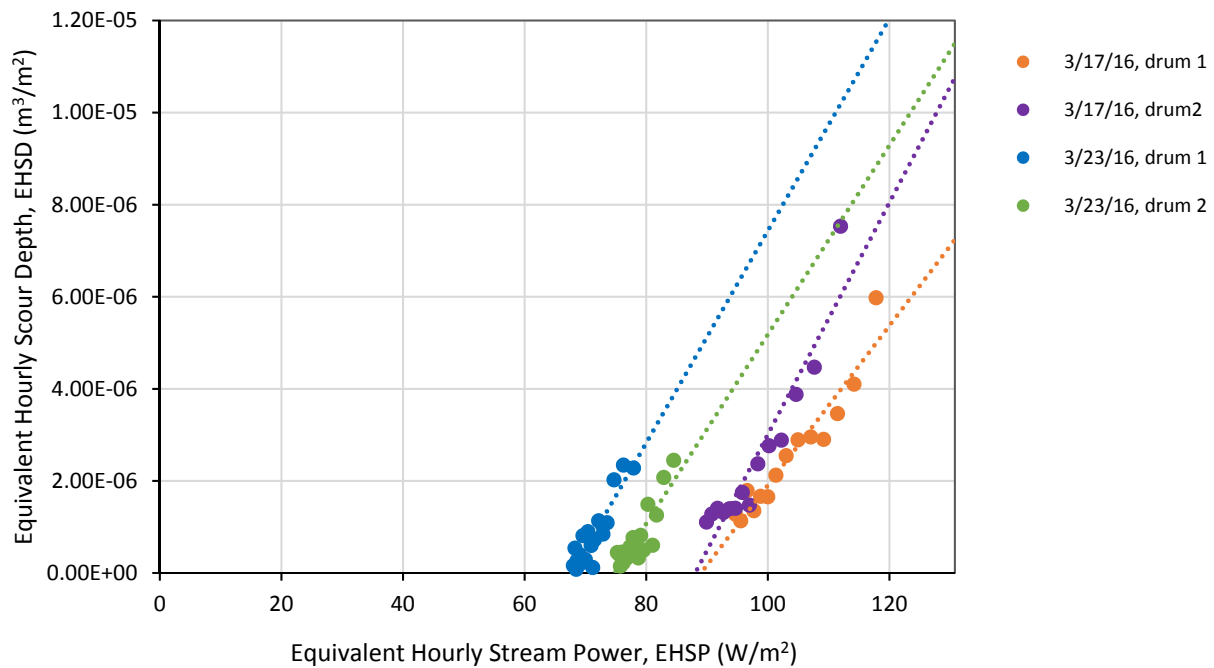


Figure B-24: Results of modified slake durability test plotted as equivalent hourly scour depth and equivalent hourly stream power for Eau Claire River (neglecting initial data point)



Wisconsin Highway Research Program
University of Wisconsin-Madison
1415 Engineering Drive
2204 Engineering Hall
Madison, WI 53706
608.890.4966
<http://wisdotresearch.wi.gov/whrp>